Distribution Agreement

In presenting this thesis or dissertation as a partial fulfillment of the requirements for an advanced degree from Emory University, I hereby grant to Emory University and its agents the non-exclusive license to archive, make accessible, and display my thesis or dissertation in whole or in part in all forms of media, now or hereafter known, including display on the world wide web. I understand that I may select some access restrictions as part of the online submission of this thesis or dissertation. I retain all ownership rights to the copyright of the thesis or dissertation. I also retain the right to use in future works (such as articles or books) all or part of this thesis or dissertation.

Signature:

_____ _____
Ian J. Pavelich   Date

Molecular mechanisms governing
regulation of toxin-antitoxin systems in bacteria

By

Ian J. Pavelich
Doctor of Philosophy

Department of Chemistry

_____[Advisor's signature]
Christine M. Dunham, Ph.D.
Advisor

_____[Advisor's signature]
Vincent Conticello, Ph.D.
Committee Member

_____[Advisor's signature]
Khalid Salaita, Ph.D.
Committee Member

Accepted:

_____
Kimberly Jacob Arriola, Ph.D., MPH
Dean of the James T. Laney School of Graduate Studies

_____
Date

Molecular mechanisms governing
regulation of toxin-antitoxin systems in bacteria

By
Ian J. Pavelich
B.S., Biomolecular Engineering (2016)
Milwaukee School of Engineering

Advisor: Christine M. Dunham, Ph.D.

An abstract of
A dissertation submitted to the Faculty of the
James T. Laney School of Graduate Studies of Emory University
in partial fulfillment of the requirements for the degree of
Doctor of Philosophy
in Chemistry
2021

Abstract

Molecular mechanisms governing
regulation of toxin-antitoxin systems in bacteria

By Ian J. Pavelich

Bacteria utilize a vast array of systems to control their growth and metabolism. Tightly regulating the process of DNA replication, transcription, and/or translation significantly alters the fate of the cell, especially in response to stress. Modules termed "toxin-antitoxin systems" are encoded in all bacteria and impact essential cellular processes upon activation. Toxins, which are the effector molecules of these systems, are unique in that they are intracellularly beneficial for survival. They are not excreted to kill neighboring bacteria. Instead, their interaction with downstream targets impacts cellular metabolism as to aid bacteria in surviving a notably variable panel of stresses. In this dissertation, the molecular mechanisms governing the regulation of toxin-antitoxin systems are investigated by applying structural and biochemical approaches to a pair of distinct, well-characterized systems: *Escherichia coli yefMyoeB* and *Proteus vulgaris higBhigA*.

First, prior studies of the YoeB toxin of *yefMyoeB* reveal that YoeB adopts a novel dimeric conformation in contrast to other toxins that are monomeric. Dimeric YoeB is just as active as an engineered monomeric YoeB variant. However, dimeric YoeB is more thermostable. This is important as YoeB is activated during heat stress in which adopting a more thermostable form is advantageous. Second, studies of *higBhigA* reveal that *higBhigA* is not regulated by any classically established method of autoregulation in toxin-antitoxin systems. Typically, regulation of toxin-antitoxin complexes is via a negative feedback loop and is sensitive to changing levels of toxin, which affect the ability of these complexes to bind and repress further activity from their own operon. In contrast to this, *higBhigA* appears to be insensitive to changing levels of toxin HigB.

Together, these studies reveal novel insights into how toxins can target protein synthesis, and the role they play in self-regulation. As toxins can drastically affect available cellular building blocks and metabolism, it is important to understand their regulation in mechanistic detail. The knowledge of how YoeB utilizes a dimeric form to tolerate heat stress, or how *higBhigA* is regulated without the use of excess toxin, provides additional insight into the numerous mechanisms bacteria utilize to evade environmental stress.

Molecular mechanisms governing
regulation of toxin-antitoxin systems in bacteria

By
Ian J. Pavelich
B.S., Biomolecular Engineering (2016)
Milwaukee School of Engineering

Advisor: Christine M. Dunham, Ph.D.

A dissertation submitted to the Faculty of the
James T. Laney School of Graduate Studies of Emory University
in partial fulfillment of the requirements for the degree of
Doctor of Philosophy
in Chemistry
2021

Table of Contents

Table of Figures

Table of Tables

Abbreviations

Abbreviation	Meaning
A site	Aminoacyl site
C. crescentus	*Caulobacter crescentus*
CbtA	Toxin protein CbtA (cytoskeleton binding toxin) of YeeU-CbtA (1)
ccd	*ccd* (coupled cell death or control of cell death) locus of mini-F plasmid (2, 3)
CcdA	Antitoxin protein CcdA of *ccd* locus
CcdB	Toxin protein CcdB of *ccd* locus
ChAd	Chaperone addiction
Clp	Caseinolytic protease
DinJ	Antitoxin protein DinJ (DNA-damage inducible protein J) of DinJ-YafQ (4)
DNA	Deoxyribonucleic acid
Doc	Toxin protein Doc (death on curing) of P1 plasmid addiction operon (5)
E. coli	*Escherichia coli*
EF-G	Elongation factor G
EF-Tu	Elongation factor thermo unstable
Fic	Filamentation induced by cAMP (6)
fit	*fit* (fast intracellular trafficking phenotype) operon (7)
FitA	Antitoxin protein FitA of *fit* operon

FitB	Toxin protein FitB of *fit* operon
GhoS	Antitoxin protein GhoS (gho̲st cell phenotype) of GhoS-GhoT (8)
GhoT	Toxin protein GhoT (gho̲st cell phenotype toxin) of GhoS-GhoT (8)
GraA	Antitoxin protein GraA (g̲rowth r̲ate a̲ffecting a̲ntitoxin) of GraT-GraA (9)
GraT	Toxin protein GraT (g̲rowth r̲ate a̲ffecting t̲oxin) of GraT-GraA (9)
hic	*hic* (*Haemophilus influenzae* (*hif̲*) c̲ontiguous) operon (10)
HicA	Toxin protein HicA of *hic*
HicB	Antitoxin protein HicB of *hic*
hig	*hig* (h̲ost i̲nhibition of g̲rowth) operon of plasmid Rts1 (11)
HigA	Antitoxin protein of *hig* operon
HigB	Toxin protein of *hig* operon
HigB	Toxin protein HigB
hip	*hip* (hi̲gh p̲ersistence mutant encoding) operon (12)
HipA	Toxin protein HipA of *hip* operon
HipB	Antitoxin protein HipB of *hip* operon
HTH	Helix-turn-helix
IPTG	Isopropylthio-β-galactoside
Kid	Toxin protein Kid (ki̲lling d̲eterminant) of plasmid R1 (13)
Kis	Antitoxin protein Kis (ki̲lling s̲upresor) of plasmid R1 (13)

LB	Lysogeny broth
Lon	<u>Lon</u>g filament phenotype protease
maz	*maz* (ma-ze meaning "what is it" in Hebrew; originally identified as an unknown ORF downstream of *relA*) operons (14)
MazE	Antitoxin protein MazE of *maz* operons
MazF	Toxin protein MazF of *maz* operons
M. tuberculosis	*Mycobacterium tuberculosis*
mqs	*mqs* (<u>m</u>otility <u>q</u>uorum-<u>s</u>ensing regulator) operon (15)
MqsA	Antitoxin protein MqsA of *mqs* operon
MqsR	Toxin protein MqsR of *mqs* operon
mRNA	Messenger RNA
N. gonorrhoeae	*Neisseria gonorrhoeae*
$OD_{\#}$	Optical density at a specific wavelength, '#'
P. vulgaris	*Proteus vulgaris*
par	*par* (<u>par</u>tition system) operons of plasmid R1, RK2 (16-18)
ParD	Antitoxin protein ParD of *par* operon
ParE	Toxin protein ParE of *par* operon
PDB	Protein Data Bank
pem	*pem* (<u>P</u>lasmid for <u>e</u>mergency <u>m</u>aintenance) operon of plasmid R1 (19)
Phd	Antitoxin protein Phd (<u>p</u>revent <u>h</u>ost <u>d</u>eath) of P1 plasmid addiction operon (5)

phd/doc	P1 plasmid addiction operon encoding *phd/doc* (5)
PSK	Post-segregational killing
P_{TA}	Toxin-antitoxin system operon promoter
R. felis	*Rickettsia felis*
rel	*rel* operon; Mutations to the *rel* operon impair the stringent response, and the accompanying mutants are termed <u>*relaxed*</u> (20)
RelB	Antitoxin protein RelB of the *rel* operon
RelE	Toxin protein RelE of the *rel* operon
RHH	Ribbon-helix-helix
RNA	Ribonucleic acid
rRNA	Ribosomal RNA
S. dublin	*Salmonella dublin*
S. enterica LT2	*Salmonella enterica* serovar Typhimurium LT2
S. flexneri	*Shigella flexneri*
S. pyogenes	*Streptococcus pyogenes*
SecB	Chaperon protein SecB (<u>sec</u>retory system protein B) of the Sec system (21)
SocA	Antitoxin protein SocA of SocA-SocB
SocB	Toxin protein SocB (<u>s</u>uppressor <u>of</u> <u>C</u>lpXP) of SocA-SocB (22)
SpoVT/AbrB	SpoVT(stage <u>V</u> <u>spo</u>rulation protein <u>T</u>)-AbrB (bacterial <u>a</u>nti<u>b</u>iotic <u>r</u>esistance protein <u>B</u>) domain superfamily (23, 24)
SRL	Sarcin-rich loop of 23S rRNA

SymE	Toxin protein SymE (<u>S</u>OS-induced *yjiQ* gene with similarity to <u>Maz</u><u>E</u>) of SymE-SymR (25)
SymR	Antitoxin non-coding RNA SymR (<u>sym</u>biotic <u>R</u>NA) of SymE-SymR (25)
tRNA	Transfer RNA
vap	*vap* (<u>v</u>irulence-<u>a</u>ssociated <u>p</u>rotein encoding) operons (26)
VapB	Antitoxin protein VapB of *vap* operons
VapC	Toxin protein VapC of *vap* operons
YafQ	Toxin protein YafQ of DinJ-YafQ
YeeU	Antitoxin protein YeeU of YeeU-CbtA
YoeB	Toxin protein YoeB of YefM-YoeB

Chapter 1

Introduction to toxin–antitoxin systems in bacteria

1.1 Abstract

Bacteria employ complex mechanisms to survive in the extreme gamut of Earth's environments and respond to environmental stimuli they encounter (e.g., nutrient deprivation, hypoxia, temperature fluctuations, phage infection, and antibiotic exposure). Small gene pairs termed toxin-antitoxin systems support such adaption and aid bacteria in survival. These gene pairs or systems are bifunctional macromolecules depending upon the environmental conditions they encounter. First, in non-stress or normal conditions, the toxin-antitoxin system acts as a transcriptional repressor to prevent their own expression and to allow for optimal bacterial growth. Second, upon encountering a change in environment or stress, bacteria undergo a functional switch whereby proteolysis of the antitoxin occurs, freeing the toxin. Liberated toxin inhibits growth by preventing essential cellular processes including membrane biogenesis, replication, transcription, and translation. Much remains unclear about how these systems are activated and regulated. Questions are proposed herein exploring the molecular mechanisms by which toxin-antitoxin systems are regulated using microbiology, molecular biology, and biomolecular chemistry.

1.2 Toxin-antitoxin systems in bacteria

Toxin-antitoxin systems are gene pairs which in the simplest context encode a "toxin" and antidote-like "antitoxin" that counteract the activity of the toxin. It is important to note that although the term "toxin" is used, they are not to be confused with traditional exotoxins, like bacteriocins. Bacteriocins are two protein components where one component is a toxin that is excreted to kill closely related strains of bacteria, but not the host via suppression of its binding partner, the antidote protein. The nomenclature of bacteriocins is derived from the species of the producing strain with a *-cin* suffix appended. For example, *E. coli* secretes colicin proteins to kill neighboring related strains of *E. coli* (27). This is achieved through targeting a wide range of possible downstream targets, much like the toxins of toxin-antitoxin systems. Bacteria even encode immunity proteins to protect themselves from their own bacteriocins, much like an antitoxin. The key difference between these systems is that toxin components of toxin-antitoxin systems remain intracellular and are beneficial for cell survival (28).

Toxin-antitoxin systems were first discovered through their role in plasmid maintenance (2, 29). Cells that lose a complete toxin-antitoxin locus from their plasmids are prevented from growing due to insufficient amounts of antitoxin to block toxin activity. Thus, plasmids that carry and maintain a complete toxin-antitoxin locus are stabilized and their inheritance in progeny cells are favored. This is also termed "post-segregational killing" (PSK) since cells without a complete toxin-antitoxin locus can be killed by unchecked toxin activity over time. Since the discovery of the first toxin-antitoxin operon *ccd* on the *E. coli* F plasmid (2), many others followed including *parD/pem* on the *E. coli* R1/R100

plasmid, *vap* of the *S. dublin* plasmid, *phd/doc of* bacteriophage P1, *par* of *E. coli* plasmid RK2, *hig* of *P. vulgaris* plasmid Rts1*, and rel* of *E. coli* plasmid P307 (5, 17, 18, 30-32).

It is now understood that toxin-antitoxin systems are ubiquitous across bacterial plasmids as well as chromosomes, with bacterial strains like *E. coli* and *M. tuberculosis* sporting dozens of toxin-antitoxin systems (33). In addition to their abundance, these systems are also functionally diverse. Currently, six types of toxin-antitoxin loci are known and are categorized by the cellular makeup of their components (RNA or protein) (Table 1.1) (34). Types I and III are the only types in which components of the toxin-antitoxin system can be RNA (35). Both components of type I are RNA wherein the antitoxin is an antisense RNA that binds directly to toxin mRNA. Alternatively type III antitoxins are RNAs that bind toxin protein directly for inhibition. In contrast, types II, IV, and VI consist of components that are both proteins, but differ significantly in how the antitoxin neutralizes the toxin (34). Type II antitoxins form a tight complex together with cognate toxin, thus sequestering the toxin to inactivate it. In contrast, type IV antitoxins do not bind the toxin directly, but instead interact with the target of the toxin. For example, the *E. coli* antitoxin YeeU (of YeeU-CbtA) binds to cytoskeletal proteins and promotes bundling of filaments (36). Once bundled, toxin CbtA can no longer interact with the cytoskeletal proteins to inhibit their activity. Thus, through changes induced by the antitoxin, the toxin can no longer affect cellular activity. Finally, antitoxins in type VI systems neutralize toxins by stimulating the degradation of the toxin. In the *C. crescentus* SocA-SocB system, antitoxin SocA achieves this through its ability to bind both toxin SocB and Clp protease. Clp proteases then degrades the entire complex. Thus, SocA promotes degradation of SocB (22).

The focus of studies contained herein are type II toxin-antitoxin (protein-protein) systems, which are by far the most well-studied and characterized (37). Both antitoxins and toxins of type II systems have low sequence identity (5-11%) (33, 38). While this would initially suggest that these systems are highly unrelated, surprisingly each component shares several structural similarities and there are numerous homologs of toxin-antitoxin systems across bacteria (39).

1.3 Regulation of toxin-antitoxin activity

In normal growth conditions, toxin-antitoxin genes are regulated as a negative feedback loop where they function as repressors of their own transcription. The toxin-antitoxin complex binds to DNA operators upstream that overlap with its promoter and prevents further expression. Upon encountering external stimuli (e.g., nutrient starvation, heat shock, etc.), bacteria undergo a functional switch whereby the antitoxin is proteolyzed, releasing the toxin. Free toxin is then able to inhibit growth by preventing essential cellular processes. Removal of stimuli results in a switch back to homeostatic conditions, where the antitoxin is no longer proteolyzed and resumes toxin sequestration and transcriptional auto-repression. Thus, toxin-antitoxin systems modulate essential cellular processes to shift cells' focus away from growth and toward survival in stressful conditions. Type II antitoxin proteins contain a DNA-binding motif which allows the antitoxin to repress at operator sites within the promoters of toxin-antitoxin genes. Toxin proteins are either recruited to their cognate antitoxins bound at these operator sites or the toxin-antitoxin complex binds to operators where they function as co-repressors, allowing the system to

4

be responsive to changes in toxin expression levels. Type II toxin-antitoxin systems manage this transcriptional auto-repression in the following different ways: (i) using "conditional cooperativity" where the system is responsive to changes in toxin levels (40-45); (ii) as simple on/off switches (46); (iii) through regulation influenced by chaperones (tri-partite systems) which enable proper folding of the antitoxin to bind and repress toxin (47-49); or (iv) by crosstalk between systems (50).

Some type II toxin-antitoxin systems are responsive to changing levels of toxin and most are regulated by a mechanism termed "conditional cooperativity". In this mechanism, toxin-antitoxin loci are sensitive to the changing ratios of toxins to antitoxins *conditional* to environmental stimuli sensed by the cell. In addition, antitoxins alone or toxin-antitoxin complexes can bind at operator sites embedded in the promoters. Binding of multiple complexes at adjacent operator sites can exert a *cooperative* effect and enhance transcriptional repression (51). Thus, a transcriptional response based on changing ratios of toxins and antitoxins *conditional* to the environmental stimuli in the cell and exhibiting *cooperative* binding at operator sites is called conditional cooperativity. Systems like *E. coli* CcdB-CcdA, RelB-RelE*,* and bacteriophage P1 Phd-Doc are all regulated by conditional cooperativity (40-42). Even though these systems share a regulatory model, there are slight differences in how regulation occurs. This is because each of these systems has a distinct structural organization that alters toxin-antitoxin complex affinity. Doc toxin of PhD-Doc can bind to PhD at either "high" and "low" affinity binding sites, which help to stabilize the complex until a critical level of toxin is reached (52). CcdB-CcdA uses a similar high/low-binding site mechanism (40), whereas RelB-RelE does not

exhibit this behavior. RelE likely does bind to RelB with different levels of affinity unlike the PhD-Doc system (53). Instead, the cooperative effect likely stems from interactions between neighboring complexes bound to adjacent operators and located close together (54).

However, some systems are not responsive to changing levels of toxin and instead, they function as on/off transcriptional switches. Toxin-antitoxin complexes still form higher-ordered complexes when bound to their DNA operators but there appears to be no conditionality or cooperativity within the mechanism of repression. One example of this is *E. coli* DinJ-YafQ (46). The DinJ-YafQ antitoxin-toxin complex is incalcitrant to changing levels of toxin, even on a fully occupied operator in which both operator sites are occupied. Thus, the ability of DinJ-YafQ to repress its own transcription is likely not conditional to changing levels of toxin. Further, binding of a single DinJ-YafQ at one operator site achieves similar transcriptional repression as two DinJ-YafQ complexes binding at two operator sites indicating there is no cooperativity between adjacent DinJ-YafQ complexes. Instead of conditional cooperativity, these data suggest that *E. coli* DinJ functions as an on/off switch.

Tripartite systems like *E. coli* O157:H7 *paaRAE2, S. pyogenes ω-ε-ζ,* plasmid encoded *pasABC*, and *M. tuberculosis higBA-secB* all encode a third regulatory component (47-49). In these systems, the behavior of the toxin-antitoxin system is modified by the third component. In the most well-studied example, *M. tuberculosis higBA-secB* is regulated by the chaperone SecB (49). Chaperone SecB mediates proper folding of the HigA

antitoxin by recognition of specific ChAd (<u>ch</u>aperone-<u>ad</u>diction) amino acid sequences such that it can bind cognate toxin. In the absence of SecB, the HigA antitoxin cannot fold properly and cannot sequester toxin. Thus, encoding a third component provides another layer of regulatory control over toxin-antitoxin systems.

Components of some toxin-antitoxin systems have an additional ability to interact with other systems in a regulatory model termed "crosstalk". The best illustration of this is by the *E. coli* type V system GhoS-GhoT (8, 50). Toxin GhoT activity can be enhanced by the degradation of GhoS (the antitoxin of GhoT) by *E. coli* toxin MqsR. The way MqsR achieves this is by cleavage of the GhoS antitoxin mRNA. Toxin GhoT does not contain these sites, so its transcript is selectively enriched upon MqsR activation (50). Importantly, *E. coli* MqsR-MqsA is a type II toxin-antitoxin system, whereas GhoS-GhoT is a type V system, suggesting that there may be hierarchies of toxin-antitoxin systems that control one another. As GhoS antitoxin is a RNase that cleaves toxin GhoT mRNA, GhoT might otherwise never be activated without the influence of MqsR. Thus, crosstalk between systems provides another level of regulatory control within toxin-antitoxin systems.

Finally, there are systems like *E. coli* MqsR-MqsA (55) and *P. putida* GraT-GraA (56) that don't resemble any of the types of regulation described above. For instance, in MqsR-MqsA, antitoxin MqsA binds tightly to its operator and is mutually exclusive with MqsR toxin binding. Similarly, toxin GraT of GraT-GraA also does not function as a co-repressor. GraA antitoxin alone is sufficient to repress the *graTgraA* operon, which is destabilized once toxin GraT binds. This is because in contrast to MqsA, GraA maintains two distinct

sites for toxin and DNA binding like many other antitoxins. Yet, GraT still cannot bind GraA-DNA. This type of diversity suggests there may be other modes of toxin-antitoxin regulation yet to be discovered.

1.4 Diversity of type II antitoxins

Type II antitoxins generally contain two motifs: an N-terminal DNA-binding motifs to bind operator DNA and a C-terminal toxin-binding motif for sequestering toxin. In addition, many type II antitoxins are obligate dimers, which influences the number of antitoxins bound at operator binding sites for transcriptional repression. Many type II toxin-antitoxin system structures have been solved using X-ray crystallography, resulting in four different DNA motifs (57).

The four types of DNA-binding motifs in type II antitoxins include (i) helix-turn-helix (HTH), (ii) ribbon-helix-helix (RHH), (iii) SpoVT/AbrB, and (iii) Phd/YefM motifs, of which the first two are the most common (Figure 1.2) (57). A HTH motif is a complete DNA-binding motif within a *single* antitoxin and contains two short α-helices separated by a short turn as in *E. coli* HipB-HipA (58), MqsR-MqsA (59, 60) and *P. vulgaris* HigB-HigA (61). In contrast, RHH motifs require the *dimerization* of two antitoxins and are composed of two antiparallel β-strands followed by two α-helices as in *E. coli* RelB-RelE (54), DinJ-YafQ (46), ParD-ParE (62), CcdB-CcdA (63, 64), *N. gonorrhoeae* FitA-FitB (65), and *M. tuberculosis* VapB-VapC (66-68). This means that an HTH-containing antitoxin dimer contains two DNA-binding motifs whereas only a single RHH motif is formed by dimerization of antitoxins. Thus, antitoxins that contain RHH motifs can potentially bind

twice as many operator sites as compared to antitoxins with HTH motifs. This difference is important as changing the oligomeric states of toxin-antitoxin complexes bound at DNA can affect the degree to which transcriptional repression is achieved (see Chapter 3). SpoVT/AbrB motifs are more complex than RHH, sporting three or four anti-parallel β-strands that pack against each other to form the DNA-binding domain as in *E. coli* MazE-MazF (69-71), *R. felis* VapB-VapC and *S. flexneri* VapB-VapC (72, 73). Finally, the Phd/YefM motif is a unique fold containing a mixture of α-helices and β-strands and found in *E. coli* Phd-Doc (52) and YefM-YoeB (74).

Toxin-binding domains of antitoxins are harder to categorize. Generally, toxin-binding domains are located at the C termini of antitoxins and contain intrinsically disordered regions that gain tertiary structure upon binding to its cognate toxin. The most obvious mechanism by which toxin can be sequestered is by blocking the toxin's active site (75). This is achieved by antitoxins like *E. coli* RelB (54) whose C-terminus wraps around the toxin and displaces a RelE α-helix from its catalytically competent position, thus inactivating RelE (76). However, this mechanism does not hold true for all antitoxins. For example, the C-terminus of *P. vulgaris* HigA does not mask the active site once bound, and the active site remains completely open. In addition, antitoxins can also neutralize toxin activity by the use of co-factors or by providing structural insertions (75). For example, antitoxin VapB prevents toxin VapC from binding its cofactor Mg^{2+} by locking VapC in a catalytically unfavorable conformation where it is unable to bind Mg^{2+} (66). Alternatively, antitoxin Phd donates an entire α-helix into the filamentation induced by cAMP proteins (Fic) fold of Doc toxin (77). The Fic-like fold on Doc is otherwise missing

the extra α-helix found in Fic proteins. Donation of the α-helix from antitoxin PhD completes the Fic-like fold in Doc, resulting in a tightly bound and sequestered toxin. These examples illustrate that the toxin-binding domain is also diverse in mechanism.

1.5 Diversity of type II toxins and targets

The two largest superfamilies of type II toxins are the RelE and MazF families. There are also smaller families including Zeta, Doc, HipA, VapC, and others which continue to expand as more toxin-antitoxin systems are studied (38). Most of these toxins function as microbial ribonucleases (RNases), which has led to a secondary categorization as ribosome-dependent or -independent.

Ribosome-dependent toxins typically disrupt active translation by either binding to and/or interacting with an actively translating ribosome for functionality. This is then followed by cleavage specifically within the aminoacyl (A) site of the ribosome, which is where tRNA binds and interacts with mRNA to be decoded. Cleavage occurs between the second or third nucleotide of the A-site codon. The best example of these are RelE superfamily members including *E. coli* RelE, YafQ, YoeB, and *Proteus vulgaris* HigB (46, 61, 74, 78). Although these ribosome-dependent toxins are within the same superfamily, they can cleave a variety of codons using sets of diverse residues in their active sites.

In contrast, ribosome-independent toxins do not rely on the presence of an actively translating ribosome for RNase activity and instead cleave free mRNA with recognition sequences that range from 3 to 7 nucleotides long. The largest of these families is the

MazF family which largely cleave free mRNA transcripts (similar to *E. coli* HicA and MqsR) (10, 25, 79, 80). In addition, many VapC toxins cleave free tRNA or rRNA (81, 82). *S. flexneri* toxin VapC inhibits translation by cleaving between nucleotides 38-39 in the junction of the anticodon stem-loop of initiator tRNA^{fMet} (83), thus preventing translation from ever beginning. Alternatively, *M. tuberculosis* toxin VapC cleaves at the sarcin-rich loop (SRL) of 23S rRNA (82). The SRL triggers the GTPase activity of both EF-Tu and EF-G which are elongation factors critical to the process of translation. EF-Tu is responsible for shuttling aminoacyl-tRNA to the ribosome in complex with GTP, and EF-G is responsible for translocation of tRNA and mRNA through the ribosome (84, 85). Unsurprisngly then, cleavage of the sarcin loop thus arrests translation. Toxin Doc of Phd-Doc of bacteriophage P1 also inhibits translation through EF-Tu (84, 86). However, Doc achieves this through an alternate mechanism. Doc phosphorylates at a single site in domain III of EF-Tu which prevents the binding of aminoacylated tRNAs and thus halts translation. Finally, *E. coli* HipA of HipB-HipA inhibits translation by phosphorylation of glutamyl-tRNA synthetase (87).

Type II toxins can also target the machinery of DNA replication. *E. coli* CcdB of CcdB-CcdA (a MazF homolog) and ParE of ParD-ParE (a RelE homolog) both inhibit DNA replication by inhibiting DNA gyrase, preventing DNA from unwinding during replication (3, 88). Interestingly, CcdB is unique from other family members because it inhibits DNA gyrase, even though it contains a similar RNase fold to that of MazF. This is because CcdB does not contain an RNA binding site, and instead has a dimer of helices that interact with DNA gyrase (89). Thus, free toxin inhibits growth by disrupting essential

cellular processes such as translation and replication and for that reason, must be tightly regulated.

1.6 Activation of toxin-antitoxin systems

Toxin-antitoxin systems were originally discovered as plasmid maintenance modules (90, 91) but they have now been implicated in more processes in bacteria including phage defense, anti-addiction (anti-PSK), plasmid displacement, or stress responses (37). Some type III and type IV toxin-antitoxin systems can trigger cell death in response to phage infection, although the mechanism by which this is achieved is still unknown (92, 93). The roles of toxin-antitoxin systems in plasmid anti-addiction and displacement are more well understood. It has been clearly demonstrated that antitoxins can neutralize toxins from homologous systems and thus prevent addiction to that system (94). In addition, toxin-antitoxin systems can also provide a competitive advantage to a plasmid in order to outcompete conjugative plasmids with identical (incompatible) replicons (95). Once toxin-antitoxin systems were identified on bacterial chromosomes, their purported roles in stress responses expanded quickly. Initially, systems like *E. coli* RelB-RelE and MazE-MazF were implicated in nutritional stress like amino acid or nutrient deprivation (80, 96, 97). These conditions are typically induced using L-serine hydroxamate (an L-serine analogue that binds and inhibits seryl-tRNA synthetase (98)) or through restricting amino acids. Uncharged tRNAs on the ribosome are sensed by RelA synthetase, which causes inactivation of protein synthesis through a process called the stringent response. RelA produces the signaling messenger guanosine tetra or pentaphosphate ((p)ppGpp) (99, 100). RNA polymerase is targeted by ppGpp and regulates transcription of numerous

12

genes. RelB-RelE is also activated as part of this response as evidenced by elevated transcript and RelE toxin levels *in vivo* (96).

Alternatively, *E. coli* YefM-YoeB is activated in response to thermal stress (101). Translational arrest often leads to mRNA degradation in the ribosome A site resulting in truncated A-site codons that prevent further decoding and produce stalled translation complexes (102-104). Such non-productive ribosomes can normally be "rescued" by quality control rescue systems in bacteria, like tmRNA-SmpB in a response called trans-translation. However, in cells that lack tmRNA-SmpB, exposure to an elevated temperature can surprisingly restore A-site cleavage activity (101). It was determined that ribosome-dependent toxin *E. coli* YoeB was also upregulated and is responsible for mRNA cleavage. To determine this, ribosomes were stalled using an mRNA transcript that encodes a Pro–Pro peptide motif. Stretches of proline residues favor the *trans* conformation, which can hinder translation by destabilizing the peptidyl (P) site of the ribosome (105, 106). The transcript also encoded an A-site codon recognized by YoeB upstream of the Pro-Pro motif. Indeed, A-site cleavage activity could only be rescued in cells that encoded the *yefMyoeB* system expressing YoeB toxin (101). Interestingly, cleavage of mRNA was not observed in transcripts where translation was terminated before reaching the Pro-Pro motif. This fact, combined with the observation that YoeB was only active at elevated temperatures, suggested that YoeB does not function to cleave A-site mRNA to *inhibit* translation, like RelE. Instead, YoeB is likely limited to ribosomes that have stalled during heat stress, and instead works to *promote* recycling of stalled ribosomes by cleaving in the A site to allow rescue factors like tmRNA-SmpB to

bind and initiate *trans*-translation.

Many toxin-antitoxin genes also appear upregulated in response to other factors like DNA damage or antibiotics (107). For instance, the *E. coli dinJyafQ* operon contains a consensus LexA binding site upstream of its promoter and is likely to be regulated by DNA damage (108). LexA is a transcriptional repressor of the SOS (Save Our Souls) regulon, which contains several genes that promote DNA repair in response to damage (4, 109-113). Prysak and coworkers demonstrated that LexA can bind at its consensus sequence within the *dinJyafQ* operator, suggesting DinJ-YafQ is involved in the SOS response (114). However, *dinJyafQ* provided no discernable beneficial phenotype when DNA damage was induced by UV radiation or antibiotic mitomycin C, which alkylates DNA. Cells lacking *dinJyafQ* recovered just as quickly as wild-type cells (114). In addition, the implications of YafQ expression after DNA damage have yet to be investigated. The role of bacterial toxin-antitoxin systems in antibiotic stress has proven more controversial. It was previously shown that toxin-antitoxin gene pairs could mediate bacterial persistence to antibiotics (12) . This was further explored by correlating deletion of type II toxin-antitoxin gene pairs with reduced levels of antibiotic persistence in bacterial culture (115). However, the deletion strains were contaminated with prophage and those results could not be replicated even in newly constructed strains (116, 117). Why other toxin-antitoxin systems are upregulated in response to antibiotics remains unclear. For example, *dinJyafQ* and *relBrelE* mRNA transcript levels are ~40-fold and >20,000-fold higher respectively in cells that have been treated with antibiotic rifampicin (107). As rifampicin inhibits RNA polymerase, this result is surprising, and should be investigated

further.

1.7 Questions addressed

There are several confirmed and contested roles that type II toxin-antitoxin systems play in aiding bacterial survival in response to environmental stimuli (37). There are still questions in key areas of toxin-antitoxin regulation that remain to be answered. These include understanding toxins whose function (see Chapter 2), regulation (see Chapter 3), or activation remain unclear (see Chapter 4).

In Chapter 2, I discuss how the toxin YoeB is activated during thermal stress and binds to the bacterial ribosome to regulate protein synthesis or translation. Translation is a finely tuned process by which the ribosome reads the genetic code on mRNA and adds the corresponding amino acid delivered by tRNAs to synthesize proteins quickly but accurately. I studied how YoeB cleaves specific mRNA codons in the A site of the ribosome to selectively alter translation globally in the cell. YoeB is the sole member of the RelE toxin superfamily that binds the ribosome as a dimer, whereas all other toxins are monomeric. YoeB also displays broad codon specificity as a ribosome-dependent mRNase. To determine the biological relevance of these properties, I solved multiple x-ray crystal structures of dimeric YoeB bound to the ribosome with different mRNA codons. Our structures provide the structural basis for how YoeB makes specific interactions with the mRNA for optimal codon cleavage, but still accommodates a wide range of codons for cleavage. I further engineered a monomeric YoeB variant and showed similar endonuclease activity as compared to its dimeric form, indicating a dimer is not necessary

for activity. I also determined that dimeric YoeB is more thermostable than monomeric YoeB strongly correlating with its upregulation during heat stress. By demonstrating that the sole dimeric type II toxin does not require its dimeric state for mRNase activity, this work expanded our knowledge of the complexity with which toxins alter essential cellular processes, in this case thermal stress. These results culminated in a co-first-author paper in the Oxford Academic Journal *Nucleic Acids Research* and an invited talk from organizers of the first-ever Toxin-Antitoxin Workshop, hosted by the European Molecular Biology Organization.

In Chapter 3, to continue to explore how toxin-antitoxin systems are regulated, I next studied the regulation of the *higBA* toxin-antitoxin operon, which was originally identified on a plasmid-associated antibiotic resistant *Proteus vulgaris* from a post-operative bacterial infection (11, 118, 119). To tightly regulate its own expression, antitoxin proteins function as transcriptional auto-repressors with additional regulation imparted by conditional cooperativity. However, our study of the *hig* operon demonstrated that *higBA* is regulated via a simple on/off transcriptional switch that is incalcitrant to changing toxin levels, not through conditional cooperativity. I solved X-ray crystal structures of the DNA-bound HigB-HigA complexes in both a trimeric and tetrameric state. Our structures suggest that each oligomeric state is remarkably similar, and that a trimeric HigB-HigA$_2$ could repress transcription just as efficiently as a fully occupied tetramer. To confirm this, I engineered and expressed a trimer-only variant of HigB-HigA$_2$ and found that indeed there is little difference in transcriptional repression based on whether the second HigB monomer is bound. We also found that no cooperativity exists between *hig* operators.

Thus, HigB-HigA does not regulate the *hig* operon using conditional cooperativity. These results add to the growing diversity of mechanisms used to balance transcriptional responses of these abundant bacterial gene pairs, and my first-author paper describing such is currently in revision at the American Society of Microbiology journal *mBio*.

In Chapter 4, I discuss how antitoxins become susceptible to proteolysis when external environmental stimuli activate the system. Some antitoxins contain intrinsically disordered regions at their C termini that may be selectively recognized by proteases. However, not all antitoxins contain intrinsically disordered termini and thus how instability of the antitoxin leads to proteolysis is unclear. Three toxin-antitoxin pairs from *E. coli* (DinJ-YafQ*, RelB-RelE,* and YefM-YoeB*)* are examined to determine which antitoxin regions are necessary for toxin sequestration, antitoxin stability, and antitoxin recognition for proteolysis. These systems were selected because although the toxins are structural homologues, the manner in which the antitoxins repress their toxins is different. Further, each system is activated in response to different stimuli and therefore may undergo proteolysis in different ways.

Type II toxin-antitoxin systems are ubiquitous protein-protein complexes that can influence many cellular processes in response to environmental stimuli, which can include antibiotics (120). Originally discovered for their role in plasmid maintenance and phage resistance (90-92), it has been suggested that toxin-antitoxins can contribute to bacterial persistence (12, 121-125). This may allow for the formation of a small subpopulation of 'persister' cells that exhibit a non-heritable ability to subsist during antibiotic treatment,

which has been linked to patient reinfection by bacterial pathogens (126-128). However, there are a few controversies in the field that complicate our understanding of the influence toxin-antitoxin systems truly exert once activated. One issue is that the strains used in some studies linking toxin-antitoxin systems to bacterial persistence contained prophages and gave erroneous results (116, 117). Because this experimental error was not caught for some time, bacterial persistence became the defining role for toxin-antitoxin systems, and activation of these systems during other stress responses did not receive as much attention. Another concern is that previous experiments rely on overexpression of toxin which likely do not accurately reflect the amount of toxin present *in vivo*. As these complexes are normally tightly repressed and sensitive to slight expression changes, overwhelming a cell with toxin overexpression from an inducible construct may amplify the effect of the toxin *in vivo*. It's possible that this toxin overexpression occurs to a level the toxin-antitoxin system could never actually achieve. In Chapter 5, I discuss how my results have advanced the field, the state of the field, and how our understanding of toxin-antitoxin systems in bacteria may evolve in the future.

1.8 Figures & Tables
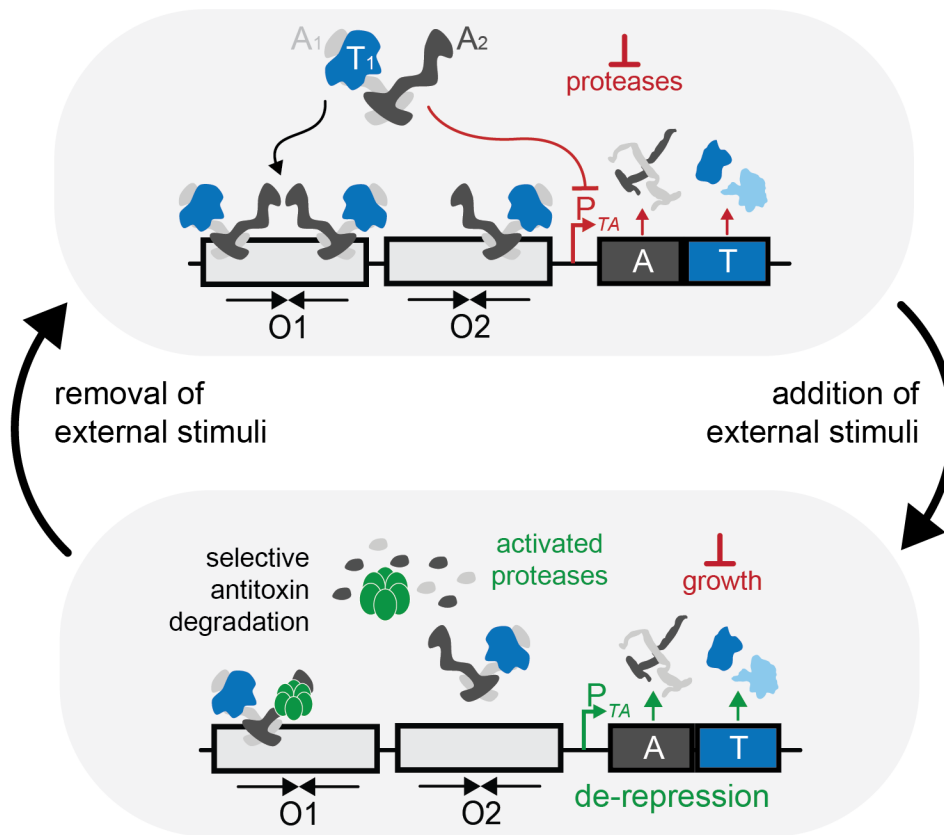
Figure 1.1 – Type II toxin-antitoxin system expression.

Normally, expression of toxin (T) and antitoxin (A) result in the formation of a tight complex that binds upstream of the promoter (P_{TA}) at operator regions (O1, O2). Upon sensing external stimuli, proteases selectively degrade antitoxins, and the operon is de-repressed.
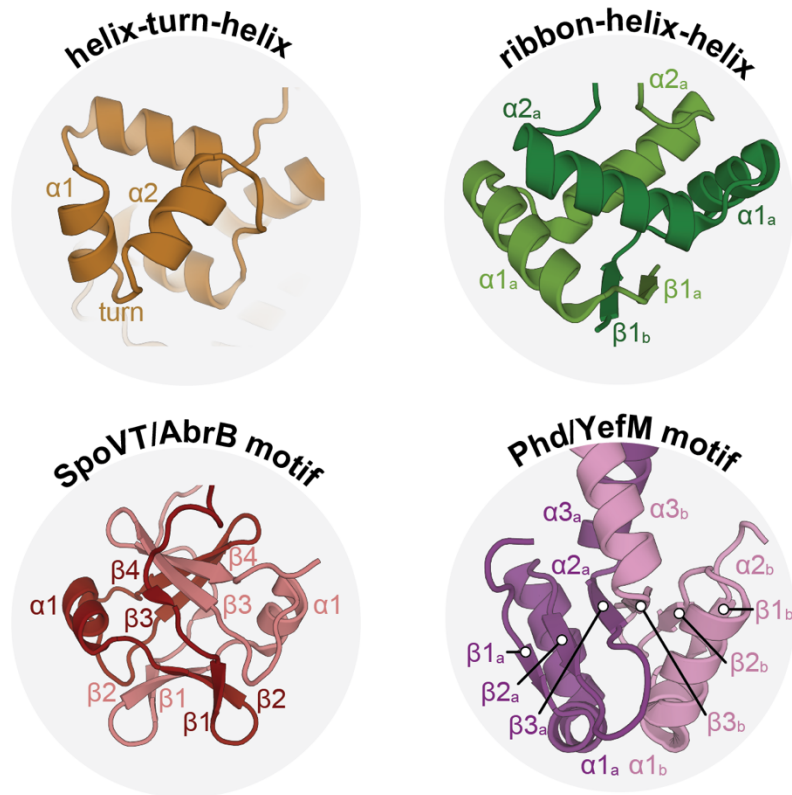
Figure 1.2 – The four types of DNA-binding domains in type II antitoxins.

DNA binding domains containing motifs of (**A**) helix-turn-helix (from *P. vulgaris* HigA, PDB code 6WFP), (**B**) ribbon-helix-helix (from *E. coli* RelB, PDB code 4FXE), (**C**) SpoVT/AbrB (from *E. coli* MazE, PDB code 2MRN, DNA binding domain termed "β-sandwich"), and (**D**) Phd/YefM (from *E. coli* YefM, PDB code 2A6Q) are shown.
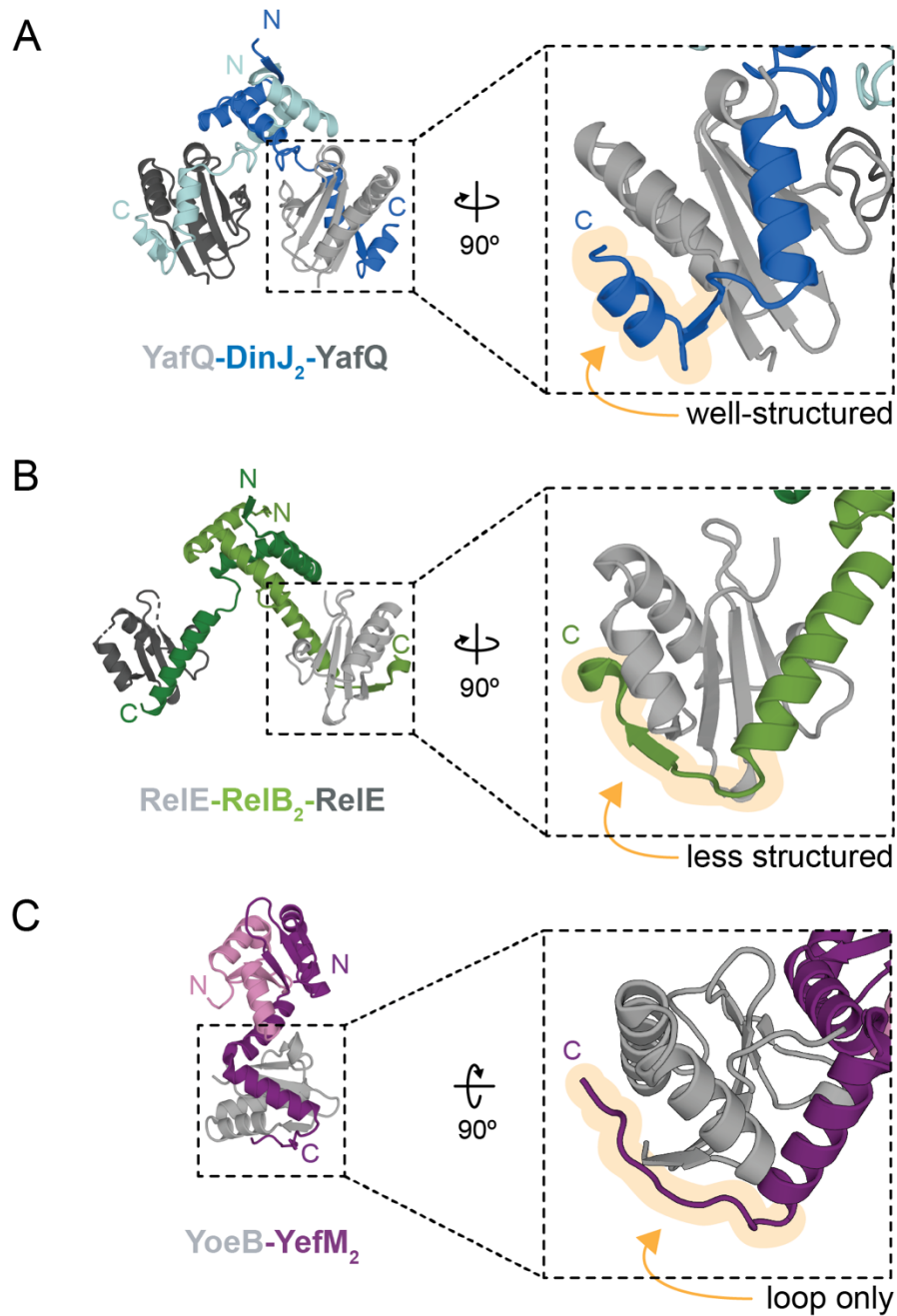
Figure 1.3 – Diversity in toxin-binding domains in type II antitoxins.

Oligomeric states and C-terminal structure of (**A**) DinJ, (**B**) RelB, and (**C**) YefM (PDB codes 4Q2U, 4FXE, and 2A6Q) shown bound to their cognate toxins (gray).
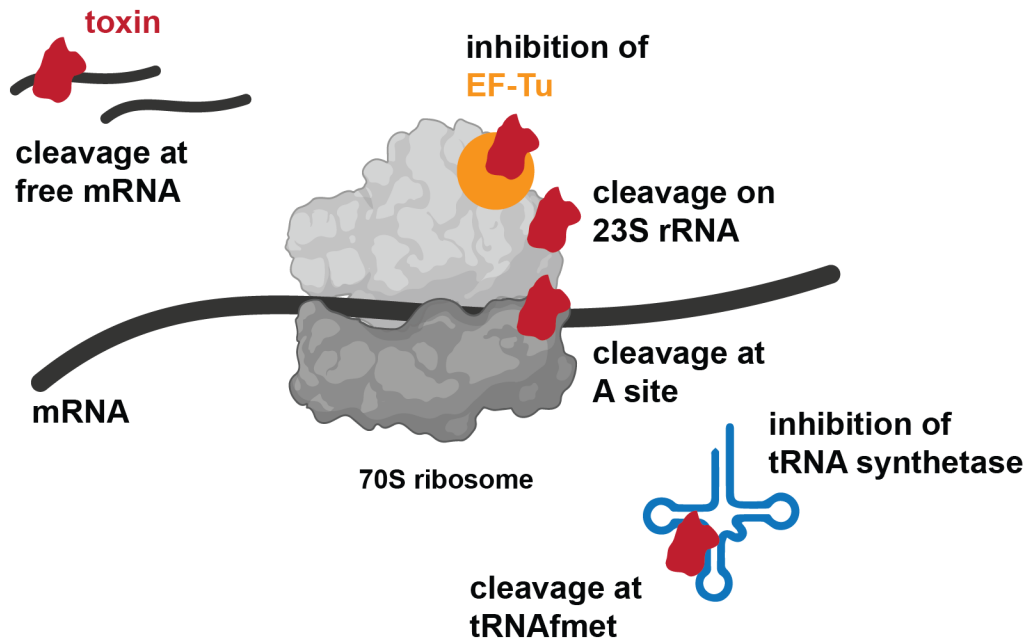
Figure 1.4 – Diversity in toxin activity in translation in type II families.

Type II toxins can exert translational regulation in a number of ways, including cleaving both free and translating mRNA, cleaving tRNA or rRNA directly, or inhibiting tRNA synthetases or EF-Tu by phosphorylation.

Table 1.1 – Six types of toxin-antitoxin systems.

Type	Antitoxin	Toxin	Mode of Toxin Neutralization
I	Antisense RNA	mRNA	Antisense mRNA of the antitoxin binds to the mRNA of the toxin, inhibiting translation of toxin
II	Protein	Protein	Antitoxin directly binds toxin
III	mRNA	Protein	Antitoxin mRNA binds toxin directly to inactivate toxin
IV	Protein	Protein	Antitoxin directly binds substrate of the toxin, preventing activity
V	Protein	mRNA	Antitoxin targets and degrades toxin mRNA, preventing toxin formation
VI	Protein	Protein	Antitoxin functions as a proteolytic adaptor, binding to the toxin and promoting its degradation

1.9 References

1. Tan Q, Awano N, Inouye M. YeeV is an *Escherichia coli* toxin that inhibits cell division by targeting the cytoskeleton proteins, FtsZ and MreB. Mol Microbiol. 2011;79(1):109-18. Epub 2010/12/21. doi: 10.1111/j.1365-2958.2010.07433.x. PubMed PMID: 21166897; PMCID: PMC3021753.

2. Ogura T, Hiraga S. Mini-F plasmid genes that couple host cell division to plasmid proliferation. Proc Natl Acad Sci U S A. 1983;80(15):4784-8. Epub 1983/08/01. doi: 10.1073/pnas.80.15.4784. PubMed PMID: 6308648; PMCID: PMC384129.

3. Bernard P, Couturier M. Cell killing by the F plasmid CcdB protein involves poisoning of DNA-topoisomerase II complexes. J Mol Biol. 1992;226(3):735-45. Epub 1992/08/05. doi: 10.1016/0022-2836(92)90629-x. PubMed PMID: 1324324.

4. Lewis LK, Harlow GR, Gregg-Jolly LA, Mount DW. Identification of high affinity binding sites for LexA which define new DNA damage-inducible genes in *Escherichia coli*. J Mol Biol. 1994;241(4):507-23. Epub 1994/08/26. doi: 10.1006/jmbi.1994.1528. PubMed PMID: 8057377.

5. Lehnherr H, Maguin E, Jafri S, Yarmolinsky MB. Plasmid addiction genes of bacteriophage P1: doc, which causes cell death on curing of prophage, and phd, which prevents host death when prophage is retained. J Mol Biol. 1993;233(3):414-28. Epub 1993/10/05. doi: 10.1006/jmbi.1993.1521. PubMed PMID: 8411153.

6. Kawamukai M, Matsuda H, Fujii W, Nishida T, Izumoto Y, Himeno M, Utsumi R, Komano T. Cloning of the fic-1 gene involved in cell filamentation induced by cyclic AMP and construction of a delta fic *Escherichia coli* strain. J Bacteriol. 1988;170(9):3864-9. Epub 1988/09/01. doi: 10.1128/jb.170.9.3864-3869.1988. PubMed PMID: 2842288; PMCID: PMC211382.

7. Hopper S, Wilbur JS, Vasquez BL, Larson J, Clary S, Mehr IJ, Seifert HS, So M. Isolation of *Neisseria gonorrhoeae* mutants that show enhanced trafficking across polarized T84

epithelial monolayers. Infect Immun. 2000;68(2):896-905. Epub 2000/01/20. doi: 10.1128/IAI.68.2.896-905.2000. PubMed PMID: 10639460; PMCID: PMC97219.

8. Wang X, Lord DM, Cheng HY, Osbourne DO, Hong SH, Sanchez-Torres V, Quiroga C, Zheng K, Herrmann T, Peti W, Benedik MJ, Page R, Wood TK. A new type V toxin-antitoxin system where mRNA for toxin GhoT is cleaved by antitoxin GhoS. Nat Chem Biol. 2012;8(10):855-61. Epub 2012/09/04. doi: 10.1038/nchembio.1062. PubMed PMID: 22941047; PMCID: PMC3514572.

9. Tamman H, Ainelo A, Ainsaar K, Horak R. A moderate toxin, GraT, modulates growth rate and stress tolerance of *Pseudomonas putida*. J Bacteriol. 2014;196(1):157-69. Epub 2013/10/29. doi: 10.1128/JB.00851-13. PubMed PMID: 24163334; PMCID: PMC3911119.

10. Jorgensen MG, Pandey DP, Jaskolska M, Gerdes K. HicA of *Escherichia coli* defines a novel family of translation-independent mRNA interferases in bacteria and archaea. J Bacteriol. 2009;191(4):1191-9. Epub 2008/12/09. doi: 10.1128/JB.01013-08. PubMed PMID: 19060138; PMCID: PMC2631989.

11. Tian QB, Hayashi T, Murata T, Terawaki Y. Gene product identification and promoter analysis of *hig* locus of plasmid Rts1. Biochem Biophys Res Commun. 1996;225(2):679-84. Epub 1996/08/14. doi: 10.1006/bbrc.1996.1229. PubMed PMID: 8753818.

12. Moyed HS, Bertrand KP. *hipA*, a newly recognized gene of *Escherichia coli* K-12 that affects frequency of persistence after inhibition of murein synthesis. J Bacteriol. 1983;155(2):768-75. Epub 1983/08/01. PubMed PMID: 6348026; PMCID: PMC217749.

13. Bravo A, Ortega S, de Torrontegui G, Diaz R. Killing of *Escherichia coli* cells modulated by components of the stability system ParD of plasmid R1. Mol Gen Genet. 1988;215(1):146-51. Epub 1988/12/01. doi: 10.1007/BF00331316. PubMed PMID: 3071737.

14.   Metzger S, Dror IB, Aizenman E, Schreiber G, Toone M, Friesen JD, Cashel M, Glaser G. The nucleotide sequence and characterization of the *relA* gene of *Escherichia coli*. J Biol Chem. 1988;263(30):15699-704. Epub 1988/10/25. PubMed PMID: 2844820.

15.   Gonzalez Barrios AF, Zuo R, Hashimoto Y, Yang L, Bentley WE, Wood TK. Autoinducer 2 controls biofilm formation in *Escherichia coli* through a novel motility quorum-sensing regulator (MqsR, B3022). J Bacteriol. 2006;188(1):305-16. Epub 2005/12/15. doi: 10.1128/JB.188.1.305-316.2006. PubMed PMID: 16352847; PMCID: PMC1317603.

16.   Gerdes K, Molin S. Partitioning of plasmid R1. Structural and functional analysis of the *parA* locus. J Mol Biol. 1986;190(3):269-79. Epub 1986/08/05. doi: 10.1016/0022-2836(86)90001-x. PubMed PMID: 3023637.

17.   Roberts RC, Helinski DR. Definition of a minimal plasmid stabilization system from the broad-host-range plasmid RK2. J Bacteriol. 1992;174(24):8119-32. Epub 1992/12/01. PubMed PMID: 1459960; PMCID: PMC207551.

18.   Bravo A, de Torrontegui G, Diaz R. Identification of components of a new stability system of plasmid R1, ParD, that is close to the origin of replication of this plasmid. Mol Gen Genet. 1987;210(1):101-10. Epub 1987/11/01. doi: 10.1007/BF00337764. PubMed PMID: 3323833.

19.   Tsuchimoto S, Ohtsubo H, Ohtsubo E. Two genes, *pemK* and *pemI*, responsible for stable maintenance of resistance plasmid R100. J Bacteriol. 1988;170(4):1461-6. Epub 1988/04/01. doi: 10.1128/jb.170.4.1461-1466.1988. PubMed PMID: 2832364; PMCID: PMC210989.

20.   Stent GS, Brenner S. A genetic locus for the regulation of ribonucleic acid synthesis. Proc Natl Acad Sci U S A. 1961;47:2005-14. Epub 1961/12/15. doi: 10.1073/pnas.47.12.2005. PubMed PMID: 13916843; PMCID: PMC223254.

21. Randall LL, Hardy SJ. SecB, one small chaperone in the complex milieu of the cell. Cell Mol Life Sci. 2002;59(10):1617-23. Epub 2002/12/12. doi: 10.1007/pl00012488. PubMed PMID: 12475171.

22. Aakre CD, Phung TN, Huang D, Laub MT. A bacterial toxin inhibits DNA replication elongation through a direct interaction with the beta sliding clamp. Mol Cell. 2013;52(5):617-28. Epub 2013/11/19. doi: 10.1016/j.molcel.2013.10.014. PubMed PMID: 24239291; PMCID: PMC3918436.

23. Bagyan I, Hobot J, Cutting S. A compartmentalized regulator of developmental gene expression in *Bacillus subtilis*. J Bacteriol. 1996;178(15):4500-7. Epub 1996/08/01. doi: 10.1128/jb.178.15.4500-4507.1996. PubMed PMID: 8755877; PMCID: PMC178216.

24. Strauch MA, Perego M, Burbulys D, Hoch JA. The transition state transcription regulator AbrB of *Bacillus subtilis* is autoregulated during vegetative growth. Mol Microbiol. 1989;3(9):1203-9. Epub 1989/09/01. doi: 10.1111/j.1365-2958.1989.tb00270.x. PubMed PMID: 2507867.

25. Kawano M, Aravind L, Storz G. An antisense RNA controls synthesis of an SOS-induced toxin evolved from an antitoxin. Mol Microbiol. 2007;64(3):738-54. Epub 2007/04/28. doi: 10.1111/j.1365-2958.2007.05688.x. PubMed PMID: 17462020; PMCID: PMC1891008.

26. Katz ME, Strugnell RA, Rood JI. Molecular characterization of a genomic region associated with virulence in *Dichelobacter nodosus*. Infect Immun. 1992;60(11):4586-92. Epub 1992/11/01. doi: 10.1128/iai.60.11.4586-4592.1992. PubMed PMID: 1398971; PMCID: PMC258206.

27. Cascales E, Buchanan SK, Duche D, Kleanthous C, Lloubes R, Postle K, Riley M, Slatin S, Cavard D. Colicin biology. Microbiol Mol Biol Rev. 2007;71(1):158-229. Epub 2007/03/10. doi: 10.1128/MMBR.00036-06. PubMed PMID: 17347522; PMCID: PMC1847374.

28. Van Melderen L, Saavedra De Bast M. Bacterial toxin-antitoxin systems: more than selfish entities? PLoS genetics. 2009;5(3):e1000437. doi: 10.1371/journal.pgen.1000437. PubMed PMID: 19325885; PMCID: PMC2654758.

29. Jensen RB, Gerdes K. Programmed cell death in bacteria: proteic plasmid stabilization systems. Mol Microbiol. 1995;17(2):205-10. Epub 1995/07/01. doi: 10.1111/j.1365-2958.1995.mmi_17020205.x. PubMed PMID: 7494469.

30. Pullinger GD, Lax AJ. A *Salmonella dublin* virulence plasmid locus that affects bacterial growth under nutrient-limited conditions. Mol Microbiol. 1992;6(12):1631-43. Epub 1992/06/01. doi: 10.1111/j.1365-2958.1992.tb00888.x. PubMed PMID: 1495391.

31. Tian QB, Ohnishi M, Tabuchi A, Terawaki Y. A new plasmid-encoded proteic killer gene system: cloning, sequencing, and analyzing *hig* locus of plasmid Rts1. Biochem Biophys Res Commun. 1996;220(2):280-4. Epub 1996/03/18. doi: 10.1006/bbrc.1996.0396. PubMed PMID: 8645296.

32. Gronlund H, Gerdes K. Toxin-antitoxin systems homologous with *relBE* of *Escherichia coli* plasmid P307 are ubiquitous in prokaryotes. J Mol Biol. 1999;285(4):1401-15. Epub 1999/01/26. doi: 10.1006/jmbi.1998.2416. PubMed PMID: 9917385.

33. Pandey DP, Gerdes K. Toxin-antitoxin loci are highly abundant in free-living but lost from host-associated prokaryotes. Nucleic Acids Res. 2005;33(3):966-76. Epub 2005/02/19. doi: 10.1093/nar/gki201. PubMed PMID: 15718296; PMCID: PMC549392.

34. Harms A, Brodersen DE, Mitarai N, Gerdes K. Toxins, Targets, and Triggers: An Overview of Toxin-Antitoxin Biology. Mol Cell. 2018;70(5):768-84. Epub 2018/02/06. doi: 10.1016/j.molcel.2018.01.003. PubMed PMID: 29398446.

35. Brantl S, Jahn N. sRNAs in bacterial type I and type III toxin-antitoxin systems. FEMS Microbiol Rev. 2015;39(3):413-27. Epub 2015/03/27. doi: 10.1093/femsre/fuv003. PubMed PMID: 25808661.

36. Masuda H, Tan Q, Awano N, Wu KP, Inouye M. YeeU enhances the bundling of cytoskeletal polymers of MreB and FtsZ, antagonizing the CbtA (YeeV) toxicity in *Escherichia coli*. Mol Microbiol. 2012;84(5):979-89. Epub 2012/04/21. doi: 10.1111/j.1365-2958.2012.08068.x. PubMed PMID: 22515815.

37. Fraikin N, Goormaghtigh F, Van Melderen L. Type II Toxin-Antitoxin Systems: Evolution and Revolutions. J Bacteriol. 2020;202(7). Epub 2020/01/15. doi: 10.1128/JB.00763-19. PubMed PMID: 31932311; PMCID: PMC7167474.

38. Leplae R, Geeraerts D, Hallez R, Guglielmini J, Dreze P, Van Melderen L. Diversity of bacterial type II toxin-antitoxin systems: a comprehensive search and functional analysis of novel families. Nucleic Acids Res. 2011;39(13):5513-25. Epub 2011/03/23. doi: 10.1093/nar/gkr131. PubMed PMID: 21422074; PMCID: PMC3141249.

39. Goeders N, Van Melderen L. Toxin-antitoxin systems as multilevel interaction systems. Toxins (Basel). 2014;6(1):304-24. Epub 2014/01/18. doi: 10.3390/toxins6010304. PubMed PMID: 24434905; PMCID: PMC3920263.

40. Afif H, Allali N, Couturier M, Van Melderen L. The ratio between CcdA and CcdB modulates the transcriptional repression of the *ccd* poison-antidote system. Mol Microbiol. 2001;41(1):73-82. Epub 2001/07/17. doi: 10.1046/j.1365-2958.2001.02492.x. PubMed PMID: 11454201.

41. Overgaard M, Borch J, Jorgensen MG, Gerdes K. Messenger RNA interferase RelE controls *relBE* transcription by conditional cooperativity. Mol Microbiol. 2008;69(4):841-57. Epub 2008/06/06. doi: 10.1111/j.1365-2958.2008.06313.x. PubMed PMID: 18532983.

42. Magnuson R, Yarmolinsky MB. Corepression of the P1 addiction operon by Phd and Doc. J Bacteriol. 1998;180(23):6342-51. Epub 1998/11/26. doi: 10.1128/JB.180.23.6342-6351.1998. PubMed PMID: 9829946; PMCID: PMC107722.

43.   Johnson EP, Strom AR, Helinski DR. Plasmid RK2 toxin protein ParE: purification and interaction with the ParD antitoxin protein. J Bacteriol. 1996;178(5):1420-9. Epub 1996/03/01. PubMed PMID: 8631720; PMCID: PMC177817.

44.   Monti MC, Hernandez-Arriaga AM, Kamphuis MB, Lopez-Villarejo J, Heck AJ, Boelens R, Diaz-Orejas R, van den Heuvel RH. Interactions of Kid-Kis toxin-antitoxin complexes with the *parD* operator-promoter region of plasmid R1 are piloted by the Kis antitoxin and tuned by the stoichiometry of Kid-Kis oligomers. Nucleic Acids Res. 2007;35(5):1737-49. Epub 2007/02/24. doi: 10.1093/nar/gkm073. PubMed PMID: 17317682; PMCID: PMC1865072.

45.   Winther KS, Gerdes K. Regulation of enteric *vapBC* transcription: induction by VapC toxin dimer-breaking. Nucleic Acids Res. 2012;40(10):4347-57. Epub 2012/01/31. doi: 10.1093/nar/gks029. PubMed PMID: 22287572; PMCID: PMC3378870.

46.   Ruangprasert A, Maehigashi T, Miles SJ, Giridharan N, Liu JX, Dunham CM. Mechanisms of toxin inhibition and transcriptional repression by *Escherichia coli* DinJ-YafQ. The Journal of biological chemistry. 2014;289(30):20559-69. doi: 10.1074/jbc.M114.573006. PubMed PMID: 24898247; PMCID: PMC4110269.

47.   Hallez R, Geeraerts D, Sterckx Y, Mine N, Loris R, Van Melderen L. New toxins homologous to ParE belonging to three-component toxin-antitoxin systems in *Escherichia coli* O157:H7. Mol Microbiol. 2010;76(3):719-32. Epub 2010/03/30. doi: 10.1111/j.1365-2958.2010.07129.x. PubMed PMID: 20345661.

48.   Volante A, Soberon NE, Ayora S, Alonso JC. The Interplay between Different Stability Systems Contributes to Faithful Segregation: *Streptococcus pyogenes* pSM19035 as a Model. Microbiol Spectr. 2014;2(4):PLAS-0007-2013. Epub 2015/06/25. doi: 10.1128/microbiolspec.PLAS-0007-2013. PubMed PMID: 26104212.

49.   Bordes P, Sala AJ, Ayala S, Texier P, Slama N, Cirinesi AM, Guillet V, Mourey L, Genevaux P. Chaperone addiction of toxin-antitoxin systems. Nat Commun.

2016;7:13339. Epub 2016/11/09. doi: 10.1038/ncomms13339. PubMed PMID: 27827369; PMCID: PMC5105189.

50.   Wang X, Lord DM, Hong SH, Peti W, Benedik MJ, Page R, Wood TK. Type II toxin/antitoxin MqsR/MqsA controls type V toxin/antitoxin GhoT/GhoS. Environ Microbiol. 2013;15(6):1734-44. Epub 2013/01/08. doi: 10.1111/1462-2920.12063. PubMed PMID: 23289863; PMCID: PMC3620836.

51.   Overgaard M, Borch J, Jørgensen MG, Gerdes K. Messenger RNA interferase RelE controls *relBE* transcription by conditional cooperativity. Molecular Microbiology. 2008;69(4):841-57. doi: 10.1111/j.1365-2958.2008.06313.x. PubMed PMID: 18532983.

52.   Garcia-Pino A, Balasubramanian S, Wyns L, Gazit E, De Greve H, Magnuson RD, Charlier D, van Nuland NA, Loris R. Allostery and intrinsic disorder mediate transcription regulation by conditional cooperativity. Cell. 2010;142(1):101-11. Epub 2010/07/07. doi: 10.1016/j.cell.2010.05.039. PubMed PMID: 20603017.

53.   Overgaard M, Borch J, Gerdes K. RelB and RelE of *Escherichia coli* form a tight complex that represses transcription via the ribbon-helix-helix motif in RelB. Journal of molecular biology. 2009;394(2):183-96. doi: 10.1016/j.jmb.2009.09.006. PubMed PMID: 19747491; PMCID: PMC2812701.

54.   Bøggild A, Sofos N, Andersen KR, Feddersen A, Easter AD, Passmore LA, Brodersen DE. The crystal structure of the intact *E. coli* RelBE toxin-antitoxin complex provides the structural basis for conditional cooperativity. Structure (London, England : 1993). 2012;20(10):1641-8. doi: 10.1016/j.str.2012.08.017. PubMed PMID: 22981948; PMCID: PMC3507626.

55.   Brown BL, Lord DM, Grigoriu S, Peti W, Page R. The *Escherichia coli* toxin MqsR destabilizes the transcriptional repression complex formed between the antitoxin MqsA and the mqsRA operon promoter. J Biol Chem. 2013;288(2):1286-94. Epub 2012/11/23. doi: 10.1074/jbc.M112.421008. PubMed PMID: 23172222; PMCID: PMC3543012.

56. Talavera A, Tamman H, Ainelo A, Konijnenberg A, Hadzi S, Sobott F, Garcia-Pino A, Horak R, Loris R. A dual role in regulation and toxicity for the disordered N-terminus of the toxin GraT. Nat Commun. 2019;10(1):972. Epub 2019/03/01. doi: 10.1038/s41467-019-08865-z. PubMed PMID: 30814507; PMCID: PMC6393540.

57. Chan WT, Espinosa M, Yeo CC. Keeping the Wolves at Bay: Antitoxins of Prokaryotic Type II Toxin-Antitoxin Systems. Front Mol Biosci. 2016;3:9. Epub 2016/04/06. doi: 10.3389/fmolb.2016.00009. PubMed PMID: 27047942; PMCID: PMC4803016.

58. Schumacher MA, Piro KM, Xu W, Hansen S, Lewis K, Brennan RG. Molecular mechanisms of HipA-mediated multidrug tolerance and its neutralization by HipB. Science. 2009;323(5912):396-401. Epub 2009/01/20. doi: 10.1126/science.1163806. PubMed PMID: 19150849; PMCID: PMC2764309.

59. Brown BL, Grigoriu S, Kim Y, Arruda JM, Davenport A, Wood TK, Peti W, Page R. Three dimensional structure of the MqsR:MqsA complex: a novel TA pair comprised of a toxin homologous to RelE and an antitoxin with unique properties. PLoS Pathog. 2009;5(12):e1000706. Epub 2009/12/31. doi: 10.1371/journal.ppat.1000706. PubMed PMID: 20041169; PMCID: PMC2791442.

60. Brown BL, Wood TK, Peti W, Page R. Structure of the *Escherichia coli* antitoxin MqsA (YgiT/b3021) bound to its gene promoter reveals extensive domain rearrangements and the specificity of transcriptional regulation. J Biol Chem. 2011;286(3):2285-96. Epub 2010/11/12. doi: 10.1074/jbc.M110.172643. PubMed PMID: 21068382; PMCID: PMC3023523.

61. Schureck MA, Maehigashi T, Miles SJ, Marquez J, Cho SE, Erdman R, Dunham CM. Structure of the *Proteus vulgaris* HigB-(HigA)2-HigB toxin-antitoxin complex. J Biol Chem. 2014;289(2):1060-70. Epub 2013/11/22. doi: 10.1074/jbc.M113.512095. PubMed PMID: 24257752; PMCID: PMC3887174.

62.   Oberer M, Zangger K, Gruber K, Keller W. The solution structure of ParD, the antidote of the ParDE toxin antitoxin module, provides the structural basis for DNA and toxin binding. Protein Sci. 2007;16(8):1676-88. Epub 2007/07/28. doi: 10.1110/ps.062680707. PubMed PMID: 17656583; PMCID: PMC2203376.

63.   Madl T, Van Melderen L, Mine N, Respondek M, Oberer M, Keller W, Khatai L, Zangger K. Structural basis for nucleic acid and toxin recognition of the bacterial antitoxin CcdA. J Mol Biol. 2006;364(2):170-85. Epub 2006/09/30. doi: 10.1016/j.jmb.2006.08.082. PubMed PMID: 17007877.

64.   De Jonge N, Garcia-Pino A, Buts L, Haesaerts S, Charlier D, Zangger K, Wyns L, De Greve H, Loris R. Rejuvenation of CcdB-poisoned gyrase by an intrinsically disordered protein domain. Mol Cell. 2009;35(2):154-63. Epub 2009/08/04. doi: 10.1016/j.molcel.2009.05.025. PubMed PMID: 19647513.

65.   Mattison K, Wilbur JS, So M, Brennan RG. Structure of FitAB from *Neisseria gonorrhoeae* bound to DNA reveals a tetramer of toxin-antitoxin heterodimers containing pin domains and ribbon-helix-helix motifs. J Biol Chem. 2006;281(49):37942-51. Epub 2006/09/20. doi: 10.1074/jbc.M605198200. PubMed PMID: 16982615.

66.   Miallau L, Faller M, Chiang J, Arbing M, Guo F, Cascio D, Eisenberg D. Structure and proposed activity of a member of the VapBC family of toxin-antitoxin systems. VapBC-5 from *Mycobacterium tuberculosis*. J Biol Chem. 2009;284(1):276-83. Epub 2008/10/28. doi: 10.1074/jbc.M805061200. PubMed PMID: 18952600; PMCID: PMC2610494.

67.   Min AB, Miallau L, Sawaya MR, Habel J, Cascio D, Eisenberg D. The crystal structure of the Rv0301-Rv0300 VapBC-3 toxin-antitoxin complex from *M. tuberculosis* reveals a Mg(2)(+) ion in the active site and a putative RNA-binding site. Protein Sci. 2012;21(11):1754-67. Epub 2012/09/27. doi: 10.1002/pro.2161. PubMed PMID: 23011806; PMCID: PMC3527712.

68.   Lee IG, Lee SJ, Chae S, Lee KY, Kim JH, Lee BJ. Structural and functional studies of the *Mycobacterium tuberculosis* VapBC30 toxin-antitoxin system: implications for the design of novel antimicrobial peptides. Nucleic Acids Res. 2015;43(15):7624-37. Epub 2015/07/08. doi: 10.1093/nar/gkv689. PubMed PMID: 26150422; PMCID: PMC4551927.

69.   Kamada K, Hanaoka F, Burley SK. Crystal structure of the MazE/MazF complex: molecular bases of antidote-toxin recognition. Mol Cell. 2003;11(4):875-84. Epub 2003/04/30. doi: 10.1016/s1097-2765(03)00097-2. PubMed PMID: 12718874.

70.   Loris R, Marianovsky I, Lah J, Laeremans T, Engelberg-Kulka H, Glaser G, Muyldermans S, Wyns L. Crystal structure of the intrinsically flexible addiction antidote MazE. J Biol Chem. 2003;278(30):28252-7. Epub 2003/05/14. doi: 10.1074/jbc.M302336200. PubMed PMID: 12743116.

71.   Zorzini V, Buts L, Schrank E, Sterckx YG, Respondek M, Engelberg-Kulka H, Loris R, Zangger K, van Nuland NA. *Escherichia coli* antitoxin MazE as transcription factor: insights into MazE-DNA binding. Nucleic Acids Res. 2015;43(2):1241-56. Epub 2015/01/08. doi: 10.1093/nar/gku1352. PubMed PMID: 25564525; PMCID: PMC4333400.

72.   Mate MJ, Vincentelli R, Foos N, Raoult D, Cambillau C, Ortiz-Lombardia M. Crystal structure of the DNA-bound VapBC2 antitoxin/toxin pair from *Rickettsia felis*. Nucleic Acids Res. 2012;40(7):3245-58. Epub 2011/12/06. doi: 10.1093/nar/gkr1167. PubMed PMID: 22140099; PMCID: PMC3326315.

73.   Dienemann C, Boggild A, Winther KS, Gerdes K, Brodersen DE. Crystal structure of the VapBC toxin-antitoxin complex from *Shigella flexneri* reveals a hetero-octameric DNA-binding assembly. J Mol Biol. 2011;414(5):713-22. Epub 2011/11/01. doi: 10.1016/j.jmb.2011.10.024. PubMed PMID: 22037005; PMCID: PMC3384007.

74.   Kamada K, Hanaoka F. Conformational change in the catalytic site of the ribonuclease YoeB toxin by YefM antitoxin. Mol Cell. 2005;19(4):497-509. Epub 2005/08/20. doi: 10.1016/j.molcel.2005.07.004. PubMed PMID: 16109374.

75. Blower TR, Salmond GP, Luisi BF. Balancing at survival's edge: the structure and adaptive benefits of prokaryotic toxin-antitoxin partners. Curr Opin Struct Biol. 2011;21(1):109-18. Epub 2011/02/15. doi: 10.1016/j.sbi.2010.10.009. PubMed PMID: 21315267.

76. Li GY, Zhang Y, Inouye M, Ikura M. Inhibitory mechanism of *Escherichia coli* RelE-RelB toxin-antitoxin module involves a helix displacement near an mRNA interferase active site. J Biol Chem. 2009;284(21):14628-36. Epub 2009/03/20. doi: 10.1074/jbc.M809656200. PubMed PMID: 19297318; PMCID: PMC2682910.

77. Garcia-Pino A, Christensen-Dalsgaard M, Wyns L, Yarmolinsky M, Magnuson RD, Gerdes K, Loris R. Doc of prophage P1 is inhibited by its antitoxin partner Phd through fold complementation. J Biol Chem. 2008;283(45):30821-7. Epub 2008/09/02. doi: 10.1074/jbc.M805654200. PubMed PMID: 18757857; PMCID: PMC2576525.

78. Neubauer C, Gao YG, Andersen KR, Dunham CM, Kelley AC, Hentschel J, Gerdes K, Ramakrishnan V, Brodersen DE. The structural basis for mRNA recognition and cleavage by the ribosome-dependent endonuclease RelE. Cell. 2009;139(6):1084-95. Epub 2009/12/17. doi: 10.1016/j.cell.2009.11.015. PubMed PMID: 20005802; PMCID: PMC2807027.

79. Zhang Y, Zhang J, Hoeflich KP, Ikura M, Qing G, Inouye M. MazF cleaves cellular mRNAs specifically at ACA to block protein synthesis in *Escherichia coli*. Mol Cell. 2003;12(4):913-23. Epub 2003/10/29. doi: 10.1016/s1097-2765(03)00402-7. PubMed PMID: 14580342.

80. Christensen-Dalsgaard M, Jørgensen MG, Gerdes K. Three new RelE-homologous mRNA interferases of *Escherichia coli* differentially induced by environmental stresses. Molecular Microbiology. 2010;75(2):333-48. doi: 10.1111/j.1365-2958.2009.06969.x.

81. Winther KS, Gerdes K. Ectopic production of VapCs from Enterobacteria inhibits translation and trans-activates YoeB mRNA interferase. Mol Microbiol. 2009;72(4):918-30. Epub 2009/04/30. doi: 10.1111/j.1365-2958.2009.06694.x. PubMed PMID: 19400780.

82.   Winther KS, Brodersen DE, Brown AK, Gerdes K. VapC20 of *Mycobacterium tuberculosis* cleaves the sarcin-ricin loop of 23S rRNA. Nat Commun. 2013;4:2796. Epub 2013/11/15. doi: 10.1038/ncomms3796. PubMed PMID: 24225902.

83.   Winther KS, Gerdes K. Enteric virulence associated protein VapC inhibits translation by cleavage of initiator tRNA. Proc Natl Acad Sci U S A. 2011;108(18):7403-7. Epub 2011/04/20. doi: 10.1073/pnas.1019587108. PubMed PMID: 21502523; PMCID: PMC3088637.

84.   Zhou J, Lancaster L, Donohue JP, Noller HF. Crystal structures of EF-G-ribosome complexes trapped in intermediate states of translocation. Science. 2013;340(6140):1236086. Epub 2013/07/03. doi: 10.1126/science.1236086. PubMed PMID: 23812722; PMCID: PMC3979973.

85.   Schuette JC, Murphy FVt, Kelley AC, Weir JR, Giesebrecht J, Connell SR, Loerke J, Mielke T, Zhang W, Penczek PA, Ramakrishnan V, Spahn CM. GTPase activation of elongation factor EF-Tu by the ribosome during decoding. EMBO J. 2009;28(6):755-65. Epub 2009/02/21. doi: 10.1038/emboj.2009.26. PubMed PMID: 19229291; PMCID: PMC2666022.

86.   Castro-Roa D, Garcia-Pino A, De Gieter S, van Nuland NAJ, Loris R, Zenkin N. The Fic protein Doc uses an inverted substrate to phosphorylate and inactivate EF-Tu. Nat Chem Biol. 2013;9(12):811-7. Epub 2013/10/22. doi: 10.1038/nchembio.1364. PubMed PMID: 24141193; PMCID: PMC3836179.

87.   Germain E, Castro-Roa D, Zenkin N, Gerdes K. Molecular mechanism of bacterial persistence by HipA. Mol Cell. 2013;52(2):248-54. Epub 2013/10/08. doi: 10.1016/j.molcel.2013.08.045. PubMed PMID: 24095282.

88.   Jiang Y, Pogliano J, Helinski DR, Konieczny I. ParE toxin encoded by the broad-host-range plasmid RK2 is an inhibitor of *Escherichia coli* gyrase. Molecular Microbiology.

2002;44(4):971-9. doi: DOI 10.1046/j.1365-2958.2002.02921.x. PubMed PMID: WOS:000175531300007.

89. Hoffer ED, Miles SJ, Dunham CM. The structure and function of *Mycobacterium tuberculosis* MazF-mt6 toxin provide insights into conserved features of MazF endonucleases. J Biol Chem. 2017;292(19):7718-26. Epub 2017/03/17. doi: 10.1074/jbc.M117.779306. PubMed PMID: 28298445; PMCID: PMC5427253.

90. Gerdes K, Rasmussen PB, Molin S. Unique type of plasmid maintenance function: postsegregational killing of plasmid-free cells. Proc Natl Acad Sci U S A. 1986;83(10):3116-20. Epub 1986/05/01. PubMed PMID: 3517851; PMCID: PMC323463.

91. Tsuchimoto S, Nishimura Y, Ohtsubo E. The stable maintenance system *pem* of plasmid R100: degradation of PemI protein may allow PemK protein to inhibit cell growth. J Bacteriol. 1992;174(13):4205-11. PubMed PMID: 1624414; PMCID: PMC206196.

92. Fineran PC, Blower TR, Foulds IJ, Humphreys DP, Lilley KS, Salmond GP. The phage abortive infection system, ToxIN, functions as a protein-RNA toxin-antitoxin pair. Proc Natl Acad Sci U S A. 2009;106(3):894-9. Epub 2009/01/07. doi: 10.1073/pnas.0808832106. PubMed PMID: 19124776; PMCID: PMC2630095.

93. Dy RL, Przybilski R, Semeijn K, Salmond GP, Fineran PC. A widespread bacteriophage abortive infection system functions through a Type IV toxin-antitoxin mechanism. Nucleic Acids Res. 2014;42(7):4590-605. Epub 2014/01/28. doi: 10.1093/nar/gkt1419. PubMed PMID: 24465005; PMCID: PMC3985639.

94. Saavedra De Bast M, Mine N, Van Melderen L. Chromosomal toxin-antitoxin systems may act as antiaddiction modules. J Bacteriol. 2008;190(13):4603-9. Epub 2008/04/29. doi: 10.1128/JB.00357-08. PubMed PMID: 18441063; PMCID: PMC2446810.

95. Cooper TF, Heinemann JA. Postsegregational killing does not increase plasmid stability but acts to mediate the exclusion of competing plasmids. Proc Natl Acad Sci U S A.

2000;97(23):12643-8. Epub 2000/11/01. doi: 10.1073/pnas.220077897. PubMed PMID: 11058151; PMCID: PMC18817.

96. Christensen SK, Mikkelsen M, Pedersen K, Gerdes K. RelE, a global inhibitor of translation, is activated during nutritional stress. Proceedings of the National Academy of Sciences of the United States of America. 2001;98(25):14328-33. doi: 10.1073/pnas.251327898. PubMed PMID: 11717402; PMCID: PMC64681.

97. Christensen SK, Gerdes K. RelE toxins from bacteria and Archaea cleave mRNAs on translating ribosomes, which are rescued by tmRNA. Mol Microbiol. 2003;48(5):1389-400. Epub 2003/06/06. PubMed PMID: 12787364.

98. Pizer LI, Merlie JP. Effect of serine hydroxamate on phospholipid synthesis in *Escherichia coli*. J Bacteriol. 1973;114(3):980-7. Epub 1973/06/01. doi: 10.1128/jb.114.3.980-987.1973. PubMed PMID: 4576413; PMCID: PMC285354.

99. Magnusson LU, Farewell A, Nyström T. ppGpp: a global regulator in *Escherichia coli*. Trends in microbiology. 2005;13(5):236-42. doi: 10.1016/j.tim.2005.03.008. PubMed PMID: 15866041.

100. Potrykus K, Cashel M. (p)ppGpp: still magical? Annual Review of Microbiology. 2008;62(1):35-51. doi: 10.1146/annurev.micro.62.081307.162903. PubMed PMID: 18454629.

101. Janssen BD, Garza-Sanchez F, Hayes CS. YoeB toxin is activated during thermal stress. Microbiologyopen. 2015;4(4):682-97. Epub 2015/07/07. doi: 10.1002/mbo3.272. PubMed PMID: 26147890; PMCID: PMC4554461.

102. Sunohara T, Jojima K, Yamamoto Y, Inada T, Aiba H. Nascent-peptide-mediated ribosome stalling at a stop codon induces mRNA cleavage resulting in nonstop mRNA that is recognized by tmRNA. RNA. 2004;10(3):378-86. Epub 2004/02/19. doi: 10.1261/rna.5169404. PubMed PMID: 14970383; PMCID: PMC1370933.

103.   Sunohara T, Jojima K, Tagami H, Inada T, Aiba H. Ribosome stalling during translation elongation induces cleavage of mRNA being translated in *Escherichia coli*. J Biol Chem. 2004;279(15):15368-75. Epub 2004/01/28. doi: 10.1074/jbc.M312805200. PubMed PMID: 14744860.

104.   Hayes CS, Sauer RT. Cleavage of the A site mRNA codon during ribosome pausing provides a mechanism for translational quality control. Mol Cell. 2003;12(4):903-11. Epub 2003/10/29. doi: 10.1016/s1097-2765(03)00385-x. PubMed PMID: 14580341.

105.   Krafczyk R, Qi F, Sieber A, Mehler J, Jung K, Frishman D, Lassak J. Proline codon pair selection determines ribosome pausing strength and translation efficiency in bacteria. Commun Biol. 2021;4(1):589. Epub 2021/05/19. doi: 10.1038/s42003-021-02115-z. PubMed PMID: 34002016; PMCID: PMC8129111.

106.   Huter P, Arenz S, Bock LV, Graf M, Frister JO, Heuer A, Peil L, Starosta AL, Wohlgemuth I, Peske F, Novacek J, Berninghausen O, Grubmuller H, Tenson T, Beckmann R, Rodnina MV, Vaiana AC, Wilson DN. Structural Basis for Polyproline-Mediated Ribosome Stalling and Rescue by the Translation Elongation Factor EF-P. Mol Cell. 2017;68(3):515-27 e6. Epub 2017/11/04. doi: 10.1016/j.molcel.2017.10.014. PubMed PMID: 29100052.

107.   Muthuramalingam M, White JC, Bourne CR. Toxin-Antitoxin Modules Are Pliable Switches Activated by Multiple Protease Pathways. Toxins. 2016;8(7):214. doi: 10.3390/toxins8070214. PubMed PMID: 27409636; PMCID: PMC4963847.

108.   Hu Y, Benedik MJ, Wood TK. Antitoxin DinJ influences the general stress response through transcript stabilizer CspE. Environ Microbiol. 2012;14(3):669-79. Epub 2011/10/27. doi: 10.1111/j.1462-2920.2011.02618.x. PubMed PMID: 22026739.

109.   Radman M. SOS repair hypothesis: phenomenology of an inducible DNA repair which is accompanied by mutagenesis. Basic Life Sci. 1975;5A:355-67. Epub 1975/01/01. doi: 10.1007/978-1-4684-2895-7_48. PubMed PMID: 1103845.

110.   Little JW, Mount DW. The SOS regulatory system of *Escherichia coli*. Cell. 1982;29(1):11-22. Epub 1982/05/01. doi: 10.1016/0092-8674(82)90085-x. PubMed PMID: 7049397.

111.   Markham BE, Harper JE, Mount DW, Sancar GB, Sancar A, Rupp WD, Kenyon CJ, Walker GC. Analysis of mRNA synthesis following induction of the *Escherichia coli* SOS system. J Mol Biol. 1984;178(2):237-48. Epub 1984/09/15. doi: 10.1016/0022-2836(84)90142-6. PubMed PMID: 6208364.

112.   Sassanfar M, Roberts JW. Nature of the SOS-inducing signal in *Escherichia coli*. The involvement of DNA replication. J Mol Biol. 1990;212(1):79-96. Epub 1990/03/05. doi: 10.1016/0022-2836(90)90306-7. PubMed PMID: 2108251.

113.   Maslowska KH, Makiela-Dzbenska K, Fijalkowska IJ. The SOS system: A complex and tightly regulated response to DNA damage. Environ Mol Mutagen. 2019;60(4):368-84. Epub 2018/11/18. doi: 10.1002/em.22267. PubMed PMID: 30447030.

114.   Prysak MH, Mozdzierz CJ, Cook AM, Zhu L, Zhang Y, Inouye M, Woychik NA. Bacterial toxin YafQ is an endoribonuclease that associates with the ribosome and blocks translation elongation through sequence-specific and frame-dependent mRNA cleavage. Molecular Microbiology. 2009;71(5):1071-87. doi: 10.1111/j.1365-2958.2008.06572.x. PubMed PMID: 19210620.

115.   Maisonneuve E, Shakespeare LJ, Jorgensen MG, Gerdes K. Bacterial persistence by RNA endonucleases. Proc Natl Acad Sci U S A. 2011;108(32):13206-11. Epub 2011/07/27. doi: 10.1073/pnas.1100186108. PubMed PMID: 21788497; PMCID: PMC3156201.

116.   Harms A, Fino C, Sorensen MA, Semsey S, Gerdes K. Prophages and Growth Dynamics Confound Experimental Results with Antibiotic-Tolerant Persister Cells. Mbio. 2017;8(6). Epub 2017/12/14. doi: 10.1128/mBio.01964-17. PubMed PMID: 29233898; PMCID: PMC5727415.

117. Goormaghtigh F, Fraikin N, Putrins M, Hallaert T, Hauryliuk V, Garcia-Pino A, Sjodin A, Kasvandik S, Udekwu K, Tenson T, Kaldalu N, Van Melderen L. Reassessing the Role of Type II Toxin-Antitoxin Systems in Formation of *Escherichia coli* Type II Persister Cells. Mbio. 2018;9(3). Epub 2018/06/14. doi: 10.1128/mBio.00640-18. PubMed PMID: 29895634.

118. Terawaki Y, Takayasu H, Akiba T. Thermosensitive replication of a kanamycin resistance factor. J Bacteriol. 1967;94(3):687-90. Epub 1967/09/01. doi: 10.1128/jb.94.3.687-690.1967. PubMed PMID: 4166554; PMCID: PMC251939.

119. Terawaki Y, Rownd R. Replication of the R factor Rts1 in *Proteus mirabilis*. J Bacteriol. 1972;109(2):492-8. Epub 1972/02/01. PubMed PMID: 4550810; PMCID: PMC285167.

120. Gerdes K, Christensen SK, Løbner-Olesen A. Prokaryotic toxin-antitoxin stress response loci. Nature reviews Microbiology. 2005;3(5):371-82. doi: 10.1038/nrmicro1147. PubMed PMID: 15864262.

121. Dorr T, Vulic M, Lewis K. Ciprofloxacin causes persister formation by inducing the TisB toxin in *Escherichia coli*. PLoS Biol. 2010;8(2):e1000317. Epub 2010/02/27. doi: 10.1371/journal.pbio.1000317. PubMed PMID: 20186264; PMCID: PMC2826370.

122. Kaspy I, Rotem E, Weiss N, Ronin I, Balaban NQ, Glaser G. HipA-mediated antibiotic persistence via phosphorylation of the glutamyl-tRNA-synthetase. Nat Commun. 2013;4:3001. Epub 2013/12/18. doi: 10.1038/ncomms4001. PubMed PMID: 24343429.

123. Helaine S, Cheverton AM, Watson KG, Faure LM, Matthews SA, Holden DW. Internalization of Salmonella by macrophages induces formation of nonreplicating persisters. Science. 2014;343(6167):204-8. Epub 2014/01/11. doi: 10.1126/science.1244705. PubMed PMID: 24408438.

124. Tripathi A, Dewan PC, Siddique SA, Varadarajan R. MazF-induced Growth Inhibition and Persister Generation in *Escherichia coli*. The Journal of biological chemistry. 2014;289(7):4191-205. doi: 10.1074/jbc.M113.510511.

125.   Maisonneuve E, Gerdes K. Molecular Mechanisms Underlying Bacterial Persisters. Cell. 2014;157(3):539-48. doi: 10.1016/j.cell.2014.02.050. PubMed PMID: 24766804.

126.   Lewis K. Persister cells, dormancy and infectious disease. Nat Rev Microbiol. 2007;5(1):48-56. Epub 2006/12/05. doi: 10.1038/nrmicro1557. PubMed PMID: 17143318.

127.   Norton JP, Mulvey MA. Toxin-antitoxin systems are important for niche-specific colonization and stress resistance of uropathogenic *Escherichia coli*. PLoS Pathog. 2012;8(10):e1002954. Epub 2012/10/12. doi: 10.1371/journal.ppat.1002954. PubMed PMID: 23055930; PMCID: PMC3464220.

128.   Kedzierska B, Hayes F. Emerging Roles of Toxin-Antitoxin Modules in Bacterial Pathogenesis. Molecules. 2016;21(6). Epub 2016/06/21. doi: 10.3390/molecules21060790. PubMed PMID: 27322231.

Chapter 2

Monomeric YoeB toxin retains RNase activity but adopts an obligate dimeric form for thermal stability

Ian J. Pavelich, Tatsuya Maehigashi, Eric D. Hoffer, Ajchareeya Ruangprasert, Stacey J. Miles, and Christine M. Dunham

2.1 Abstract

Chromosomally-encoded toxin-antitoxin complexes are ubiquitous in bacteria and regulate growth through the release of the toxin component typically in a stress-dependent manner. Type II ribosome-dependent toxins adopt a RelE-family RNase fold and inhibit translation by degrading mRNAs while bound to the ribosome. Here, we present biochemical and structural studies of the *Escherichia coli* YoeB toxin interacting with both a UAA stop and an AAU sense codon in pre- and post-mRNA cleavage states to provide insights into possible mRNA substrate selection. Both mRNAs undergo minimal changes during the cleavage event in contrast to type II ribosome-dependent RelE toxin. Further, the 16S rRNA decoding site nucleotides that monitor the mRNA in the aminoacyl (A) site adopt different orientations depending upon which toxin is present. Although YoeB is a RelE family member, it is the sole ribosome-dependent toxin that is dimeric. We show that engineered monomeric YoeB is active against mRNAs bound to both the small and large subunit. However, the stability of monomeric YoeB is reduced ~20°C, consistent with potential YoeB activation during heat shock in *E. coli* as previously demonstrated. These data provide a molecular basis for the ability of YoeB to function in response to thermal stress.

2.2 Introduction

Regulation of gene expression through the activation of the SOS, stringent, and heat shock responses during changing environmental conditions is critical for bacterial survival (1–3). These responses generally result in an overall inhibition of cell growth. During the stringent response, inhibition of cell growth occurs by halting gene expression (4). Although originally identified for their role in plasmid maintenance (5–7), toxin-antitoxin complexes are chromosomally encoded and inhibit growth in response to stress including DNA damage, nutrient starvation, reactive chemical species, heat shock and can aid in the transition to an antibiotic-tolerant or persistent state (8–12). In the past decade, toxin-antitoxin loci have been found to be ubiquitous throughout bacteria and archaea (13). Understanding the regulation and function of toxin-antitoxin complexes in gene expression will unravel their roles in stress responses and thus, antibiotic tolerance.

Toxin–antitoxin pairs are organized into six classes defined by the molecular composition of the toxin and antitoxin components, and how they interact with each other. Type II complexes, in which both the toxin and the antitoxin are proteins, are the best-studied and most abundant systems (reviewed in (12)). During nutrient-rich growth, the expression of toxin–antitoxin pairs is regulated via a negative feedback loop where the DNA-binding antitoxin binds at operator regions that overlap with its promoter region. Toxin and antitoxin proteins form tightly associating complexes and, in some cases, different toxin and antitoxin stoichiometric levels can regulate optimal transcriptional repression (14–16). Stress causes antitoxin proteolysis by cellular proteases, releasing its cognate toxin to inhibit downstream cellular targets. Although two type II toxins

inactivate DNA gyrase (17,18), the majority inhibit protein synthesis and RNA metabolism by degrading messenger RNAs, transfer RNAs, ribosomal RNA, or by modification of tRNAs, aminoacyl synthetases or elongation factors (19–30). It is not clear why type II toxins predominately target protein synthesis. However, given the enormous cellular resources devoted to translational regulation in bacteria, one hypothesis is that inhibition of translation may represent a facile mechanism to respond quickly to environmental changes (4).

A subclass of type II toxins that disrupt translation are ribosome-dependent RNases (for review see (12,31)). Ribosome-dependent toxins are small proteins (~8–13 kDa) that adopt a conserved microbial RNase-fold containing a concave active site and are members of the RelE superfamily including *Escherichia* coli RelE, YafQ, YoeB, and *Proteus vulgaris* HigB (32–36). These RNases degrade mRNAs actively undergoing translation on the ribosome, specifically within the A site, the same site where tRNA binds to the ribosome to interact with mRNA codons for decoding. To date, most of these toxins only target the coding regions of mRNAs and can recognize both sense and stop codons but not AUG start codons (20, 37–39). HigB and YafQ toxins primarily target codons that are commonly found after the AUG start codon suggesting they may interfere with the initiation phase of translation (38, 40–42). Although ribosome-dependent toxins share a common RNase fold representing the larger RelE superfamily, their sequence identities are extremely low, which makes them difficult to identify. Specifically, active site residues are highly variable which may give rise to markedly different substrate preferences and thus, by extension, may allow the degradation of different mRNA codons. The structure

of RelE bound to the 70S along with *in vitro* functional assays suggest a substrate preference of the CAG glutamine codon and stop codons (preference of UAG > UAA > UGA) (20,33) (all codons shown in the 5′-3′ direction). Additional studies suggest a wider range of mRNAs targeted by RelE with a N–R–R codon preference, where N and R indicate any nucleotide and purines, respectively (43). In contrast, HigB prefers an adenosine at the third nucleotide position in the codon while YafQ seems to only recognize an AAA lysine codon (37,40,41). Similar to the broad codon specificity of RelE, YoeB cleaves UAA stop and AAA lysine codons (39,44), but can also recognize AAU asparagine, CUG leucine, GCG alanine, and GCU alanine codons (45). In the 70S-YoeB structure solved with a UAA stop codon in a pre-cleavage state, the preference for N-R-R codons was rationalized by how YoeB interacts with its mRNA substrate (46), although this contradicts the wide range of codons YoeB can cleave (39,45). During our structural comparison of the HigB toxin bound to the 70S ribosome with the 70S-RelE and 70S-YoeB structures, we identified that the mRNA was incorrectly modeled in the 70S-YoeB structure potentially obscuring key details about YoeB codon recognition (46). We remodeled the mRNA in unbiased electron density to better understand how YoeB recognizes the UAA codon (41). While the remodeling of mRNA provided some insights into the comparison of YoeB with other ribosome-dependent toxins, outstanding questions remain including how YoeB recognizes sense codons and whether YoeB influences the mRNA position after cleavage.

RelE superfamily members are typically monomeric proteins whether in the apo form, bound to its cognate antitoxin, or when bound to the ribosome (33,35,36,41). However,

YoeB binds to the 70S ribosome as a dimer but the biological relevance of this oligomeric state remained unclear (46). Additionally, how YoeB recognizes different codons and whether significant conformational changes occur post cleavage is unknown. Here, we examine YoeB bound to both the UAA stop codon and asparagine AAU sense codon in pre- and post-cleavage states on the ribosome. Our results indicate that YoeB has loose overall codon specificity but makes specific interactions with the mRNA codon possibly for optimal mRNA cleavage. Furthermore, to test the requirements of the YoeB dimer, we engineer a YoeB monomer and test for activity either with mRNA positioned on the 30S subunit or the 70S. We demonstrate that the YoeB monomer retains activity confirming the YoeB dimer is not required for function. Interestingly, we find that the engineered monomeric YoeB is ~20°C less stable than the wild-type YoeB dimer, consistent with YoeB being the only type II toxin activated during thermal stress, thus providing a molecular basis for its action (47).

2.3 Materials and Methods

2.3a Strains and plasmids

The *E. coli* strains BL21 Gold (DE3) pLysS (F⁻*ompT hsdS* (r$_B$⁻m$_B$) *dcm*⁺ Tet^r*gal* λ(DE3) *endA* Hte [pLysS Cam^r]) (Agilent/Stratagene) was used for the purification of YefM, YoeB and YoeB variant proteins. Plasmids used in this study are listed in Table 2.1. The pET21c-*yefM-yoeB* was a generous gift from Professor Masayori Inouye (Robert Wood Johnson Medical School, NJ, USA).

2.3b Purification of YefM, YoeB, and YoeB variants

BL21 Gold (DE3) pLysS cells containing pET21c-*yefM-yoeB* were grown in lysogeny broth (LB) medium supplemented with 200 µg/ml ampicillin at 37°C to an OD$_{600}$ of 0.5–0.7 and induced with 0.4 mM IPTG. Cultures were grown for 3 h before harvesting cells by centrifugation at 3500 × *g* for 30 min. Cell pellets were resuspended in lysis buffer containing 20 mM Tris–HCl pH 7.5, 250 mM KCl, 0.1% Triton X-100, 5 mM β-mercaptoethanol, 0.1 mM phenylmethylsulfonyl fluoride and 0.1 mM benzamidine. Cells were lysed by sonication and centrifuged at 20 000 × *g* for 30 min to obtain the supernatant containing the YefM–YoeB(His)$_6$ complex. Cleared lysate was applied to a HisTrap FF Crude™ Ni^{2+}-Sepharose column (GE Healthcare) pre-equilibrated with binding buffer containing 40 mM Tris–HCl pH 7.5, 250 mM KCl, 20 mM imidazole, 5 mM MgCl$_2$, 10% glycerol and 5 mM β-mercaptoethanol. After the lysate was loaded, the column was washed for an additional 20 column volumes with the same buffer.

For wild-type YoeB and YefM purification, denaturing buffer containing binding buffer plus

6 M guanidine-HCl was applied for 15 column volumes to denature the bound YoeB–YefM complex to elute YefM. Elution fractions containing denatured YefM were combined, shock refolded by rapid dilution into binding buffer followed by filtration using 0.45 µm steriflip (Millipore). YefM was applied to a Superdex 75 SEC column (GE Healthcare) in a buffer containing 40 mM Tris–HCl pH 7.5, 250 mM KCl, 5 mM $MgCl_2$ and 5 mM β-mercaptoethanol. Denatured $YoeB(His)_6$ was refolded on the Ni^{2+}column by slowly removing guanidine-HCl in 20 column volumes and >8 hrs. $YoeB(His)_6$ was eluted in a buffer containing 300 mM imidazole. Fractions containing $YoeB(His)_6$ were combined and applied to Superdex 75 SEC column in the same buffer as YefM.

For monomer YoeB W5A and W5A/W10A variants purifications, cleared lysate was applied to a HisTrap FF Crude^{TM} Ni^{2+} sepharose column (GE Healthcare) and washed as described above, however, reduced guanidine–HCl (2 M) was applied to partially disrupt the YefM–YoeB complex, followed by gradual removal of guanidine-HCl from the column. Bound proteins (YefM-YoeB and free YoeB mix) were then eluted from the column by applying elution buffer containing 300 mM imidazole. The later fractions containing mostly free YoeB mutant, judged by SDS-PAGE, were applied to Superdex 75 SEC column (GE Healthcare) to further purify the monomeric YoeB.

The purity of all proteins was determined to be >95% by SDS-PAGE analysis and their concentrations were determined by the Bradford assay (Biorad). Purified proteins were divided into ~10 µl aliquots, flash froze in liquid nitrogen, and stored at −80°C until further use.

2.3c *In vitro* mRNA cleavage assays

Escherichia coli 30S and 70S were purified from MRE600 cells as previously described (40,42). Purified *E. coli* 30S or 70S (1.2 μM) were programmed with 5′- [^{32}P]-labeled mRNA (0.6 μM; 5′-GCCAAGGAGGUAAAAAUG<u>AAU</u>CAGA-3′ or 5′-GCCAAGGAGGUAAAAAUG<u>UAA</u>CAGA-3′) at 37°C for 6 min in 50 mM KCl, 10 mM NH₄Cl, 10 mM Mg(OAc)₂ and 5 mM HEPES, pH 7.5. *E. coli* tRNA^{fMet} (3 μM; Chemical Block) was incubated for 30 min while YoeB (0.6 μM) was incubated for 10 min at 37°C, followed by incubation at room temperature for additional 20 min. The reaction was stopped by the addition of formamide loading dye and incubation at 65°C for 2 min. Reactions were resolved on a 18% polyacrylamide-8M Urea gel, the gel dried and exposed to a phosphoimager. Cleavage activities were quantified with ImageQuant TL™ (GE Healthcare) using the 1D gel analysis function to compare the cleavage band intensities across all lanes. Two technical replicates of the *in vitro* cleavage assays were performed.

2.3d *Thermus thermophilus* 30S complex formation and crystallization

30S subunits were purified, crystallized, and cryoprotected as has been previously described (48). The mRNAs were chemically synthesized (ThermoFisher, Dharmacon) with the sequence 5′-<u>AAU</u> AAA-3′ with <u>AAU</u> representing the A-site codon (Table 2.2). After cryoprotection, 100 μM mRNA and 220 μM YoeB were soaked into empty 30S crystals for at least 12 hrs. Crystals were flash cooled by plunging into liquid nitrogen and stored for data collection.

2.3e *Thermus thermophilus* 70S complex formation, crystallization, and structure determination

70S ribosomes were purified as previously described (49). Complex formation was performed as described for the mRNA cleavage assay. Four x-ray datasets were collected at the Northeastern Collaborative Access Team (NE-CAT) 24-ID-C facility at the Advanced Photon Source at Argonne National Laboratory (Argonne, IL). These datasets included the 3.7 Å-structure of the 30S bound to YoeB, the 3.2 Å-structure of the 70S bound to YoeB with a non-cleavable mRNA (pre-cleavage state with an A-site AAU codon), the 3.1 Å-structure of the 70S bound to YoeB with mRNA (post-cleavage state with an A-site AAU codon), and the 3.5 Å-structure of the 70S bound to YoeB with mRNA (post-cleavage state with an A-site UAA codon). The post-cleavage state structures were obtained by incubating 70S-YoeB complexes with a 25-nucleotide mRNA similar to the *in vitro* cleavage assays. The mRNA is cleaved during the crystallization trials as seen previously for the 70S-RelE and 70S-HigB structures (33,41). A total of 45° of data with 0.2° oscillations (30S-YoeB) and 90° of data with 0.15° oscillations (70S-YoeB) were collected on a PILATUS pixel 6M-F detector (DECTRIS Ltd., Switzerland) using 0.972 or 0.9795 Å radiation, respectively (Table 2.3). Data were integrated and scaled using the program XDS (50) and molecular replacement was performed using the PHENIX software suite (51). Iterative rounds of refinement in PHENIX and model building were performed using the program Coot (52).

For the 30S-YoeB dataset, the structure was solved by molecular replacement using PDB

code 1J5E as the search model (53). An initial round of refinement was performed with each ribosomal subunit defined as a rigid group, followed by coordinate and grouped ADP refinement (per residue) with ten rigid groups determined by TLS server (54). $F_o – F_c$ electron density maps indicated that the YoeB dimer was positioned in the A site (Figure 2.8). Each monomer of the YoeB dimer model from the PDB code 4V8X (46) was rigid docked. Individual refinement of the RNA coordinates was performed with tight restraints. Final refinement of the structures including YoeB gave crystallographic R_{work}/R_{free} = 20.6/22.4%. Residues 1–84 of the YoeB in direct contact with the decoding center (denoted as YoeB[a]) and residues 1–84 on the second YoeB (YoeB[b]) were built.

The 70S structures were solved by molecular replacement using PDB code 4V6F as the search model with mRNA and tRNA ligands removed (55). In each 70S-YoeB structure, F_o-F_c electron density maps show an unambiguous signal for mRNA, P-site tRNA[fMet] and the YoeB dimer in the A site. YoeB was initially docked in the A site using the previous YoeB structure solved in the absence of the ribosome to avoid any bias in the modeling (PDB code 2A6S) (32). In particular, YoeB residues that interact with mRNA (Glu46, Arg59, Glu62, Arg65, His83 and His84) were extensively remodeled to fit the $F_o – F_c$ difference density. Iterative rounds of refinement in PHENIX and model building in Coot were performed (51,52). These unbiased maps allowed modeling of both mRNA and YoeB. The final YoeB model was built for residues 1–84 for both YoeB monomers (Figure 2.8).

2.3f Site-directed mutagenesis

The plasmid pBAD33-*yoeB* and pET21c-*yefM-yoeB* were kind gifts from Professor Masayori Inouye (Robert Wood Johnson Medical School, NJ, USA) and served as templates for site-directed mutagenesis using the QuikChange Lightning Kit (Agilent). Primers are shown in Table 2.4.

2.3g Differential scanning fluorimetry

Purified wild-type YoeB, YoeB W5A or YoeB W5A/W10A variants (5 µM) were used in the DSF experiments. SYPRO Orange dye (Invitrogen) was added at a 1:1000 dilution. Reactions were heated at a rate of 0.5°C per min, using a StepOne Plus Real Time PCR system (ThermoFisher) and fluorescence was recorded using the ROX filter (602 nm). Data were analyzed by normalizing fluorescence and then fitting the curves using the Boltzmann equation to determine the melting temperature (T_m) (GraphPad Prism, version 8.0.2). Non-linear regression fitting to a Boltzmann sigmoidal curve was performed to determine the T_m of each sample. A one-way ANOVA was performed with Dunnett post-hoc analysis (n = 2, F = 1234, df = 5, $P \leq 0.0001$). The T_m of wild-type YoeB is significantly different as compared to the YoeB W5A and YoeB W5A/W10A variants (mean difference of 20.6°C and 21.1°C respectively, adjusted P = <0.0001). Experiments were performed in triplicate with two independent replicates for each variant.

2.4 Results

2.4a YoeB cleaves mRNA bound to both the 30S subunit and the 70S

YoeB cleaves both sense and stop codons (39,45) and has been shown to associate with free 50S and 70S albeit in the absence of mRNA (39,45). Given that mRNA is located on the 30S subunit in the mRNA path, it is currently unclear how the toxin interacts with the large subunit. Indeed, although the *P. vulgaris* HigB also appears to bind to the 50S in polysome profiles (38), HigB can cleave mRNA bound to only the small subunit (42). Considering that YoeB cleaves sense codons (39,44,45), we reasoned that YoeB may also recognize a 30S initiation-like complex. To test this possibility, we performed *in vitro* mRNA cleavage assays where we incubated purified wild-type YoeB with the *E. coli* 30S or 70S ribosome programmed with a 25-nucleotide mRNA and *E. coli* tRNA^{fMet} in the peptidyl(P) site of the ribosome. When YoeB binds to the 70S, both an asparagine AAU sense and a UAA stop codon are cleaved to form a product that runs on a denaturing gel at ~19 nucleotides as compared to standards (Figure 2.1A). RNAs containing a 3′ phosphate typically run 1–2 nucleotides faster than 3′ dephosphorylated RNAs (56). Since YoeB-mediated cleavage resulted in mRNA containing a 3′ phosphate (46), we hypothesize that our cleavage product means YoeB cleaves the phosphodiester backbone between the second and third nucleotide of the A-site codon (between nucleotides 20 and 21 in our mRNA) consistent with previous results (39). We also found that YoeB cleaves mRNA bound to the 30S (Figure 2.1A). However, YoeB is unable to cleave the mRNA to completion on the 30S subunit similar to HigB toxin mRNA cleavage on the 30S (42). In addition, another mRNA product is observed indicating that YoeB can

cleave the mRNA at two different locations when bound to the 30S. Possibilities for this include that the mRNA moves in the context of the 30S or that in the absence of the 50S, both YoeB monomers are needed for its optimal positioning to cleave the mRNA codon.

2.4b Molecular recognition of the 30S subunit by the YoeB dimer

Our biochemical results above indicate that YoeB can cleave mRNA bound to the 30S in contrast to polysome profiles that showed YoeB did not bind the 30S subunit (39,45). To understand the molecular basis of the interaction of YoeB with 30S and mRNA, we next solved a 3.8-Å X-ray crystal structure of the complex (Table 2.1 and Figure 2.1B). *Thermus thermophilus* 30S subunits were purified and crystallized as previously described (48) and a short six nucleotide mRNA and purified wild-type YoeB were soaked into preformed 30S crystals. The mRNA contains an A-site AAU asparagine codon containing 2′-O-methyl (2′-OMe) modifications at all three A-site positions to prevent cleavage. $2F_o - F_c$ electron density maps clearly show that YoeB interacts with the 30S subunit as a dimer (Figure 2.1B and Figure 2.8A). Unfortunately, the mRNA is not visible which is similar to the 30S-HigB structure we previously solved (42). One possible reason for this is that in the 30S crystal lattice, the 3′ end of the 16S rRNA and the 16S rRNA spur from an adjacent molecule in the asymmetric unit mimic a P-site codon and anticodon stem–loop, respectively. As we previously suggested, the absence of the P-site tRNA and mRNA codon may prevent the binding of the small mRNA in the A site (42). Nonetheless, this structure provides insights into how the dimeric YoeB toxin recognizes the small subunit.

Monomeric *E. coli* YoeB is a 10.2 kDa protein and forms a compact globular structure consisting of a five-stranded β-sheet and two α-helices (32). Consistent with the way the 70S-YoeB structure was previously described (46), the YoeB monomer closest to the mRNA path is referred to as YoeB[a] and the more distant monomer as YoeB[b]. In general, the YoeB dimer occupies the A site between the 30S head and the body domains (Figure 2.1B). The binding site of YoeB[a] overlaps completely with that of the anticodon stem-loop of the tRNA and YoeB[a] also interacts with the shoulder domain of the 30S subunit (Figures 2.1B and 2.2). The position of YoeB[b] does not overlap with where tRNA binds and instead packs against the 30S head domain, contacting 16S rRNA helix 31 (h31) (Figure 2.1B and D). The overall YoeB dimer arrangement on the 30S is similar to when bound to the 70S (46) with a root mean-square deviation (r.m.s.d.) of 1.2 Å, for 168 equivalent Cα atoms (84 residues in each YoeB chain). Additionally, YoeB, in the context of the 30S-YoeB structure, is similar to the structure of YoeB in the YefM$_2$-YoeB toxin-antitoxin complex as well as to the previously determined 70S-YoeB structure (r.m.s.d. = 1.5–1.6 Å) (32).

Although α-helix 2 (α2) in each YoeB monomer is enriched with basic residues that theoretically could interact with the negatively charged backbone of 16S rRNA, only YoeB[a] makes extensive interactions with the ribosome (Figure 2.1C). YoeB[a] contacts the 30S head and body domains via 16S rRNA helix 18 (h18) and helix 44 (h44), respectively. Residue Arg22 is within hydrogen bonding distance to the phosphate backbone oxygens of nucleotide U531 in h18. Weak electrostatic interactions are formed between YoeB[a] residues Lys26 and Gly43 with the phosphate backbone oxygens of C519 while

Lys42 contacts the 2′-OH of C519 (Figure 2.1C). In contrast, YoeB[b] makes weak interactions with the 16S rRNA located in the 30S head domain (Figure 2.1D). YoeB[b] residues Lys21, Arg22 and Lys25 are adjacent to the backbone of 16S rRNA h34 but likely only form weak electrostatic interactions (>3.5 Å). Additional weak electrostatic interactions are made between YoeB residues Lys32, Arg35 and Arg36 with helix 31 (h31) of the head domain of the 30S. Although ribosomal S12 residues Glu40 and Lys44 interact with YoeB bound to the 70S (46), in the context of the 30S, YoeB slightly shifts away from S12 thus ablating these interactions.

2.4c Molecular mechanism of YoeB recognition of a UAA stop codon

YoeB cleaves AAA lysine, AAU asparagine, UAA stop, CUG leucine and GCG alanine codons on the ribosome in the A site (39). As previously described, a structure of the 70S with YoeB bound to an A-site UAA stop codon in a pre-cleavage state contained an incorrect modeling of the mRNA (46). To directly compare how ribosome-dependent toxins RelE, HigB and YoeB interact with their mRNA substrates on the ribosome, we rebuilt and refined the mRNA into unbiased electron density (41). We found that YoeB induces a similar conformation of the A-site codon as compared to the RelE and HigB toxin (33,41). The rebuilt mRNA indicates that YoeB conserved residues Glu46, Lys49 and Asn51 interact with the first (U4) and the second (A5) nucleotides of the mRNA within the A site (Figure 2.3A) (mRNA numbering starts with +1 in the P site with A-site nucleotides numbered 4–6). Although this structure provided insights into how the YoeB dimer interacted with the 70S in a pre-cleavage state, how YoeB interacted with a UAA stop codon after mRNA cleavage was necessary to determine which YoeB residues are

important for activity. For example, HigB residues move considerably after mRNA cleavage and pre- and post-cleavage structures provided significant insights into its mechanism (41). Therefore, we solved a 3.5-Å x-ray crystal structure of 70S bound to YoeB and mRNA containing an A-site UAA stop codon that undergoes cleavage during the crystallization process (Figure 2.3, Figure 2.8D and Table 2.1). The post-cleavage state was solved using unmodified 25-mer mRNA and cleavage was indicated by a lack of electron density for the third nucleotide (A6) of the A-site codon (Figure 2.9). In both pre- and post-cleavage states of YoeB bound to an UAA stop codon, YoeB adopts an almost identical conformation with an r.m.s.d. of 1.2 Å for equivalent 168 Cα atoms (84 residues in each YoeB chain). Although the YoeB dimer appeared to colocalize with both the 70S or 50S subunit in polysome profile assays (39) but not the 30S subunit, there are no interactions between YoeB and the 50S subunit in this structure (Figure 2.10).

When bacterial toxins bind to the A site of the ribosome to cleave the mRNA phosphodiester backbone, the mRNA is dramatically pulled into the toxin active site (33,41) (Figure 2.11). Upon YoeB binding to the A-site codon, we find that the mRNA is similarly pulled into the YoeB active site in slight contrast to what was previously published (41,46). In the pre-cleavage state, the side chain amine group of YoeB[a] residue Asn51 forms a π-π stacking interaction with the nucleobase of first nucleotide of the A-site codon U4 (Figure 2.3A). Given the nonspecific nature of this interaction, it appears that any nucleotide could be accommodated at this position consistent with primer extension analysis of mRNAs cleaved by YoeB (45). In contrast to the absence of interactions with the first nucleotide position of the codon, YoeB[a] surrounds the second and third A-site

59

nucleotides (Figure 2.3A). In the incorrect build of A5 (46), it appears there are base-specific interactions with the sidechains of highly conserved YoeB[a] residues Arg59, Arg65 and Tyr84. However, in our rebuild, Arg65 and Tyr84 are too distant to interact with A5, however, Arg65 interacts with the scissile phosphate and the O4′ of the ribose of A6 (Figure 2.3A). Interactions with the second A5 nucleotide not observed in the previous 70S-YoeB structure include the interaction of Glu46 with the 2′-OH and the base-specific interaction of Lys49 (Figure 2.3A). The sidechain of Glu46 forms a hydrogen bond with the 2′-OH of A5 and the backbone oxygen and amine groups of Lys49 form hydrogen bonds with the Hoogsteen face of A5 that adopts a *syn* conformation. Only cytosine in an *anti* confirmation can fulfill this hydrogen bonding pattern (Figure 2.12). At the third nucleotide position of the A-site codon (A6), YoeB[a] residues Glu63 and His83 (β4) stack with the A6 nucleobase. A6 undergoes a 180° rotation around its phosphate backbone as compared to when tRNA is present, where its nucleobase forms stabilizing stacking interactions with His83 and Glu63 (Figure 2.3B).

Upon mRNA cleavage by YoeB, the position of U4 and A5 minimally changes however, YoeB[a] moves slightly away from the mRNA path. This movement results in an ablation of the stacking and the hydrogen bonding interactions between Asn51 and U4 and Glu46 with the 2′-OH of A5 (Figure 2.3B). The formation of the 3′-phosphate positions YoeB[a] residues Arg59, Arg65, and Tyr84 within hydrogen bonding distance (Figure 2.3B and C). Together, these two structures indicate that while any nucleotide can be accommodated in the first position, the hydrogen bonding network formed between the second position (A5) and stacking interactions at the third position (A6) with YoeB

residues seem to impose some constraints on which nucleotides would be a good YoeB substrate.

2.4d Molecular mechanism of YoeB recognition of a AAU asparagine sense codon

YoeB also cleaves the AAU sense codon in addition to the UAA stop codon (39,45). Given that YoeB[a] appears to select for the UAA stop codon by extensive interactions with the third nucleotide (Figure 2.3A), and these two codons differ at this third position, we solved x-ray crystal structures of 70S-YoeB bound to a 25-mer mRNA containing an A-site AAU codon in a pre- and post-cleavage states to 3.2 and 3.1 Å, respectively (Figure 2.4, Figure 2.8C, D, and Table 2.1). In these structures with the AAU codon, the first nucleotide in the codon is positioned closer to the P-site tRNA enabling interactions between the ribose O4′ atom of nucleotide 36 and the N6 atom of U4 but the stacking interaction between Asn51 and U4 is no longer observed (Figures 2.3A and 2.4A). In both UAA and AAU codons, there is an adenosine at the second nucleotide position. In the two 70S-YoeB structures, there is conservation in how YoeB interacts with A5 suggesting that differences in the codon do not change how YoeB recognizes the nucleotide at the second position. At the third position, substitution of an adenine with a uridine still causes a reorientation of the nucleobase towards the mRNA path, however, U6 does not stack between Glu63 and His83 (Figure 2.4A and Figure 2.13). In the post-cleavage state, YoeB[a] residues Arg59 and Tyr84 move towards the mRNA to hydrogen bond with the newly formed 3′ phosphate while Arg65 maintains interactions with the phosphate (Figure 2.4B and C). These interactions were previously observed (46). Together, these structures suggest that while purines stack more efficiently with the third nucleotide of the

61

A-site codon upon YoeB binding, this interaction is not essential considering that YoeB still cleaves codons containing pyrimidines at the third position.

2.4e YoeB-induced conformational changes of the decoding center

When tRNA binds to the 70S A site, the mRNA-tRNA pair is monitored by 16S rRNA nucleotides and ribosomal protein S12 in the decoding center (57). During this decoding process, 16S rRNA nucleotides G530, A1492 and A1493 monitor the codon-anticodon interaction to determine if the interaction is cognate. A1492 and A1493 flip from an internal loop in 16S rRNA h44 to probe for Watson-Crick base-pairing at the first and second positions of the codon–anticodon interaction. At the same time, G530 moves inward to form a single hydrogen bond with A1492 and flips from a *syn* to an *anti* conformation to interact with the second and third codon positions. Additionally, the entire 30S shoulder domain moves inward towards the intersubunit space of the A site and these conformational changes collectively contribute to tRNA selection (58,59). YoeB binding also induces similar conformational rearrangements of 16S rRNA nucleotides however, there are slight differences as compared to the process of tRNA selection. In the structure of the pre-cleavage 70S bound to a UAA stop codon, binding of YoeB causes A1492 and A1493 to flip out of h44 to interact with mRNA and YoeB residues Glu46, Pro47 and Lys49, as previously seen (46). Although A1913 of 23S rRNA Helix 69 (H69) moves during tRNA decoding to interact with A1492, upon YoeB binding, the position of A1913 remains constant because YoeB[a] binding occupies this space (Figure 2.5B). However, in the post-cleavage state, A1492 rotates ~150° back into h44 (Figure 2.5C). This movement places A1492 adjacent to A1913 where it partially stacks with A1913 ablating

interactions with YoeB[a]. In both pre and post-cleavage states, YoeB binding inserts Lys44 (of the α2–β2 loop) and Arg59 (β2) residues between G530 and A1492 thus preventing interactions between these two nucleotides that are usually required for correct tRNA selection (Figure 2.14). These interactions with the decoding nucleotides are preserved in the 70S structures bound to the AAU sense codon.

2.4f Monomeric YoeB retains ribosome-dependent ribonuclease activity yet is thermally unstable

Our data presented here and the previous YoeB structure bound to the ribosome demonstrate that YoeB binds to both the 30S and 70S as a dimer (46). The YoeB dimer interface is formed by hydrophobic surfaces of α1 and α2 from each YoeB monomer and a hydrogen bonding network between residues Glu7, Tyr13, Gln17, Asn28 and Arg35 (Figure 2.6A and Figure 2.15). Two tryptophan residues, Trp5 and Trp10, form a hydrophobic pocket and are also involved in the formation of the YefM-YoeB toxin-antitoxin complex via interactions with C-terminal residues of YoeB (32). Since all known ribosome-dependent toxins are monomers including RelE, YafQ and HigB (33,36,40,41,60), it is unclear why YoeB adopts a dimeric form. To test whether a YoeB monomer retains RNase activity, we introduced alanine mutations of W5A and W5A/W10A in an attempt to disrupt the tryptophan cluster and thus engineer a YoeB monomer. Wild-type YoeB dimer elutes as a compact dimer at ~16 kDa as determined by size exclusion chromatography (SEC) while the apparent molecular weight of both purified YoeB W5A and YoeB W5A/W10A is ~11 kDa indicating that YoeB is a monomer (Figure 2.6B).

We next tested whether YoeB W5A and YoeB W5A/W10A variants cleave mRNA in the context of 30S and 70S ribosomes using the in vitro cleavage assay previously described. Both YoeB variants cleave AAU and UAA codons on the 70S to near completion similar to wild-type YoeB (Figure 2.6C and Figure 2.16). In the context of the 30S subunit, the YoeB W5A and YoeB W5A/W10A variants cleave AAU and UAA codons on mRNA to ~55 and 65% completion, respectively as compared to ~80% on the 70S ribosome (Figures 2.1A and 2.6C). However, YoeB variants do not produce an additional cleavage band on the 30S in contrast to wild-type YoeB cleavage on the 30S subunit (Figures 2.1A and 2.6C). It is not clear the exact reason for the disappearance of this extra band when YoeB is monomeric but it may indicate that YoeB[b] affects the position of YoeB[a] and this somehow prevents the movement of mRNA that produces an extra mRNA cleavage band (Figure 2.1A). These data indicate that an engineered YoeB monomer can cleave ribosome-bound mRNA and somehow this oligomeric state influences the position of the mRNA in the context of the 30S only.

YoeB is activated during thermal stress (47) and therefore we wondered whether one role of a YoeB dimer is for thermal stability. To test this, we performed differential scanning fluorescence (DSF) experiments of wild-type YoeB, YoeB W5A and YoeB W5A/W10A proteins. Wild-type YoeB has a melting temperature (T_m) of 63.3°C while the YoeB W5A and YoeB W5A/W10A variants are ~20°C less stable (Figure 2.6D). These data suggest that the YoeB dimer is stabilized and active during thermal stress consistent with data from the Hayes group (47).

2.5 Discussion

In this study, we focus on understanding the mechanism of action of the type II toxin, YoeB. YoeB is an endonuclease that cleaves mRNA bound to the ribosome but only in the A site, the site where tRNAs are brought to the ribosome for decoding of the mRNA codon. We find that YoeB is capable of cleaving mRNA codons on both the 30S and 70S ribosomes suggesting that interactions with the 50S are not required for YoeB activity. We further solved an x-ray crystal structure of YoeB bound to the 30S, revealing extensive interactions of YoeB[a] with the decoding center while YoeB[b] minimally interacts with the 30S. Given that YoeB can cleave codons immediately downstream of the AUG start codon in a subset of mRNA tested (39), our results indicate that YoeB targets mRNAs even during the initiation phase of translation before recruitment of the 50S. Although YoeB is active as a dimer, our experiments show that a dimeric oligomeric state is not essential for cleavage of the mRNA by YoeB. Instead, YoeB likely forms a dimer to persist during thermal stress in which it is upregulated (47).

Traditional RNases, including type II ribosome-dependent toxins, display a wide range of substrate specificity. As with other type II toxins, YoeB cleaves between the second and third nucleotide of the mRNA codon presented in the A site and appears to target a range of codons most commonly at the beginning of the coding region or at stop codons (39,46). The previously reported structure of YoeB bound to a 70S containing an A-site UAA stop codon in a pre-cleavage state suggested that any nucleotide could be accommodated at the first nucleotide position of the codon due to a lack of base-specific interactions (46). Although this structure provided insights into potential YoeB mRNA specificity, the mRNA

65

was incorrectly modeled as we previously discussed upon comparison with type II HigB toxin bound to the 70S ribosome (41). This prompted us to rebuild the mRNA and examine how YoeB interacts with its mRNA substrate. Here, we further extend these studies to determine how YoeB residues change after mRNA cleavage of the UAA stop codon and additionally how YoeB cleaves the sense UAA codon. In the rebuild, YoeB[a] Lys49 makes nucleobase-specific interactions that define which nucleotide is allowed at the second position of the codon while Glu46 stabilizes the nucleotide by interactions with its 2′-OH (Figure 2.3A). It is clear that cytosine can make similar interactions as adenosine if it adopts an *anti* conformation, which is similar to how HigB recognizes A and C codons at this second position (41). YoeB[a] residues Arg65 and His83 interact with the scissile phosphate while Glu63 and His83 stack with A6 or the third nucleotide of the codon (Figure 2.3). A post-cleavage state reveals that Arg65 maintains interactions with the 3′-phosphate and Arg59 moves towards the 3′-phosphate, both events likely important in stabilizing the transition state of the reaction. These structures begin to provide insights into the mechanism of YoeB cleavage of mRNA.

To extend our understanding of potential codon specificity by YoeB, we also solved structures in both the pre-and post-cleavage states bound to an AAU sense codon. Interestingly, A4 contacts the P-site tRNA at nucleotide 36 unlike when a uridine is present at this first position (Figure 2.4A and B). Regardless, clearly this is not an important interaction as all four nucleotides are found at the first position in codons cleaved by YoeB (39,44). Interactions of YoeB[a] residue Lys49 with A5 are preserved in both UAA and AAU codons bound to the 70S providing evidence that the identity of surrounding nucleotides,

66

that is, the first and third nucleotides in the codon, do not alter how the second nucleotide is pulled from the mRNA path to present the scissile phosphate for cleavage (Figures 2.3 and 2.4). Modeling of other nucleotides at the second position indicates that while a cytosine may be accommodated, either a guanosine or uridine would not maintain this hydrogen-binding pattern (Figure 2.12), consistent with *in vivo* cleavage assays (32,39,44). At the third nucleotide position, although A6 in the UAA structure is clearly stabilized by stacking interactions with Glu63 and His83, this stacking is ablated when A6 is substituted with U6. YoeB mediated mRNA cleavage assays indicate YoeB can cleave codons containing a guanine at this position, suggesting there may be subtle nucleotide specificity at this third position (45) (Figures 2.3A, 2.4A, and 2.13). This is consistent with previous observations that the majority of nucleobases recognized by YoeB in the third position are purines (32,39,44,45). Overall, these data provide accumulating evidence that YoeB has loose codon specificity.

The 30S decoding center undergoes conformational rearrangements regardless of when tRNAs or translation factors bind and this includes when type II toxins RelE, HigB and YoeB bind (33,41,46). Surprisingly, ribosome-dependent toxins induce slightly different conformational changes of the decoding center that may be reflective of how such stalled ribosome complexes are recycled after toxin departure (Figure 2.7). During decoding, 16S rRNA nucleotides A1492, A1493 and G530 along with S12 residues monitor mRNA-tRNA interactions and concurrently, the 30S adopts a closed state resulting in the shoulder domain moving towards the A site. Comparison of pre- and post-cleavage states induced by RelE reveals that the decoding center changes very little (Figure 2.7C and D)

(33). 16S rRNA nucleotide A1492 is pulled from h44, G530 moves to a *syn* conformation, however, A1493 remains stacked with A1913. The absence of A1493 movement towards G530 indicates that this is not a fully closed state. Toxin HigB also induces an incomplete closing of the A site but there are differences between pre- and post-cleavage states (Figure 2.7E and F) (41). For example, upon HigB binding but before mRNA cleavage has occurred, A1492 rather than A1493, partially stacks with A1913. After cleavage by HigB, A1492 moves ~45° away from A1913. Interestingly, YoeB induces changes that are distinct from changes induced by either RelE or HigB (Figures 2.5, 2.7A and B). In the pre-cleavage state with YoeB bound, both A1492 and A1493 are flipped from h44 and G530 adopts a *syn* conformation, all changes that reflect a closed state (Figure 2.7A). After cleavage, A1492 flips back into h44 however, it does not stack with A1913 (Figure 2.7B). In all 70S structures containing the three toxins, A1492 is prevented from interacting with G530 by a toxin loop that functions as a physical barrier to prevent the ribosome adopting fully closed states. The differences that toxins exert upon the A-site may be due to their physical size and surrounding electrostatic interactions (Figure 2.17). RelE and HigB proteins are slightly smaller than the monomeric YoeB, but more importantly, YoeB occupies more space in the A site to more fully interact with A1492, A1493 and A1913 (Figure 2.17D). Additionally, this extended position of YoeB may be aided by the surrounding negative electrostatic surface of the 50S in relation to the distal YoeB[b] monomer (Figure 2.17E). For example, there is only one point of opposing charges between the 50S and YoeB[b] that could potentially result in repelling YoeB[b] from the 50S surface towards the A site (Figure 2.11 and 2.17E). This repelling may result in YoeB[b] somehow influencing the position of YoeB[a] important for interactions with the

codon. Support for this includes the additional mRNA cleavage band in cleavage assays with only the 30S that then is ablated when engineered monomeric YoeB is tested. Thus, the dimeric state of YoeB may account for the more closed state of the A site as compared to RelE and HigB (Figure 2.7).

What are the consequences of the binding of toxin that induce different conformations of A-site decoding nucleotides? One possibility is that variations of open and closed states could influence toxin release after cleavage. For example, toxins that remain bound to the ribosomes post cleavage could, in addition to the inhibition of translation, also protect ribosomes that are queued on mRNAs from other toxins that cleave rRNA such as *E. coli* MazF, *M. tuberculosis* MazF-mt6 and MazF-mt9 (61–64). In addition to protection, toxin-bound ribosomes would also prevent ribosome recycling. Conversely, other toxins that rapidly dissociate from the ribosome would have the opportunity to cleave many mRNAs thus inhibiting translation to a larger extent. In line with this argument, toxins such as RelE and YoeB that appear to have loose specificity may help combat nutritional deficiencies arising from stress by targeting the majority of transcripts to promote recycling of nascent chains to help replenish nutrients such as amino acids. Future studies aimed at understanding the steps after toxin RNase activity would provide important insights into these downstream events.

The question of why YoeB is a dimer while all other structurally homologous ribosome-dependent toxins are monomers motivated us to test whether the dimeric form is related to its activity. Engineered monomeric YoeB appears to be as active as the wild-type YoeB

dimer indicating the dimeric state is not a requirement for function. Recent studies by the Hayes group demonstrate YoeB is the sole ribosome-dependent toxin that cleaves mRNA during elevated temperatures in *E. coli* (47). These cleaved mRNAs are then recognized by tmRNA-SmpB, ArfA, or ArfB for the release of the nascent chain required for the recycling of ribosomes. Consistent with these data, the YoeB dimer is more thermal stable than the YoeB monomer rationalizing why YoeB has evolved to be dimeric during heat shock (Figure 2.6D).

Expression of type II toxin-antitoxin systems is typically regulated via a negative feedback loop where stress attenuates antitoxin proteolysis leading to transcriptional de-repression. Whether specific stresses activate different toxins is unknown, however, it has been shown that nutritional stress causes rapid activation of *E. coli* RelBE, MazEF, HicAB, YafNO, YgiNM, and YgiUT toxin-antitoxin complexes (23) while other systems may be regulated by the SOS response (*E. coli* YafQ-DinJ) (37), antibiotics (*P. vulgaris* HigB) (65) and more recently, thermal stress (*E. coli* YoeB-YefM) (47). While traditional RNases monitor whether mRNAs are functional, these toxins serve more as a stress-specific mechanism of translational inhibition. Many outstanding questions remain regarding the activation, regulation, and downstream effects of toxins on bacterial physiology, however, our mechanistic insights into YoeB activity expands our understanding of ribosome-dependent toxins activated during thermal stress.

2.6 Acknowledgements

2.7 Funding

2.8 Figures & Tables

Figure 2.1 – *E. coli* YoeB recognizes the 30S A site.

(**A**) In vitro cleavage assays of [32]P-5′-labeled mRNA bound to either a 70S or 30S programmed with P-site tRNA[fMet]. The mRNA sequence contains a ribosome binding site (rbs) and E-, P- and A-site codons are shown above the mRNA sequence (tick lines are shown for every 10 nucleotides). The A-site codons contained either an AAU asparagine or UAA stop codon. Ribosome complexes were formed as described in the Methods section. YoeB was incubated for 10 mins and reactions were quenched and monitored by denaturing PAGE. Both codons are cleaved by YoeB when bound to a 30S and 70S complex (lanes 10–13). Cleavage on the 30S occurs to a lesser extent and an extra band is observed (lanes 11 and 13). Full length mRNA is denoted by a closed arrowhead, cleavage product by an open arrowhead and the extra mRNA band by a gray arrowhead.

Neither codon is cleaved in the absence of YoeB (lanes 6–9). 19-, 20- and 25-nucleotide

mRNA standards and AAU and UAA containing mRNAs are shown for comparison (lanes

1–5). (**B**) A 3.7 Å-structure of Thermus thermophilus 30S-YoeB where YoeB binds in the

A site as a dimer between the head, body, and shoulder domains. The YoeB monomer

closest to the mRNA path is shown in green (YoeB[a]) while the distal YoeB monomer is

shown in pink (YoeB[b]). 16S rRNA helices (h18, h31, h34, and h44) and proteins (S12,

S19) that YoeB interacts with are indicated in dark gray and blue, respectively. (**C**)

YoeB[a] interactions with 16S rRNA h18 and S12 of the 30S. (**D**) YoeB[b] makes weak

electrostatic interactions with 16S rRNA h34 and h31.
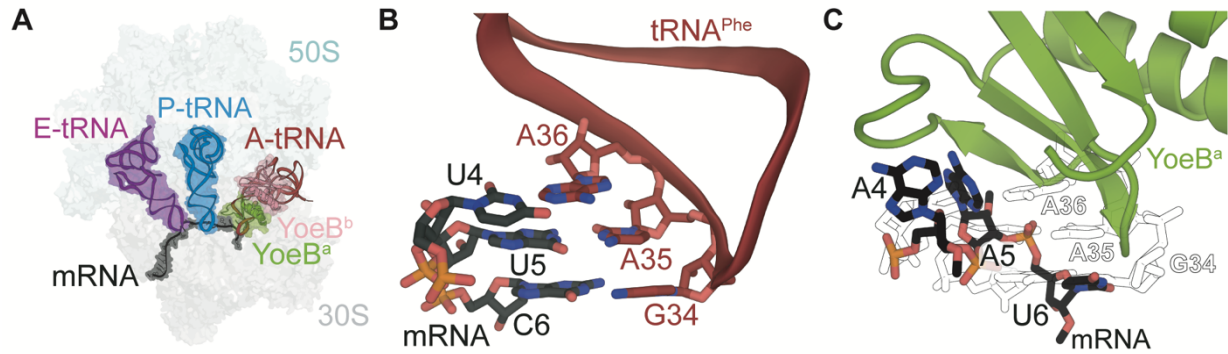
Figure 2.2 – YoeB binds in the A site normally occupied by A-site tRNA.

(**A**) View of the *Thermus thermophilus* 70S ribosome with dimeric YoeB bound in a UAA post-cleavage state. 50S and 30S subunits are shown as background and A-, P- and E-site tRNAs are shown in red, blue and purple, respectively. The YoeB monomer closest to the mRNA path is shown in green (YoeB[a]). The YoeB dimer overlaps with the position of A-tRNA[Phe] (PDB code 4V5I). (**B**) tRNA[Phe] interaction with its cognate mRNA codon in the A site. (**C**) The mRNA (black) is re-positioned for cleavage by YoeB[a] as compared to the normal anticodon stem loop and mRNA pairing from (B) shown in outline.
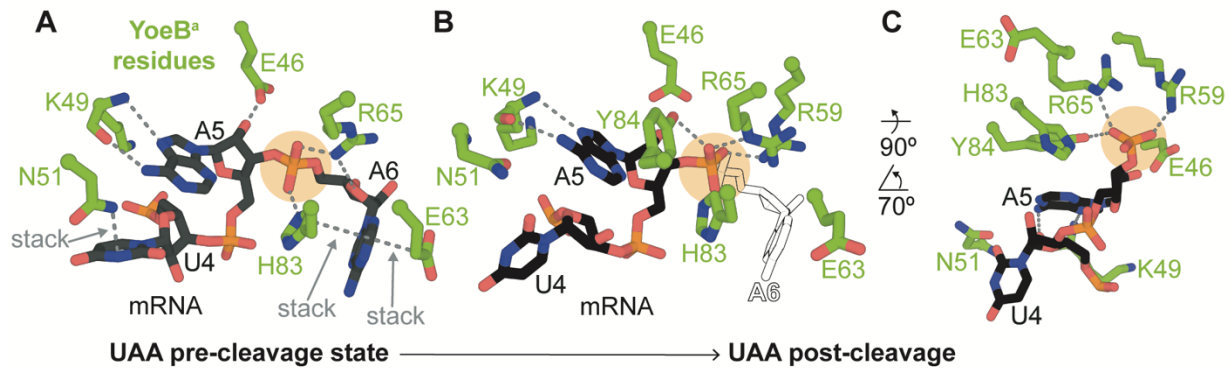
Figure 2.3 – The influence of YoeB on the mRNA path when bound to an UAA stop codon.

(**A**) Our remodel of the interactions between the A-site UAA stop codon and YoeB in a pre-cleavage state (PDB code 4V8X, remodeled). The scissile phosphate is highlighted in orange. (**B**) In a post-cleavage state (PDB code 6OXI, this study), interactions between the A-site UAA stop codon and YoeB. The position of the cleaved A6 is shown in outline for comparison. (**C**) Upon cleavage, Arg59, Arg65 and Tyr84 interact with the 3′-phosphate.
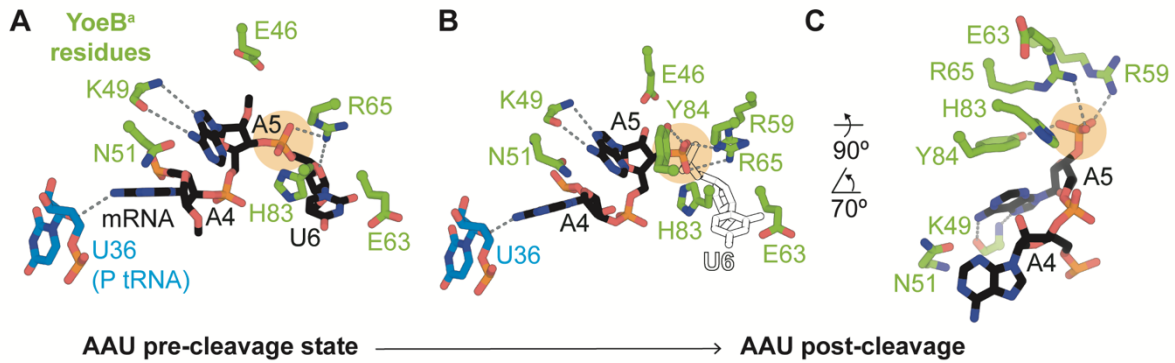
Figure 2.4 – The influence of YoeB on the mRNA path when bound to an AAU sense codon.

(**A**) Interactions between YoeB residues and the A-site AAU asparagine codon in a pre-cleavage state. The scissile phosphate is highlighted in orange (PDB code 6OXA). (**B**) In a post-cleavage state (PDB code 6OTR), interactions between YoeB residues and the A-site asparagine codon. The position of the cleaved U6 is shown in outline for comparison. (**C**) Upon YoeB-mediated cleavage, Arg59, Arg65 and Tyr84 interact with the phosphate.
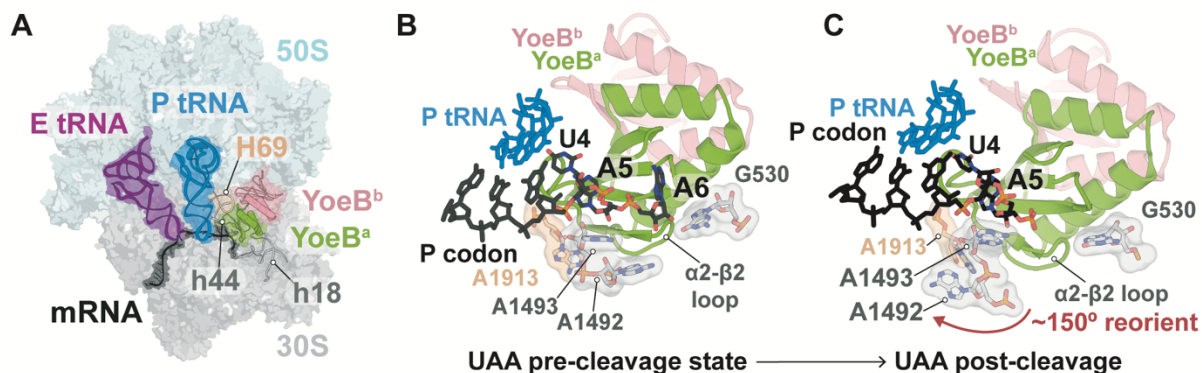
Figure 2.5 – The influence of YoeB on the mRNA path when bound to a UAA stop codon.

(**A**) Structure of dimeric YoeB bound to the *Thermus thermophilus* 70S ribosome. Color scheme is the same as in Figure 2.1. YoeB[a] interacts with 16S rRNA helices h18 and h44 (gray) and 23S rRNA helix H69 (gold) adjacent to the mRNA path (black). P- and E-site tRNAs are shown as blue and purple, respectively. (**B**) YoeB[a] interacts with the A-site decoding center when bound to a UAA stop codon in a pre-cleavage state (by the inclusion of 2′-OCH$_3$ at all three A-site nucleotides) solved by Feng *et al.* (46). All three A-site nucleotides (U4, A5, A6) are shown in black, and are monitored by 16S rRNA nucleotides A1492, A1493, and G530 of h44 (gray) and 23S rRNA A1913 (gold). We rebuilt the mRNA as previously published (41). The P-site mRNA codon (black) and anticodon nucleotide (blue) are shown for perspective. (**C**) A 70S-YoeB post-cleavage state where the α2-β2 loop of YoeB prevents A1492 forming hydrogen bonds with G530.
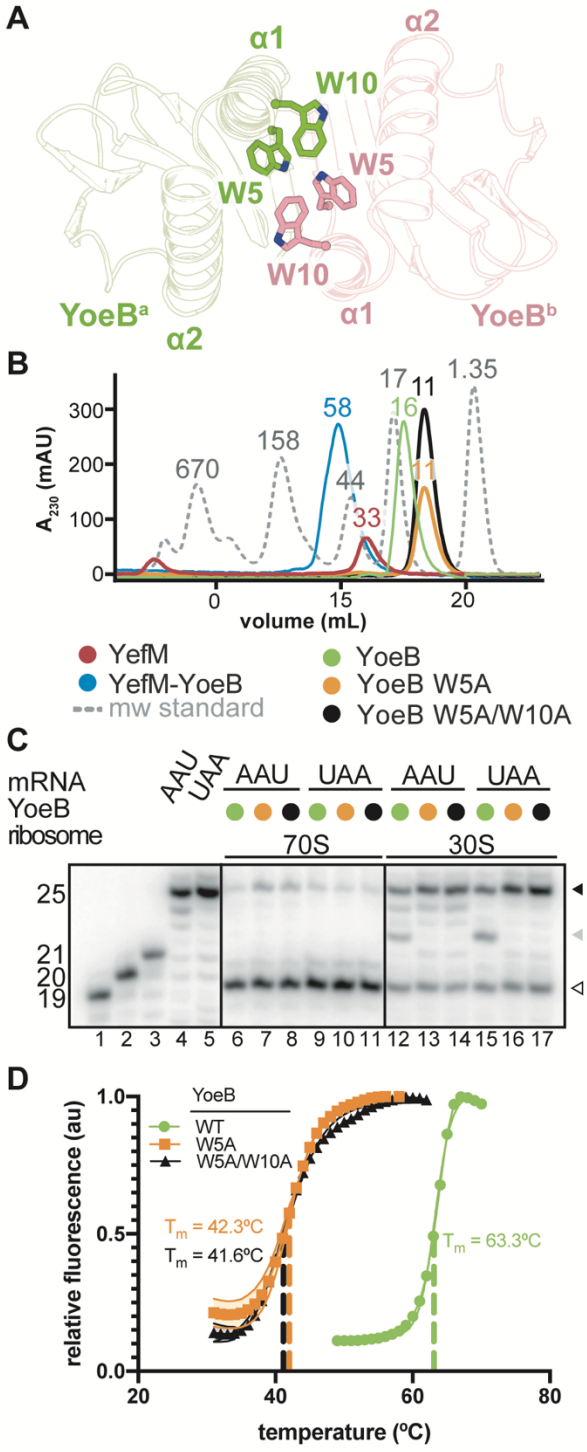
Figure 2.6 – Monomeric YoeB is active but is less thermal stable.

(**A**) YoeB residues W5 and W10 of each YoeB monomer comprise the dimer interface

and were selected for mutagenesis experiments to create a monomeric YoeB. (**B**) Size exclusion chromatography of purified YoeB, YefM-YoeB, and YoeB variants indicating that the W5A and W5A/W10A variants are monomeric. The number above each peak denotes the molecular weight in kDa. Approximate molecular weights of YefM, YefM-YoeB, and YoeB are 27.9 kDa, 59.6 kDa, and 22.4 kDa, respectively. YoeB variants W5A and W5A/W10A elute at ~11 kDa. (**C**) *In vitro* cleavage assays of ^{32}P-5′-labeled mRNA bound to either a 70S or 30S programmed with P-site tRNA^{fMet}. The mRNA sequence used in these assays is the same as in Figure 2.1A. Both mRNAs are cleaved by YoeB when bound to a 30S and 70S complex. YoeB variants W5A and W5A/W10A are both active in cleaving mRNA bound to either the 30S or 70S as compared to wild-type YoeB. Full length mRNA is denoted by a closed arrowhead, cleavage product by an open arrowhead and the extra mRNA band by a gray arrowhead.19-, 20- and 25-mer mRNA standards and AAU and UAA containing mRNAs are shown for comparison (lanes 1–5). The line separating the gels indicates each region of the figure were taken from different parts of a single gel. (**D**) DSF assays demonstrate that wild-type YoeB (green, T_m = 63.3°C) is more thermostable than YoeB variants W5A (orange, T_m = 42.3°C) or W5A/W10A (black, T_m = 41.6°C). Fluorescence values were normalized to the highest tested temperature and the boundary of each line represents the mean ± SD of values of three independent experiments.
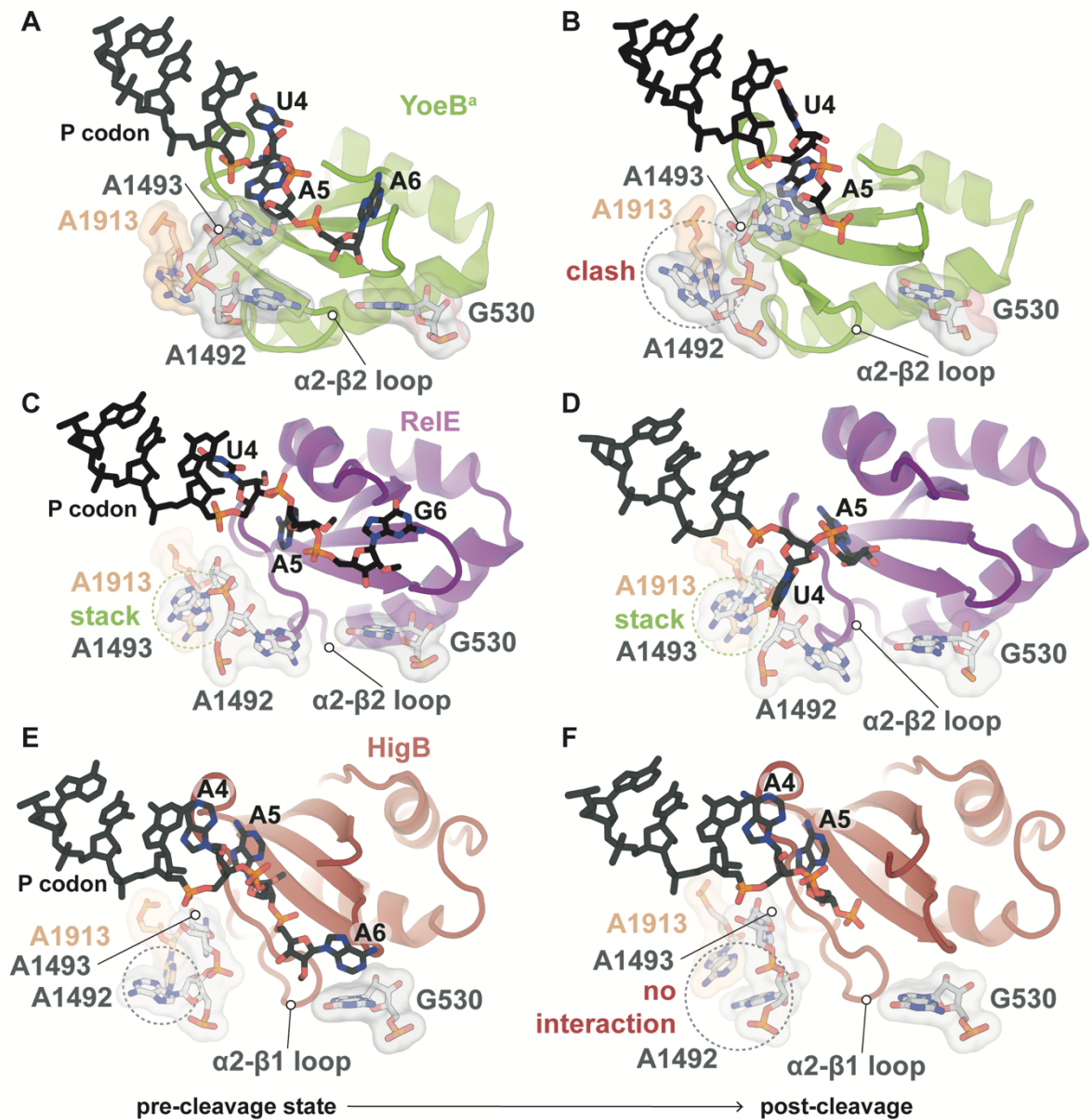
Figure 2.7 – Comparison of the influence of YoeB, RelE and HigB toxins on the mRNA path.

(**A**) Interaction of YoeB with the A-site decoding center bound to a UAA stop codon in a pre-cleavage state is shown (PDB code 4V8X, remodeled). All three A-site nucleotides (U4, A5, A6) are monitored by 16S rRNA A1492, A1493, and G530, and 23S rRNA

A1913. (**B**) Interaction of YoeB with the A-site decoding center bound to a UAA stop codon in a post-cleavage state is shown (PDB code 6OXI, this study). Reorientation of A1492 post-cleavage results in a clash with A1913 of H69. (**C**) Interaction of RelE with the A-site decoding center bound to a UAG stop codon in a pre-cleavage state is shown (33). All three A-site nucleotides (U4, A5, G6; black) are monitored by 16S rRNA A1492, A1493, and G530 and 23S rRNA A1913. (**D**) Interaction of RelE with the A-site decoding center bound to a UAG stop codon in a post-cleavage state is shown (33). There is little to no significant conformational changes between the two states. In both cases, the RelE α2-β2 loop prevents A1492 from forming hydrogen bonds with G530. (**E**) Interaction of HigB with the A-site decoding center bound to a AAA lysine codon in a pre-cleavage state is shown (41). All three A-site nucleotides (A4, A5, A6) are monitored by 16S rRNA A1492, A1493, and G530, and 23S rRNA A1913. In this state, A1492 only partially interacts with A1913. (**F**) Interactions of HigB with the A-site decoding center bound to a AAA lysine codon in a post-cleavage state is shown (41). In this state, A1492 moves away from and no longer stacks with A1913. In both cases, the HigB α2-β2 loop prevents A1492 from forming hydrogen bonds with G530.
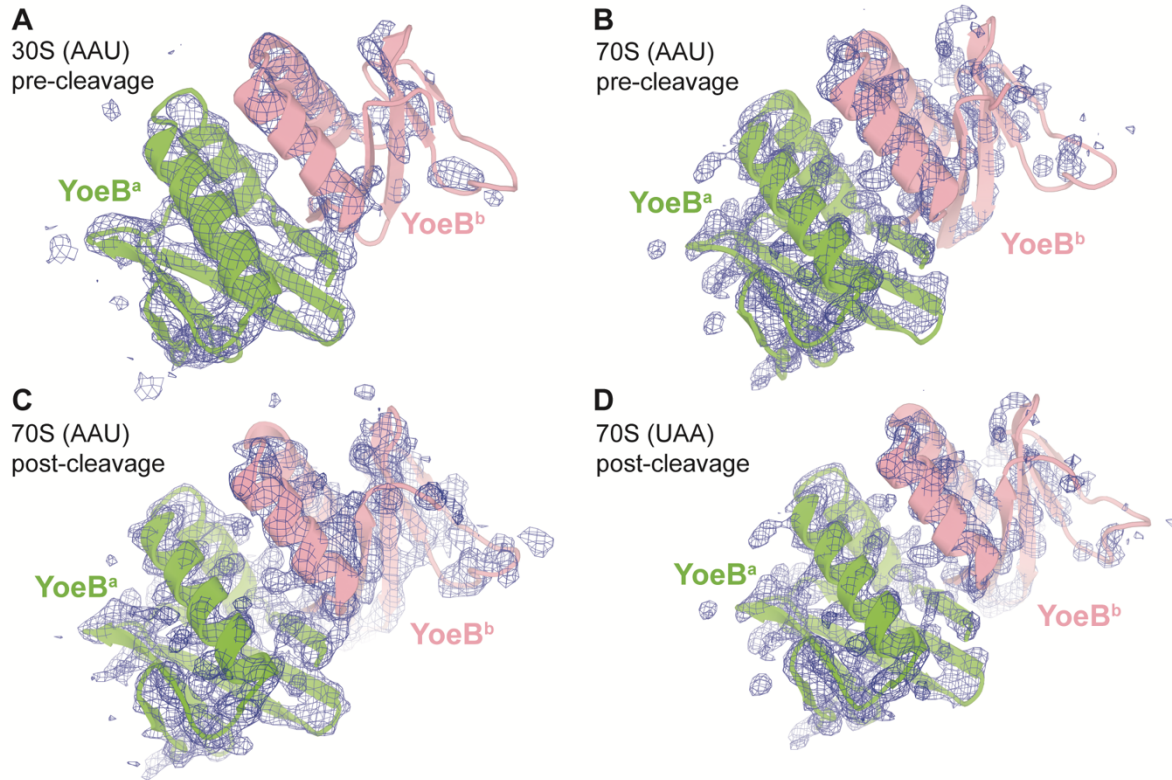
Figure 2.8 – Electron density maps of YoeB bound to the ribosome.

(A) 2Fo-Fc electron density maps (contoured at 1σ) for the YoeB dimer (green and pink) is shown for the 3.7-Å x-ray crystal structure of 30S-YoeB (PDB ID 6NY6); **(B)** the 3.2-Å x-ray crystal structure of 70S-YoeB bound to the A-site AAU asparagine codon in a pre-cleavage state (PDB ID 6OXA); **(C)** the 3.1-Å x-ray crystal structure of the 70S-YoeB bound to the A-site AAU asparagine codon in a post-cleavage state (PDB ID 6OTR); and **(D)** the 3.5-Å x-ray crystal structure of 70S-YoeB post-cleavage state containing an A-site UAA stop codon (PDB ID 6OXI).
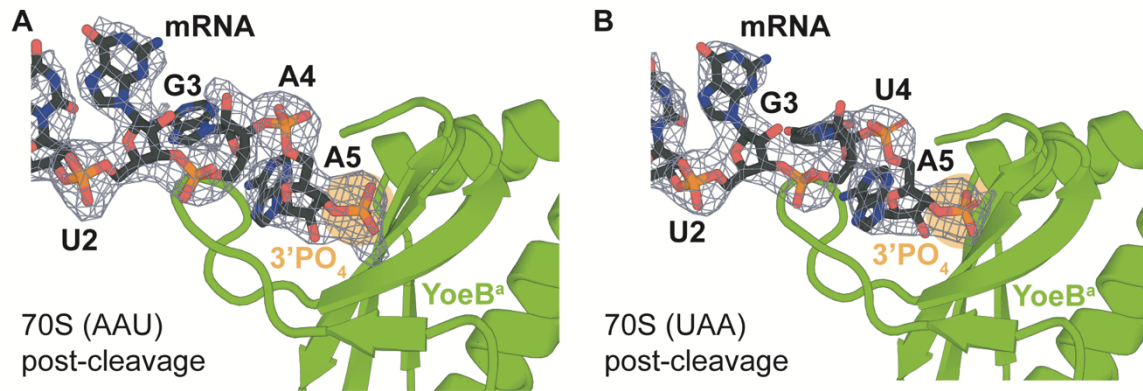
Figure 2.9 – YoeB-mediated mRNA cleavage results in a 3'-phosphate.

(A) A 3.1-Å x-ray crystal structure of 70S-YoeB bound to an A-site AAU asparagine codon in a post-cleavage state is shown (PDB ID 6OTR). 2Fo-Fc electron density map (contoured to 1σ) for mRNA (black) in the A site is shown. The 3'-phosphate resulting from cleavage between the second and third nucleotides of the A-site codon (after A5) is circled in orange. **(B)** A 3.5-Å x-ray crystal structure of the 70S-YoeB bound to an UAA stop codon in a post-cleavage state is shown (PDB ID 6OXI).
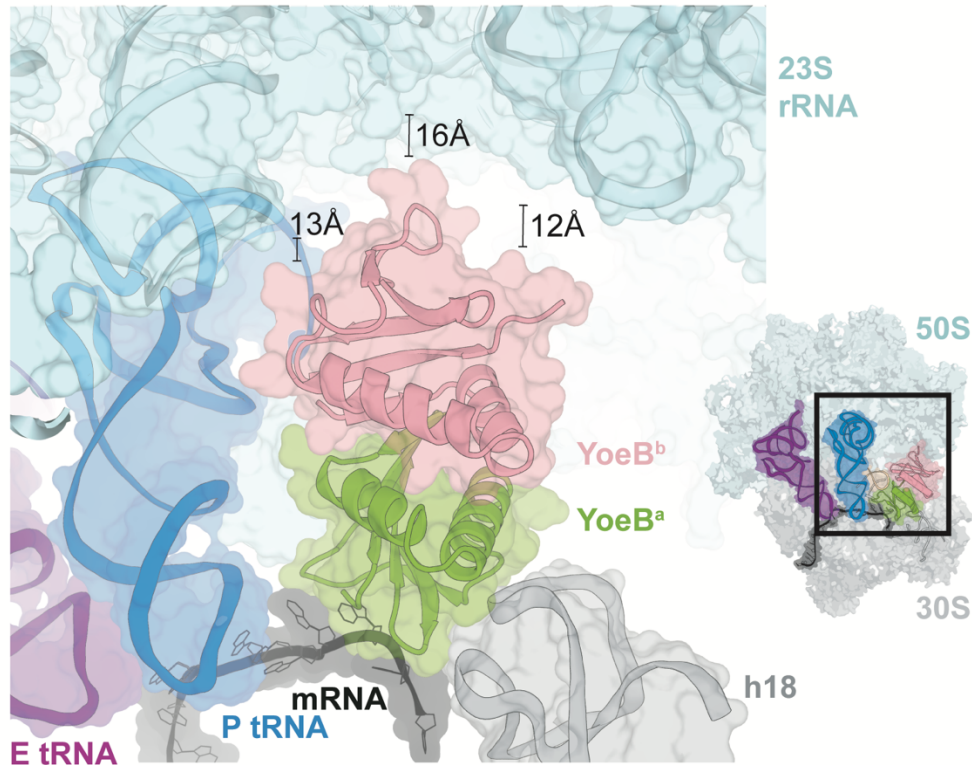
Figure 2.10 – YoeB[b] and the 50S subunit minimally interact.

Pre-cleavage structure of dimeric YoeB bound to the *Thermus thermophilus* 70S ribosome containing an AAU codon (50S and 30S subunits are shown as blue and gray, respectively). The closest points of contact between the backbone of YoeB[b] (pink) and 23S rRNA (cyan ribbon and surface) are shown (13 Å, 16 Å, 12 Å). Distances were measured from the Cα of YoeB[b] residues Glu40, His50, and Tyr84, to the backbone phosphate of 23S rRNA nucleotide C885, Cα of ribosomal protein L25 residue Val180, and backbone phosphate of 23S rRNA nucleotide U1066, respectively. P- and E-site tRNAs are shown in blue and purple, respectively. The YoeB monomer closest to the mRNA path is shown in green (YoeB[a]) and the distal YoeB[b] is shown in pink. Inset: A zoomed out figure of the entire ribosomal complex.
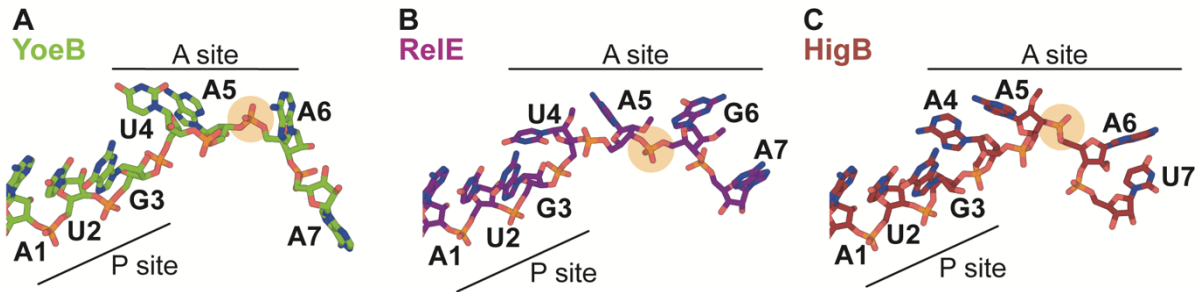
Figure 2.11 – Structural comparison of type II toxins YoeB, RelE, and HigB and their influence on the mRNA path.

(A) The location of the mRNA when YoeB binds to the A site (this study, PDB ID 6OXA; YoeB not shown), **(B)** upon RelE binding (PDB ID 4V7J; RelE not shown) and **(C)** upon HigB binding (PDB ID 4YPB; HigB not shown). In each case, the mRNA is re-positioned to expose the scissile phosphate between nucleotides 5 and 6 of the A-site codon. The P-site mRNA nucleotide is labeled starting from +1. The 3'-phosphate resulting from cleavage between the second and third nucleotides of the A-site codon (after A5) is circled in orange.
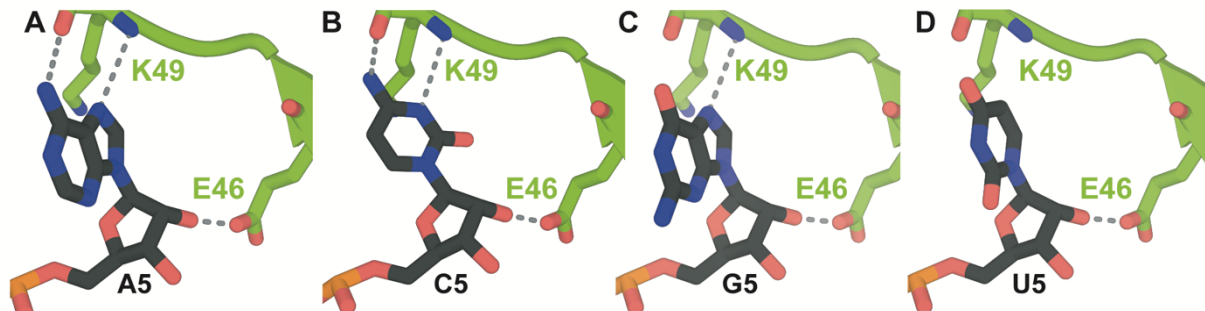
Figure 2.12 – YoeB recognizes either A or C nucleotides at the second position of the mRNA codon.

(A) A5 adopts an *anti* conformation to form hydrogen bonds with Glu46 and Lys49, as seen in our 70S- YoeB pre-cleavage state structure bound to a UAA codon. In all panels, YoeB is removed for clarity. **(B)** A model for C5 in an *anti* conformation at the second nucleotide position shows that a cytosine would be able to form the same hydrogen bonding network as in panel (A). **(C)** A model for G5 at the second nucleotide position shows that a guanosine would be unable to form the same hydrogen bonding network as in panel (A). **(D)** A model for U5 at the second nucleotide position shows that a uridine would be being unable to form the same hydrogen bonding network as in panel (A).
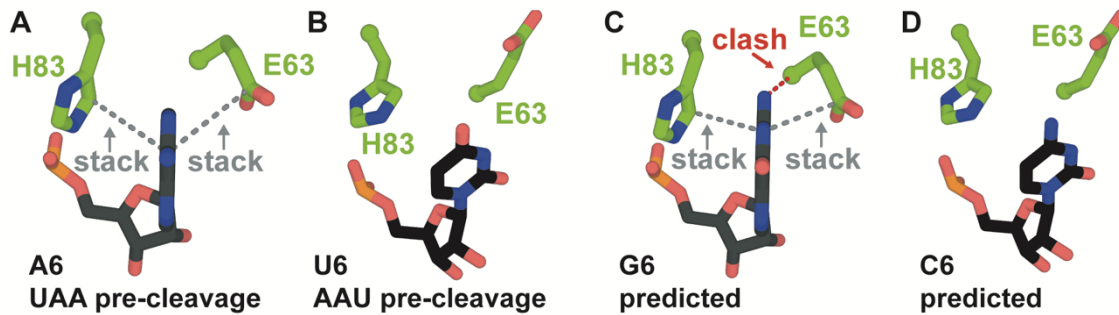
Figure 2.13 – YoeB residues His83 and Glu63 stack with A6, but not U6.

(A) In the 70S-UAA pre- cleavage state with remodeled mRNA, YoeB[a] residues Glu63 and His83 stack (grey dotted lines) with the A6 nucleobase. **(B)** In the 70S-AAU pre-cleavage state (PDB ID 6OXA), U6 does not form the same stacking interaction as in panel (A). Modeling of position A6 with either **(C)** G6 or **(D)** C6 indicates that a purine, but not pyrimidine, would be able to form the same stacking interaction as in panel (A). The backbone of YoeB near residues Glu63 (β2-3 loop) and His83 (after β4) would have to adjust slightly to avoid a potential steric clash when accommodating a G nucleobase as shown in panel (**C**).
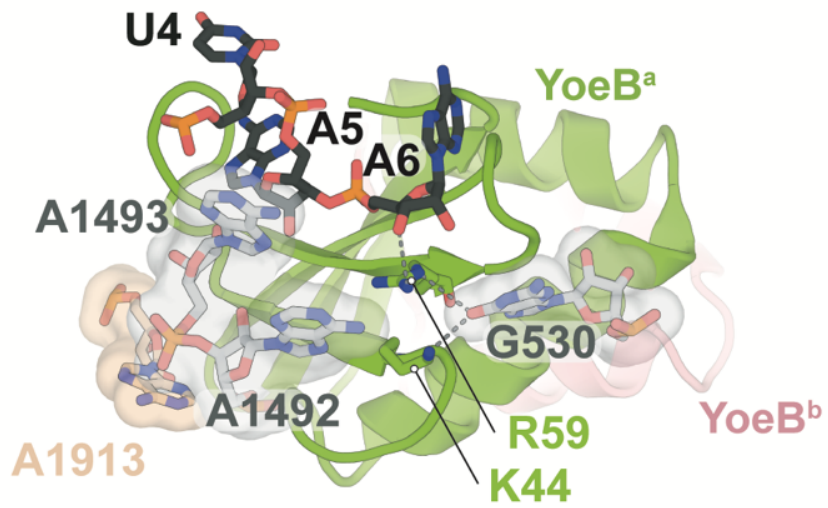
Figure 2.14 – YoeB prevents the interaction between 16S rRNA residues G530 and A1492.

YoeB[a] residues Lys44 and Arg59 form a hydrogen bonding network (grey dashed lines) between G530 and A1492, preventing direct interaction. Color scheme is the same as in Figure 2.1.
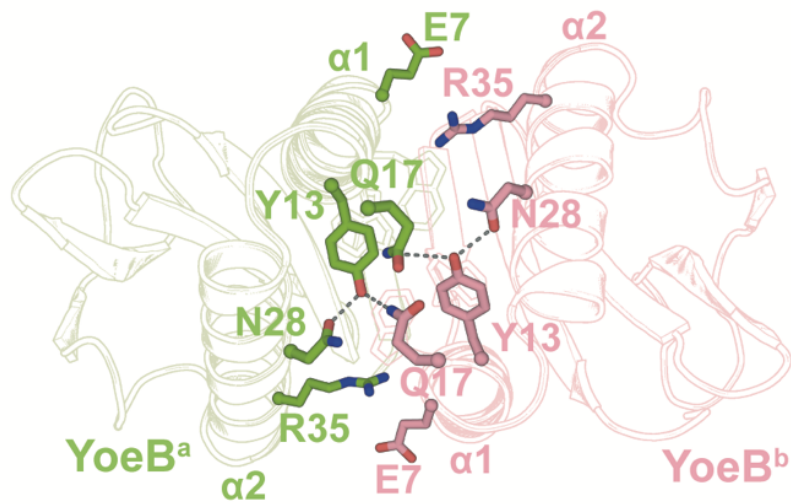
Figure 2.15 – Network of hydrogen bonds between the dimer interface of YoeB[a] and YoeB[b].

YoeB[a] residues (green) that form hydrogen bonds with YoeB[b] residues (pink).
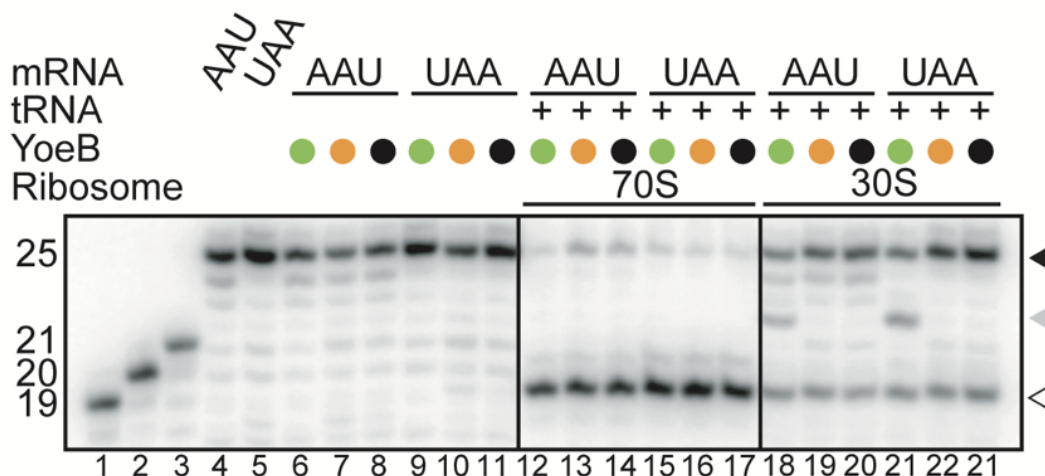
Figure 2.16 – *In vitro* **cleavage assays of** [32]**P-labeled mRNA bound to either a 70S or 30S programmed with P-site tRNA**[fMet]**.**

This figure is identical to Figure 2.6C, except with the addition of control lanes 6-11.The mRNA sequence is the same as shown in Figure 2.1A. Ribosome complexes were formed as described in the Methods section, YoeB was incubated for 10 mins and reactions were quenched and monitored by denaturing PAGE. Both the AAU and UAA mRNAs are cleaved by YoeB when bound to a 30S and 70S complex (lanes 12-21). YoeB variants W5A and W5A/W10A (denoted as ● and ●, respectively) cleave mRNA bound to either the 30S or 70S as compared to wild-type YoeB (●). Full length mRNA is denoted by a closed arrowhead (▲), cleavage product between the second and the third nucleotide of the mRNA codon by an open arrowhead (△) and the extra mRNA band by a gray arrowhead (▲). 19, 20 and 25-mer mRNA standards are shown in lanes 1-3. Controls with mRNA and YoeB variants alone are shown in lanes 6-11. The line separating the gels indicates each region of the figure were taken from different parts of a single gel.
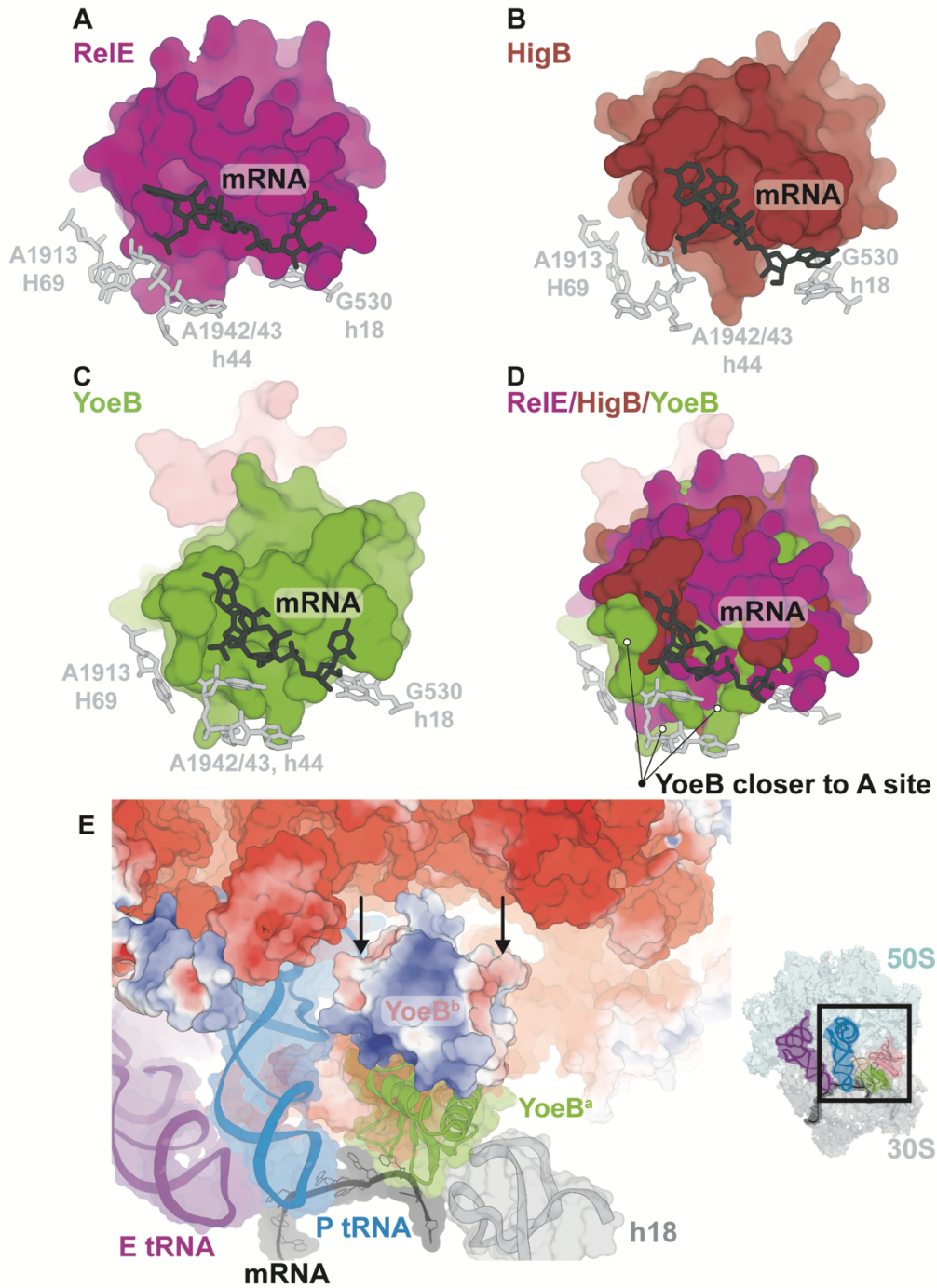
Figure 2.17 – Size and electrostatic surrounding of YoeB help induce conformational changes in the A site.

The positioning of **(A)** RelE (33), **(B)** HigB (69), **(C)** YoeB (this study; PDB ID 6OXA), or

(D) RelE, HigB and YoeB in the A site surrounded by mRNA (black) and H69 residue A1913, h44 residues A1492 and A1493, and h18 G530 (gray) is shown. YoeB occupies more space close to A1913 and nucleotides A1492 and A1493 than any of the other toxins. **(E)** The electrostatic surface potential of YoeB[b] and the 50S subunit are shown, where red and blue depict acidic and basic electrostatic potential respectively. Color scheme and inset is as in Figure 2.10. Two regions of overall negative charge on YoeB[b] are repelled by the overall negative concave surface of the 50S ribosome. Electrostatic potential maps were generated using the Adaptive Poisson-Boltzmann Solver (APBS) plug-in for PyMol version 2.3.1.

Table 2.1 – Data collection and refinement statistics.

	30S-YoeB AAU pre-cleavage	70S-YoeB AAU pre-cleavage	70S-YoeB AAU post-cleavage	70S-YoeB UAA post-cleavage
Data Collection				
Space Group	$P\,4_1\,2_1\,2$	$P\,2_1\,2_1\,2_1$	$P\,2_1\,2_1\,2_1$	$P\,2_1\,2_1\,2_1$
Wavelength (Å)	0.9792	0.9795	0.9795	0.9795
Cell dimensions				
a, b, c (Å)	401.710, 401.710, 175.4400	212.791, 453.079, 608.934	213.364, 451.705, 607.630	214.676, 453.509, 609.501
α, β, γ (degrees)	90, 90, 90	90, 90, 90	90, 90, 90	90, 90, 90
Resolution (Å)	49.83-3.74	126.40-3.25	144.00-3.12	126.50-3.50
	(3.87-3.74)	(3.37-3.25)	(3.23-3.12)	(3.62-3.50)
R_{pim} (%)	4.2 (48.5)	14.5 (74.0)	12.5 (75.9)	13.8 (70.7)
I/σI	11.11 (1.38)	6.05 (1.08)	6.60 (1.12)	5.98 (1.12)
Completeness (%)	97.21 (91.49)	93.43 (75.60)	98.56 (99.31)	98.03 (95.30)
Redundancy	3.3 (2.6)	3.3 (2.3)	3.7 (3.8)	3.2 (3.3)
$CC_{1/2}$	0.999 (0.673)	0.990 (0.348)	0.994 (0.370)	0.994 (0.373)
Refinement				
Reflections	143,160 (13,288)	854,004 (68,654)	1,014,860 (101,652)	729,071 (70,397)
R_{work}/R_{free} (%)	20.6/22.4	23.0/25.6	23.2/25.8	21.6/24.6
No. of atoms	53,249	298,432	298,517	295,153
B-factors (Å^2)				
Overall	171.02	88.93	80.57	101.81
Macromolecule	171.19	89.10	80.68	102.02
Ligand/ion	124.92	45.16	48.00	42.90
Root mean square deviations				
Bond lengths (Å)	0.008	0.006	0.009	0.007
Bond angles (degrees)	1.16	1.02	1.38	1.18

Data for the highest-resolution shell is shown in parentheses.

Table 2.2 – Bacterial strains and plasmids used in Chapter 2.

Strain/plasmid	Description	Source
E. coli strain	Genotype	Reference
BL21-Gold(DE3)pLysS	F- *ompT hsdS$_\beta$(r$_\beta$-m$_\beta$-) dcm$^+$* Tet^r *gal* λ(DE3) *endA* Hte [pLysS Cam^r]	Novagen
BW25113	Δ(*araD-araB)567 ΔlacZ4787(::rrnB-4) lacIp-400(lacIQ)λ- rpoS396*(Am) *rph-1* Δ(*rhaD-rhaB)568 rrnB-4 hsdR514*	(70)
Plasmid	Content	Reference
pBAD33	Expression vector with Cm^r-cassette, P$_{BAD}$ promoter, pACYC184 origin, araC coding sequence, and ara operator	(71)
pBAD-*yoeB*	pBAD33 with *yoeB* gene (5'- NdeI/BamHI -3')	(72)
pBAD-*yoeB*(W5A)	pBAD33 with *yoeB*(W5A) gene (5'- NdeI/BamHI -3')	This paper
pBAD-*yoeB*(W5A·W10A)	pBAD33 with *yoeB*(W5A·W10A) gene (5'- NdeI/BamHI -3')	This paper
pET21c	Expression vector with Amp^r-casette, T7-promoter, pBR322 origin, lacI-coding sequence, lac operator	Novagen
pET21c-*yefM-yoeB*(his$_6$)	pET21c with *yefM* and C-terminal (His)$_6$-*yoeB* genes (5'- NdeI/XhoI -3')	(72)
pET21c-*yefM-yoeB*(his$_6$) (W5A)	pET21c with *yefM* and C-terminal (His)$_6$-*yoeB*(W5A) genes (5'- NdeI/XhoI -3')	This paper
pET21c-*yefM-yoeB*(his$_6$) (W5A·W10A)	pET21c with *yefM* and C-terminal (His)$_6$-*yoeB*(W5A·W10A) genes (5'- NdeI/XhoI -3')	This paper

Table 2.3 – mRNAs used in Chapter 2.

mRNA	Sequence (5' to 3')
AAU (30S-pre)	<u>AAU</u>A$_m$A$_m$A$_m$
AAU (70S-pre)	GCCAAGGAGGUAAAAAUGA$_m$A$_m$U$_m$CAGA
AAU (70S-post)	GCCAAGGAGGUAAAAAUG<u>AAU</u>CAGA
UAA (70S-post)	GCCAAGGAGGUAAAAAUG<u>UAA</u>CAGA

Underlined portions of sequences represent the A-site codon and a 2'-OCH$_3$ modification is depicted as a lower "m".

Table 2.4 – Oligos used in site-directed mutagenesis in Chapter 2.

Oligo pair	Sequence (5' to 3')	Source
W5A, pBAD TM208_F t30g_g31c TM208_R t30g_g31c_R	ggagatatacatatgaaactaatcgcgtctgaggaatcatgggatgatt aatcatcccatgattcctcagacgcgattagtttcatatgtatatctcc	This study
W10A, pBAD TM0209c_F t45g_g46c TM0209c_R t45g_g46c_R	aactaatcgcgtctgaggaatcagcggatgattatctgtactg cagtacagataatcatccgctgattcctcagacgcgattagtt	This study
W5A, pET21c TM204_F, t305g_g306c TM204_R, t305g_g306c_R	gacattattgagtgaaactaatcgcgtctgaggaatcatgggatgatt aatcatcccatgattcctcagacgcgattagtttcactcaataatgtc	This study
W10A, pET21c TM205c_F, t320g_g321c TM205c_R, t320g_g321c_R	aactaatcgcgtctgaggaatcagcggatgattatctgtactg cagtacagataatcatccgctgattcctcagacgcgattagtt	This study
W5A/W10A, pET21c TM0220 TM0220_AS_pET21c	ggatccatatgaaactaatcgcgtctgagg tctcgctcgagataatgataacgacatgc	This study

2.9 References

1. Richter, K., Haslbeck, M. and Buchner, J. (2010) The heat shock response: life on the verge of death. *Mol Cell*, **40**, 253-266.

2. Boutte, C.C. and Crosson, S. (2013) Bacterial lifestyle shapes stringent response activation. *Trends Microbiol*, **21**, 174-180.

3. Kreuzer, K.N. (2013) DNA damage responses in prokaryotes: regulating gene expression, modulating growth patterns, and manipulating replication forks. *Cold Spring Harbor perspectives in biology*, **5**, a012674.

4. Starosta, A.L., Lassak, J., Jung, K. and Wilson, D.N. (2014) The bacterial translation stress response. *FEMS Microbiol Rev*, **38**, 1172-1201.

5. Hiraga, S., Jaffe, A., Ogura, T., Mori, H. and Takahashi, H. (1986) F plasmid ccd mechanism in *Escherichia coli*. *J Bacteriol*, **166**, 100-104.

6. Gerdes, K., Rasmussen, P.B. and Molin, S. (1986) Unique type of plasmid maintenance function: postsegregational killing of plasmid-free cells. *Proc Natl Acad Sci U S A*, **83**, 3116-3120.

7. Gerdes, K., Poulsen, L.K., Thisted, T., Nielsen, A.K., Martinussen, J. and Andreasen, P.H. (1990) The *hok* killer gene family in gram-negative bacteria. *New Biol*, **2**, 946-956.

8. Christensen, S.K., Mikkelsen, M., Pedersen, K. and Gerdes, K. (2001) RelE, a global inhibitor of translation, is activated during nutritional stress. *Proc Natl Acad Sci U S A*, **98**, 14328-14333.

9. Christensen, S.K. and Gerdes, K. (2003) RelE toxins from bacteria and Archaea cleave mRNAs on translating ribosomes, which are rescued by tmRNA. *Mol*

Microbiol, **48**, 1389-1400.

10. Norton, J.P. and Mulvey, M.A. (2012) Toxin-antitoxin systems are important for niche-specific colonization and stress resistance of uropathogenic *Escherichia coli*. *PLoS Pathog*, **8**, e1002954.

11. Helaine, S., Cheverton, A.M., Watson, K.G., Faure, L.M., Matthews, S.A. and Holden, D.W. (2014) Internalization of Salmonella by macrophages induces formation of nonreplicating persisters. *Science*, **343**, 204-208.

12. Page, R. and Peti, W. (2016) Toxin-antitoxin systems in bacterial growth arrest and persistence. *Nat Chem Biol*, **12**, 208-214.

13. Pandey, D.P. and Gerdes, K. (2005) Toxin-antitoxin loci are highly abundant in free-living but lost from host-associated prokaryotes. *Nucleic Acids Res*, **33**, 966-976.

14. Afif, H., Allali, N., Couturier, M. and Van Melderen, L. (2001) The ratio between CcdA and CcdB modulates the transcriptional repression of the *ccd* poison-antidote system. *Mol Microbiol*, **41**, 73-82.

15. Overgaard, M., Borch, J., Jorgensen, M.G. and Gerdes, K. (2008) Messenger RNA interferase RelE controls *relBE* transcription by conditional cooperativity. *Mol Microbiol*, **69**, 841-857.

16. Garcia-Pino, A., Balasubramanian, S., Wyns, L., Gazit, E., De Greve, H., Magnuson, R.D., Charlier, D., van Nuland, N.A. and Loris, R. (2010) Allostery and intrinsic disorder mediate transcription regulation by conditional cooperativity. *Cell*, **142**, 101-111.

17. Bernard, P. and Couturier, M. (1992) Cell killing by the F plasmid CcdB protein involves poisoning of DNA-topoisomerase II complexes. *Journal of molecular*

biology, **226**, 735-745.

18. Jiang, Y., Pogliano, J., Helinski, D.R. and Konieczny, I. (2002) ParE toxin encoded by the broad-host-range plasmid RK2 is an inhibitor of *Escherichia coli* gyrase. *Mol Microbiol*, **44**, 971-979.

19. Zhang, Y., Zhang, J., Hoeflich, K.P., Ikura, M., Qing, G. and Inouye, M. (2003) MazF cleaves cellular mRNAs specifically at ACA to block protein synthesis in *Escherichia coli*. *Mol Cell*, **12**, 913-923.

20. Pedersen, K., Zavialov, A.V., Pavlov, M.Y., Elf, J., Gerdes, K. and Ehrenberg, M. (2003) The bacterial toxin RelE displays codon-specific cleavage of mRNAs in the ribosomal A site. *Cell*, **112**, 131-140.

21. Zhang, Y., Zhang, J., Hara, H., Kato, I. and Inouye, M. (2005) Insights into the mRNA cleavage mechanism by MazF, an mRNA interferase. *J Biol Chem*, **280**, 3143-3150.

22. Jorgensen, M.G., Pandey, D.P., Jaskolska, M. and Gerdes, K. (2009) HicA of *Escherichia coli* defines a novel family of translation-independent mRNA interferases in bacteria and archaea. *J Bacteriol*, **191**, 1191-1199.

23. Christensen-Dalsgaard, M., Jorgensen, M.G. and Gerdes, K. (2010) Three new RelE-homologous mRNA interferases of *Escherichia coli* differentially induced by environmental stresses. *Mol Microbiol*, **75**, 333-348.

24. Winther, K.S. and Gerdes, K. (2011) Enteric virulence associated protein VapC inhibits translation by cleavage of initiator tRNA. *Proc Natl Acad Sci U S A*, **108**, 7403-7407.

25. Winther, K.S., Brodersen, D.E., Brown, A.K. and Gerdes, K. (2013) VapC20 of *Mycobacterium tuberculosis* cleaves the Sarcin-Ricin loop of 23S rRNA. *Nature*

communications, **4**, 2796.

26. Germain, E., Castro-Roa, D., Zenkin, N. and Gerdes, K. (2013) Molecular mechanism of bacterial persistence by HipA. *Mol Cell*, **52**, 248-254.

27. Castro-Roa, D., Garcia-Pino, A., De Gieter, S., van Nuland, N.A., Loris, R. and Zenkin, N. (2013) The Fic protein Doc uses an inverted substrate to phosphorylate and inactivate EF-Tu. *Nat Chem Biol*, **9**, 811-817.

28. Cruz, J.W., Rothenbacher, F.P., Maehigashi, T., Lane, W.S., Dunham, C.M. and Woychik, N.A. (2014) Doc toxin is a kinase that inactivates elongation factor Tu. *J Biol Chem*, **289**, 19276.

29. Cheverton, A.M., Gollan, B., Przydacz, M., Wong, C.T., Mylona, A., Hare, S.A. and Helaine, S. (2016) A Salmonella Toxin Promotes Persister Formation through Acetylation of tRNA. *Mol Cell*, **63**, 86-96.

30. Wilcox, B., Osterman, I., Serebryakova, M., Lukyanov, D., Komarova, E., Gollan, B., Morozova, N., Wolf, Y.I., Makarova, K.S., Helaine, S. *et al.* (2018) *Escherichia coli* ItaT is a type II toxin that inhibits translation by acetylating isoleucyl-tRNAIle. *Nucleic Acids Res*, **46**, 7873-7885.

31. Harms, A., Brodersen, D.E., Mitarai, N. and Gerdes, K. (2018) Toxins, Targets, and Triggers: An Overview of Toxin-Antitoxin Biology. *Mol Cell*, **70**, 768-784.

32. Kamada, K. and Hanaoka, F. (2005) Conformational change in the catalytic site of the ribonuclease YoeB toxin by YefM antitoxin. *Mol Cell*, **19**, 497-509.

33. Neubauer, C., Gao, Y.G., Andersen, K.R., Dunham, C.M., Kelley, A.C., Hentschel, J., Gerdes, K., Ramakrishnan, V. and Brodersen, D.E. (2009) The structural basis for mRNA recognition and cleavage by the ribosome-dependent endonuclease

RelE. *Cell*, **139**, 1084-1095.

34. Heaton, B.E., Herrou, J., Blackwell, A.E., Wysocki, V.H. and Crosson, S. (2012) Molecular structure and function of the novel BrnT/BrnA toxin-antitoxin system of *Brucella abortus*. *J Biol Chem*, **287**, 12098-12110.

35. Schureck, M.A., Maehigashi, T., Miles, S.J., Marquez, J., Cho, S.E., Erdman, R. and Dunham, C.M. (2014) Structure of the *Proteus vulgaris* HigB-(HigA)2-HigB toxin-antitoxin complex. *J Biol Chem*, **289**, 1060-1070.

36. Ruangprasert, A., Maehigashi, T., Miles, S.J., Giridharan, N., Liu, J.X. and Dunham, C.M. (2014) Mechanisms of Toxin Inhibition and Transcriptional Repression by *Escherichia coli* DinJ-YafQ. *J Biol Chem*, **289**, 20559-20569.

37. Prysak, M.H., Mozdzierz, C.J., Cook, A.M., Zhu, L., Zhang, Y., Inouye, M. and Woychik, N.A. (2009) Bacterial toxin YafQ is an endoribonuclease that associates with the ribosome and blocks translation elongation through sequence-specific and frame-dependent mRNA cleavage. *Mol Microbiol*, **71**, 1071-1087.

38. Hurley, J.M. and Woychik, N.A. (2009) Bacterial toxin HigB associates with ribosomes and mediates translation-dependent mRNA cleavage at A-rich sites. *J Biol Chem*, **284**, 18605-18613.

39. Zhang, Y. and Inouye, M. (2009) The inhibitory mechanism of protein synthesis by YoeB, an *Escherichia coli* toxin. *J Biol Chem*, **284**, 6627-6638.

40. Maehigashi, T., Ruangprasert, A., Miles, S.J. and Dunham, C.M. (2015) Molecular basis of ribosome recognition and mRNA hydrolysis by the *E. coli* YafQ toxin. *Nucleic Acids Res*, **43**, 8002-8012.

41. Schureck, M.A., Dunkle, J.A., Maehigashi, T., Miles, S.J. and Dunham, C.M. (2015)

Defining the mRNA recognition signature of a bacterial toxin protein. *Proc Natl Acad Sci U S A*, **112**, 13862-13867.

42. Schureck, M.A., Maehigashi, T., Miles, S.J., Marquez, J. and Dunham, C.M. (2016) mRNA bound to the 30S subunit is a HigB toxin substrate. *RNA*, **22**, 1261-1270.

43. Hurley, J.M., Cruz, J.W., Ouyang, M. and Woychik, N.A. (2011) Bacterial toxin RelE mediates frequent codon-independent mRNA cleavage from the 5' end of coding regions *in vivo*. *J Biol Chem*, **286**, 14770-14778.

44. Christensen-Dalsgaard, M. and Gerdes, K. (2008) Translation affects YoeB and MazF messenger RNA interferase activities by different mechanisms. *Nucleic Acids Res*, **36**, 6472-6481.

45. Christensen, S.K., Maenhaut-Michel, G., Mine, N., Gottesman, S., Gerdes, K. and Van Melderen, L. (2004) Overproduction of the Lon protease triggers inhibition of translation in *Escherichia coli*: involvement of the *yefM-yoeB* toxin-antitoxin system. *Mol Microbiol*, **51**, 1705-1717.

46. Feng, S., Chen, Y., Kamada, K., Wang, H., Tang, K., Wang, M. and Gao, Y.G. (2013) YoeB-ribosome structure: a canonical RNase that requires the ribosome for its specific activity. *Nucleic Acids Res*, **41**, 9549-9556.

47. Christensen, S.K. and Gerdes, K. (2004) Delayed-relaxed response explained by hyperactivation of RelE. *Mol Microbiol*, **53**, 587-597.

48. Janssen, B.D., Garza-Sanchez, F. and Hayes, C.S. (2015) YoeB toxin is activated during thermal stress. *Microbiologyopen*, **4**, 682-697.

49. Clemons, W.M., Jr., Brodersen, D.E., McCutcheon, J.P., May, J.L., Carter, A.P., Morgan-Warren, R.J., Wimberly, B.T. and Ramakrishnan, V. (2001) Crystal structure

of the 30 S ribosomal subunit from *Thermus thermophilus*: purification, crystallization and structure determination. *Journal of molecular biology*, **310**, 827-843.

50. Selmer, M., Dunham, C.M., Murphy, F.V.t., Weixlbaumer, A., Petry, S., Kelley, A.C., Weir, J.R. and Ramakrishnan, V. (2006) Structure of the 70S ribosome complexed with mRNA and tRNA. *Science*, **313**, 1935-1942.

51. Kabsch, W. (2010) Xds. *Acta crystallographica*, **66**, 125-132.

52. Adams, P.D., Afonine, P.V., Bunkoczi, G., Chen, V.B., Davis, I.W., Echols, N., Headd, J.J., Hung, L.W., Kapral, G.J., Grosse-Kunstleve, R.W. *et al.* (2010) PHENIX: a comprehensive Python-based system for macromolecular structure solution. *Acta crystallographica*, **66**, 213-221.

53. Emsley, P., Lohkamp, B., Scott, W.G. and Cowtan, K. (2010) Features and development of Coot. *Acta crystallographica*, **66**, 486-501.

54. Wimberly, B.T., Brodersen, D.E., Clemons, W.M., Jr., Morgan-Warren, R.J., Carter, A.P., Vonrhein, C., Hartsch, T. and Ramakrishnan, V. (2000) Structure of the 30S ribosomal subunit. *Nature*, **407**, 327-339.

55. Painter, J. and Merritt, E.A. (2006) Optimal description of a protein structure in terms of multiple groups undergoing TLS motion. *Acta crystallographica*, **62**, 439-450.

56. Jenner, L.B., Demeshkina, N., Yusupova, G. and Yusupov, M. (2010) Structural aspects of messenger RNA reading frame maintenance by the ribosome. *Nat Struct Mol Biol*, **17**, 555-560.

57. Cruz-Reyes, J., Piller, K.J., Rusche, L.N., Mukherjee, M. and Sollner-Webb, B. (1998) Unexpected electrophoretic migration of RNA with different 3' termini causes a RNA sizing ambiguity that can be resolved using nuclease P1-generated

sequencing ladders. *Biochemistry*, **37**, 6059-6064.

58. Clemons, W.M., Jr., May, J.L., Wimberly, B.T., McCutcheon, J.P., Capel, M.S. and Ramakrishnan, V. (1999) Structure of a bacterial 30S ribosomal subunit at 5.5 A resolution. *Nature*, **400**, 833-840.

59. Ogle, J.M., Murphy, F.V., Tarry, M.J. and Ramakrishnan, V. (2002) Selection of tRNA by the ribosome requires a transition from an open to a closed form. *Cell*, **111**, 721-732.

60. Ying, L. and Fredrick, K. (2016) Epistasis analysis of 16S rRNA ram mutations helps define the conformational dynamics of the ribosome that influence decoding. *RNA*, **22**, 499-505.

61. Hoffer, E.D., Maehigashi, T., Fredrick, K. and Dunham, C.M. (2018) Ribosomal ambiguity (ram) mutations promote the open (off) to closed (on) transition and thereby increase miscoding. *Nucleic Acids Res*.

62. Schureck, M.A., Repack, A., Miles, S.J., Marquez, J. and Dunham, C.M. (2016) Mechanism of endonuclease cleavage by the HigB toxin. *Nucleic Acids Res*, **44**, 7944-7953.

63. Schifano, J.M., Edifor, R., Sharp, J.D., Ouyang, M., Konkimalla, A., Husson, R.N. and Woychik, N.A. (2013) Mycobacterial toxin MazF-mt6 inhibits translation through cleavage of 23S rRNA at the ribosomal A site. *Proc Natl Acad Sci U S A*, **110**, 8501-8506.

64. Schifano, J.M., Vvedenskaya, I.O., Knoblauch, J.G., Ouyang, M., Nickels, B.E. and Woychik, N.A. (2014) An RNA-seq method for defining endoribonuclease cleavage specificity identifies dual rRNA substrates for toxin MazF-mt3. *Nature*

communications, **5**, 3538.

65. Hoffer, E.D., Miles, S.J. and Dunham, C.M. (2017) The structure and function of *Mycobacterium tuberculosis* MazF-mt6 toxin provide insights into conserved features of MazF endonucleases. *J Biol Chem*, **292**, 7718-7726.

66. Culviner, P.H. and Laub, M.T. (2018) Global Analysis of the E. coli Toxin MazF Reveals Widespread Cleavage of mRNA and the Inhibition of rRNA Maturation and Ribosome Biogenesis. *Mol Cell*, **70**, 868-880 e810.

67. Tian, Q.B., Ohnishi, M., Tabuchi, A. and Terawaki, Y. (1996) A new plasmid-encoded proteic killer gene system: cloning, sequencing, and analyzing *hig* locus of plasmid Rts1. *Biochem Biophys Res Commun*, **220**, 280-284.

68. Selmer, M., Dunham, C.M., Murphy, F.V.t., Weixlbaumer, A., Petry, S., Kelley, A.C., Weir, J.R. and Ramakrishnan, V. (2006) Structure of the 70S ribosome complexed with mRNA and tRNA. *Science*, **313**, 1935-1942.

69. Schureck, M.A., Dunkle, J.A., Maehigashi, T., Miles, S.J. and Dunham, C.M. (2015) Defining the mRNA recognition signature of a bacterial toxin protein. *Proc Natl Acad Sci U S A*, **112**, 13862-13867.

70. Datsenko, K.A. and Wanner, B.L. (2000) One-step inactivation of chromosomal genes in *Escherichia coli* K-12 using PCR products. *Proc Natl Acad Sci U S A*, **97**, 6640-6645.

71. Guzman, L.M., Belin, D., Carson, M.J. and Beckwith, J. (1995) Tight regulation, modulation, and high-level expression by vectors containing the arabinose PBAD promoter. *J Bacteriol*, **177**, 4121-4130.

72. Zhang, Y. and Inouye, M. (2009) The inhibitory mechanism of protein synthesis by

YoeB, an *Escherichia coli* toxin. *J Biol Chem*, **284**, 6627-6638.

Chapter 3

Transcriptional repression of the *hig* toxin-antitoxin locus is independent of HigBHigA toxin-antitoxin oligomeric state

Ian Pavelich, Marc A. Schureck, Dongxue Wang, Eric D. Hoffer, Pooja Srinivas, Michelle Boamah, Kimberly Zaldana, Nina Onuoha, Stacey J. Miles, C. Denise Okafor, and Christine M. Dunham

This work is in revision at mBio. Figure numbers and formatting has been slighted edited.

3.1 Abstract

Ubiquitous bacterial type II toxin-antitoxin (TA) gene pairs are regulated via a negative feedback loop whereby their expression is typically responsive to changing levels of toxins at the transcriptional level. While this mechanism can explain how certain TA complexes are regulated, accumulating evidence suggests diversity in this regulation. One system for which the negative feedback loop is not well defined is the plasmid-encoded HigBHigA TA pair originally identified in a post-operative infection with antibiotic-resistant *Proteus vulgaris*. In contrast to other type II TA modules, we find that each *hig* operator functions independently and excess toxin does not contribute to a significant increase in de-repression *in vivo*. Two x-ray crystal structures of HigBHigA bound to *hig* reveal that either a trimer (HigBHigA$_2$) or a tetramer (HigB$_2$HigA$_2$) toxin-antitoxin complex can bind to repress transcription. Comparison of the two structures reveals similar interactions with *hig* are maintained suggesting increasing HigB toxin levels may not result in greater transcriptional repression. Consistent with this result, molecular dynamic simulations reveal both oligomeric states exhibit similar dynamics. Engineering a dedicated trimeric HigBHigA complex does not regulate transcriptional repression. We propose that HigBHigA functions via a simple on/off transcriptional switch regulated by antitoxin proteolysis. The present studies thus expand the known diversity of how these abundant bacterial protein pairs are regulated.

3.2 Introduction

Bacterial toxin-antitoxin (TA) genes are bicistronic operons found in mobile genetic elements and bacterial chromosomes (1-3). There are six different types of TA modules and in each case, the characteristics of the antitoxin distinguishes which type the module belongs to. Type II TA modules are the most abundant and best studied and consist of toxin and antitoxin protein components. These systems form architecturally diverse macromolecular complexes in the absence of external stimuli and during nutrient-rich growth. Although these gene pairs were first identified on plasmids and in bacteriophages (4-9), TAs are highly abundant in free-living bacteria where they appear to have different functions. In their role in plasmid maintenance, the toxin component can induce post-segregational killing if both genes are not inherited (6). In the past few years, conflicting experimental data on the endogenous activities of TAs have led to ambiguity and controversy surrounding their roles in bacterial physiology (10).

Expression of type II TA pairs is autoregulated at the transcriptional level via a negative feedback loop (10-12). Antitoxin proteins contain both a toxin binding domain and a DNA-binding motif to repress at operator sites that overlap with the promoters of TA genes. Toxin proteins are either recruited to their cognate antitoxins bound at these operator sites or the TA complex binds to operators where they function as co-repressors, allowing the system to be responsive to changes in toxin expression levels. Further, TAs can form different oligomeric complexes when bound at operator sites that depends on the ratio of toxin to antitoxin, resulting in a conditional response on transcription called "conditional cooperativity" (e.g. *ccdBccdA*, *relBrelE* and *phddoc*) (13-16). In this mechanism, toxin

binding is enhanced at low molar levels of the toxins-antitoxin but once a high molar ratio is achieved, the toxin functions as a co-repressor. However, conditional cooperativity is not able to describe how all type II TAs are transcriptionally regulated and these outliers include Escherichia coli *mqsRA, hicAhicB* and *dinJyafQ*, and *Proteus vulgaris higBA* (17-20).

The structural diversity and distinct toxin- and DNA-binding motifs of different type II antitoxin proteins may partially explain why they can exert different mechanisms of autoregulation (11). Antitoxins contain ribbon-helix-helix (RHH), helix-turn-helix (HTH), Phd/YefM or SpoVT/AbrB DNA-binding motifs, with RHH and HTH being the most common (19, 21-26). The type of DNA binding motif affects transcriptional repression. HTH-containing antitoxins contain a complete DNA-binding motif while RHH-containing antitoxins contain a half site requiring antitoxin dimerization for DNA binding. TA operons usually contain multiple operator sites and antitoxin binding at adjacent sites can lead to cooperativity and an increase in transcriptional repression (15, 16, 27). Antitoxins are particularly susceptible to proteases especially during changing cellular conditions (28). This reduction in antitoxin concentration increases free toxin levels that when released can inhibit growth. Free toxin can also interact with antitoxins bound at their operators changing the toxin-antitoxin ratio of the TA complex during repression. Changing oligomeric states can lead to changes in how TAs bind to their operator and influence the extent of repression as in the case of the *ccdBccdA, relBrelE*, and *phddoc* systems (Figure 3.1) (15, 16, 23). In the case of the *hicBhicA*, *mqsRmqsA*, and *graTgraA* systems, the toxin competes for antitoxin binding with the operator and solely functions as a de-

repressor (17, 20, 29). Alternatively, other TA systems function as simple on/off transcriptional switches (e.g. *dinJyafQ* and *higBhigA*) (18, 19). While there exists some experimental evidence that distinguishes between these two modes of regulation, the molecular basis for each mechanism is ambiguous because there is little or no structural evidence to support changing toxin-antitoxin molar ratios as a foundation for each model.

The <u>h</u>ost <u>i</u>nhibition of <u>g</u>rowth BA (*higBhigA*) TA module was first identified on the antibiotic-resistance plasmid Rts1 associated with *Proteus vulgaris* and discovered post-operatively in an urinary tract infection (30, 31) (we call this TA pair "HigBHigA" to denote both the HigB toxin and HigA antitoxin proteins). The HigB toxin belongs to the RelE family of toxins, resembles a microbial ribonuclease and cleaves mRNA substrates bound to a translating ribosome (19, 32-35). Although HigBHigA TA pairs are found chromosomally in *E. coli* and in *Pseudomonas putida* and these HigB toxins are also RelE family members (29, 36-38), the structural organization and the regulation of these systems compared to the *P. vulgaris* associated module is different (19). For example, while all known HigA homologs contain a HTH DNA-binding motif, the *P. vulgaris* associated antitoxin binds to each of its operator sites (O1 and O2) in a non-cooperative manner (19, 39). Here, we solve X-ray crystal structures that reveal that the HigBHigA complex binds to its DNA operator as two defined oligomeric ratios, $HigBHigA_2$ and $HigB_2HigA_2$. Although different ratios of type II toxin-antitoxins complex have been proposed to illicit differences in transcriptional repression, we find that both oligomeric forms appear to repress transcription. Further, HigBHigA binds each operator site independent in contrast to other type II modules. These results show an increasing level

of diversity in how toxin-antitoxin modules are transcriptionally regulated and, most surprisingly, even with the *higBhigA* family.

3.3 Materials & Methods

3.3a Strains and plasmids

E. coli BL21(DE3) cells were used for expression of His_6-HigA, His_6-HigBHigA and HigBHigA-His_6 proteins from pET28a, pET28a and pET21c vectors, respectively as previously reported (19). *E. coli* BW25113 cells were used for all β-gal experiments and HigB(H54A)-His_6 expression (49). All point mutations were introduced by site-directed mutagenesis and sequences were verified by DNA sequencing (Genewiz).

3.3b HigA, HigB, and HigBHigA expression and purification

The His_6-HigA, His_6-HigBHigA and HigBHigA-His_6 protein complexes were overexpressed and purified as previously described with minor modifications (19). These differences included incubation of His_6-HigA at 18°C overnight after protein induction and removal of the His_6 tag from His_6-HigA and His_6-HigBHigA with thrombin prior to gel filtration chromatography. HigB(H54A) protein was overexpressed and purified as previously described (45).

3.3c Crystallization, data collection and structure determination of HigBHigA-O2 DNA complexes

The complex was formed by mixing either His_6-HigBHigA or selenomethionine-derivatized HigBHigA-His_6 (both in 40 mM Tris-HCl, pH 7.5, 250 mM KCl, 5 mM $MgCl_2$, and 5 mM β-mercaptoethanol) with O2 operator DNA (10 mM Tris, pH 8, 100 mM NaCl, and 1 mM EDTA) at one $HigB_2HigA_2$ tetramer to one O2 dsDNA molar ratio. The complexes were diluted to 5.95 mg/mL HigBHigA and 1.55 mg/mL O2 DNA by the

addition of buffer (20 mM Tris, pH 8, 10 mM $MgCl_2$, and 100 mM NaCl). Crystals of HigBHigA bound to O2 DNA were grown by sitting drop vapor diffusion and crystallized in 0.2 M $CaCl_2$ and 10-25% (w/v) polyethylene glycol 3,350 at 20°C. Both crystal forms grew after two days and were cryoprotected by serially increasing the concentration of ethylene glycol in the mother liquor from 10-30% (w/v) followed by flash freezing in liquid nitrogen.

Two X-ray datasets were collected at the Northeastern Collaborative Access Team (NE-CAT) 24-ID-C and Southeast Regional Collaborative Access Team (SER-CAT) 22-ID facilities at the Advanced Photon Source (APS) at the Argonne National Laboratory (Table 3.1). For the tetrameric $HigB_2HigA_2$-O2 complex, 360° of data (0.5° oscillations) were collected on a PILATUS 6M-F detector (DECTRIS Ltd., Switzerland) using 0.9792 Å radiation. For the trimeric $HigBHigA_2$-O2 complex, 90° of data (0.5° oscillations) were collected on a MARMOSAIC 300 mm CCD detector (Rayonix, L.L.C., USA) using 1.0 Å radiation. XDS was used to integrate and scale the data (50). The tetrameric $HigB_2HigA_2$-O2 structure was solved by single wavelength anomalous diffraction phasing using AutoSol from the PHENIX software suite (51) and thirteen heavy atom sites were found. The trimeric $HigBHigA_2$-O2 structure was solved using the structure of the $HigA_2$ dimer (PDB code 6CF1) as a molecular replacement search model in the PHENIX software suite. XYZ coordinates, real space, and B-factors (isotropic) were refined iteratively in PHENIX and model building was performed using the program Coot (52). Final refinement of the structures gave crystallographic R_{work}/R_{free} of 17.6/21.8% for trimeric $HigBHigA_2$-O2 and 17.5/22.1% for tetrameric $HigB_2HigA_2$-O2. All figures were created in PyMol (53).

3.3d Molecular dynamics simulations

Starting models for molecular dynamics (MD) simulations were prepared from PDB codes 6W6U (HigB$_2$HigA$_2$-O2) and 6WFP (HigBHigA$_2$-O2). Simulations were performed on the tetrameric or trimeric HigBHigA structures in the absence or presence of O2 DNA (HigB$_2$HigA$_2$-O2, HigBHigA$_2$-O2, HigB$_2$HigA$_2$ and HigBHigA$_2$). All complexes were prepared using the Xleap module of AmberTools 18 (54), the ff14SB forcefield for protein atoms (55) and the OL15 forcefield (56) for DNA. Complexes were solvated in an octahedral box of TIP3P water (57) with a 10 Å buffer. Ions were added to each complex to achieve a final concentration of 150 mM NaCl. Minimization was performed in three rounds, each employing steepest descent (5000 steps) followed by conjugate gradient (5000 steps). In the first round, restraints of 500 kcal/mol-Å^2 were applied to all solute atoms. In the second round, solute restraints were reduced to 100 kcal/mol-Å^2. All restraints were removed in the third round. Complexes were heated from 0 to 300 K with a 100-ps run with constant volume periodic boundaries and restraints of 10-kcal/mol-Å^2 on solute atoms. All MD simulations were performed using AMBER2018 (54, 58, 59). Two stages of equilibration were performed: 10 ns MD in the NPT ensemble with 10-kcal/mol-Å^2 restraints on solute atoms, followed by an additional 10 ns MD run with restraints reduced to 1 kcal/mol-Å^2. Finally, all restraints were removed and 1 microsecond production simulations obtained for each complex. Long-range electrostatics were evaluated with a cutoff of 10 Å and all heavy atom-hydrogen bonds were fixed with the SHAKE algorithm (60). Following MD, the CPPTRAJ module (61) of AmberTools 18 was used to calculate root mean square fluctuations (RMSF) of each protein reside in each

complex.

3.3e Electrophoretic mobility shift assays (EMSAs)

To construct the dsDNA for the EMSA, pairs of complementary single-stranded oligonucleotides were diluted to 2 µM each in 100 mM NaCl, 10 mM Tris-HCl pH8. The O1-O2, O1-O2(scrambled), O1(scrambled)-O2, O1(scrambled)-O2(scrambled) oligonucleotide mixtures (Table 3.2) of the *hig* promoter fragment were incubated in boiling water and then cooled at room temperature overnight. The dsDNA oligos were diluted to 150 nM in EMSA binding buffer (100 mM NaCl, 10 mM $MgCl_2$, 5% glycerol, 0.01 mg/mL bovine serum albumin). Purified wild-type HigBHigA protein was diluted to 10 µM in EMSA binding buffer and serially diluted to give a series of protein concentrations ranging from 25 nM to 0.8 µM. The binding reactions were incubated on ice for 20 min and 10 µL of each reaction was loaded onto 8% native, polyacrylamide-0.5X TBE/10% glycerol gels (50 mM Tris-HCl pH 8, 50 mM boric acid, 5 mM EDTA, 10% glycerol) and subjected to electrophoresis at 110 V limiting on ice for 60 min. To visualize the DNA and DNA-protein complexes, the gels were stained with SYBR green nucleic acid gel stain (ThermoFisher Scientific) in 0.5X TBE/10% glycerol for 30 min with gentle agitation and then the fluorescence was imaged with a Typhoon Trio phosphoimager (GE Healthcare; 488 nm excitation and 526 nm emission). Assays were performed in duplicate with representative gels shown. Band intensities for both free and bound *hig* DNA were quantified with ImageQuant 1D gel analysis software using the rolling ball background subtraction. For HigBHigA bound to either O1 or O2, the binding data were fit using a one site-specific binding equation (Y (specific binding, µM) = Bmax * X / [K_D + X]) in GraphPad

Prism 9.0.0.

3.3f Dianthus binding assays

To determine the affinity of HigBHigA binding when both operators are available, we monitored the change in fluorescence of a 12.5 nM Cy5-labeled *hig* DNA operator (in EMSA binding buffer) upon the addition of increasing amounts of HigBHigA. Purified wild-type HigBHigA was diluted to 325 nM in EMSA binding buffer and serially diluted to give a series of protein concentrations ranging from 50 nM to 325 nM. Reactions were incubated on ice for 10' min. Fluorescence was measured using a Dianthus NT.23 Pico (NanoTemper Technologies) instrument. Fluorescence values were baseline corrected and plotted against HigBHigA concentration. Data of three independent measurements were fit using a specific binding equation with Hill slope equation (Y (specific binding) = Bmax * X^h, /(KD^h+X^h; h = Hill slope) in GraphPad Prism 9.0.0.

3.3g Differential scanning fluorimetry (DSF)

The thermal stability of wild-type HigBHigA and HigB(L5ext)HigA were assessed using a Tycho NT.6 instrument (NanoTemper). Protein was heated at 0.1ºC steps over a temperature range of 35ºC to 95ºC, during which intrinsic fluorescence at 350 and 330 nm was measured. Inflection temperature (T_i) was determined for each apparent unfolding transition from the temperature-dependent change in the ratio of 350 and 330 nm measurements. Assays were performed in triplicates.

3.3h β-galactosidase assays

The *hig* operon was chemically synthesized (IDT), digested and ligated into a pQF50

vector with *lacZ* downstream (pQF50-*hig* constructs). *E. coli* BW25113 transformed with

pQF50-*hig* variants or pBAD33-*higB*(H54A) were used for all experiments. The β-gal

assays in the absence or presence of HigB(H54A) were performed using a method

previously described (39). In both approaches, activity in Miller Units (M.U.) was

measured using the formula: total activity (M.U.) = $(1000*OD_{420})$ / (OD_{600} * volume of

culture used (mL) * 0.5). Assays were performed in triplicate with two technical replicates.

Error bars represent the mean ± SD of values of three independent experiments

performed in technical replicates (raw values shown as dots). Asterisks in the *higBA* group

(blue bars) represent results of a two-tailed Student's t-test in the *higBA* group comparing

% repression of *higBA* operon without HigB(H54A) to *higBA* operon with addition of

HigB(H54A) ($p < 0.001$, t = 44.73, df = 4, ****). Asterisks in the *higB*(L5ext)*higA* group

(pink bars) represent results of a two-tailed Student's t-test comparing % repression of

higB(L5ext)*higA* operon without HigB(H54A) to *higB*(L5ext)*higA* operon with addition of

HigB(H54A) ($p = 0.0163$, t = 4.01, df = 4, *).

3.3i Western blot analysis

E. coli BW25113 cells were transformed with pBAD33-*higB*(H54A) and grown in LB

medium supplemented with 25 μg/mL chloramphenicol at 37 ºC and 0.2% L-arabinose.

Samples were collected and resuspended in lysis buffer (20 mM Tris-HCl pH 7.5, 250

mM KCl, 0.1% Triton X-100, 5 mM β-ME, 0.1 mM benzamidine, 0.1 mM PMSF), free/thaw

cycled 10 times (frozen for 2 minutes in liquid nitrogen, thawed at 37 ºC for 2 minutes,

vortexed for 5 seconds), and diluted to 0.2 OD with Laemmli buffer (20% glycerol, 62.5

mM Tris-HCl, 2% SDS, 0.025% bromophenol blue, and 0.025% β-ME). Samples were

loaded onto a 4-20% TGX SDS-PAGE gel at 0.2OD/lane and run at 125 V for 80 minutes. Gels were removed, washed 3 times, and allowed to equilibrate in western transfer buffer (25 mM Tris-base, 192 mM glycine, 20% methanol, pH 8) for 15 minutes. The gels were then assembled into the blotting cassette and allowed to transfer to Immobilon-FL (Millipore) membranes at 100 V for 45 minutes. Membranes were removed from the blotting cassette and directly blocked with TBS-TT (20 mM Tris-base, 150 mM NaCl, 0.05% tween-20, 0.05% Triton X-100, pH 7.6) containing 3% blocking agent (BioRad), and left shaking overnight at 4 ºC. The next day, membrane were removed from buffer, washed with TBS-TT 3 times for 10 minutes each, and incubated with primary antibody polyclonal rabbit anti-HigBA (a kind gift from Prof. Nancy Woychik) at a 1:12,500 dilution in TBS-TT containing 3% blocking agent for 1 hour at room temperature. Membrane was removed and washed 6 times with TBS-TT for 10 minutes each and then incubated with Goat anti-Rabbit IgG (whole molecule) Peroxidase conjugated secondary antibody (Sigma A0545) at a 1:75,000 dilution for 1 hour at room temperature shaking. Membrane was removed and washed 6 times with TBS-TT for 10 minutes each, and left shaking overnight at room temperature in TBS-TT. The next day, membrane was removed from TBS-TT and washed for 60 minutes at room temperature in TBS (20 mM Tris-base, 150 mM NaCl, pH 7.6). Afterwards, a 1:1 ECL solution (Thermo Pierce) was freshly mixed, pipetted onto the membrane, and allowed to sit in a light-blocked box for 5 minutes for chemiluminescent detection. Membrane was plastic wrapped, placed into an x-ray film cassette, an x-ray film applied on top of the membrane, and exposed for 30 minutes in the closed cassette and subsequently developed with a Konica Minolta SRX-101A automated film developer following manufacturer's instructions.

3.4 Results

3.4a Structure of HigB$_2$HigA$_2$-O2 DNA

The HigBHigA complex forms a tetrameric assembly with two HigB monomers and a HigA dimer (HigB$_2$HigA$_2$) (19). Each HigA antitoxin contains a single HTH DNA-binding motif and forms an obligate dimer, meaning that two HigA antitoxins in one HigB$_2$HigA$_2$ complex bind two inverted repeats of a single DNA operator (19, 39). To determine how HigBHigA interacts with its operator DNA, we pursued a high-resolution X-ray crystal structure of HigBHigA bound to a single operator, O2. We performed crystallization trials using two HigBHigA constructs: a six histidine (His$_6$) affinity tag located at the N terminus of HigB and a His$_6$ affinity tag located at the C terminus of HigA. Both HigBHigA variants crystallized in the same condition, however, each resulted in a different ratio of HigB and HigA bound to O2. The HigBHigA-His$_6$-O2 complex crystalized in the monoclinic space group C2, was determined to 2.4 Å resolution by single wavelength anomalous diffraction phasing and contained a HigA$_2$ dimer bound to two HigB monomers (Figure 3.2). The His$_6$-HigBHigA-O2 complex crystalized in the tetragonal space group I4$_1$, was determined by molecular replacement using the previously determined HigA$_2$ model (PDB code 6CF1) to 2.8 Å resolution and contained a HigA$_2$ dimer bound to a single HigB (Figure. 3.3 and Table 3.1). In both structures, residues 1–91 were built for each HigB monomer (92 total residues) and all nucleotides (1–21) were built for the O2 DNA duplex (Figure 3.9). Residues 1–101 and 1–102 in the HigB$_2$HigA$_2$ structure and residues 1–91 and 1–95 in the HigBHigA$_2$ structure were modeled (104 total residues) (Figure 3.9).

The HTH motif in HigA consists of α2, loop 3 and α3 and this region interacts with the

major groove of the operator O2 DNA (Figure 3.2A). In the tetrameric $HigB_2HigA_2$-O2 structure, HigA contacts the T_{-1}, G_{-2}, T_{-3}, A_{-4} O2 sequence on the *hig* negative strand (39) (Figures 3.2A, B). HigA residue Arg40 interacts with the Hoogsteen face of G_{-2} to make the only sequence-specific protein-DNA contact. Residues Thr34 and Thr37 (from α3) contact the phosphate of G_{+7} while the sidechains of Ser23 (from loop 2), Ser39 (from α3), and Lys45 (from α3) are all within hydrogen bonding distance of nucleotides T_{-7}, A_{-6}, T_{-5}, and T_{-4}, respectively which are located on the opposite DNA strand (Figure 3.10). Additionally, Ala36 and Thr34 form van der Waals interactions with the nucleobase C5 methyl of A_{-3}. These interactions are similar to those previously observed in the $HigA_2$-O2 DNA interaction (39) and are also present between HigA and O2 on the opposite strand, indicating that HigB binding to form the tetrameric $HigB_2HigA2$-O_2 complex does not change interactions of $HigA_2$ with O2.

The termini of antitoxins are typically intrinsically disordered contributing to their proteolysis during external stimuli. In the free $HigA_2$ structure (39), the N terminus is disordered (Figures S3A and B). Upon HigB binding, the HigA termini becomes ordered both in the free $HigB_2HigA_2$ structure (19) and upon binding DNA ($HigB_2HigA_2$-O2 DNA) (Figure 2C and Figures S3C and D). The N- and C-termini of HigA form intramolecular interactions in addition to interactions with α1 of an adjacent HigB in the crystal lattice (Figures 3.11A and B). Specifically, N-terminal residues Arg2 (side chain) and Gln3 (backbone carbonyl) form salt bridges with C-terminal residues Glu80 and Arg77, respectively, and these interactions presumably stabilize the termini. Thus, binding of HigB stabilizes HigA both in the presence or absence of DNA.

Comparison of the overall architecture of $HigB_2HigA_2$-O2 DNA to $HigB_2HigA_2$ (19) or $HigA_2$ (39) reveals subtle changes that may be important for O2 DNA binding and transcriptional repression. Aligning analogous HigA monomers from the $HigB_2HigA_2$-O2 and the $HigB_2HigA_2$ structures (PDB code 4MCX) reveals a ~14° displacement of the adjacent, second HigA protomer (Figure 3.2D). Similarly, comparison of the free $HigA_2$ dimer (PDB code 6CF1) to $HigB_2HigA_2$-O2 also shows rotation of HigA upon DNA binding, although the movement is not as large as compared to when HigB is present (~8° rotation versus a ~14° rotation) (Figure 3.12). Thus, $HigA_2$ reorients to bind DNA and HigB binding to a $HigA_2$-DNA complex minimally influences the protein-DNA interface.

3.4b Structure of $HigBHigA_2$-O2 DNA

As noted above, both the tetrameric $HigB_2HigA_2$-O2 DNA and trimeric $HigBHigA_2$-O2 DNA crystal forms formed in the same crystallization conditions and resulted in two different macromolecular structures (Table 3.1). Interestingly, not all of the interactions seen in tetrameric $HigB_2HigA_2$-DNA are conserved in the trimeric $HigBHigA_2$-O2 structure. While critical interactions of HigA with the T_{-1}, G_{-2}, T_{-3}, A_{-4} recognition sequence are maintained, α2 and α3 of the HTH DNA-binding motif slightly moves away from O2, no longer positioning Ser23 and Lys45 to hydrogen bond with the phosphates of T_{-7} and T_{-4} (Figure 3.3B and Figure 3.10).

Global comparison of the $HigB_2HigA_2$-O2 structure with the $HigBHigA_2$-O2 structure reveal only a ~1° difference emphasizing how similar the two structures are (Figure 3.3D).

Likewise, there are very little differences in the position of HigA$_2$ bound to O2 (39) in the absence or presence of HigB. Thus, it does not appear that HigB binding influences the position of HigA$_2$ on DNA. It appears the largest structural change results from either HigA$_2$ or HigB$_n$HigA$_2$ binding to DNA (~14° rotation, where "n" denotes either a single HigB or two HigB monomers; Figure 3.2D). Previously we described how HigA N-terminal residues Arg2 and Gln3 interact with its C-terminal residues Arg77 and Glu80 in the HigB$_2$HigA$_2$-O2 structure (Figure 3.2C). We find that even a single HigB binding can cause these termini residues to become ordered (Figure 3C and Figure 3.11E).

A curious crystallization note for the trimeric HigBHigA$_2$-O2 complex is that there is an adjacent molecule in the neighboring asymmetric unit that overlaps with the missing HigB (Figure 3.13). This ejection of HigB from the HigBHigA complex is surprising given the known tight interactions of TA complexes where affinities are typically sub-nanomolar (17, 40-42). Therefore, we think it is unlikely that the trimeric HigBHigA$_2$-O2 complex results from crystal packing. Interestingly, the structures of both HigBHigA complexes with the different placement of the His$_6$ tag were solved and both found to be tetrameric HigB$_2$HigA$_2$ in the absence of DNA. Taken together, we propose that there is likely a mixture of both trimeric and tetrameric HigBHigA complexes bound to DNA in solution consistent with mixed ratios of toxin-antitoxin from other systems {Garcia-Pino, 2010 #2009}.

3.4c HigB$_2$HigA$_2$-O2 and HigBHigA$_2$-O2 complexes exhibit similar dynamics

The structure of the trimeric HigBHigA$_2$-O2 complex is intriguing as most models that

describe the transcriptional regulation of type II TA systems conclude that such a toxin-antitoxin ratio is more stable than the fully loaded complex (16, 22, 42). However, prior to our new structure, there has been no biochemical or direct evidence for the existence of this oligomeric state. To assess the dynamics of both complexes in the presence or absence of O2, we performed molecular dynamics (MD) simulations of four complexes: $HigB_2HigA_2$ and $HigBHigA_2$ in the presence or absence of O2 (Figure 3.4). The trimeric $HigBHigA_2$ complex in the absence of DNA has not been solved and we generated the model based upon the $HigBHigA_2$-O2 structure. We obtained 1 microsecond-long MD trajectories of each complex and subsequently performed root mean square fluctuation (RMSF) analysis. This analysis reveals overall comparable dynamics: in tetrameric $HigB_2HigA_2$, binding to O2 only marginally affects dynamics, with the largest effects observed at intrinsically flexible regions such as the C termini of HigA monomers (residues 94-102) and loop 3 of HigB (residues 56-62) (Figure 3.4A). In trimeric $HigBHigA_2$, similar trends are observed, confirming that both oligomeric states represent similarly stable, DNA-bound complexes (Figure 3.4B). One noted difference is that in the trimeric $HigBHigA_2$-O2 complex, the C-termini of one of the two HigAs is disordered and is not modeled. Two HigB monomers binding causes the C-termini of HigA to regain order but while the C-termini of both HigA monomers can be modeled, this region still exhibits dynamic behavior.

3.4d HigBHigA binding at O1 or O2 operators is independently regulated

The *hig* promoter (P*hig*) is negatively autoregulated by the HigBHigA complex binding at operators O1 and O2 that overlap with the -35 and -10 promoter sites (31) (Figure 3.5A).

To determine if we could build oligomeric complexes *in vitro*, we monitored the binding of

the HigBHigA complex to *hig* (O1 and O2) using an electrophoretic mobility shift assay

(EMSA) (Figure 3.5B). The HigBHigA complex was purified according to previously

published protocols and the DNA probe used in the EMSA consists of the entire 61

basepair (bp) operator region (Table 3.2). To determine whether HigBHigA binds with high

affinity to either O1 or O2, all 21 nucleotides in each operator were randomized

individually (39). Each of these 21 nucleotides located in either O1 or O2 were previously

shown to be protected upon HigA binding (43). Therefore, any change in the mobility of

the DNA band using a scrambled O1 or O2 would represent binding of HigBHigA to a

single operator. HigBHigA binds to each of the two sites represented as a single molecular

weight shift and both result in similar dissociation binding constants (0.36 ± 0.09 µM for

O1 and 0.24 ± 0.04 µM for O2) (Figure 3.5B and Table 3.3). HigBHigA was unable to bind

to operator DNA containing both scrambled O1 and O2 (Figure 3.14). Titration of

HigBHigA with a constant amount of *hig* causes two molecular weight shifts, indicating

binding of HigBHigA at each operator site (Figure 3.5C, top). To determine a quantitative

measure of binding of HigBHigA to both operators, we used a Cy5-labeled *hig* containing

both O1 and O2 (61 bp). Increasing concentration of HigBHigA were added to *hig* that

resulted in a dissociation binding constant of 0.24 ± 0.09 µM. The data were plotted to

yield a Hill coefficient of 0.87 which indicates that the system is non-cooperative.

Additionally, the K_D can explain both binding of HigBHigA at both O1 and O2 which is

similar to what was acquired when binding at each site was measured independently.

Together, these data indicate that HigBHigA recognizes each operator independently to

form a high affinity interaction. This observation appears to be an important distinction

from other type II TAs where TA complexes binding at an operator influences the binding of TAs at adjacent operators (Figure 3.1).

3.4e Both trimeric HigBHigA$_2$ and tetrameric HigB$_2$HigA$_2$ repress P*hig*

At this point, we assume the majority of the HigBHigA complex used in the EMSA is tetrameric HigB$_2$HigA$_2$ for two reasons. First are the prior HigB$_2$HigA$_2$ structures that reveal the complex to be tetrameric (19). And second, if there were multiple oligomeric states of HigBHigA binding that would be observed in the EMSA as an increase in the number of bands present, which we do not observe (Figure 3.5B). To test whether a trimeric HigBHigA$_2$ complex represses transcription to the same extent as HigB$_2$HigA$_2$, we attempted to engineer such a variant. Comparison of the HigB$_2$HigA$_2$ structure with the HigB$_2$HigA$_2$-O2 DNA structure shows that the two HigB monomers move closer to each other to accommodate binding to DNA (Figure 3.6A). In particular, HigB loop 5 (L5) located at the interface of the HigB monomers moves ~4Å (Figure 3.6A). We therefore extended L5 by the addition of a short, flexible sequence of four residues (Asn, Gly, Asn, Gly (NGNG) called HigB(L5ext)HigA$_2$). This extension is predicted to prevent concurrent binding of two HigB monomers to HigA$_2$ (Figure 3.6A). Expression and purification of HigB(L5ext)HigA$_2$ showed a delayed elution of the complex from the size exclusion column as compared to wild-type HigB$_2$HigA$_2$ (Figure 3.6B), at a volume corresponding to a molecular weight of 42 kDa (compared to 56 kDa for wild-type HigB$_2$HigA$_2$). The difference in apparent molecular weights indicates that the HigB(L5ext)HigA$_2$ complex is ~14 kDa smaller than the wild-type complex which roughly corresponds to a HigB monomer (molecular weight of ~13 kDa). To assess its thermal stability, we performed

nano-differential scanning fluorimetry (nano-DSF) which provides information on the melting temperature (T_m) of the complex. Since this measurement is not at equilibrium, the inflection point is known as T_i. HigB(L5ext)HigA$_2$ is ~5ºC less thermostable than wild-type HigB$_2$HigA$_2$ (60.5ºC vs. 54.0ºC) consistent with an altered oligomeric state (Figure 3.6C).

To compare the differences of wild-type HigBHigA (which we presume is predominantly HigB$_2$HigA$_2$) to trimeric HigB(L5ext)HigA$_2$ transcriptional repression *in vivo*, we designed a series of constructs that encode *lacZ* in three different contexts: downstream of the P*hig* promoter (pQF50-P*hig-lacZ*), downstream of P*hig* but also containing *higB*(H54A)*higA* (pQF50-P*hig-higB*(H54A)*higA-lacZ*), and downstream of P*hig* but also containing *higB*(L5ext)*higA* (pQF50-P*hig-higB*(L5ext)*higA-lacZ*). Although there is a weak predicted promoter for HigA (called P*higA*), this promoter is not controlled by HigBHigA and therefore, its influence is minimal (44). The HigB(H54A) variant was used because this amino acid change renders the HigB toxin inactive and thereby prevents inhibition of growth (34, 45). We also tested whether HigB(H54A) binds to HigA and we confirm the mutation does not prevent the HigBHigA interaction (Figure 3.15A). As expected, P*hig* alone shows high β-gal activity (~3300 MUs, normalized to 0% repression) because of the absence of transcriptional repressor HigA. When both HigB and HigA are expressed (P*hig-higBhigA-lacZ*), there is little β-gal activity indicating robust HigA repression at P*hig* (~17 MUs; ~99.5% repression) (Figure 3.7). In the presence of trimeric HigB(L5ext)HigA$_2$, there is similar repression as wild-type HigBHigA (~55 MUs; ~98.3% repression).

One possibility that we wanted to explore was whether *hig* is responsive to changing HigB toxin levels *in vivo* considering that toxin overexpression in the *phddoc*, *ccdBccdA* and *relErelB* systems can relieve repression (15, 16, 27). For this assay, we overexpressed the same HigB(H54A) variant whose expression was previously detected by Western blot analysis (34, 45). We additionally confirm that in these strains containing different *lacZ* constructs that we observe HigB(H54A) expression and that this mutation does not prevent HigB from binding to HigA (Figure 3.15B). Overexpression of HigB(H54A) shows a minor effect on repression of P*hig-higBhigA* where β-gal activity increases from ~17 MUs to ~94 MUs (repression of 97.2% vs. 99.5%; Figure 3.7) while the full activity of P*hig* is ~3300 MUs. In the case of the engineered HigB(L5ext)HigA$_2$, excess HigB(H54A) expression also has a minimal effect on repression where β-gal activity increases from ~55 MUs to ~67 MUs (98.3% vs 97.9% (excess HigB) Figure 3.7). These data suggest *hig* repression is minimally influenced by changing ratios of HigB toxin to HigA antitoxin.

3.5 Discussion

The roles of bacterial TA modules have been controversial owing to experimental errors in the construction of *E. coli* TA deletion strains and the ambiguity over what activates toxin expression, antitoxin proteolysis and the release of toxin (10, 46, 47). While these activities are still under debate, the way these modules are transcriptionally autoregulated is known to clearly contribute to their changing expression patterns in response to external stimuli although many outstanding questions remain (15, 16, 27). One question is how changing ratios of TA complexes influence physical interactions with their DNA operators and the assembly and/ or cooperativity of TA complexes bound at adjacent operator sites.

In this study, we focus on the regulation of the *higBhigA* TA module first identified on the antibiotic-resistance Rts1 plasmid associated with a urinary tract infection caused by *P. vulgaris* (31). Our prior work revealed that while the *P. vulgaris* HigB toxin adopts a canonical microbial ribonuclease fold that is similar to other members of the RelE family (19), the structure of the HigA antitoxin and its autoregulation of *hig* revealed important differences as compared to other known type II modules. For example, HigA does not contain intrinsically disordered termini, HigA did not wrap around the HigB toxin to suppress toxicity, and the binding of the HigB toxin does not influence repression at *hig* (19, 45). All of these differences center on the diversity of the HigA antitoxin, strongly suggesting that autoregulation of transcription may also be different. We therefore sought to understand how the *higBhigA* operon is regulated and how its diverse architecture might influence its transcriptional repression.

130

Other type II TA modules including *ccdBccdA*, *kiskid*, *relBrelE* and *phddoc* are all regulated by changing toxin levels (15, 16, 23, 48). In the case of *relBrelE* where the RelE toxin is very similar to HigB, the trimeric RelB$_2$RelE is proposed to bind with high affinity to the *rel* operator (16, 22) while the tetrameric RelB$_2$RelE$_2$ represents a low affinity complex for *rel* that causes de-repression. However, the tetrameric RelB$_2$RelE$_2$ is the only state that has been observed (22). This model permits the system to be responsive to changing levels of toxin but at this point, there is limited biochemical and structural data that corresponds to these changing oligomeric states.

The structure of *P. vulgaris* HigBHigA in the absence of *hig* reveals a tetrameric architecture with two HigB and two HigA protomers (HigB$_2$HigA$_2$) (19). The HigB toxin does not influence the affinity of HigA for *hig* and thus, *hig* does not appear to be regulated by conditional cooperativity. Therefore, it was surprising when we serendipitously solved two different structures of the HigBHigA-O2 complexes that differ in their molar ratios of HigA antitoxin to the HigB toxin (Figures. 3.2 and 3.3). The different oligomeric HigBHigA complexes bound to *hig* thus capture, for the first time, how different ratios of toxin-antitoxin complexes interact with their operator despite the *higBhigA* operon not regulated by these changing toxin ratios. The trimeric HigBHigA$_2$-O2 DNA structure was especially unexpected given that the tetrameric HigB$_2$HigA$_2$ form predominates in the absence of operator (19). In an attempt to perturb the system *in vivo* by increasing HigB concentrations in the presence of the HigBHigA complex bound at O1 and O2 operators, we find no observable change in repression in contrast to other TA systems (Figure 3.7).

131

Engineering of a forced trimeric HigBHigA$_2$ complex revealed similar levels of transcriptional repression (Figure 3.7). The molecular interactions of each HigBHigA complex with *hig* are largely maintained, suggesting that different HigB amounts may not contribute to changes in repression for this system. Molecular dynamic simulations of both the trimeric and tetrameric HigBHigA-O2 complexes show each complex have similar dynamics when bound to DNA, offering further support for the ability of both oligomeric states to contribute to repression (Figure 3.4). Together, these data support a model where *hig* is incalcitrant to changing levels of toxin and may instead, be influenced solely by HigA proteolysis.

Most comparisons to this point have been made of HigBHigA to other type II modules however, HigBHigA shares high sequence (29%) and structural similarity (overall r.m.s.d. of 2.5 Å for residues 23–92) with the GraTGraA system from *Pseudomonas putida* (29) (Figure 3.8). Despite these similarities, there are several key differences in regulation. Although the GraT toxin adopts a microbial ribonuclease fold similar to HigB, the N-terminal 23 amino acids are disordered while in the HigB structure, these residues form interactions with a HigA monomer. Further, GraA binding to its operator causes high levels of repression yet the GraT toxin is unable to bind to GraA while simultaneously bound to DNA. While both GraT and HigB toxins are not co-repressors in contrast to other type II toxins, in fact, the way these two structurally similar toxins function is completely different. The GraT toxin dissociates GraA antitoxin from its operator causing de-repression while HigB can bind to HigA-operator complex. Additionally, the binding of the GraA antitoxin at its operator is highly cooperative while this is not the case for HigA

antitoxin. This diversity between GraTGraA and HigBHigA is surprising but adds to the rich diversity of toxin-antitoxin modules even among complexes within the same family and that appear, at first glance, to be the same.

The results presented here provide new insight into the transcriptional regulation of the plasmid-associated *hig* operon and add to the growing diversity of mechanisms used to balance transcriptional responses of these abundant bacterial gene pairs. In the future, additional biophysical studies are needed to reconcile the role of changing macromolecular complex formation in the regulation of TA pairs and to align these properties with transcriptional responsiveness.

3.6 Acknowledgements

3.7 Funding

Figure 3.1 – Diverse transcriptional control mechanisms that regulate expression of toxin-antitoxin complexes.

Toxin (T) and antitoxin (A) proteins form multimeric complexes that bind operator sites (O1 and O2) that overlap with their promoters (P_{TA}) to repress transcription. (**A**) In some type II toxin-antitoxin systems, changing levels of toxins (due to antitoxin proteolysis) that bind to the repressor complex leads to steric clashes and/or changes in affinity causing de-repression. In this case, the system functions as a molecular rheostat responsive to toxin levels. (**B**) In contrast, other toxin-antitoxin systems are not sensitive to changes in toxin concentrations and thus function as on/off transcriptional switches dependent on

antitoxin depletion from proteolysis.
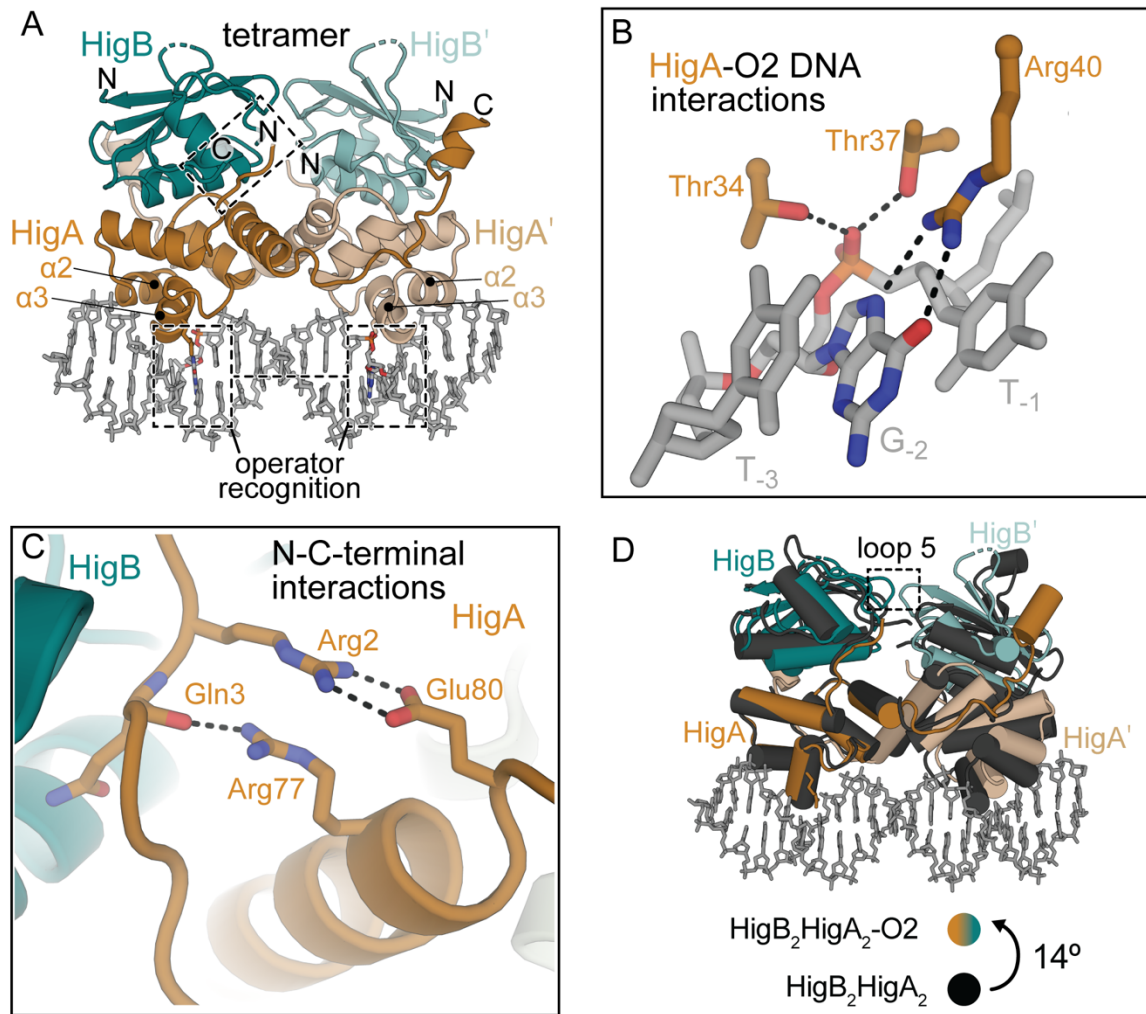
Figure 3.2 – Structure of tetrameric HigB$_2$HigA$_2$ bound to O2 DNA.

(**A**) The 2.4-Å structure of tetrameric HigB$_2$HigA$_2$-O2 DNA complex (PDB code 6W6U). HigA recognizes the T$_{-1}$, G$_{-2}$, T$_{-3}$, A$_{-4}$ DNA operator region via α2 and α3. N and C-terminal regions of HigA are boxed. (**B**) HigA Arg40 makes the only sequence specific interactions with the nucleobase of G$_{-2}$ while HigA residues Thr34 and Thr37 (both from α3) stably interact with the phosphate of G$_{-2}$. (**C**) The N- and C-terminal residues of HigA become ordered upon both HigB binding. HigA residue Arg77 forms a hydrogen bond with the backbone carbonyl of Gln3 and Arg2 and Glu80 interact via a salt bridge. (**D**) Comparison

of the tetrameric HigB$_2$HigA$_2$ complex (all black; PDB code 4MCX) and HigB$_2$HigA$_2$-O2

DNA complex (PDB code 4MCX) reveal a ~14º rotation of HigB$_2$HigA$_2$ away from DNA

that allows recognition.
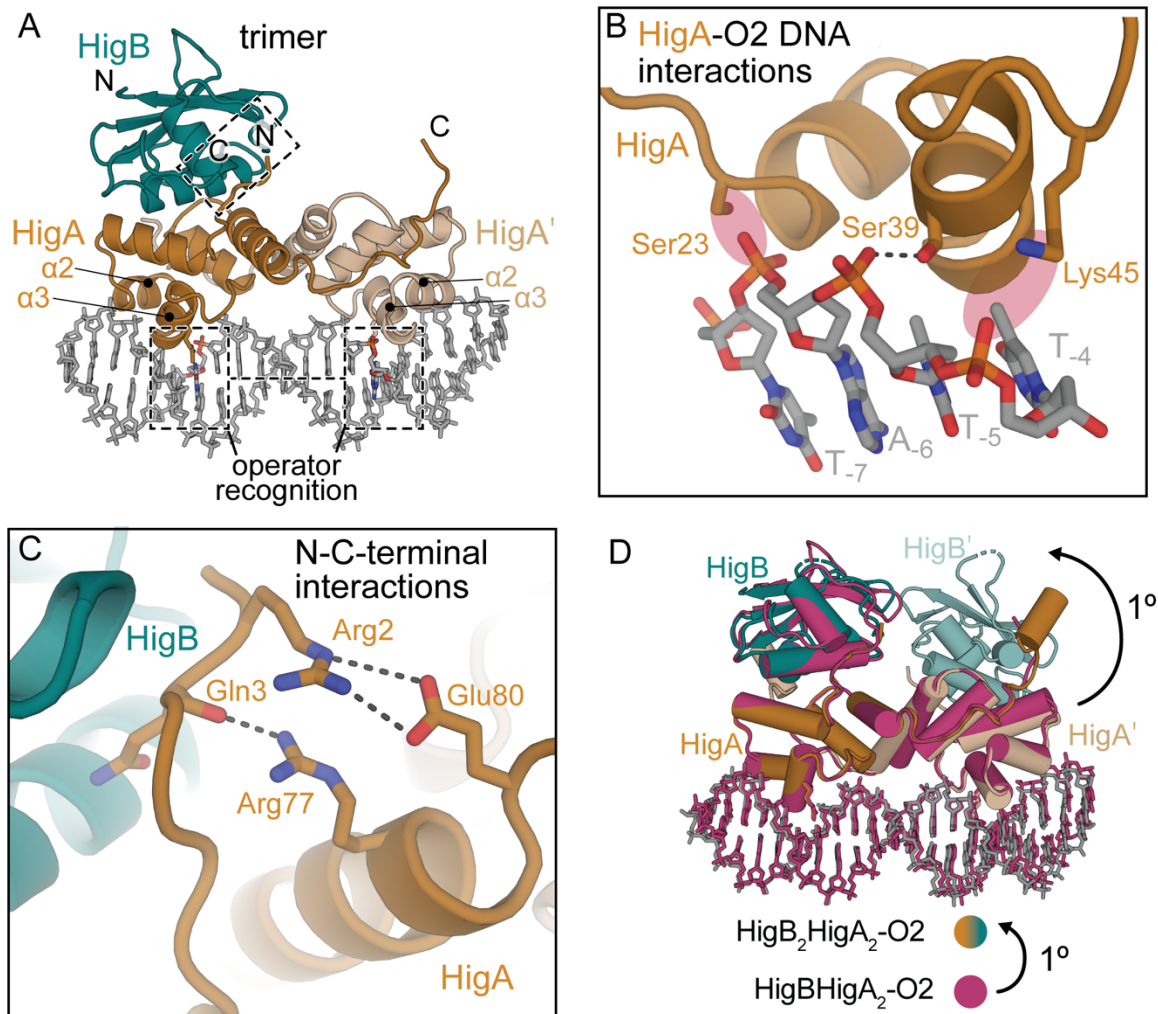
Figure 3.3 – Structure of trimeric HigBHigA$_2$ bound to O2 DNA.

(**A**) The 2.8-Å structure of trimeric HigBHigA$_2$-O2 DNA (PDB code 6WFP). HigA recognizes the T$_{+6}$, G$_{+7}$, T$_{+8}$, A$_{+9}$ DNA region via α2 and α3. N and C-terminal regions of HigA are boxed. (**B**) In the HigB$_2$HigA$_2$-O2 DNA structure (PDB code 6W6U), HigA residues Ser23, Ser39, and Lys45 interact with the backbone phosphate of T$_{-7}$, T$_{-5}$, and T$_{-4}$ respectively to rigidify the T$_{-1}$, G$_{-2}$, T$_{-3}$, A$_{-4}$ sequence for nucleotide-specific recognition on the opposite strand. In the trimeric HigBHigA$_2$-O2 structure, only Ser39 interacts with the phosphate backbone and Ser23 and Lys45 are too distant (red highlighted region).

(**C**) The N- and C-terminal residues of HigA become ordered upon a single HigB monomer binding similar to when two HigB monomers bind (Figure 3.4C). (**D**) Comparison of trimeric HigBHigA$_2$-O2 DNA (pink; PDB code 6WFP) and tetrameric HigB$_2$HigA$_2$-O2 DNA (PDB code 6W6U) are incredibly similar with an r.m.s.d of 0.7 Å (for 1479 equivalent atoms) and less than a ~1° rotation.
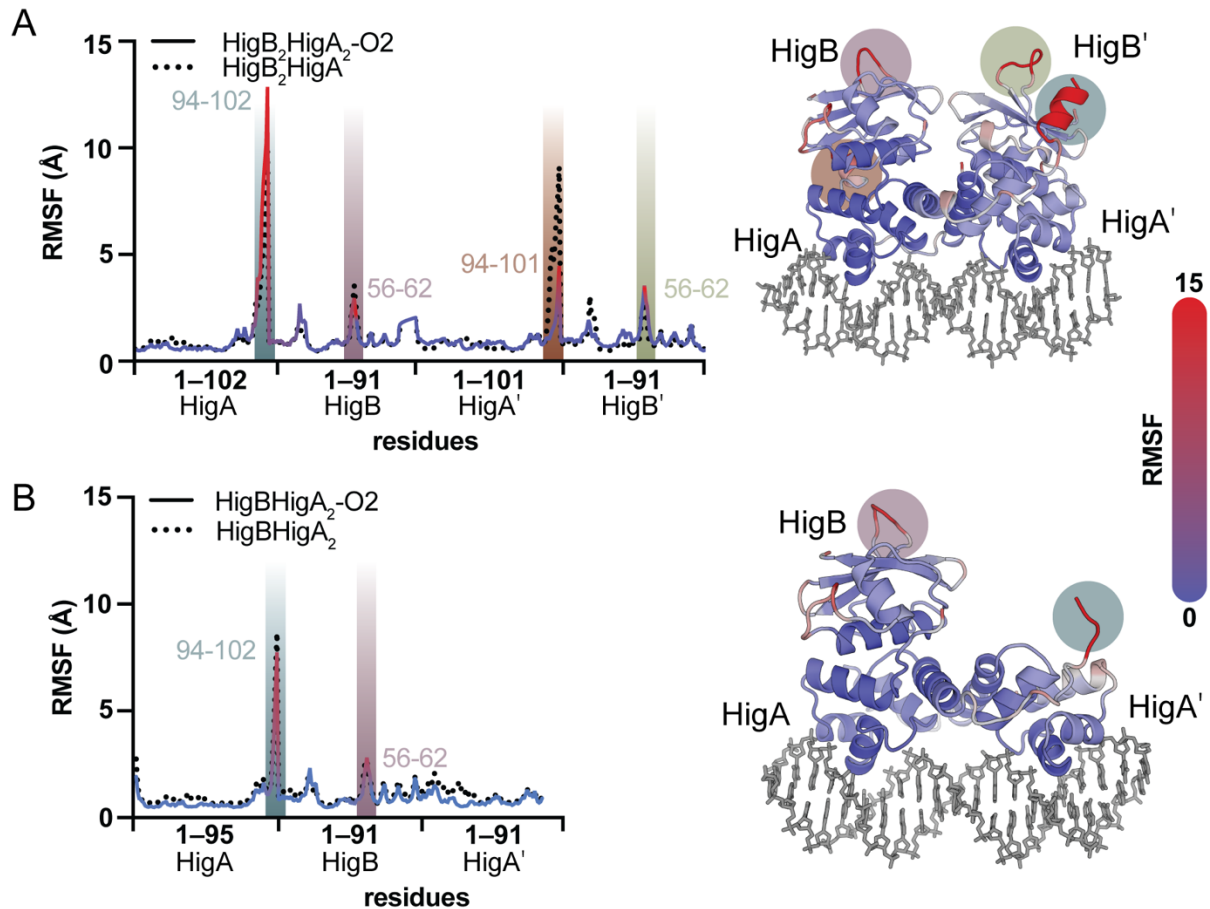
Figure 3.4 – Trimeric HigBHigA₂ and tetrameric HigB₂HigA₂ exhibit similar dynamics in the presence or absence of O2 DNA.

Root-mean-square-fluctuations (RMSFs) of Cα atoms for each residue in the (**A**) HigBHigA₂ or (**B**) HigB₂HigA₂ complexes are calculated from 1 ms MD trajectories. Regions that have increased RMSFs are indicated with highlighted bars that correspond to their positions on the HigBHigA-O2 structures (right). High RMSF spikes correlate to either labile C termini of HigA or HigB loop regions with colored circles corresponding to the highlighted bars on the left.
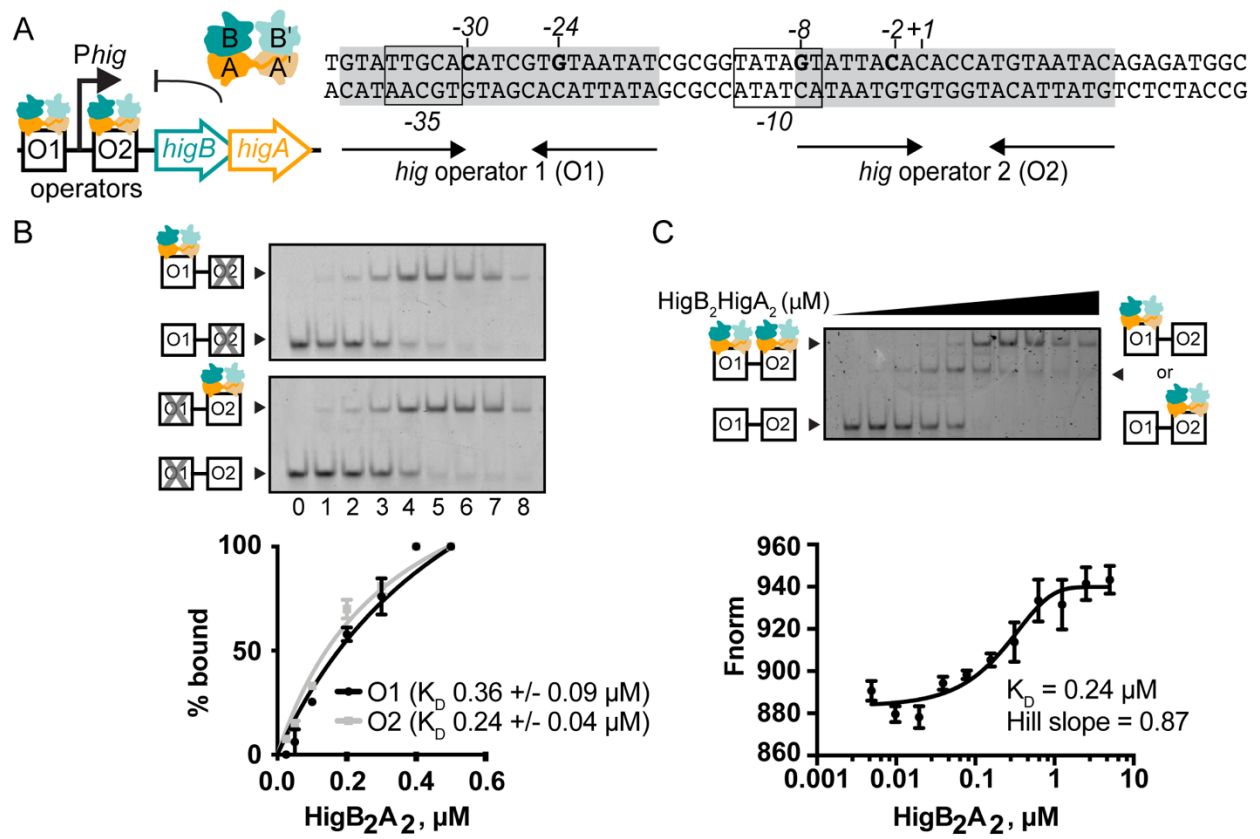
Figure 3.5 – Binding of HigB₂HigA₂ to a single operator is sufficient for transcriptional repression of the *hig* operon.

(**A**) *Left*, organization of the *hig* operon containing the operators O1 and O2, the P*hig* promoter, *higB* toxin and *higA* antitoxin genes. *Right*, the nucleotide sequences of O1 and O2, with the +1 transcriptional start site and the -35 and -10 sites indicated. The sequence recognized by HigA is shown in grey and operator nucleotides C_{-30}, G_{-24}, G_{-8}, and C_{-2} important for HigA binding are shown in bold. (**B**) EMSA of HigB₂HigA₂ binding to wild-type P*hig* (top), O1 only (O2 scrambled; middle), and O2 only (O1 scrambled; bottom) DNA. Band intensities were plotted from EMSAs as the percent of HigB₂HigA₂ bound to DNA versus HigB₂HigA₂ concentration (concentrations used: 0, 0.025, 0.05, 0.1, 0.2, 0.3,

0.4, 0.5, 0.6, 0.7, 0.8). Curves represent the fit from which K_Ds were calculated.
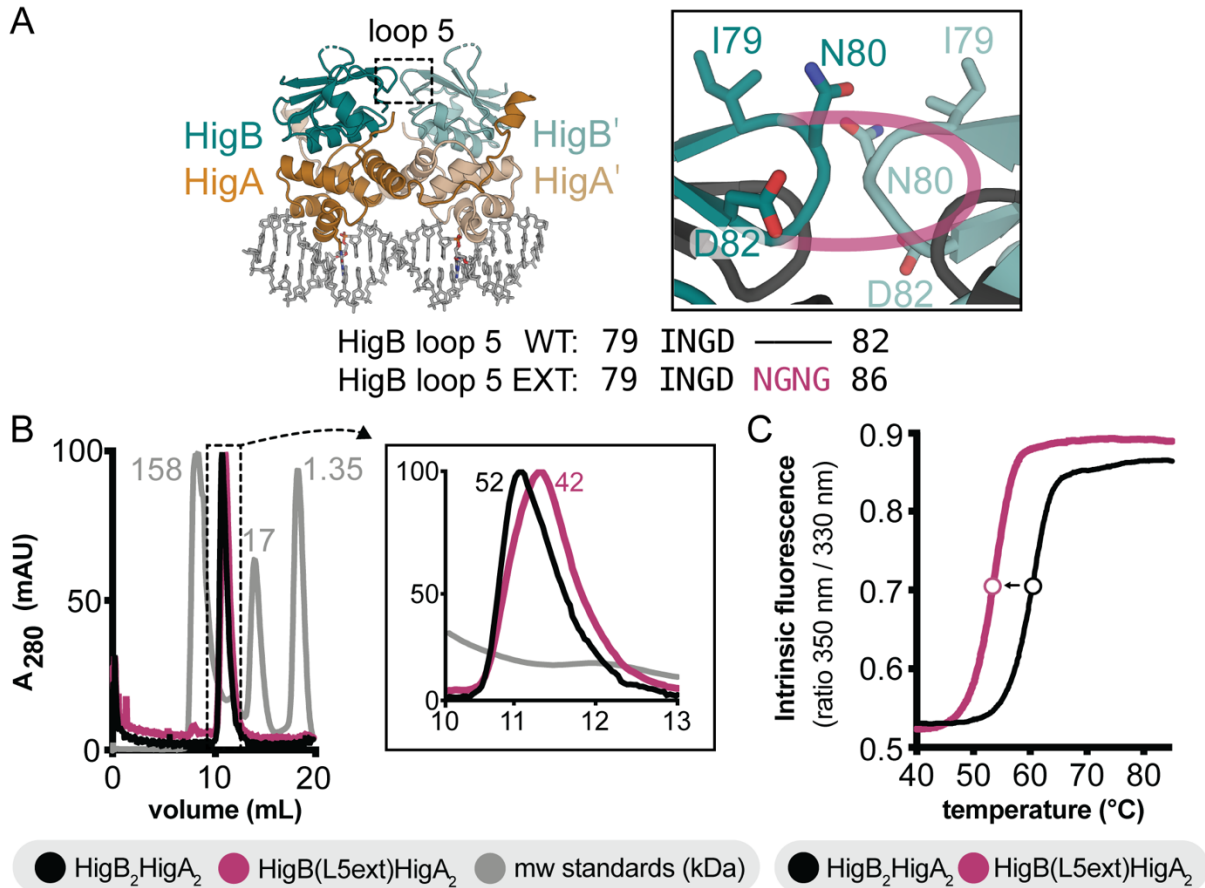
Figure 3.6 – Engineering a trimeric HigBHigA₂ complex.

(**A**) To prevent two HigB monomers from binding, loop 5 (L5) of HigB was extended by the insertion of four residues (Asn, Gly, Asn, Gly; NGNG; "L5ext", magenta) after residue Asp82. The dotted box indicating the L5 region of two HigB monomers is zoomed in (*right*). The theoretical extension of L5 is shown in magenta with the wild-type HigB and HigB(L5ext) amino acid alignment shown underneath. (**B**) Size exclusion chromatography of purified wild-type HigB₂HigA₂ shows an elution volume that corresponds to a molecular weight of 52 kDa. HigB(L5ext)HigA₂ complex (magenta) elutes at a volume corresponding to a molecular weight of 42 kDa with the inset showing a zoomed in view. Molecular weight standards are shown in grey. (**C**) Nano-DSF analysis

of wild-type HigB$_2$HigA$_2$ (black) and HigB(L5ext)HigA$_2$ (magenta) shows that the HigB(L5ext)HigA$_2$ complex has ~5°C lower T$_i$ value than HigB$_2$HigA$_2$. Fluorescence values were normalized to the highest tested temperature and the boundary of each line represents the mean ± SD of values of three independent experiments.
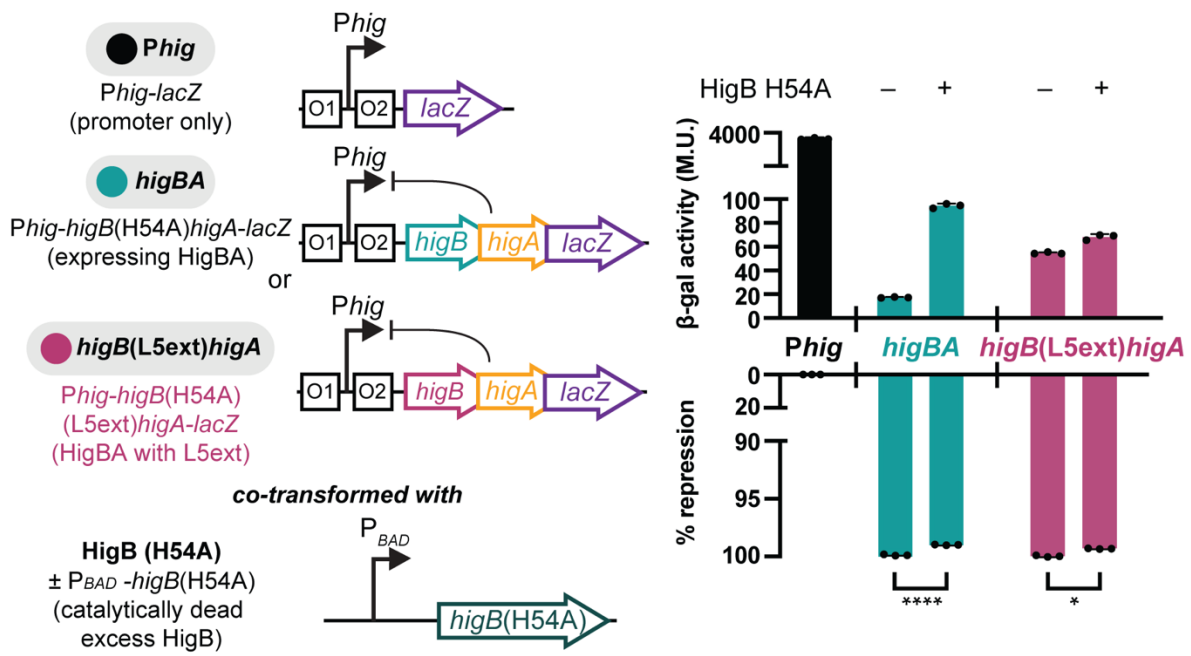
Figure 3.7 – Trimeric HigB(L5ext)HigA$_2$ is sufficient to repress transcription of P*hig*.

β-gal assays of *E. coli* BW25113 transformed with either pQF50-P*hig-lacZ* (P*hig* only), pQF50-P*hig-higB*(H54A)*higA-lacZ* (*higBhigA*), pQF50-P*hig-higB*(L5ext)*higA-lacZ* (*higB*(L5ext)*higA*)*,* and/or pBAD33-*higB*(H54A*)*. Raw Miller Units are shown on the top portion of the graph, while the same values are converted to % repressed and shown on the bottom portion (normalized to P*hig*). P*hig* only demonstrates the maximum amount of β-gal activity (black bar, 0% repression). Constructs containing either a wild-type HigBHigA (blue bars) or a HigB(L5ext)HigA variant (pink bars) both repress transcription (first bar in each group). Excess HigB expression (using a catalytically inactive H54A variant) results a small but statistically significant difference in repression (second bars in each group). Error bars represent the mean ± SD of values of three independent experiments (raw values shown as dots). Asterisks in the *higBA* group (blue bars)

represent results of a two-tailed Student's t-test in the *higBA* group comparing % repression of *higBA* operon without HigB(H54A) to *higBA* operon with addition of HigB(H54A) (p < 0.001, t = 44.73, df = 4, ****). Asterisks in the *higB*(L5ext)*higA* group (pink bars) represent results of a two-tailed Student's t-test comparing % repression of *higB*(L5ext)*higA* operon without HigB(H54A) to *higB*(L5ext)*higA* operon with addition of HigB(H54A) (p = 0.0163, t = 4.01, df = 4, *).
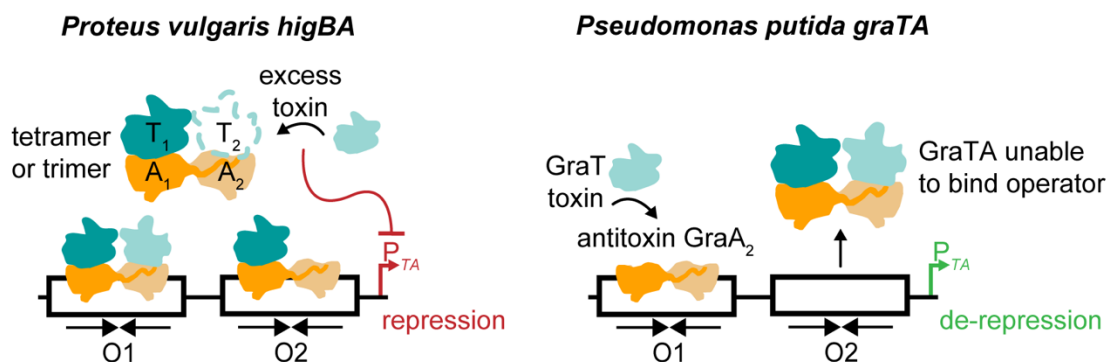
Figure 3.8 – Diverse modes of transcriptional repression occur even among evolutionarily conserved *higBA* family members.

Toxin (T) and antitoxin (A) proteins form multimeric complexes that bind operator sites (O1 and O2) that overlap with their promoters (P_{TA}) to repress transcription. In the *P. vulgaris higBhigA* system (left), diverse oligomeric complexes of HigBHigA sufficiently repress transcription. In contrast, the GraT toxin of the *graTgraA* toxin-antitoxin system acts as a de-repressor for the *gra* operon by binding to the GraA antitoxin relieving repression. *graTgraA* and *higBhigA* have high sequence identity and structural homology indicating that even among evolutionarily conserved *higBhigA* family members, the modes of transcriptional repression vary significantly.
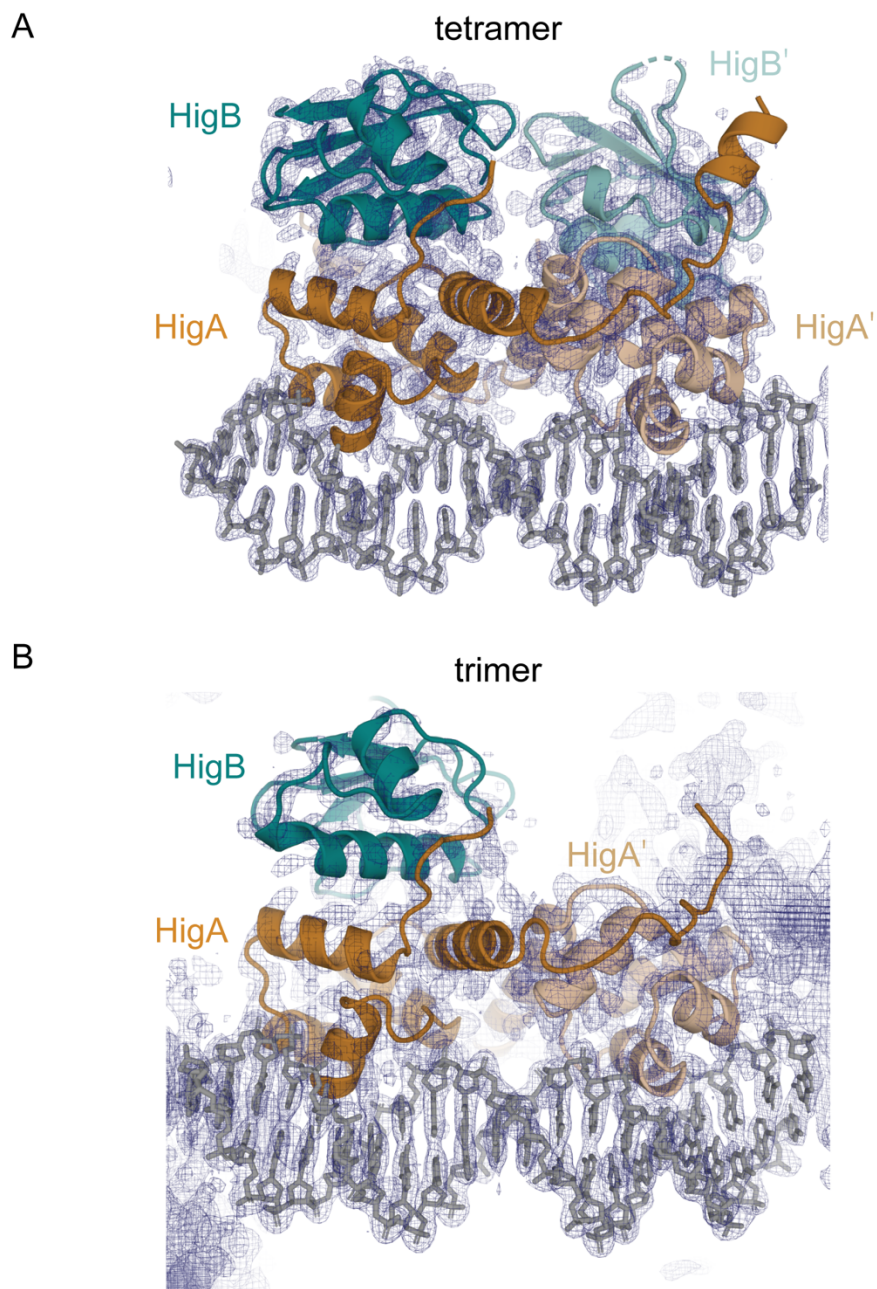
Figure 3.9 – Electron density maps of HigB$_2$-HigA$_2$-O2 and HigB-HigA$_2$-O2.

2F$_o$-F$_c$ electron density maps (contoured at 1σ) for the HigBHigA complex (HigB in teal, HigA in orange) are shown for the (**A**) 2.4-Å X-ray crystal structure of tetrameric

HigB$_2$HigA$_2$ (PDB code 6W6U) and (**B**) the 2.8-Å X-ray crystal structure of trimeric

HigBHigA$_2$ (PDB code 6WFP) complexes bound to O2 (grey).
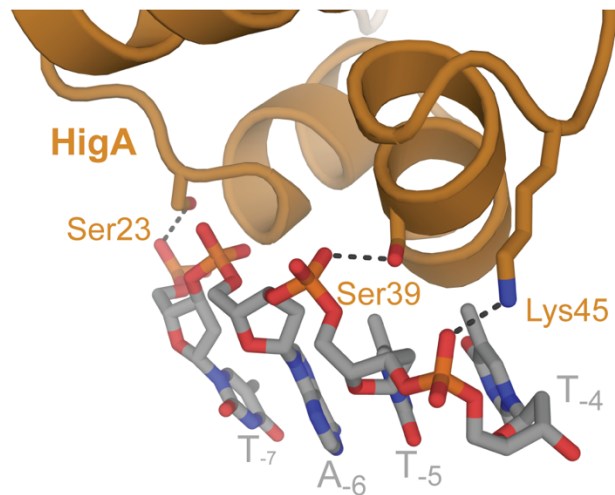
Figure 3.10 – HigA$_2$-DNA interactions in HigB$_2$HigA$_2$-O2 structure.

In the HigB$_2$HigA$_2$-O2 structure (PDB code 6W6U), HigA residues Ser23, Ser39, and Lys45 interact with the backbone phosphate of T$_{-7}$, T$_{-5}$, and T$_{-4}$, respectively to rigidify the T$_{+6}$, G$_{+7}$, T$_{+8}$, A$_{+9}$ sequence for nucleotide-specific recognition on the opposite strand. In the trimeric HigBHigA$_2$-O2 structure, only Ser39 maintains interactions with the phosphate backbone while Ser23 and Lys45 are too distant (Figure 3.3B, red highlighted region).
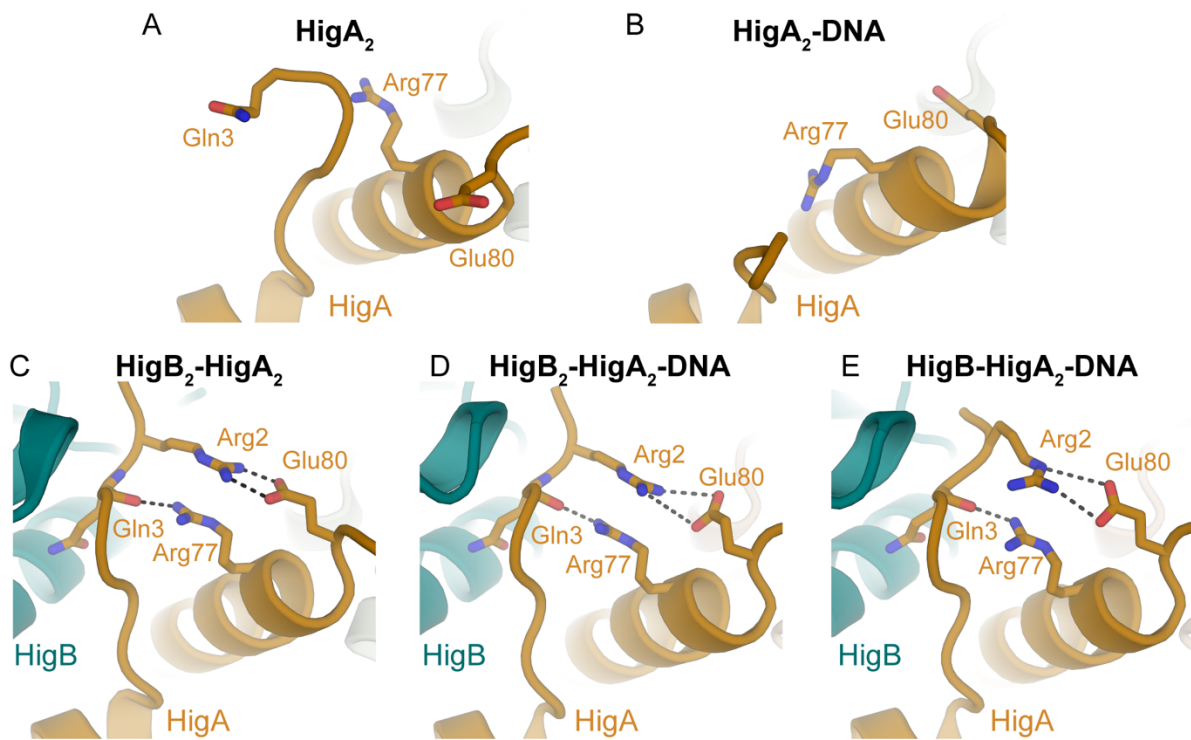
Figure 3.11 – HigA N-C terminal interactions become ordered upon HigB binding.

In the structure of (**A**) the HigA$_2$ dimer (PDB code 6CF1) or (**B**) the HigA$_2$ dimer bound to O2 DNA (PDB code 6CHV), the HigA N-terminus is disordered in the absence of HigB. HigB binding ordered the N- and C-termini residues of HigA in the (**C**) HigB$_2$HigA$_2$ structure (PDB code 4MCX), the (**D**) HigB$_2$HigA$_2$-O2 structure (PDB code 6W6U), and the (**E**) HigBHigA$_2$-O2 structure (PDB code 6WFP). Arg77 forms interactions with the backbone carbonyl of Gln3 and Arg2 and Glu80 form salt bridges.
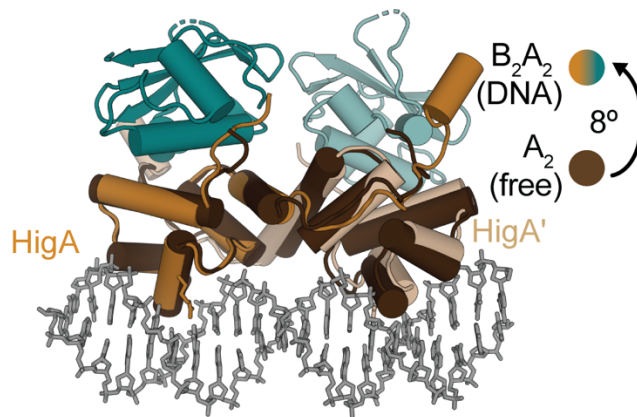
Figure 3.12 – Influence of HigB toxin on HigA$_2$ interactions with O2.

Comparison of apo HigA$_2$ dimer (brown; PDB code 6CF1) and tetrameric HigB$_2$HigA$_2$-O2 (PDB code 6W6U) is shown. The apo HigA$_2$ dimer reorients ~8° away from O2 to accommodate binding of one or two HigB monomers. Structures are aligned a single HigA (left).
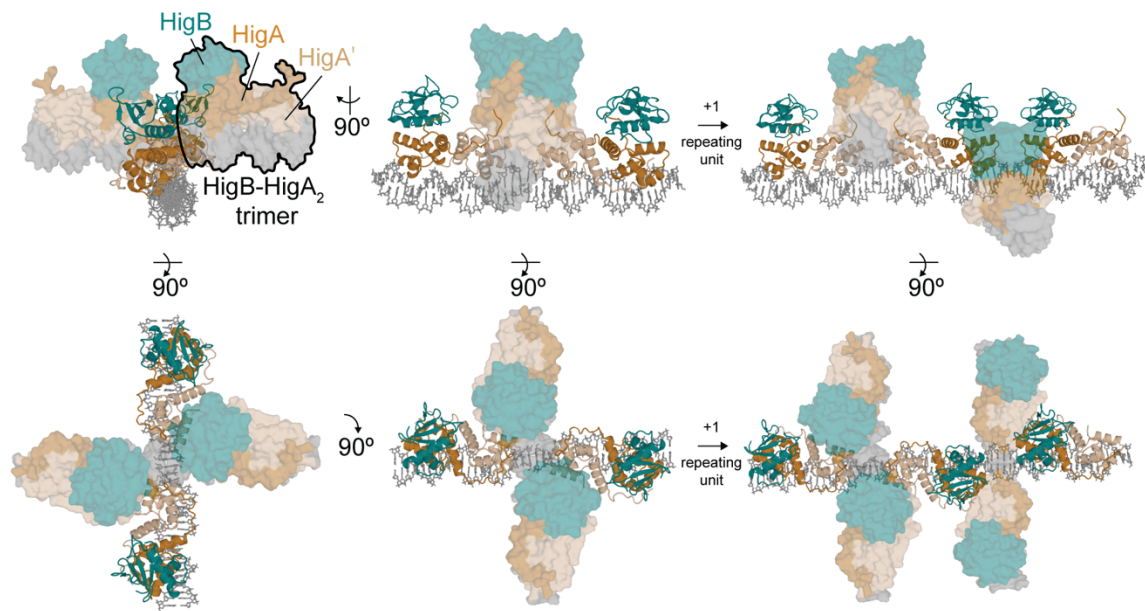
Figure 3.13 – Packing of the trimeric HigBHigA$_2$.

The repeating asymmetric unit of the HigBHigA$_2$-O2 structure. Each repeating unit packs on DNA in such a way that two HigBHigA$_2$-O2 complexes (shown as surface) interact with another two HigBHigA$_2$-O2 complexes (shown as cartoon).
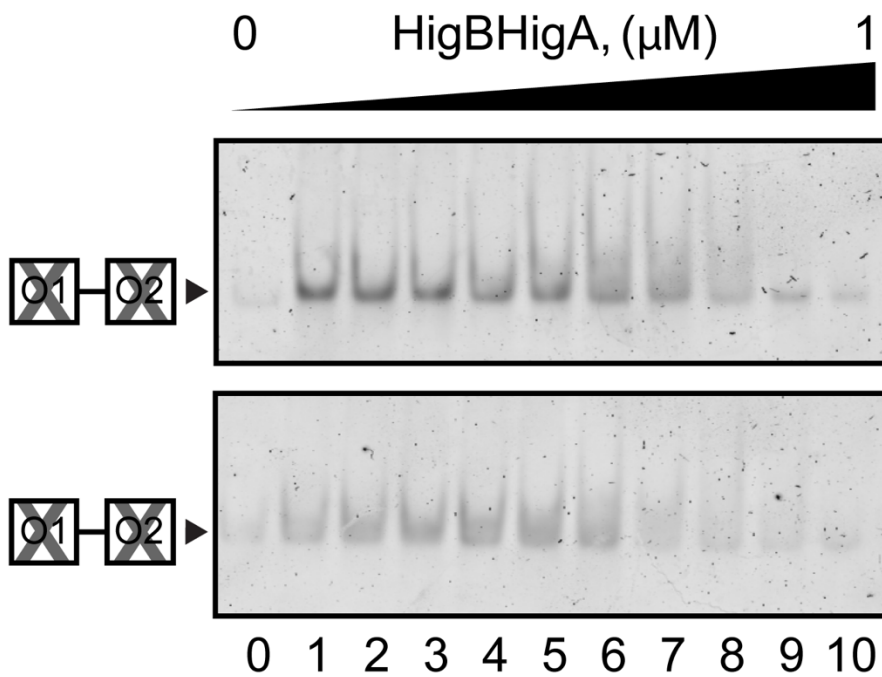
Figure 3.14 – HigBHigA is unable to bind to *hig* if both operators are scrambled.

EMSA of HigBHigA inability to bind P*hig* DNA where both O1 and O2 sites have been scrambled (concentrations used: 0, 0.025, 0.05, 0.1, 0.2, 0.3, 0.4, 0.5, 0.6, 0.7, 0.8).
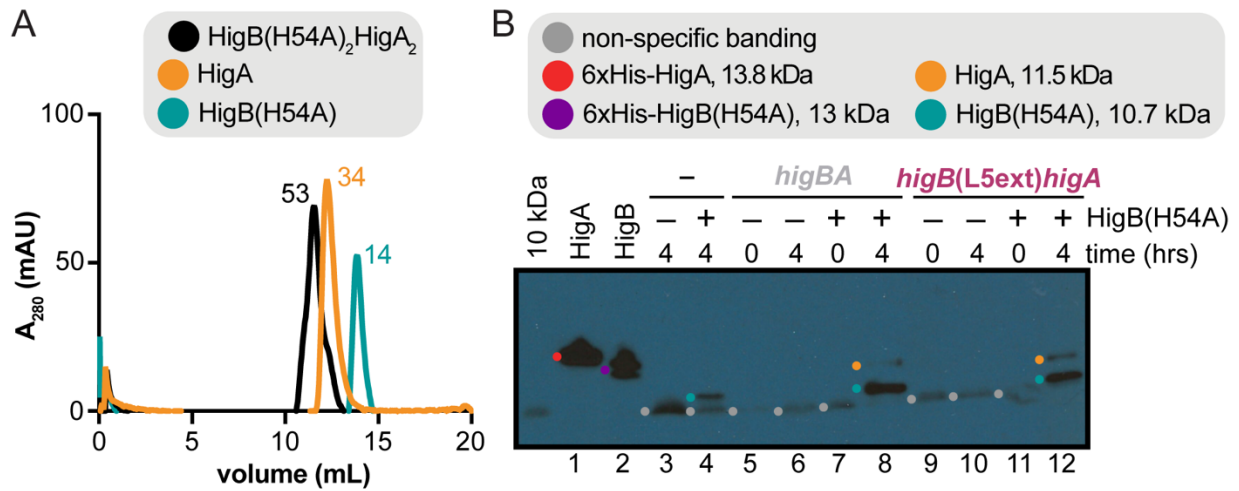
Figure 3.15 – HigB(H54A) catalytic mutant is stably expressed and can bind HigA.

(**A**) Size exclusion chromatography of purified HigB(H54A) incubated with HigA shows an elution volume that corresponds to a molecular weight of 53 kDa, consistent with the molecular weight reported herein for $HigB_2HigA_2$ (52 kDa). HigB(H54A) elutes at a volume that corresponds to approximately 14 kDa, consistent with His_6-tagged HigB protein. Elution volume and corresponding molecular weight of HigA alone provided as a control. (**B**) Western blotting using an anti-HigBA polyclonal antibody reveals HigB(H54A) is stably expressed in cells containing only pBAD33-*higB*(H54A) ("*higB*", lanes 3–4), pQF50-*higB*(H54A)-*higA*-*lacZ* and pBAD33-*higB*(H54A) ("*higBA*", lanes 5–8), or pQF50-*higB*(H54A)(L5ext)-*higA*-*lacZ* and pBAD33-*higB*(H54A) ("*higB*(L5ext)*higA*", lanes 9–12). HigB(H54A) is only detected when induced with arabinose (represented by –/+) and after four hours. These are the same strains and conditions used in β-gal assays presented herein

Table 3.1 – Data collection and refinement statistics.

	Tetrameric HigB$_2$HigA$_2$ 6W6U	Trimeric HigBHigA$_2$ 6WFP
Data Collection		
Space Group	C2	I4$_1$
Wavelength (Å)	0.9792	1.0
Cell dimensions		
a, b, c (Å)	98.15, 98.13, 147.19	139.82, 139.82, 80.8
α, β, γ (°)	90, 109.49, 90	90, 90, 90
Resolution (Å)	67.32-2.4	34.98-2.8
	(2.49-2.4)	(2.9-2.8)
R$_{pim}$ (%)	4.0 (33.8)	2.08 (18.34)
I/σI	13.43 (2.71)	22.41 (4.19)
Completeness (%)	97.24 (97.27)	94.50 (68.50)
Redundancy	3.8 (3.8)	7.2 (7.3)
CC$_{1/2}$	0.996 (0.86)	0.999 (0.975)
Refinement		
Reflections	50,142 (4,955)	18,256 (1,296)
R$_{work}$/R$_{free}$ (%)	17.5/22.1	17.6/21.8
No. of atoms	8,143	3,180
B-factors (Å^2)		
Overall	57.38	69.98
Macromolecule	57.55	70.54
Ligand/ion	69.96	78.58
Root mean square deviations		
Bond lengths (Å)	0.003	0.011
Bond angles (°)	0.53	1.51

Data for the highest-resolution shell is shown in parentheses.

Table 3.2 – List of oligonucleotides and plasmids used in Chapter 3.

	Genotype
BW25113	*Escherichia coli Δ(araBAD)567 Δ(rhaBAD)568 ΔlacZ4787(::rrnB-3) hsdR514 rph-1*
BL21(DE3)	*Escherichia coli* strain *B F⁻ ompT gal dcm lon hsdS_B(r_B⁻-m_B⁻) λ(DE3 [lacI lacUV5-T7p07 ind1 sam7 nin5]) [malB⁺]_{K-12} (λ^S)*

Oligonucleotides	Sequence
O1-O2 dsDNA pHigA_F pHigA_R	5' TGTATTGCACATCGTGTAATATCGCGGTATAGTATTACACACCATGTAATACAGAGATGGC 3' 3' ACATAACGTGTAGCACATTATAGCGCCATATCATAATGTGTGGTACATTATGTCTCTACCG 5'
O1-O2(scr) dsDNA pHigA_F_Scra2 pHigA_R_Scra2	5' TGTATTGCACATCGTGTAATATCGCGGTATA<u>CAGCC</u>ATGTGGACACCCCCGG</u>AGAGATGGC 3' 3' ACATAAACGTGTAGCACATTATAGCGCCATA<u>GTCGG</u>TACACCTGTGGGGGCC</u>TCTCTACCG 5'
O1(scr)-O2 dsDNA pHigA_F_Scra1 pHigA_R_Scra1	5'T<u>CAGCCATGTGGACACCCCCGG</u>CGCGGTATAGTATTACACACCATGTAATACAGAGATGGC 3' 3'A<u>GTCGGTACACCTGTGGGGGCC</u>GCGCCATATCATAATGTGTGGTACATTATGTCTCTACCG 5'
O2 dsDNA pHigA_O2_F pHigA_O2_R	5' GTATTACACACCATGTAATAC 3' 3' CATAATGTGTGGTACATTATG 5'

Plasmid	Content or reference
pBAD33	(62)
pQF50	(63)
pET28a-His₆-*higA*	(64)
pET28a-His₆-*higBhigA*	(65)
pET21c-*higBhigA*-His₆	(65)
pQF50-P*hig-lacZ*	(66)
pQF50-P*hig-higA-lacZ*	(66)
pQF50-P*hig-higA*(Δ84-104)-*lacZ*	(66)
pQF50-P*hig*(G₋₂₄T/C₋₃₀A)-*lacZ*	This study
pQF50-P*hig*(G₋₂₄T/C₋₃₀A)-*higA-lacZ*	This study
pQF50-P*hig*(G₋₂₄T/C₋₃₀A)-*higA*(Δ84-104)-*lacZ*	This study
pQF50-P*hig*(G₋₈T/C₋₂A)-*lacZ*	This study
pQF50-P*hig*(G₋₈T/C₋₂A)-*higA-lacZ*	This study
pQF50-P*hig*(G₋₈T/C₋₂A)-*higA*(Δ84-104)-*lacZ*	This study

pQF50-P*hig-higB-higA-lacZ*	This study
pQF50-P*hig-higB*(L5ext)*higA-lacZ*	This study
pBAD33-*higB*(H54A)	(67)

Table 3.3 – K_D values (best fit ± SE) for complex binding.

Complex	K_D (µM)		Fold change in K_D (O1/O2)
HigA$_2$-*hig*O1 (66)	0.14	± 0.03	
HigA$_2$-*hig*O2 (66)	0.13	± 0.03	1.1
HigA$_2$-*hig*O1O2	N.C.		
HigBHigA-*hig*O1 (this study)	0.36	± 0.09	
HigBHigA-*hig*O2 (this study)	0.24	± 0.04	1.5
HigBHigA-*hig*O1O2	N.C.		

N.C = not calculated.

3.9 References

1. D. P. Pandey, K. Gerdes, Toxin-antitoxin loci are highly abundant in free-living but lost from host-associated prokaryotes. *Nucleic Acids Res* **33**, 966-976 (2005).

2. K. S. Makarova, Y. I. Wolf, E. V. Koonin, Comprehensive comparative-genomic analysis of type 2 toxin-antitoxin systems and related mobile stress response systems in prokaryotes. *Biol Direct* **4**, 19 (2009).

3. R. Leplae *et al.*, Diversity of bacterial type II toxin-antitoxin systems: a comprehensive search and functional analysis of novel families. *Nucleic Acids Res* **39**, 5513-5525 (2011).

4. H. Karoui, F. Bex, P. Dreze, M. Couturier, Ham22, a mini-F mutation which is lethal to host cell and promotes *recA*-dependent induction of lambdoid prophage. *EMBO J* **2**, 1863-1868 (1983).

5. T. Ogura, S. Hiraga, Mini-F plasmid genes that couple host cell division to plasmid proliferation. *Proc Natl Acad Sci U S A* **80**, 4784-4788 (1983).

6. K. Gerdes, P. B. Rasmussen, S. Molin, Unique type of plasmid maintenance function: postsegregational killing of plasmid-free cells. *Proc Natl Acad Sci U S A* **83**, 3116-3120 (1986).

7. A. Bravo, G. de Torrontegui, R. Diaz, Identification of components of a new stability system of plasmid R1, ParD, that is close to the origin of replication of this plasmid. *Mol Gen Genet* **210**, 101-110 (1987).

8. S. Tsuchimoto, H. Ohtsubo, E. Ohtsubo, Two genes, *pemK* and *pemI*, responsible for stable maintenance of resistance plasmid R100. *J Bacteriol* **170**, 1461-1466 (1988).

9. H. Lehnherr, E. Maguin, S. Jafri, M. B. Yarmolinsky, Plasmid addiction genes of bacteriophage P1: *doc*, which causes cell death on curing of prophage, and *phd*, which prevents host death when prophage is retained. *Journal of molecular biology* **233**, 414-428 (1993).

10. N. Fraikin, F. Goormaghtigh, L. Van Melderen, Type II Toxin-Antitoxin Systems: Evolution and Revolutions. *J Bacteriol* **202** (2020).

11. R. Loris, A. Garcia-Pino, Disorder- and dynamics-based regulatory mechanisms in toxin-antitoxin modules. *Chemical reviews* **114**, 6933-6947 (2014).

12. R. Page, W. Peti, Toxin-antitoxin systems in bacterial growth arrest and persistence. *Nat Chem Biol* **12**, 208-214 (2016).

13. M. Gotfredsen, K. Gerdes, The *Escherichia coli relBE* genes belong to a new toxin-antitoxin gene family. *Mol Microbiol* **29**, 1065-1076 (1998).

14. R. Magnuson, M. B. Yarmolinsky, Corepression of the P1 addiction operon by Phd and Doc. *J Bacteriol* **180**, 6342-6351 (1998).

15. H. Afif, N. Allali, M. Couturier, L. Van Melderen, The ratio between CcdA and CcdB modulates the transcriptional repression of the *ccd* poison-antidote system. *Mol Microbiol* **41**, 73-82 (2001).

16. M. Overgaard, J. Borch, M. G. Jorgensen, K. Gerdes, Messenger RNA interferase RelE controls *relBE* transcription by conditional cooperativity. *Mol Microbiol* **69**, 841-857 (2008).

17. B. L. Brown, D. M. Lord, S. Grigoriu, W. Peti, R. Page, The *Escherichia coli* toxin MqsR destabilizes the transcriptional repression complex formed between the antitoxin MqsA and the *mqsRA* operon promoter. *J Biol Chem* **288**, 1286-1294

(2013).

18. A. Ruangprasert *et al.*, Mechanisms of toxin inhibition and transcriptional repression by *Escherichia coli* DinJ-YafQ. *J Biol Chem* **289**, 20559-20569 (2014).

19. M. A. Schureck *et al.*, Structure of the *Proteus vulgaris* HigB-(HigA)2-HigB toxin-antitoxin complex. *J Biol Chem* **289**, 1060-1070 (2014).

20. K. J. Turnbull, K. Gerdes, HicA toxin of *Escherichia coli* derepresses *hicAB* transcription to selectively produce HicB antitoxin. *Mol Microbiol* **104**, 781-792 (2017).

21. T. Madl *et al.*, Structural basis for nucleic acid and toxin recognition of the bacterial antitoxin CcdA. *Journal of molecular biology* **364**, 170-185 (2006).

22. A. Boggild *et al.*, The crystal structure of the intact *E. coli* RelBE toxin-antitoxin complex provides the structural basis for conditional cooperativity. *Structure* **20**, 1641-1648 (2012).

23. A. Garcia-Pino *et al.*, Allostery and intrinsic disorder mediate transcription regulation by conditional cooperativity. *Cell* **142**, 101-111 (2010).

24. C. Dienemann, A. Boggild, K. S. Winther, K. Gerdes, D. E. Brodersen, Crystal structure of the VapBC toxin-antitoxin complex from *Shigella flexneri* reveals a hetero-octameric DNA-binding assembly. *Journal of molecular biology* **414**, 713-722 (2011).

25. B. L. Brown *et al.*, Three dimensional structure of the MqsR:MqsA complex: a novel TA pair comprised of a toxin homologous to RelE and an antitoxin with unique properties. *PLoS Pathog* **5**, e1000706 (2009).

26. M. A. Schumacher *et al.*, Molecular mechanisms of HipA-mediated multidrug

tolerance and its neutralization by HipB. *Science* **323**, 396-401 (2009).

27. R. Magnuson, H. Lehnherr, G. Mukhopadhyay, M. B. Yarmolinsky, Autoregulation of the plasmid addiction operon of bacteriophage P1. *J Biol Chem* **271**, 18705-18710 (1996).

28. I. Brzozowska, U. Zielenkiewicz, Regulation of toxin-antitoxin systems by proteolysis. *Plasmid* **70**, 33-41 (2013).

29. A. Talavera *et al.*, A dual role in regulation and toxicity for the disordered N-terminus of the toxin GraT. *Nature communications* **10**, 972 (2019).

30. Y. Terawaki, H. Takayasu, T. Akiba, Thermosensitive replication of a kanamycin resistance factor. *J Bacteriol* **94**, 687-690 (1967).

31. Q. B. Tian, M. Ohnishi, A. Tabuchi, Y. Terawaki, A new plasmid-encoded proteic killer gene system: cloning, sequencing, and analyzing *hig* locus of plasmid Rts1. *Biochem Biophys Res Commun* **220**, 280-284 (1996).

32. K. Pedersen *et al.*, The bacterial toxin RelE displays codon-specific cleavage of mRNAs in the ribosomal A site. *Cell* **112**, 131-140 (2003).

33. J. M. Hurley, N. A. Woychik, Bacterial toxin HigB associates with ribosomes and mediates translation-dependent mRNA cleavage at A-rich sites. *J Biol Chem* **284**, 18605-18613 (2009).

34. M. A. Schureck, J. A. Dunkle, T. Maehigashi, S. J. Miles, C. M. Dunham, Defining the mRNA recognition signature of a bacterial toxin protein. *Proc Natl Acad Sci U S A* **112**, 13862-13867 (2015).

35. M. A. Schureck, T. Maehigashi, S. J. Miles, J. Marquez, C. M. Dunham, mRNA bound to the 30S subunit is a HigB toxin substrate. *RNA* **22**, 1261-1270 (2016).

36. H. Tamman, A. Ainelo, K. Ainsaar, R. Horak, A moderate toxin, GraT, modulates growth rate and stress tolerance of *Pseudomonas putida*. *J Bacteriol* **196**, 157-169 (2014).

37. S. Hadzi *et al.*, Ribosome-dependent *Vibrio cholerae* mRNAse HigB2 is regulated by a beta-strand sliding mechanism. *Nucleic Acids Res* **45**, 4972-4983 (2017).

38. B. S. Xu *et al.*, Conformational changes of antitoxin HigA from *Escherichia coli* str. K-12 upon binding of its cognate toxin HigB reveal a new regulation mechanism in toxin-antitoxin systems. *Biochem Biophys Res Commun* **514**, 37-43 (2019).

39. M. A. Schureck *et al.*, Structural basis of transcriptional regulation by the HigA antitoxin. *Mol Microbiol* **111**, 1449-1462 (2019).

40. M. H. Dao-Thi *et al.*, Molecular basis of gyrase poisoning by the addiction toxin CcdB. *Journal of molecular biology* **348**, 1091-1102 (2005).

41. S. K. Khoo *et al.*, Molecular and structural characterization of the PezAT chromosomal toxin-antitoxin system of the human pathogen *Streptococcus pneumoniae*. *J Biol Chem* **282**, 19606-19618 (2007).

42. M. Overgaard, J. Borch, K. Gerdes, RelB and RelE of *Escherichia coli* form a tight complex that represses transcription via the ribbon-helix-helix motif in RelB. *Journal of molecular biology* **394**, 183-196 (2009).

43. Q. B. Tian *et al.*, Specific protein-DNA and protein-protein interaction in the *hig* gene system, a plasmid-borne proteic killer gene system of plasmid Rts1. *Plasmid* **45**, 63-74 (2001).

44. Q. B. Tian, T. Hayashi, T. Murata, Y. Terawaki, Gene product identification and promoter analysis of *hig* locus of plasmid Rts1. *Biochem Biophys Res Commun* **225**,

679-684 (1996).

45. M. A. Schureck, A. Repack, S. J. Miles, J. Marquez, C. M. Dunham, Mechanism of endonuclease cleavage by the HigB toxin. *Nucleic Acids Res* **44**, 7944-7953 (2016).

46. A. Harms, C. Fino, M. A. Sorensen, S. Semsey, K. Gerdes, Prophages and Growth Dynamics Confound Experimental Results with Antibiotic-Tolerant Persister Cells. *mBio* **8** (2017).

47. F. Goormaghtigh *et al.*, Reassessing the Role of Type II Toxin-Antitoxin Systems in Formation of *Escherichia coli* Type II Persister Cells. *mBio* **9** (2018).

48. M. C. Monti *et al.*, Interactions of Kid-Kis toxin-antitoxin complexes with the *parD* operator-promoter region of plasmid R1 are piloted by the Kis antitoxin and tuned by the stoichiometry of Kid-Kis oligomers. *Nucleic Acids Res* **35**, 1737-1749 (2007).

49. K. A. Datsenko, B. L. Wanner, One-step inactivation of chromosomal genes in *Escherichia coli* K-12 using PCR products. *Proc Natl Acad Sci U S A* **97**, 6640-6645 (2000).

50. W. Kabsch, Xds. *Acta crystallographica* **66**, 125-132 (2010).

51. P. D. Adams *et al.*, PHENIX: a comprehensive Python-based system for macromolecular structure solution. *Acta crystallographica* **66**, 213-221 (2010).

52. P. Emsley, B. Lohkamp, W. G. Scott, K. Cowtan, Features and development of Coot. *Acta crystallographica* **66**, 486-501 (2010).

53. Schrodinger, LLC (2010) The PyMOL Molecular Graphics System, Version 1.3r1.

54. I. Y. B.-S. D.A. Case, S.R. Brozell, D.S. Cerutti, T.E. Cheatham, III, V.W.D. Cruzeiro, T.A. Darden, R.E. Duke, D. Ghoreishi, M.K. Gilson, H. Gohlke, A.W. Goetz, D. Greene, R Harris, N. Homeyer, Y. Huang, S. Izadi, A. Kovalenko, T. Kurtzman, T.S.

Lee, S. LeGrand, P. Li, C. Lin, J. Liu, T. Luchko, R. Luo, D.J. Mermelstein, K.M. Merz, Y. Miao, G. Monard, C. Nguyen, H. Nguyen, I. Omelyan, A. Onufriev, F. Pan, R. Qi, D.R. Roe, A. Roitberg, C. Sagui, S. Schott-Verdugo, J. Shen, C.L. Simmerling, J. Smith, R. SalomonFerrer, J. Swails, R.C. Walker, J. Wang, H. Wei, R.M. Wolf, X. Wu, L. Xiao, D.M. York and P.A. Kollman (2018) AMBER 2018. (University of California, San Francisco).

55. J. A. Maier *et al.*, ff14SB: Improving the Accuracy of Protein Side Chain and Backbone Parameters from ff99SB. *J Chem Theory Comput* **11**, 3696-3713 (2015).

56. R. Galindo-Murillo *et al.*, Assessing the Current State of Amber Force Field Modifications for DNA. *J Chem Theory Comput* **12**, 4114-4127 (2016).

57. W. L. Jorgensen, J. Chandrasekhar, J. D. Madura, R. W. Impey, M. L. Klein, Comparison of simple potential functions for simulating liquid water. *J. Chem. Phys.* **79** (1983).

58. R. Salomon-Ferrer, A. W. Gotz, D. Poole, S. Le Grand, R. C. Walker, Routine Microsecond Molecular Dynamics Simulations with AMBER on GPUs. 2. Explicit Solvent Particle Mesh Ewald. *J Chem Theory Comput* **9**, 3878-3888 (2013).

59. S. Le Grand, A. W. Gotz, R. C. Walker, SPFP: Speed without compromise—A mixed precision model for GPU accelerated molecular dynamics simulations. *Computer Physics Communications* **184**, 374-380 (2013).

60. J. C. Ryckaert, G.; Berendsen, H.J.C., Numerical integration of the cartesian equations of motion of a system with constraints: molecular dynamics of n-alkanes. *Journal of Computational Physics* **23**, 327-341 (1977).

61. D. R. Roe, T. E. Cheatham, 3rd, PTRAJ and CPPTRAJ: Software for Processing

and Analysis of Molecular Dynamics Trajectory Data. *J Chem Theory Comput* **9**, 3084-3095 (2013).

62. Guzman, L.M., Belin, D., Carson, M.J. and Beckwith, J. (1995) Tight regulation, modulation, and high-level expression by vectors containing the arabinose PBAD promoter. *J Bacteriol*, **177**, 4121-4130.

63. Farinha, M.A. and Kropinski, A.M. (1990) Construction of broad-host-range plasmid vectors for easy visible selection and analysis of promoters. *J Bacteriol*, **172**, 3496-3499.

64. Hurley, J.M. and Woychik, N.A. (2009) Bacterial toxin HigB associates with ribosomes and mediates translation-dependent mRNA cleavage at A-rich sites. *J Biol Chem*, **284**, 18605-18613.

65. Schureck, M.A., Maehigashi, T., Miles, S.J., Marquez, J., Cho, S.E., Erdman, R. and Dunham, C.M. (2014) Structure of the *Proteus vulgaris* HigB-(HigA)2-HigB toxin-antitoxin complex. *J Biol Chem*, **289**, 1060-1070.

66. Schureck, M.A., Meisner, J., Hoffer, E.D., Wang, D., Onuoha, N., Ei Cho, S., Lollar, P., 3rd and Dunham, C.M. (2019) Structural basis of transcriptional regulation by the HigA antitoxin. *Mol Microbiol*, **111**, 1449-1462.

67. Schureck, M.A., Repack, A., Miles, S.J., Marquez, J. and Dunham, C.M. (2016) Mechanism of endonuclease cleavage by the HigB toxin. *Nucleic Acids Res*, **44**, 7944-7953.

Chapter 4

Stability of toxin-antitoxin complexes governed by regulated antitoxin proteolysis

4.1 Abstract

When toxins are released in response to environmental stimuli encountered by bacteria, antitoxins first must be preferentially degraded by major cellular proteases for toxin release. As antitoxins normally bind and sequester toxin in a tight complex, proteolysis of such antitoxins is thus a critical part of toxin-antitoxin system regulation that remains largely unknown. Although antitoxin proteins have low sequence identities and can adopt diverse secondary structural motifs, they all engage and inhibit their toxin partners via their C termini, suggesting that this region may be susceptible to proteolysis. Here, in on-going work, the stability of three defined *E. coli* toxin-antitoxin systems (DinJ-YafQ*,* RelB-RelE*,* and YefM-YoeB*)* are examined. The rationale for selecting these systems is that although the toxin components are structural homologs, each antitoxin interacts with their cognate toxins in different ways. In addition, each system is regulated in response to different stimuli, suggesting they may also be regulated by different proteases. Antitoxin regions required for toxin recognition and stability were determined and will be further tested for recognition by a panel of proteases and known protease adaptors. These studies are critical for understanding how bacteria select substrates for proteolysis in response to environmental stimuli.

4.2 Introduction

Bacterial type II (protein-protein) toxin-antitoxin systems are influenced by environmental stimuli in two major ways: antitoxin proteolysis and the accompanying release of toxin. In the absence of stimuli, transcription from toxin-antitoxin loci is inhibited by binding of the toxin-antitoxin to DNA operators that overlap with its promoter. Toxin proteins form high-affinity complexes with antitoxins bound to DNA, serving as a negative feedback loop. Selective degradation of antitoxins by cellular proteases frees toxins in response to various environmental cues (Figure 1.1). Thus, toxin activation and antitoxin proteolysis are intrinsically linked, but their underlying mechanisms remain unknown. Major questions governing antitoxin proteolysis are still unanswered more than 30 years after toxin-antitoxin systems were discovered, including understanding (i) how proteases recognize and degrade antitoxins and (ii) how proteases gain stress-specificity against different toxin-antitoxin systems.

Lon and Clp are the two most well-characterized proteases in bacteria and are members of the <u>A</u>TPases <u>a</u>ssociated with various cellular <u>a</u>ctivities (AAA+) family. Together, they are responsible for degradation of more than 50% of all proteins in *E. coli* (1-3). While both proteases use ATP for energy, Lon is active alone whereas Clp has different subunits and adapters that confer specificity (4-6). Clp peptidase domains (ClpP) associate with subunits A and X (ClpAP and ClpXP) in gram-negative bacteria or with subunits C and E (ClpCP and ClpEP) in gram-positive bacteria (6). Both Lon and Clp proteases recognize and degrade antitoxins (7-10) and in some cases, both proteases degrade the same antitoxin (8, 11, 12). Antitoxin proteolysis likely occurs by different mechanisms because

of inherent differences in how the proteases work. For example, Lon recognizes exposed hydrophobic residues on misfolded proteins (13, 14) and Clp proteases require sequence specific degrons that are recognized directly by Clp or through the use of chaperones (15). The best example of this is the *ssrA* tag, which is appended to the C termini of peptides when stalled ribosomes are rescued by tmRNA-SmpB during *trans*-translation (16). It is important to note that Lon activity can also be modulated by adapters, such as in the inhibition of DNA replication or cell swarming in *C. crescentus* and *B. subtilis* (17, 18), but at present no other Lon adapters have been discovered. Although it has been suggested that exposure to stress, like DNA damage, nutrient deprivation, reactive oxygen species, or antimicrobial agents triggers Lon and Clp to degrade antitoxins (19), how this is achieved remains unclear.

The ability of antitoxins to regulate toxin activity depends on the molecular interactions between the two proteins. When most antitoxin form complexes with their cognate toxins, their C termini interact with the toxins and in some cases, these intrinsically disordered regions adopt secondary structural motifs (20). This transition from unstructured to structured has been implicated as important for antitoxin function (21). In addition, binding of the toxin by the antitoxin can influence the ability Lon and Clp to degrade antitoxins. For example, *E. coli* antitoxin CcdA of *ccdBccdA* is protected from proteolysis when in complex with cognate toxin. When CcdA is in the absence of CcdB, it is readily recognized by Lon and degraded at its C-terminus at stretches of hydrophobic residues (22). The same mechanism of recognition and degradation of Lon may also be true for the structurally distinct *E. coli* system *hipBhipA*. The C-terminus of antitoxin HipB also harbors

hydrophobic residues that are presumably recognized by Lon protease (23). Removal of the last 16 residues of the unstructured C-terminus of HipB increased the *in vitro* half-life of HipB from 74 minutes to >200 minutes, indicating that this region is recognized by Lon. Average *E. coli* protein half-life is approximately 20 hours (24), so antitoxins have relatively short half-lives. We also previously generated C-terminal truncations of DinJ and determined which regions were essential for formation of the DinJ-YafQ complex or for proteolysis by Lon (25). A trio of C-terminal DinJ truncations were designed: DinJΔ77-86, DinJΔ71-86, and DinJΔ56-86 (Figure 4.1A). DinJΔ77-86 removes α4, which packs against a hydrophobic pocket located on cognate toxin YafQ. DinJΔ71-86 is a more severe truncation as it additionally removes DinJ β2, which forms an antiparallel β-sheet with a β-strand on YafQ. DinJΔ56-86 is the most severe truncation and additionally removes α3. These truncations were made at the ends of secondary structure elements to avoid DinJ aggregation. All three truncations prevented DinJ from forming a complex with cognate toxin YafQ, indicating that DinJ α4 is the only structural element important for sequestering toxin. This would also suggest that proteases would target these regions to release toxin. To determine this, the C-terminal loop 5 (residues 74–77) and loop 3 (residues 44–50) of DinJ were replaced with a TEV protease recognition site. Replacing loop 5 resulted in DinJ no longer being proteolyzed by Lon. However, it was confirmed that loop 5 was still accessible to proteases, as expression of TEV proteolyzed DinJ. In contrast, loop 3 was not accessible to TEV. Thus, the C-terminal loop 5 of DinJ is specifically recognized by Lon for degradation. To confirm that DinJ had lost the ability to bind YafQ, both proteins were incubated together and analyzed by SEC (size-exclusion chromatography). The smallest C-terminal truncation, DinJΔ77-86, impaired the ability of

DinJ to bind YafQ as expected (25). Thus, in CcdA, HipB, and DinJ, there are hydrophobic residues recognized by Lon, but it remains unclear how proteases gain selectivity towards antitoxins in response to environmental stimuli.

To provide mechanistic insight into the role proteases play in toxin activation, proteolysis of three *E. coli* type II toxin-antitoxin systems- DinJ-YafQ (25-28), RelB-RelE (29-31), and YefM-YoeB (32-35) were examined. These systems were selected because (i) each system contains homologous toxins and yet, each antitoxin binds their toxin in a different manner and (ii) these systems are activated during different stresses and therefore could be potentially degraded by different proteases. Antitoxins DinJ, RelB, and YefM contain C termini that bury a hydrophobic region against the toxin in the context of the toxin-antitoxin complex (Figure 4.2). Such hydrophobic residues are recognized by proteases (6, 13, 36) and this suggests shared hydrophobic regions among these very different antitoxins may aid in toxin sequestration and antitoxin proteolysis. Here, we generated a series of C-terminal antitoxin truncations and tested their ability to sequester toxin. We find that each antitoxin utilizes a different range of residues within their C termini to maintain toxin sequestration. We also designed and tested a quantitative ELISA to track DinJ antitoxin degradation in cell lysates in strains expressing truncated antitoxins, or with proteases deleted. This work provides the framework for testing the role of proteases in antitoxin degradation in addition to determining which residues are recognized by proteases.

4.3 Materials & Methods

4.3a Strains and plasmids

E. coli BL21 DE3 was used for all protein expression studies. *E. coli* BW25113 was used for growth and cell viability assays, as well as generation of cell lysates for western blotting and ELISA analysis. All mutations were introduced by site-directed mutagenesis and sequences were verified by DNA sequencing (Genewiz). Strains and plasmids used in this study are summarized in Table 4.1.

4.3b Bacterial growth and cell viability assays

E. coli BW25113 were transformed with pBAD33 plasmids harboring wild-type toxin-antitoxin systems (*dinJyafQ, relBrelE*, and *yefMyoeB*)*,* truncated antitoxin variants (*dinJΔ77-86-yafQ*, *dinJΔ71-56-yafQ*, *dinJΔ56-86-yafQ*, *relBΔ75-79-relE*, *relBΔ70-79-relE*, *yefMΔ78-83-yoeB*, *yefMΔ73-83-yoeB*, and *yefMΔ53-83-yoeB*), or toxins alone (*yafQ*, *relE*, and *yoeB*) and grown in M9 medium supplemented with 0.2% casamino acids, 0.21% glycerol, 10 mM magnesium sulfate, and 25 µg/mL chloramphenicol at 37 ºC. A 1:100 overnight culture was used to inoculate fresh medium, and cells were grown to an OD_{600} of 0.2. The culture was split in half and induced with 0.2% L-arabinose or equivalent volume of water was added. 300 µL was transferred in triplicate to a 96-well clear flat-bottom polystyrene plate (ThermoFisher) and OD_{600} measurements taken every 15 min in an automated Elx808 plate reader (BioTek) at 37 ºC shaking. For cell viability assays, 100 µL of the same culture (pre-transfer to the microplate) were taken after 8 hr and serially diluted (10^6) in saline. 100 µL of the final dilution was plated on M9 agar containing the same additives as medium and left at 37 ºC for 36 hr. CFU/mL was

determined using the following formula: CFU/mL = log[(colony count * dilution factor)/volume of culture plated].

4.3c YefM and YoeB expression and purification

YefM, YefM truncation mutants, and YoeB were purified as previously described (37). The molecular weight and oligomeric state of YefM, YoeB, and YefMΔ53-83 were determined by loading purified protein either individually or mixed components pre-incubated at 37 ºC for 30 min onto a Superdex S75 column (GE Healthcare) equilibrated with buffer (40 mM Tris-HCl pH 7.5, 250 mM KCl, 5 mM MgCl$_2$, 5 mM β-mercaptoethanol (β-Me)). Molecular weights were calculated based on comparison of elution volumes of molecular weight standards (BioRad).

4.3d Western blotting analysis (DinJ, RelB, and YefM)

E. coli BW25113 were transformed with accompanying toxin-antitoxin pBAD33-*dinJ*, pBAD33-*relB* or pBAD33-*yefM* plasmids and grown in LB medium supplemented with 25 μg/mL chloramphenicol at 37 ºC and 0.2% L-arabinose. Cells were pelleted and resuspended in lysis buffer (20 mM Tris-HCl pH 7.5, 250 mM KCl, 0.1% Triton X-100, 5 mM β-Me, 0.1 mM benzamidine, 0.1 mM PMSF), freezed/thawed for 10 cycles (frozen for 2 min in liquid nitrogen, thawed at 37 ºC for 2 min, vortexed for 5 sec), and diluted with Laemmli buffer (20% glycerol, 62.5 mM Tris-HCl, 2% SDS, 0.025% bromophenol blue, and 0.025% β-Me). Samples of cell lysate were loaded onto a 4-20% tris-glycine SDS-PAGE gel in 5 μg (α-DinJ) or 10 μg (α-RelB and α-YefM) amounts and run at 125 V limiting for 80 min. Gels were removed, washed 3 times, and allowed to equilibrate in

western transfer buffer (25 mM Tris-base, 192 mM glycine, 20% methanol, pH 8.3) for 15 min. The gels were then assembled into the blotting cassette and transferred to Immobilon-FL (Millipore) membranes at 100 V limiting for 45 min. Membranes were removed from the blotting cassette and directly blocked with TBST (20 mM Tris-base, 150 mM NaCl, 0.1% tween-20, 0.05% Triton X-100, pH 7.6) containing 3% blocking agent (BioRad), and left shaking for 1 hr at room temperature (RelB) or overnight at 4 °C (DinJ, YefM). These incubation times were established previously and found to give the most optimal signal. After either 1 hr or overnight, the membranes were removed from buffer, washed with TBST 3 times for 10 min each, and incubated with α-DinJ (Covance), α-RelB (a kind gift from Dr. Kenn Gerdes) or α-YefM (Covance) primary antibody polyclonal rabbit at a 1:10,000 dilution in TBST (0.2% tween-20) containing 3% blocking agent for 1 hr at room temperature. Membrane was removed and washed 5 times with TBST for 10 min each and then incubated with goat anti-rabbit DyLight 550 secondary antibody (ThermoFisher) at a 1:10,000 dilution for 1 hr at room temperature shaking. Membranes were removed and washed 5 times with TBST for 10 min each and imaged on a Typhoon Trio (Amersham) in fluorescence mode using 532 nm excitation mode and a 580 nm band-pass filter.

4.3e Western blotting analysis (FLAG)

Post transfer, membranes were removed from the blotting cassette and directly blocked with Sigma TBS (50 mM Tris-HCl, 138 mM NaCl, 2.7 mM KCl, 0.05%, pH 8) containing 3% blocking agent (BioRad), and left shaking for 30 min at room temperature. Membranes were removed from buffer, washed with Sigma TBST 3 times for 10 min each, and

incubated with anti-FLAG M2 (Sigma) primary antibody monoclonal mouse at a 1:2,500 dilution in Sigma TBS containing 3% blocking agent overnight at 4 ºC. The membranes were removed and washed with TBS for 10 min each and incubated with ECL Plex goat anti-mouse Cy3 conjugated secondary antibody (ThermoFisher) at a 1:2,500 dilution for 1 hr at room temperature shaking. Membranes were removed and washed 4 times with TBST for 5 min each and imaged on a Typhoon Trio (Amersham) in fluorescence mode using 532 nm excitation mode and a 580 nm band-pass filter.

4.3f α-DinJ ELISA

Cell lysates containing expressed antitoxin were diluted to 0.1 mg/mL in carbonate buffer (15 mM sodium carbonate, 35 mM sodium bicarbonate, pH 9.5). 100 µL of sample (10 µg) were pipetted into the wells of a Microfluor 2 High Binding black flat-bottom plate (ThermoFisher), sealed with parafilm, and shaking for 1 hr at room temperature. All incubation steps occurred with a sealed plate and shaking. Carbonate buffer was removed and wells were washed twice with 200 µL TBS, after which the wells were incubated for 1 hr with 100 µL TBST (0.1% tween-20) containing 3% blocking agent (BioRad) at room temperature. Blocking agent was removed and wells were washed twice with 200 µL TBS, after which the wells were incubated for 1 hr with 100 µL primary antibody (1:3,333 polyclonal rabbit anti-DinJ) in TBST at room temperature. Primary antibody solution was removed and wells were washed twice with 200 µL TBS, after which the wells were incubated for 1 hr with 100 µL secondary antibody (1:6,666 polyclonal goat anti-rabbit HRP conjugated (Sigma)) in TBST at room temperature. Secondary antibody solution was removed and wells were washed twice with 200 µL TBS, after which 100 µL

of developing solution (Pierce ECL Western Blotting Substrate (ThermoFisher)) was pipetted into each well and the microplate read by a Cytation5 automated plate reader (BioTek) in luminescence (fiber) mode after 1 min incubation.

4.4 Results

4.4a C termini of DinJ and RelB, but not YefM, are essential for toxin inhibition

To determine whether the C-terminal residues of type II toxin-antitoxin systems RelB-RelE and YefM-YoeB are conserved, we introduced similar C-terminal truncations as in antitoxin DinJ. In antitoxin RelB, we introduced C-terminal truncations Δ75-79 and Δ70-79 that ablate direct interactions between RelB and cognate toxin RelE (Figure 4.1B). RelBΔ75-79 removes RelB α4 which packs directly against a hydrophobic pocket on RelE similar to YafQ (Figure 4.2). The more severe truncation, RelBΔ70-79, additionally removes RelB β1 and loop 4, which wrap around toxin RelE. However, RelB β1 does not form an antiparallel β-sheet with an accompanying β-strand from RelE, unlike in DinJ-YafQ. In addition, loop 4 of RelB (residues 66–72) is 3 residues longer than loop 5 of DinJ. We also introduced C-terminal truncations in antitoxin YefM to similarly ablate interactions with cognate toxin YoeB, which include Δ78-83, Δ73-83, and Δ53-83 (Figure 4.1C). Unlike DinJ and RelB, YefM does not contain α-helices or β-strands in its C-terminus and instead contains only loop 5 (residues 73-76). Loop 5 in YefM is similarly sized to loop 5 in DinJ (~4 residues). YefMΔ78-83 removes residues that pack against a hydrophobic region on cognate toxin YoeB (Figure 4.2). YefMΔ73-83 additionally removes YefM loop 5. YefMΔ53-83 removes the long α-helix that precedes loop 5, in case neither YefMΔ78 or Δ73-83 are sufficient to ablate toxin-antitoxin interaction. Using these YefM variants, we next monitored the effect of their overexpression on growth (OD_{600}) for 24 hrs and determined cell viability (CFU/mL) 8 hrs post-induction. Antitoxin variants unable to form complexes with their cognate toxin will release the toxin, resulting in halted growth. Inhibition of growth is an easy measure to determine whether toxin-antitoxin

complex formation occurs.

These assays were first performed using DinJ truncations. DinJ truncations Δ77-86, Δ71-86, and Δ56-86 all abrogated growth similar to YafQ toxin-only levels, suggesting that even the smallest truncation was sufficient to release toxin (Figure 4.3A). However, while each of these truncations resulted in lower cell viability (~6.5 CFU/mL) as compared to when wild-type DinJ was expressed (~8 CFU/mL), this did not match when YafQ toxin only was expressed (no measurable CFU/mL) (Figure 4.3A). Overexpression of truncated RelBΔ75-79 resulted in abrogation of growth and lowered cell viability (~6 CFU/mL) (Figure 4.3B) similar to the DinJ truncations. However, RelBΔ70-79 results in no measurable cell viability akin to RelE toxin only (Figure 4.3B). These data suggest that RelB utilizes the last 10 residues of its C-terminus to sequester toxin, whereas DinJ can utilize residues prior to 51. Overexpression of truncated YefM did not result in any growth or viability difference until at least 20 residues were deleted (Figure 4.3C). Expression of YefMΔ78-83 and Δ73-83 is indistinguishable from wild-type YefM expression. Only YefMΔ53-83, which represents removal of the long helix before the C-terminus of YefM, results in toxin release. This release is likely complete, as YefMΔ53-83 growth is abrogated and has no cell viability (Figure 4.3C). These data indicate that YefM must utilizes residues 53 to 73 to sequester toxin, which is different from both DinJ and RelB. Together, these data suggest that these antitoxins utilize their C termini in different ways to sequester toxin.

To test whether the RelBΔ75-79 and Δ70-79 or YefMΔ78-83, Δ73-83, and Δ53-83 still

biochemically form a complex with cognate toxins RelE and YoeB, we purified each protein and tested for interaction via size exclusion chromatography (SEC), similar to DinJ (Figure 4.4). YefM and YoeB elute at a volume corresponding to 36 and 12.5 kDa respectively. YefMΔ53 elutes at a similar volume of YoeB toxin, also corresponding to 12.5 kDa. We then incubated YefM variants with YoeB to form a complex before analysis by SEC. YefM-YoeB elutes at a volume corresponding to 38 kDa, but YefMΔ53-83-YoeB elutes at 12.5 kDa. This indicates that the YefMΔ53-83 truncation can no longer bind YoeB (Figure 4.4). YefMΔ78-83 and Δ73-83, and RelBΔ75-79 and Δ70-79 remain to be tested (see Discussion). These preliminary results suggest that C termini that contain little secondary structure, like in YefM are not critical in maintaining the toxin-antitoxin complex and sequestering toxin, as compared to structured C termini like that in DinJ.

4.4b 3xFLAG DinJ is artificially stabilizing

To understand how cellular proteases may regulate antitoxin levels *in vivo*, we designed a series of N-terminally FLAG tagged antitoxin constructs. Since our studies focus on the C termini of antitoxins, the FLAG tag had to be appended at the N-terminus to avoid disrupting interactions between the C termini and cognate toxins. These constructs would then be induced for antitoxin expression (either wild-type or truncated) and allow us to monitor antitoxin half-lives after the inhibition of protein synthesis by addition of spectinomycin as previously performed (38-40). (Figure 4.5). Wild-type DinJ and 3xFLAG-DinJ were detected using a α-DinJ polyclonal antibody (gift from Dr. Nancy Woychik, Rutgers (8, 25)). Detection of 3xFLAG-DinJ using an α-FLAG polyclonal antibody (Sigma F7425) was not observed. In each case, multiple secondary antibodies

were tested to ensure detection method was not a concern. In addition, two tagged protein controls were used (FT-MazF and FT-FlhD), and a secondary lot of Sigma F7425 was also tested. Switching to a new α-FLAG monoclonal M2 antibody (Sigma F3165) alleviated detection issues. Further, we confirmed that the primary α-FLAG was indeed the issue, as monoclonal M2 from Cell Signaling Technologies (CST 14793) also alleviated detection issues (results are summarized in Table 4.2). We found that appending the N-terminal 3XFLAG tag to DinJ artificially stabilized its half-life similar to when Lon protease was removed from the strain (Δlon) (Figure 4.6). We next constructed a 1xFLAG construct but were unable to detect any protein. Thus, we abandoned using the FLAG system. Our lab already had a polyclonal DinJ serum antibody, so we next sought to obtain an established antibody for RelB (of RelB-RelE) and generate an antibody against YefM (of YefM-YoeB).

4.4c Validation of anti-RelB and anti-YefM antibodies for future use

To expand the proposed studies to antitoxins RelB and YefM, we tested serum antibodies against each protein. The α-RelB antibody was a kind gift from Dr. Kenn Gerdes from the University of Copenhagen (9). The α-YefM antibody was generated by Covance against purified *E. coli* YefM (Labcorp Drug Development). Each antibody was tested for specificity in E. coli lysates in which each antitoxin had been expressed for 180 min (Figure 4.7). Each antibody was able to detect overexpressed RelB and YefM in cellular lysates.

4.4d Establishing an anti-DinJ ELISA for high-throughput screening of antitoxin half-life

To assay a wide combination of antitoxin variants and protease deletions, we sought to design a quantitative enzyme-linked immunosorbent assay (ELISA) to track antitoxin degradation in E. coli cell lysates (41, 42). We initially selected an indirect ELISA, which relies on the antitoxin being immobilized to the surface inside the wells of a microplate, after which a standard array of probing is performed (Figure 4.8A). This is because we had already established a protocol for on-hand primary and secondary antibodies. We tested a number of different factors in setting up the ELISA (Table 4.3), including whether to perform short or long incubation steps, different blocking agents, and concentrations of antibody solutions that gave the highest signal-to-noise ratio. This resulted in a functioning ELISA method (Figure 4.8B) that tracks expression and degradation of DinJ in *E. coli* cellular lysates (Fig. 4.9).

4.5 Discussion

The formation of type II toxin-antitoxin complexes typically results from the antitoxin wrapping around the toxin to suppress toxin function and does not appear to fulfill traditional ways to bury hydrophobic regions within protein-protein interactions. Previous analyses of DinJ antitoxin C-terminal truncations revealed attenuation of bacterial growth similar to toxin only expression after the removal of only 10 residues (25). However, cell viability remains relatively stable (Figure 4.2A), whereas full toxin alone results in complete inhibition of growth. To determine if antitoxins utilize conserved mechanisms to sequester toxin, *E. coli* RelB-RelE and YefM-YoeB were also examined. While RelE and YoeB toxins are homologous to YafQ toxin, their cognate antitoxins all interact with toxins in different ways. The C termini of DinJ and RelB are structurally similar and contain two flanking α-helices. YefM lacks secondary structure in the last 10 residues in its C-terminus but contains a small loop (residues 73-76). This is a major difference between YefM and DinJ and RelB. Truncation of RelBΔ75-79 abrogates growth and reduces cell viability from ~8 to ~6 CFU/mL. Truncation of RelBΔ70-79 reduces cell viability to levels akin to RelE toxin only, which does not occur in a similar 10 residue truncation of DinJΔ77-86. It is surprising that DinJ maintains cell viability (and thus, sequestration of toxin) after removal of 30 residues, since truncation of only the last 10 residues of DinJ renders it unable to bind toxin YafQ (25). In contrast, deletion of the last 10 residues of RelB fully releases toxin. DinJ then must utilize distinct residues to interact with cognate toxin YafQ and keep it sequestered. In stark contrast, removal of at least 20 residues of YefMΔ53-83 is required to observe any abrogated growth or reduced cell viability as a consequence of YoeB release. Although YefM lacks any secondary structure in its C-terminus, it remains more

186

incalcitrant to truncations than RelB, as the shortest truncation of RelBΔ75-79 still impacts both growth and cell viability. In summary, these data suggest the stability of each toxin-antitoxin complex is governed in different ways and does not depend solely on the wrapping the C-terminus around the toxin. Distinct residues in the C termini of antitoxins maintain sequestration. For example, interactions stemming from residues 53 and 73 of YefM must accomplish toxin sequestration, since truncation of anything prior eliminates cell viability. DinJ utilizes interactions that occur even further from the C-terminus, which are before residue 51. In contrast, RelB must rely on interactions within the last 9 residues of the C-terminus, between residues 70-79. These assays should be expanded to antitoxins with intrinsically disordered C termini like CcdA and HipB (23, 43) to further explore patterns in toxin sequestration.

Antitoxin stability as a function of its half-life could be determined using ELISAs. It's possible that antitoxin truncations that reduce or remove hydrophobic regions or residues could result in increased stability against Lon protease. Hydrophobic regions or residues could be features that are critical for proteolysis and could be tested by mutating individual residues within each truncation (Figure 4.1D). For example, the C termini of CcdA and HipB hydrophobic residues are recognized by Lon. The half-lives of these antitoxins are 10 and 17 minutes *in vivo* respectively, but those values are stabilized to >120 and 200 minutes in a Lon protease deletion strain (22, 23). In addition, it is not well understood how Clp protease contributes to antitoxin proteolysis across bacteria, or if Lon equally contributes to proteolysis of all antitoxins and not just a select few. As *E. coli* DinJ-YafQ, RelB-RelE, and YefM-YoeB are upregulated during different environmental stimuli (DNA

damage, nutrient starvation, and thermal stress, respectively), there is also a possibility that these systems are targeted by different proteases. Therefore, cells expressing antitoxin variants and lacking either Lon or Clp (including subunits A, P, and X) proteases should also be used in antitoxin half-life assays. My initial quantitative ELISA against DinJ shows a 1.6-fold increase in total DinJ present in a Δlon strain as compared to wild-type (Figure 4.9). These assays should be extended to Clp proteases to determine if Clp also plays a role in antitoxin proteolysis.

Finally, adaptor proteins may help proteases gain specificity for antitoxins and thus should also be investigated. Recently, it has been demonstrated that Lon collaborates with adaptors to gain specificity against known substrates or unstructured proteins (44, 45). For example, the specificity and activity of Lon can be regulated by associating with heat shock protein Q (HspQ) (44). HspQ is a member of the heat-shock responsive family of proteins and is conserved in all kingdoms. HspQ contains a C-terminal motif through which Lon recognizes and binds HspQ, thus enhancing total proteolysis. For example, casein (a known unstructured Lon substrate) is degraded three times faster by Lon when HspQ is present (44). Lon activity can also be modulated by DnaJ/K, a widely known chaperone system that regulates levels of DNA replication protein DnaA (45). DnaA initiates DNA replication in bacteria by unwinding DNA and recruiting components necessary for replication to proceed. Critical parts of the recruitment process of DNA replication are governed by the DnaJ/K chaperone system, which includes accumulation of sufficient amounts of DnaA (46). Interestingly, depletion of the DnaJ/K system through stress-induced protein unfolding led to enhanced proteolysis of DnaA by Lon. A decrease

in cellular DnaA levels halts DNA replication to prevent cell cycle progression to survive stress. It was also suggested that depletion of DnaJ/K likely left other Lon substrates unfolded, which allosterically activated Lon against DnaA. Thus, Lon possibly surveys the proteome landscape for increasing levels of unfolded protein and can tune degradation accordingly. To test whether these adaptors are involved in antitoxin proteolysis, adaptor deletion strains ($\Delta hspQ$, $\Delta dnaJ$, $\Delta dnaK$, and $\Delta dnaJ/K$) should also be used in ELISA based assays to further explore if adaptors play a role in antitoxin proteolysis.

4.6 Figures & Tables
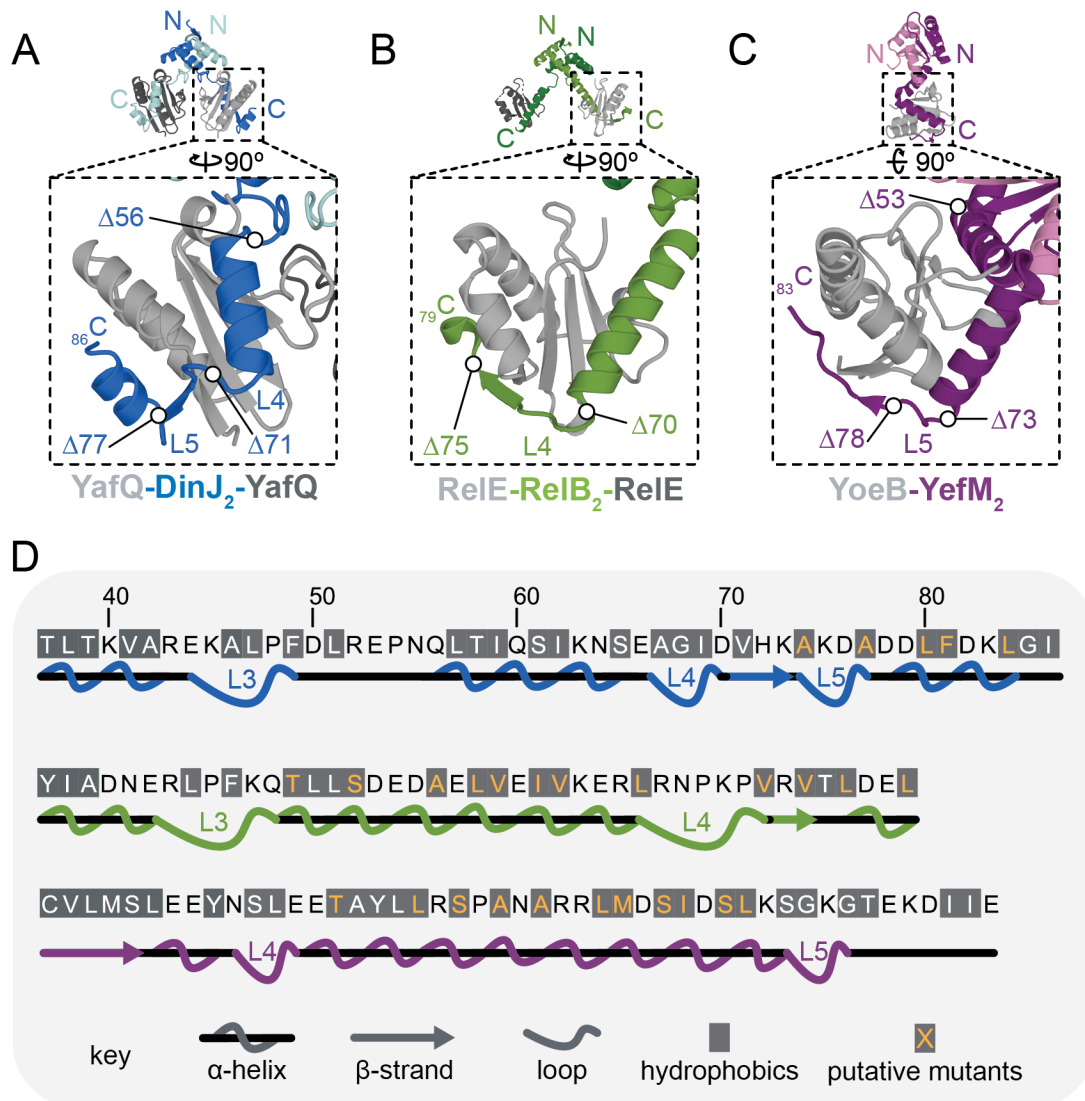
Figure 4.1 – Structures of toxin-antitoxin complexes.

C termini of (**A**) DinJ (blue), (**B**) RelB (green), and (**C**) YefM (purple) are shown bound to their cognate toxins (gray) (PDB codes 4Q2U, 4FXE, and 2A6Q). C-terminal truncations are indicated for each antitoxin. (**D**) Residue and secondary structure alignment of antitoxins from panels A–C are shown. α-helices, β-strands, and loops are indicated by symbols in the key. Hydrophobic residues are indicated with grey boxes, and putative

targets for mutation are in orange.
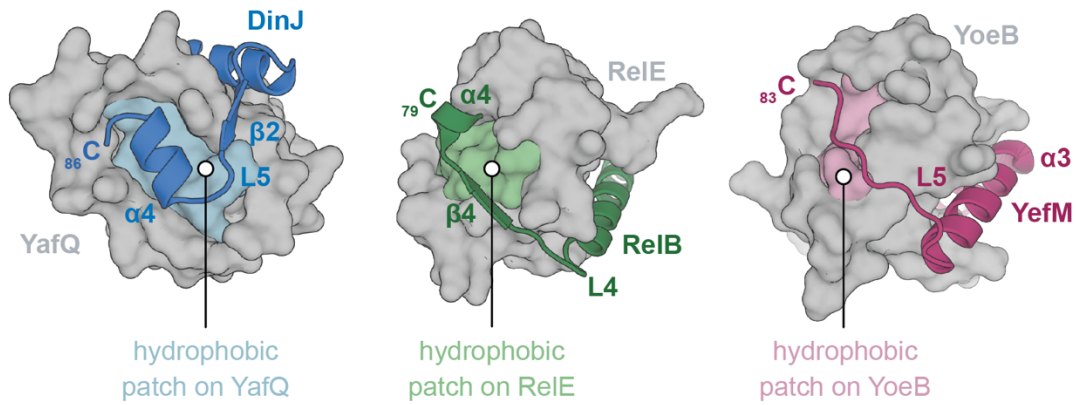
Figure 4.2 – Comparison of the hydrophobic patches of toxins near C termini of antitoxins.

(**A**) DinJ (blue) is shown bound to the YafQ toxin (gray surface representation; PDB code 4Q2U). (**B**) RelB (green) is shown bound to the RelE toxin (gray surface representation; PDB code 4FXE). (**C**) YefM (purple) is shown bound to the YoeB toxin (gray surface representation; PDB code 2A6Q). The C-terminal regions of each antitoxin and pack against a hydrophobic pocket located on the toxin (lighter shades).
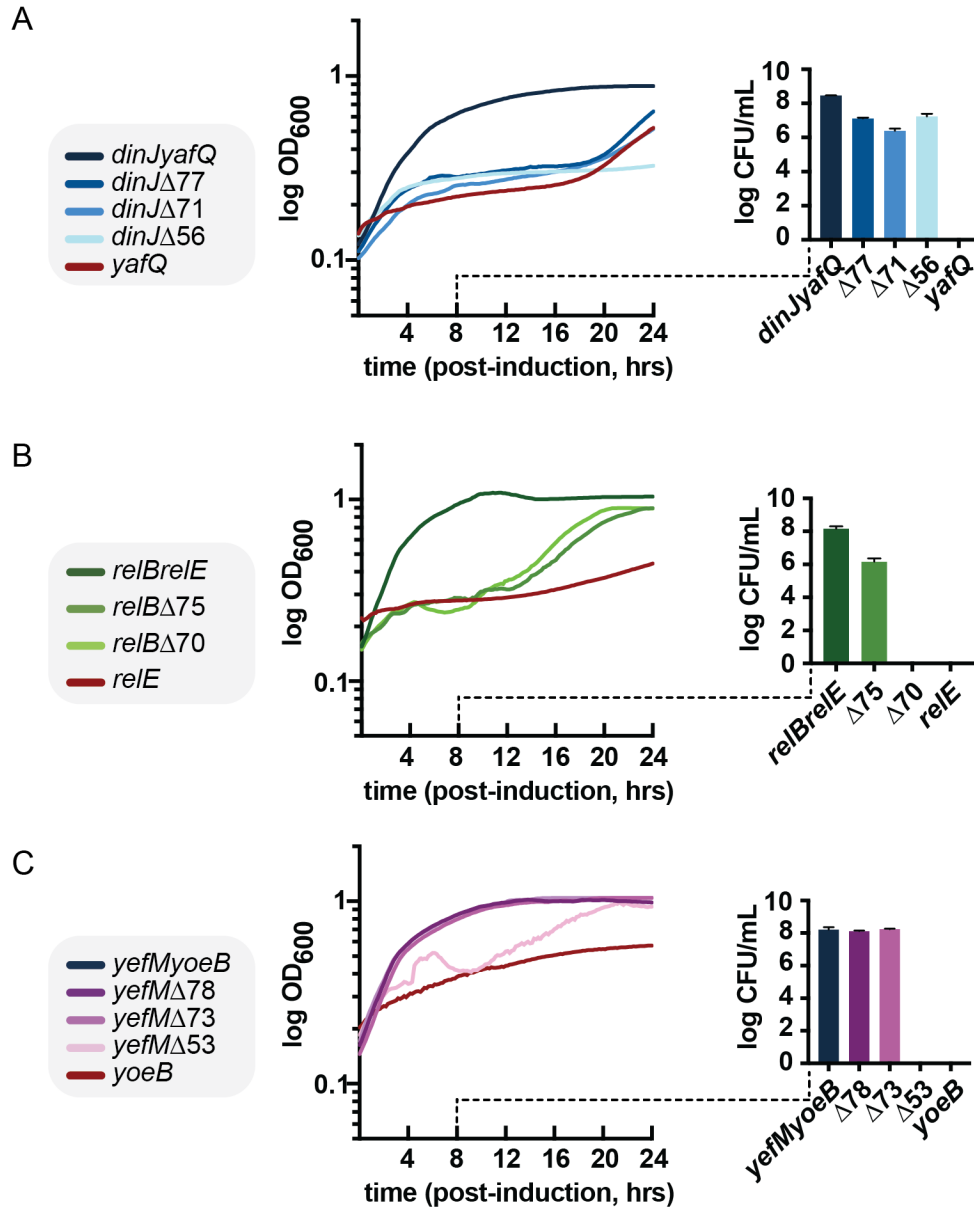
Figure 4.3 – C termini of DinJ and RelB, but not YefM, is essential for toxin suppression.

Growth curves of *E. coli* BW25113 expressing (**A**) DinJ-YafQ, (**B**) RelB-RelE, (**C**) YefM-YoeB or C-terminal truncated variants are shown. Cultures from growth assays were plated 8 hours after induction (dotted lines) and CFU/mL determined. Error bars represent SD.
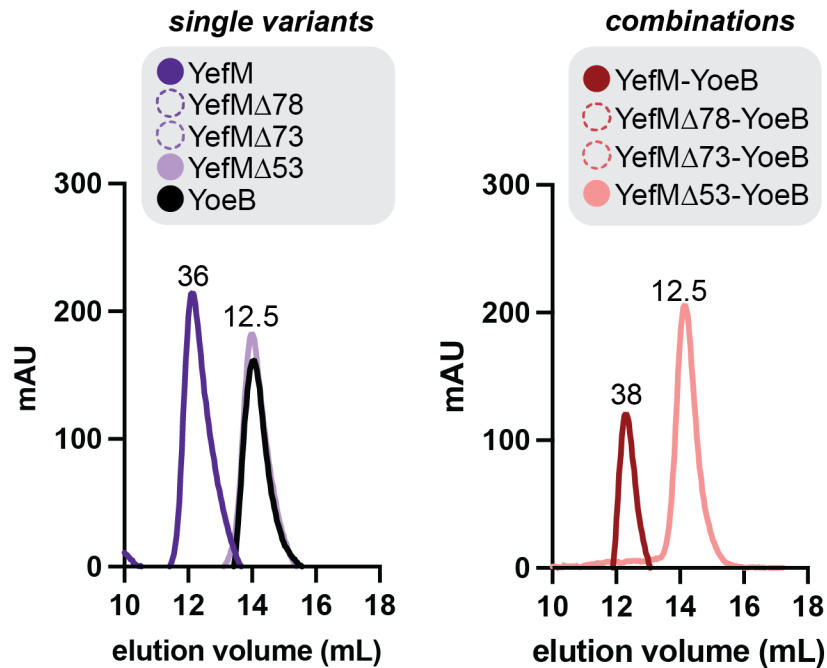
Figure 4.4 – The C-terminus of YefM may be essential for toxin suppression.

Size-exclusion chromatography (SEC) of YefM-YoeB single proteins (left) or combinations (right) are shown. YefM-YoeB elutes as a 36 kDa complex, whereas YefMΔ53-83-YoeB elutes as a single 12.5 kDa peak, which indicates elution as separate species. YefMΔ78-83 and Δ73-83 variants remain to be analyzed separately and mixed with YoeB (dotted circles).
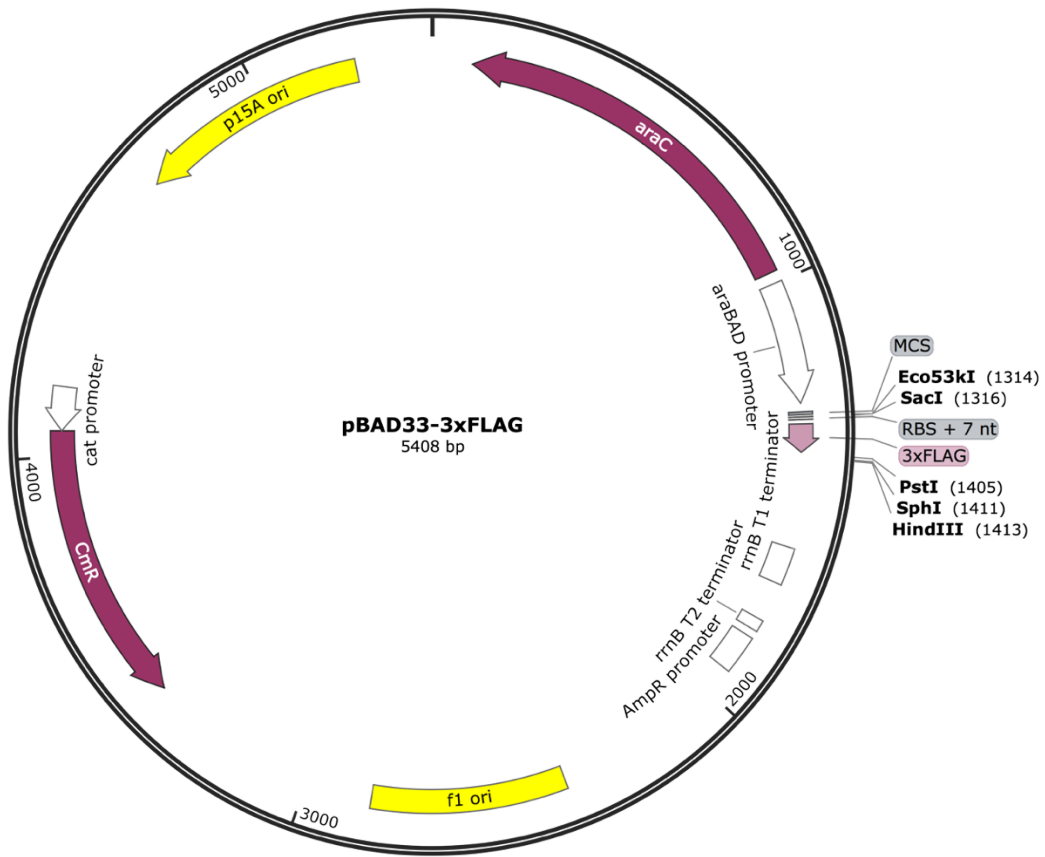
Figure 4.5 – 3xFLAG-tag-appending vector.

A pBAD33-3xFLAG plasmid was designed to append N-terminal 3xFLAG tags with a multiple cloning site containing PstI, SphI, and HindIII sites for gene insertion.
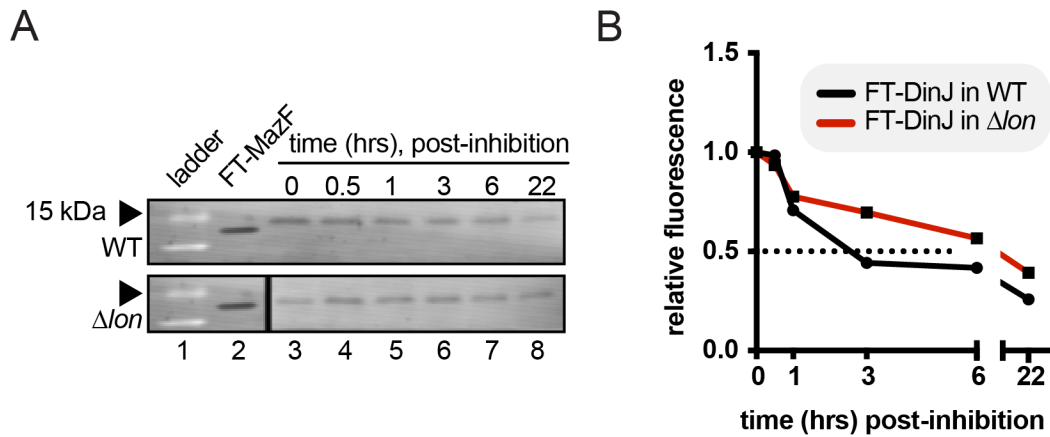
Figure 4.6 – 3xFLAG tag stabilizes antitoxins.

(**A**) Western blots against 3xFLAG-tagged DinJ in *E. coli* BW25113 and Δ*lon* strains are shown. 15 kDa and 10 kDa bands are indicated in lane 1. A flag-tagged control protein, FT-MazF is used in lane 2. Degradation of 3xFT-DinJ is tracked post-expression and translation inhibition for up to 22 hours (lanes 3–8). The intensity of these bands is quantified and normalized as relative fluorescence for comparison in (**B**).
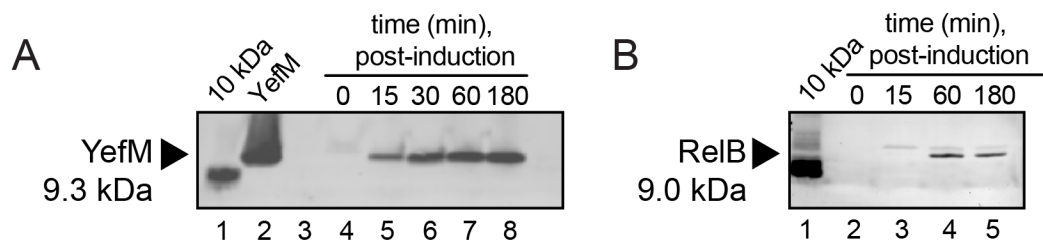
Figure 4.7 – RelB and YefM antibodies are specific to protein of interest.

Western blots of either (**A**) α-YefM or (**B**) α-RelB are shown using cell lysates in which either YefM or RelB have been expressed for up to 180 minutes. 10 kDa ladder is indicated in lane 1.
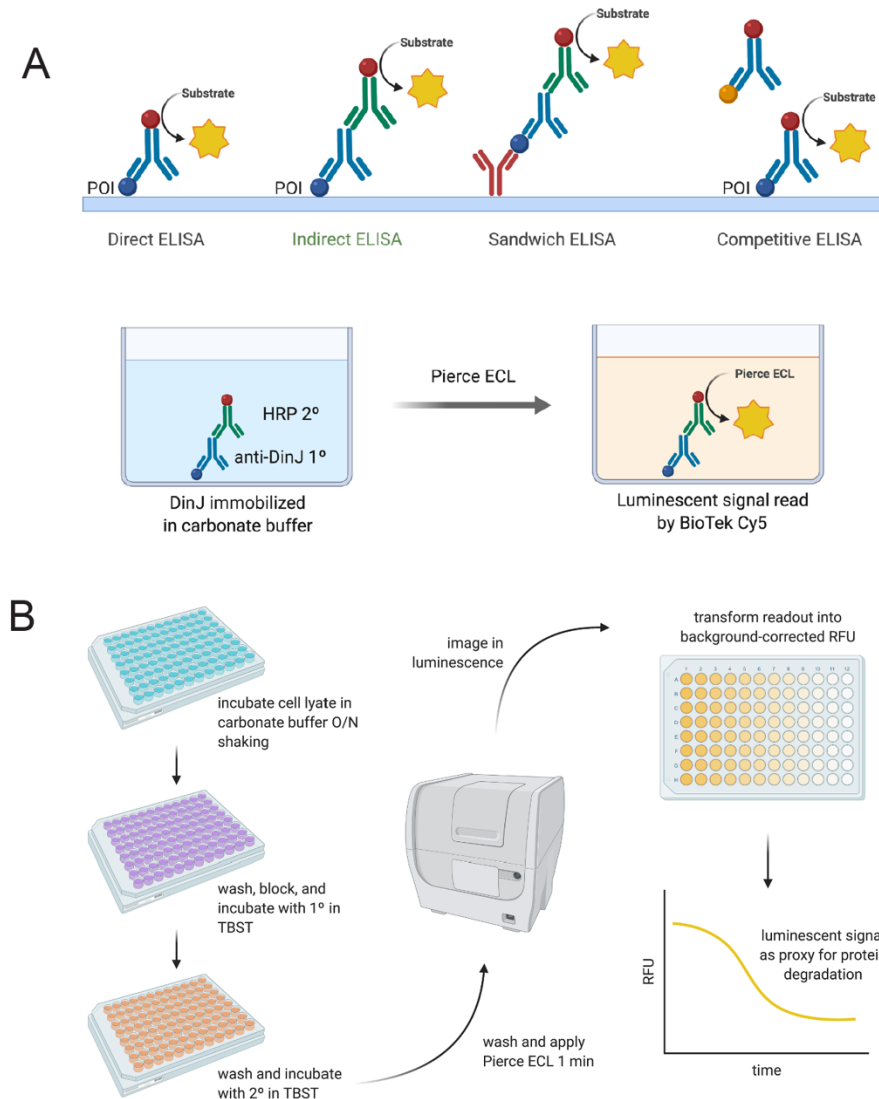
Figure 4.8 – General overview of α-DinJ ELISA.

(**A**) The α-DinJ ELISA is an indirect ELISA, where protein of interest is immobilized to the surface of microplate wells and probed with both a primary and secondary antibody. This contrasts with other ELISA methods which rely either on a primary antibody detection method (direct ELISA), protein capture (sandwich ELISA), or a competition assay (competitive ELISA). (**B**) The general wet-lab workflow of the α-DinJ ELISA is shown. Figure made with BioRender.com.
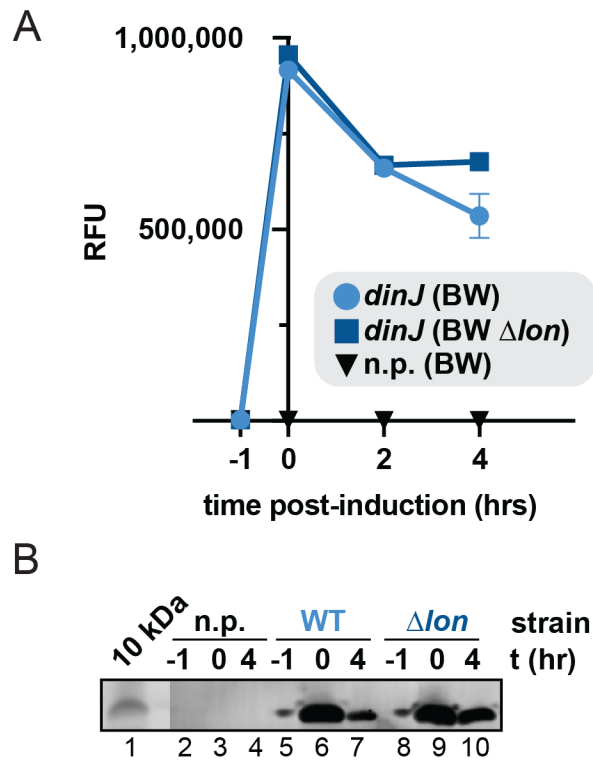
Figure 4.9 – Lon protease likely targets DinJ for proteolysis.

(**A**) DinJ is detected in cell lysates analyzed using the α-DinJ ELISA protocol near 1,000,000 RFU after 1 hour of expression. Up to 4 hours post-translation inhibition, the RFU from DinJ detection in a wild-type *E. coli* BW25113 strain is nearly 150,000 units higher (1.6-fold change) than in a Δ*lon* protease deletion strain. (**B**) The same cell lysates were also analyzed by western blot where the same pattern was observed.

Table 4.1 – Strains and plasmids used in Chapter 4.

Strain/plasmid	Description	Source
E. coli strain	Genotype	Reference
BW25113	Δ(*araD-araB*)567 Δ*lacZ4787*(::*rrnB-4*) *lacIp-400*(*lacIQ*)λ- *rpoS396*(Am) *rph-1* Δ(*rhaD-rhaB*)568 *rrnB-4* *hsdR514*	(47)
BL21DE3	F- *ompT* $hsdS_\beta(r_\beta\text{-}m_\beta\text{-})$ dcm^+ Tet^r *gal* λ(DE3) *endA* Hte [pLysS Cam^r]	Novagen
Plasmid	Content	Reference
pBAD33	Expression vector with cam^r-cassette, P_{BAD} promoter, pACYC184 origin, araC coding sequence, and ara operator	(48)
pBAD33-*dinJ-yafQ*	–	(25)
pBAD33-*dinJΔ77-86-yafQ*	–	(25)
pBAD33-*dinJΔ71-86-yafQ*	–	(25)
pBAD33-*dinJΔ56-86-yafQ*	–	(25)
pBAD33-*yafQ*	–	(25)
pBAD33-*relB-relE*	–	This study
pBAD33-*relBΔ75-79-relE*	–	This study
pBAD33-*relBΔ70-79-relE*	–	This study
pBAD33-*relE*	–	This study
pBAD33-*yefM-yoeB*	–	This study
pBAD33-*yefMΔ78-83-yoeB*	–	This study
pBAD33-*yefMΔ73-83-yoeB*	–	This study
pBAD33-*yefMΔ53-83-yoeB*	–	This study
pBAD33-*yoeB*	–	This study
pET21c	Expression vector with amp^r-	Novagen

	cassette, T7 promoter, f1 origin, and C-term His tag.	
pET21c-*yefM-yoeB-6xHis*	–	(49)
pET28a	Expression vector with kan^r-cassette, T7 promoter, f1 origin, and N/C-term His tag.	Novagen
pET28a-*yefM*	–	This study
pET28a-*yefMΔ78-83*	–	This study
pET28a-*yefMΔ78-83*	–	This study
pET28a-*yefMΔ78-83*	–	This study

201

Table 4.2 – Summary of western blot troubleshooting experiments.

Key is as follows: (✓) strong signal, (B) background banding only, (N/A) experiment not performed. Abbreviations FL, CIL, HRP/ECL are fluorescence, chemiluminescence, and horseradish-peroxidase/enzymatic chemiluminescence respectfully. Blank cells indicate no detection observed.

Primary Antibody (1º)	Secondary Antibody (2º)	DinJ	FT-MazF	FT-FlhD*	FT-DinJ
1º anti-DinJ polyclonal (Covance)	2º DyLight 550 (FL)	✓			✓
	2º Cy3 (FL)	✓			✓
	2º HRP/ECL (CIL)	✓			✓
1º anti-FLAG polyclonal (Sigma F7425)	2º DyLight 550 (FL)			B	B
	2º Cy3 (FL)			B	B
	2º HRP/ECL (CIL)			B	B
1º anti-FLAG Monoclonal M2 (CST 14793)	2º HRP/ECL (CIL)		✓		N/A
1º anti-FLAG Monoclonal M2 (Sigma F3165)	2º Cy3 (FL)		✓		✓

Table 4.3 – ELISA controls performed prior to analysis of cell lysates.

Abbreviations O/N, TBS, TBSt, and ECL are overnight, tris-buffered saline, tris-buffered saline containing tween-20, and enzymatic chemiluminescence respectively.

Control	Purpose	Result
1 hr v O/N protein	Determine the effect of protein incubation time on total output signal	No measurable effect *in vitro*
1 hr v O/N block	Determine the effect of blocking time on total output signal	No measurable effect *in vitro*
TBS v TBSt	Determine the effect of tween-20 addition in incubation steps	Tween-20 necessary – prevents background from antibody absorption
1º solution	Determine luminescence of primary antibody solution	< 100 RFU (low)
2º solution	Determine luminescence of secondary antibody solution	< 100 RFU (low)
ECL	Determine luminosity of luminescent substrate without HRP	< 100 RFU (low)
Block, 1º, 2º, ECL	Determine background of wells that have skipped protein incubation	< 100 RFU (low, tween-20 must be present in blocking and wash buffers)
Block, 1º, 2º, ECL	Determine background of wells that have skipped protein and blocking incubation	< 100 RFU (low, tween-20 must be present in blocking and wash buffers)
1º & 2º checkboard	Determine concentrations of primary and secondary that achieve high signal:noise	1º no greater dilution than 1:6,500, 2º no greater dilution than 1:25,000.

4.7 References

1. Tsilibaris V, Maenhaut-Michel G, Van Melderen L. Biological roles of the Lon ATP-dependent protease. Res Microbiol. 2006;157(8):701-13. Epub 2006/07/21. doi: 10.1016/j.resmic.2006.05.004. PubMed PMID: 16854568.

2. Maurizi MR. Proteases and protein degradation in *Escherichia coli*. Experientia. 1992;48(2):178-201. Epub 1992/02/15. doi: 10.1007/BF01923511. PubMed PMID: 1740190.

3. Van Melderen L, Aertsen A. Regulation and quality control by Lon-dependent proteolysis. Res Microbiol. 2009;160(9):645-51. Epub 2009/09/24. doi: 10.1016/j.resmic.2009.08.021. PubMed PMID: 19772918.

4. Lee I, Suzuki CK. Functional mechanics of the ATP-dependent Lon protease- lessons from endogenous protein and synthetic peptide substrates. Biochimica et biophysica acta. 2008;1784(5):727-35. doi: 10.1016/j.bbapap.2008.02.010. PubMed PMID: 18359303; PMCID: PMC2443057.

5. Gur E, Biran D, Ron EZ. Regulated proteolysis in Gram-negative bacteria--how and when? Nat Rev Microbiol. 2011;9(12):839-48. Epub 2011/10/25. doi: 10.1038/nrmicro2669. PubMed PMID: 22020261.

6. Olivares AO, Baker TA, Sauer RT. Mechanistic insights into bacterial AAA plus proteases and protein-remodelling machines. Nature Reviews Microbiology. 2016;14(1):33-44. doi: 10.1038/nrmicro.2015.4. PubMed PMID: WOS:000366399600007.

7. Gerdes K, Christensen SK, Løbner-Olesen A. Prokaryotic toxin-antitoxin stress response loci. Nature reviews Microbiology. 2005;3(5):371-82. doi: 10.1038/nrmicro1147. PubMed PMID: 15864262.

8. Prysak MH, Mozdzierz CJ, Cook AM, Zhu L, Zhang Y, Inouye M, Woychik NA. Bacterial toxin YafQ is an endoribonuclease that associates with the ribosome and blocks translation elongation through sequence-specific and frame-dependent mRNA cleavage.

Molecular Microbiology. 2009;71(5):1071-87. doi: 10.1111/j.1365-2958.2008.06572.x. PubMed PMID: 19210620.

9.   Christensen SK, Mikkelsen M, Pedersen K, Gerdes K. RelE, a global inhibitor of translation, is activated during nutritional stress. Proceedings of the National Academy of Sciences of the United States of America. 2001;98(25):14328-33. doi: 10.1073/pnas.251327898. PubMed PMID: 11717402; PMCID: PMC64681.

10.   Christensen SK, Maenhaut-Michel G, Mine N, Gottesman S, Gerdes K, Van Melderen L. Overproduction of the Lon protease triggers inhibition of translation in *Escherichia coli*: involvement of the *yefM-yoeB* toxin-antitoxin system. Molecular Microbiology. 2004;51(6):1705-17. doi: 10.1046/j.1365-2958.2003.03941.x. PubMed PMID: 10.1046/j.1365-2958.2003.03941.x.

11.   Kim Y, Wang X, Zhang XS, Grigoriu S, Page R, Peti W, Wood TK. *Escherichia coli* toxin/antitoxin pair MqsR/MqsA regulate toxin CspD. Environ Microbiol. 2010;12(5):1105-21. Epub 2010/01/29. doi: 10.1111/j.1462-2920.2009.02147.x. PubMed PMID: 20105222; PMCID: PMC3980499.

12.   Donegan NP, Marvin JS, Cheung AL. Role of adaptor TrfA and ClpPC in controlling levels of SsrA-tagged proteins and antitoxins in *Staphylococcus aureus*. J Bacteriol. 2014;196(23):4140-51. Epub 2014/09/17. doi: 10.1128/JB.02222-14. PubMed PMID: 25225270; PMCID: PMC4248875.

13.   Gur E, Sauer RT. Recognition of misfolded proteins by Lon, a AAA(+) protease. Genes & development. 2008;22(16):2267-77. doi: 10.1101/gad.1670908. PubMed PMID: 18708584; PMCID: PMC2518814.

14.   Gur E. The Lon AAA+ protease. Subcell Biochem. 2013;66:35-51. Epub 2013/03/13. doi: 10.1007/978-94-007-5940-4_2. PubMed PMID: 23479436.

15.   Battesti A, Gottesman S. Roles of adaptor proteins in regulation of bacterial proteolysis. Current opinion in microbiology. 2013;16(2):140-7. doi: 10.1016/j.mib.2013.01.002. PubMed PMID: 23375660; PMCID: PMC3646950.

16.   Keiler KC, Feaga HA. Resolving nonstop translation complexes is a matter of life or death. J Bacteriol. 2014;196(12):2123-30. Epub 2014/04/08. doi: 10.1128/JB.01490-14. PubMed PMID: 24706739; PMCID: PMC4054194.

17.   Mukherjee S, Bree AC, Liu J, Patrick JE, Chien P, Kearns DB. Adaptor-mediated Lon proteolysis restricts *Bacillus subtilis* hyperflagellation. Proceedings of the National Academy of Sciences of the United States of America. 2015;112(1):250-5. doi: 10.1073/pnas.1417419112. PubMed PMID: 25538299; PMCID: PMC4291670.

18.   Joshi KK, Chien P. Regulated Proteolysis in Bacteria: Caulobacter. Annual review of genetics. 2016;50(1):423-45. doi: 10.1146/annurev-genet-120215-035235. PubMed PMID: 27893963; PMCID: PMC5510660.

19.   Muthuramalingam M, White JC, Bourne CR. Toxin-Antitoxin Modules Are Pliable Switches Activated by Multiple Protease Pathways. Toxins. 2016;8(7):214. doi: 10.3390/toxins8070214. PubMed PMID: 27409636; PMCID: PMC4963847.

20.   Chan WT, Espinosa M, Yeo CC. Keeping the Wolves at Bay: Antitoxins of Prokaryotic Type II Toxin-Antitoxin Systems. Front Mol Biosci. 2016;3:9. Epub 2016/04/06. doi: 10.3389/fmolb.2016.00009. PubMed PMID: 27047942; PMCID: PMC4803016.

21.   Loris R, Garcia-Pino A. Disorder- and dynamics-based regulatory mechanisms in toxin-antitoxin modules. Chem Rev. 2014;114(13):6933-47. Epub 2014/05/09. doi: 10.1021/cr400656f. PubMed PMID: 24806488.

22.   Van Melderen L, Thi MH, Lecchi P, Gottesman S, Couturier M, Maurizi MR. ATP-dependent degradation of CcdA by Lon protease. Effects of secondary structure and heterologous subunit interactions. J Biol Chem. 1996;271(44):27730-8. Epub 1996/11/01. PubMed PMID: 8910366.

23.   Hansen S, Vulić M, Min J, Yen T-J, Schumacher MA, Brennan RG, Lewis K. Regulation of the *Escherichia coli* HipBA Toxin-Antitoxin System by Proteolysis. PLoS ONE. 2012;7(6):e39185-10. doi: 10.1371/journal.pone.0039185; PMCID: 22720069.

24.   Koch AL, Levy HR. Protein turnover in growing cultures of *Escherichia coli*. J Biol Chem. 1955;217(2):947-57. Epub 1955/12/01. PubMed PMID: 13271454.

25.   Ruangprasert A, Maehigashi T, Miles SJ, Dunham CM. Importance of the *E. coli* DinJ antitoxin carboxy terminus for toxin suppression and regulated proteolysis. Molecular Microbiology. 2017;104(1):65-77. doi: 10.1111/mmi.13641. PubMed PMID: 28164393.

26.   Motiejunaite R, Armalyte J, Markuckas A, Suziedeliene E. *Escherichia coli dinJ-yafQ* genes act as a toxin-antitoxin module. FEMS Microbiol Lett. 2007;268(1):112-9. Epub 2007/02/01. doi: 10.1111/j.1574-6968.2006.00563.x. PubMed PMID: 17263853.

27.   Armalyte J, Jurenaite M, Beinoraviciute G, Teiserskas J, Suziedeliene E. Characterization of *Escherichia coli dinJ-yafQ* toxin-antitoxin system using insights from mutagenesis data. J Bacteriol. 2012;194(6):1523-32. Epub 2012/01/17. doi: 10.1128/JB.06104-11. PubMed PMID: 22247505; PMCID: PMC3294823.

28.   Ruangprasert A, Maehigashi T, Miles SJ, Giridharan N, Liu JX, Dunham CM. Mechanisms of toxin inhibition and transcriptional repression by *Escherichia coli* DinJ-YafQ. The Journal of biological chemistry. 2014;289(30):20559-69. doi: 10.1074/jbc.M114.573006. PubMed PMID: 24898247; PMCID: PMC4110269.

29.   Cherny I, Overgaard M, Borch J, Bram Y, Gerdes K, Gazit E. Structural and thermodynamic characterization of the *Escherichia coli* RelBE toxin-antitoxin system: indication for a functional role of differential stability. Biochemistry. 2007;46(43):12152-63. Epub 2007/10/11. doi: 10.1021/bi701037e. PubMed PMID: 17924660.

30.   Li G-Y, Zhang Y, Inouye M, Ikura M. Structural mechanism of transcriptional autorepression of the Escherichia coli RelB/RelE antitoxin/toxin module. Journal of

molecular biology. 2008;380(1):107-19. doi: 10.1016/j.jmb.2008.04.039. PubMed PMID: 18501926.

31.   Gerdes K. Type II Toxin-Antitoxins Loci: The *relBE* Family. Prokaryotic Toxin-Antitoxins. Berlin, Heidelberg: Springer Berlin Heidelberg; 2013. p. 69-92.

32.   Cherny I, Gazit E. The YefM antitoxin defines a family of natively unfolded proteins: implications as a novel antibacterial target. J Biol Chem. 2004;279(9):8252-61. Epub 2003/12/16. doi: 10.1074/jbc.M308263200. PubMed PMID: 14672926.

33.   Cherny I, Rockah L, Gazit E. The YoeB toxin is a folded protein that forms a physical complex with the unfolded YefM antitoxin. Implications for a structural-based differential stability of toxin-antitoxin systems. J Biol Chem. 2005;280(34):30063-72. Epub 2005/06/28. doi: 10.1074/jbc.M506220200. PubMed PMID: 15980067.

34.   Kamada K, Hanaoka F. Conformational change in the catalytic site of the ribonuclease YoeB toxin by YefM antitoxin. Mol Cell. 2005;19(4):497-509. Epub 2005/08/20. doi: 10.1016/j.molcel.2005.07.004. PubMed PMID: 16109374.

35.   Nieto C, Cherny I, Khoo SK, de Lacoba MG, Chan WT, Yeo CC, Gazit E, Espinosa M. The *yefM-yoeB* toxin-antitoxin systems of *Escherichia coli* and *Streptococcus pneumoniae*: functional and structural correlation. J Bacteriol. 2007;189(4):1266-78. Epub 2006/10/31. doi: 10.1128/JB.01130-06. PubMed PMID: 17071753; PMCID: PMC1797350.

36.   Sakr S, Cirinesi AM, Ullers RS, Schwager F, Georgopoulos C, Genevaux P. Lon protease quality control of presecretory proteins in *Escherichia coli* and its dependence on the SecB and DnaJ (Hsp40) chaperones. J Biol Chem. 2010;285(30):23506-14. Epub 2010/05/28. doi: 10.1074/jbc.M110.133058. PubMed PMID: 20504766; PMCID: PMC2906341.

37.   Pavelich IJ, Maehigashi T, Hoffer ED, Ruangprasert A, Miles SJ, Dunham CM. Monomeric YoeB toxin retains RNase activity but adopts an obligate dimeric form for thermal stability.

Nucleic Acids Res. 2019. Epub 2019/09/11. doi: 10.1093/nar/gkz760. PubMed PMID: 31501867.

38. Ranquet C, Gottesman S. Translational regulation of the *Escherichia coli* stress factor RpoS: a role for SsrA and Lon. J Bacteriol. 2007;189(13):4872-9. Epub 2007/04/24. doi: 10.1128/JB.01838-06. PubMed PMID: 17449615; PMCID: PMC1913435.

39. Hughes AC, Subramanian S, Dann CE, Kearns DB. The C-Terminal Region of *Bacillus subtilis* SwrA Is Required for Activity and Adaptor-Dependent LonA Proteolysis. J Bacteriol. 2018;200(6). doi: UNSP e00659-17

10.1128/JB.00659-17. PubMed PMID: WOS:000426018300005.

40. Brown BL, Vieux EF, Kalastavadi T, Kim S, Chen JZ, Baker TA. N domain of the Lon AAA+ protease controls assembly and substrate choice. Protein Sci. 2018. Epub 2018/11/22. doi: 10.1002/pro.3553. PubMed PMID: 30461098.

41. Clark MF, Barbara DJ. A method for the quantitative analysis of ELISA data. J Virol Methods. 1987;15(3):213-22. Epub 1987/02/01. PubMed PMID: 3558703.

42. Kohl TO, Ascoli CA. Indirect Competitive Enzyme-Linked Immunosorbent Assay (ELISA). Cold Spring Harb Protoc. 2017;2017(7):pdb prot093757. Epub 2017/07/07. doi: 10.1101/pdb.prot093757. PubMed PMID: 28679706.

43. Madl T, Van Melderen L, Mine N, Respondek M, Oberer M, Keller W, Khatai L, Zangger K. Structural basis for nucleic acid and toxin recognition of the bacterial antitoxin CcdA. J Mol Biol. 2006;364(2):170-85. Epub 2006/09/30. doi: 10.1016/j.jmb.2006.08.082. PubMed PMID: 17007877.

44. Puri N, Karzai AW. HspQ Functions as a Unique Specificity-Enhancing Factor for the AAA+ Lon Protease. Mol Cell. 2017;66(5):672-83 e4. Epub 2017/06/03. doi: 10.1016/j.molcel.2017.05.016. PubMed PMID: 28575662.

45. Jonas K, Liu J, Chien P, Laub MT. Proteotoxic stress induces a cell-cycle arrest by stimulating Lon to degrade the replication initiator DnaA. Cell. 2013;154(3):623-36. doi: 10.1016/j.cell.2013.06.034. PubMed PMID: 23911325; PMCID: PMC3749246.

46. Jonas K, Chen YE, Laub MT. Modularity of the bacterial cell cycle enables independent spatial and temporal control of DNA replication. Curr Biol. 2011;21(13):1092-101. Epub 2011/06/21. doi: 10.1016/j.cub.2011.05.040. PubMed PMID: 21683595; PMCID: PMC3143580.

47. Datsenko KA, Wanner BL. One-step inactivation of chromosomal genes in *Escherichia coli* K-12 using PCR products. Proceedings of the National …2000.

48. Guzman LM, Belin D, Carson MJ, Beckwith J. Tight regulation, modulation, and high-level expression by vectors containing the arabinose PBAD promoter. J Bacteriol. 1995;177(14):4121-30. Epub 1995/07/01. doi: 10.1128/jb.177.14.4121-4130.1995. PubMed PMID: 7608087; PMCID: PMC177145.

49. Zhang Y, Inouye M. The inhibitory mechanism of protein synthesis by YoeB, an *Escherichia coli* toxin. J Biol Chem. 2009;284(11):6627-38. Epub 2009/01/07. doi: 10.1074/jbc.M808779200. PubMed PMID: 19124462; PMCID: PMC2652283.

Chapter 5

Conclusion

5.1 Abstract

Although originally identified as plasmid maintenance systems, accumulating evidence from the field seems to suggest that some toxin-antitoxin systems may also function as mechanisms of the bacterial immune response that protects cells from bacteriophages. Similar to CRISPR-Cas guided systems that can interfere with or adapt to phage DNA, or restriction-modification systems that degrade phage DNA in a site-specific manner or protect host DNA through signal modifications, one can imagine quite a few novel roles for toxin-antitoxin systems to play in the cell. For example, activation of these systems by way of antitoxin degradation could free toxins to target host RNA or remodel the cellular transcriptome in the face of environmental stimuli like DNA damage, nutrient starvation, thermal fluctuations, or antibiotic phage infection, or antibiotic exposure. Here, I discuss the current state of the field, the impact my studies have made in further understanding toxin-antitoxin systems, and finally, scientific work being conducted to address remaining questions in the field.

5.2 Introduction

Toxin-antitoxins are now understood to have a variety of roles in bacteria including plasmid maintenance via post-segregational killing, defense against phage infection, and stress (see Section 1.5). In the last 20 years, the most exciting but controversial role of toxin-antitoxin systems has been their implication in bacterial persistence against antibiotics.

It has been known for decades that bacteria can survive during antibiotic treatment without undergoing genetic mutations as seen in antibiotic resistance (1). This phenomenon is known as antibiotic tolerance and bacteria that display these phenotypic or behavioral changes are called "persisters". Persistence is achieved by the inhibition of growth and allows for the formation of a small subpopulation of persister cells, which uniquely exhibit a non-heritable ability to subsist during antibiotic treatment. Notably, bacterial persistence in pathogens has been linked to patient reinfection (2-4). Although antibiotic tolerance (as in persister cells) is distinct from antibiotic resistance because it does not rely on genetic mutations to provide immunity from antibiotics, it has recently been shown that antibiotic tolerance precedes the development of resistance (Figure 5.1) (5). Thus, understanding how tolerance functions is a major goal of antimicrobial medical research.

Toxin-antitoxin systems were first implicated in bacterial persistence through the discovery of the *E. coli* HipA toxin from the HipA-HipB toxin-antitoxin system (6-10). Screening bacteria for antibiotic tolerance resulted in a population of *E. coli* with increased

persistence (6). Most of the accumulated mutations occurred in the *hipA* toxin gene, which are within the domain important for dimerization to antitoxin HipB (11). Without dimerization, antitoxin HipB can no longer sequester and block the active site of HipA, freeing it to phosphorylate glutamyl-tRNA synthetase, which prevents aminoacylation (8). Uncharged tRNAs then activate the stringent response (Figure 5.2). Gerdes and coworkers demonstrated later that a sequential deletion of up to 10 well-studied type II toxin-antitoxin systems, including *hipAhipB,* hindered the ability of bacteria to enter a persistent state (12). In addition, overexpression of many type II RNase toxins increased the number of bacterial persister cells in the total population. In a follow-up study, the master signaling molecule (p)ppGpp was shown to indirectly control activation of toxin-antitoxin systems and bacterial persistence through the stringent response (13). Through the RelA-dependent pathway, bacteria sense nutritional stress from uncharged tRNAs on the ribosome that causes inactivation of protein synthesis by stalling and produces (p)ppGpp (Figure 5.2). One of the downstream targets of (p)ppGpp is an enzyme called exopolyphosphatase (PPX) (14). Inhibition of PPX is important, as it prevents accumulation of polyphosphate, a molecule that associates with Lon protease to enhance degradation (15). Thus, a new regulatory mechanism underlying bacterial persistence suggested that through (p)ppGpp, Lon protease could be activated against type II antitoxins to free toxins and bolster the persistence phenotype. For the first time, it appeared that modulation of bacterial persistence was a major function of toxin-antitoxin systems. However, none of these results could be reproduced and it was later determined that lambda and ϕ80 prophages were to blame for the erroneous results (16, 17).

Since then, toxin-antitoxin systems that function in bacterial persistence in addition to HipA-HipB have been identified (18, 19). These include *E. coli* toxins TisB (of TisA-TisB) and MazF (of MazE-MazF) (20, 21), but the mechanisms by which these toxins induce persistence are still unclear. The importance of toxin-antitoxin systems in bacterial persistence has also translated to animal models in pathogenic *E. coli, M. tuberculosis*, *S. typhimurium* and *B. pseudomallei* (3, 4, 22, 23). This is important as toxin-antitoxins are unique to bacteria, and thus represent desirable antimicrobial targets if specific systems can be implicated in persistent infections. For example, the PasT-PasI system promotes bacterial persistence in extraintestinal pathogenic *E. coli* (ExPEC) (3). A new druggable target for reducing persistent and recurring ExPEC infections would be powerful, as they're a major cause of bacteremia, sepsis, and urinary tract infections (24).

Because of the controversies the toxin-antitoxin field has faced in relation to bacterial persistence, simple questions regarding these systems remain important to study as they are still activated in a general way that includes degradation of antitoxin to free toxin (Figure 5.3). My graduate work has sought to provide mechanistic insight into three distinct aspects of the general toxin-antitoxin activation pathway, which are (i) toxin activation (Chapter 2), (ii) toxin-antitoxin regulation (Chapter 3), and (iii) antitoxin degradation (Chapter 4).

5.3 Toxin activity as a consequence of stress

As many type II toxins function as mRNases, we sought to further understand substrate specificity by determining the mechanism of the ribosome-dependent *E. coli* toxin YoeB

of the YefM-YoeB system (see Chapter 2). The YefM-YoeB system was first identified by homology to the previously characterized system Axe-Txe in the *E. faecium* multi-drug resistant plasmid pRUM (25). YefM-YoeB is distinct from other type II toxin-antitoxin systems in that YoeB is a dimer that binds to the ribosome. This contrasts with all other known type II ribosome-dependent toxins which bind the ribosomal A site as monomers. To determine if this oligomeric state was essential for activity, we engineered a YoeB variant that ablates binding interactions between monomers in the YoeB dimer to form a solely monomeric population of YoeB. We found monomeric YoeB to be just as active as dimeric YoeB, indicating that the dimeric version was not necessary for catalytic activity. Additionally, we observed that dimeric YoeB was more thermostable than the monomeric version. This is an interesting result as YoeB is thus far the only ribosome-dependent toxin shown to be upregulated and active during thermal stress (26).

Early work in the toxin-antitoxin field on chromosomal systems RelB-RelE and MazE-MazF suggested that in addition to plasmid maintenance, toxins could also be released as a consequence of nutritional stress (27-29). Further exploration of type II RNase toxins activation and cleavage activity expanded this idea, suggesting toxins could be activated in response to diverse stress. As type II toxins are largely RNases, it was thought that the overall purpose of these toxins was to cleave RNA to inhibit translation. For example, *E. coli* toxin RelE fulfills the role of inhibiting translation by cleaving in the A site of the ribosome in response to amino acid starvation (nutritional stress) (27). tmRNA-SmpB can then recognize and alleviate stalled ribosomes, allowing the cell to continue translation (30). tmRNA-SmpB is the complex that drives *trans*-translation, a process by which

ribosomes stalled on damaged transcripts can be rescued (31). tmRNA contains both tRNA-like and mRNA-like domains, and complexes with SmpB to mimic the anticodon stem-loop of tRNA (32). Thus, tmRNA-SmpB is accepted into the ribosomal A site containing the damaged mRNA as if it were the next tRNA encoded for, allowing translation to continue through replacement of the damaged message with tmRNA. In addition, a degradation tag is also appended to the end of the damaged protein. There is also the possibility that tmRNA has a role in kicking out the toxin from the A site, although this has never been shown.

It is possible that not every toxin shares the function of *inhibiting* translation. Although YoeB cleaves in the A site similar to RelE, it only does so on ribosomes stalled on mRNA transcripts (26). This would suggest that YoeB has an alternative role to RelE, working instead to cleave stalled transcripts at elevated temperatures to open the A site to tmRNA-SmpB, which would then bind and release the nascent chain stuck in the peptide exit tunnel (Figure 5.4). Our studies greatly expand the understanding of YoeB cleavage specificity by solving four structures of YoeB bound to the ribosome in pre- and post-cleavage states on a UAA and AAU codons. If the role of a toxin was to cleave in the ribosomal A site to enable *trans*-translation to recycle ribosomal complexes, the toxin would ideally have little-to-no specificity for its target. Our data suggests YoeB has far looser codon specificity than previously thought, which is in contrast to other toxins that are more specific, like *E. coli* toxin YafQ which recognizes only a single AAA lysine codon (33, 34). The overall non-specificity of YoeB agrees with the hypothesized role of YoeB in cleaving stalled transcripts to allow *trans*-translation to occur.

Many studies in the toxin-antitoxin field have pointed to elevated levels of toxin-antitoxin transcripts as evidence for increased toxin activity. Surprisingly, Laub and coworkers show that transcriptional activation of toxin-antitoxin systems does not always lead to freed toxin activity (35). Their study achieved this result by comparing transcriptional activation of toxin-antitoxin genes to actual toxin activity. *E. coli* were exposed to a panel of stress inducers used in the toxin-antitoxin field to determine how type II toxin-antitoxin genes are transcriptionally activated in response to stress. The panel of stressors included serine hydroxamate (nutrient starvation), chloramphenicol (translation inhibitor), trimethoprim (DNA synthesis inhibitor), hydrogen peroxide (oxidative stress inducer), a 15 ºC temperature shift (heat shock inducer), acidic medium (pH 4, acid shock inducer), and carbenicillin (cell wall synthesis inhibitor). In each case except carbenicillin, a majority of the type II toxin-antitoxin systems were transcriptionally activated. An *E. coli* strain where the ten most well-studied type II toxin-antitoxin systems were removed (Δ10) was then exposed to the same panel of stressors. In comparison to the Δ10 strain, wild-type *E. coli* did not display any advantage in growth when exposed to different stresses. Further, RNAseq revealed no evidence of endogenous toxin activity in response to the stresses mentioned above. All other studies that examine cleavage specificity of toxins have relied on overexpression of toxin. As a control, Laub and coworkers also induced toxins from overexpression constructs and observed dramatically elevated toxin activation patterns, suggesting that overexpression of toxin inflates the true effect of endogenous toxin activation. For example, in the study implicating YoeB in thermal stress, cleavage of model and heat-shock specific YoeB transcripts in the presence of

endogenous YoeB levels was not observed. This is likely because studies that had previously characterized YoeB cleavage specificity relied on YoeB overexpression constructs. These results do not mean that toxins are totally inactive, but instead suggest that their activity remains significantly lower than expected. Future studies should avoid relying on toxin overexpression and ensure that for any phenotype observed post-overexpression, the opposite phenotype can be observed if the toxin-antitoxin system is removed. Laub and co-workers have further examined cleavage activity on a mass scale with sensitive RNAseq, and even with toxin overexpression have not observed major patterns in mRNA cleavage (36).

Discrepancies in how toxin-antitoxin systems are activated during stress extend beyond total toxin activity. For instance, RelB-RelE and MazE-MazF can be activated in response to stress other than the stringent response for which they were originally identified (37). Given that the majority of the 10 most studied type II toxin-antitoxins systems were upregulated in response to the panel of stressors provided by Laub and coworkers (35), the possibility that there are master regulatory molecules that control toxin-antitoxin activity is diminishing. There are also some toxin-antitoxin systems for which the data on activation under stress is unclear. For example, while it was previously suggested that antitoxin MqsA is able to effect expression of other master regulator genes of oxidative stress and biofilm formation (38, 39), conflicting data suggest this may not be true (40). Thus, activation of toxin remains a fundamental question that should be carefully re-examined.

5.4 Type II toxin-antitoxin systems are regulated by a diverse set of mechanisms

As our understanding of toxin-antitoxin regulation has expended, we also sought to determine if the well-studied mechanism of conditional cooperativity (see Section 1.4) is conserved in systems whose regulation is not well understood, like in the *P. vularis* HigB-HigA system (Chapter 3). In addition, it had been previously suggested that changes in transcriptional repression of toxin-antitoxin operons occur in part through the different oligomeric states adopted by toxin-antitoxin systems. For example, while antitoxin alone would be sufficient for transcriptional repression, toxins would function as co-repressors as the total population of toxin increases and binds to DNA-bound antitoxin. However, structures of type II toxin-antitoxin complexes bound to DNA previously solved were only in one of the many possible oligomeric states. Here, for the first time, different oligomeric states of a toxin-antitoxin complex have now been solved. This means that at least for the HigB-HigA system, we solved structures of HigA-DNA (41) and the two possible oligomeric states of HigB-HigA bound to operator DNA (Chapter 3). This enables us to make direct comparisons between the structures to understand how HigB-HigA is regulated. If possible, solving alternate oligomeric conformations of other toxin-antitoxin complexes bound to DNA would provide a significant number of mechanistic insights into how toxin-antitoxin systems regulate their own transcription.

The most surprising result of our studies with HigB-HigA is that we found no significant difference in the ability of HigB-HigA to repress transcription based on oligomeric state. We engineered and verified a variant of HigB-HigA that is trimeric, instead of tetrameric. This was accomplished by insertion of residues into loop 5 of HigB, which causes a steric

clash if an adjacent, second HigB monomer binds, while bound to a HigA antitoxin-DNA complex. As we don't find HigB functions as a co-repressor, this mechanism is distinct from other systems like those utilized in GraT-GraA and MqsR-MqsA (42, 43), further adding to the diversity of mechanisms used to regulate toxin-antitoxin systems (see Section 1.7). Since there is little difference between the trimeric and tetrameric structures of HigBA, I hypothesize that regulation of HigBA is affected by some dynamic behavior *in vivo* that static structures cannot capture, or that these systems function at different timescales or toxin activity levels as previously described.

5.5 Toxin activation by antitoxin proteolysis remains poorly understood

There is also the simple question of how proteases suddenly and selectively become active against antitoxins whose proteolysis frees toxins. Most studies have suggested that antitoxins are largely recognized by Lon and Clp proteases (44). This has been determined by examining the impact of protease deletions on antitoxin half-lives via western blotting (28, 33, 45-53). In addition, studies have shown that changing levels of cellular proteases in response to stress are not sufficient to activate antitoxin degradation, nor do proteases target antitoxins during normal growth (44). Thus, proteases must gain some sort of specificity against antitoxins as a consequence of stress, but how this is achieved is unclear.

The prevailing model of toxin activation assumes that the increased transcription of toxin-antitoxin operons during stress was a result of antitoxin degradation, and that toxin trapped in toxin-antitoxin complexes functions as a reserve population ready to be rapidly

activated (54). In the same study that determined toxin-antitoxin transcripts are elevated while toxins are not necessarily freed, an alternative mechanism was suggested (35). While stress can indeed accelerate antitoxin degradation, antitoxin populations are never totally removed. The implication of this is that toxins that occupy toxin-binding sites on DNA-bound antitoxins are never actually freed. This raises an interesting question of how toxins can, if ever, be freed from their complex with cognate antitoxin. The few studies that have examined the affinity of toxin-antitoxin complexes have concluded that at least some of these complexes bind with affinity in the sub-nanomolar range (43, 48). This is further complicated by the fact that plasmid-borne and chromosomal toxin-antitoxin systems appear to behave differently. For example, toxins in plasmid-borne toxin-antitoxin systems like CcdA-CcdB are liberated when new synthesis stops following plasmid loss (52). This is evidenced by a marked defect in growth, indicating antitoxin CcdA has been degraded and toxin CcdB released. The same behavior does not apply to chromosomal toxin-antitoxin systems like YefM-YoeB or MqsR-MqsA (35). Even after synthesis of these systems is halted, no growth defect is observed, indicating toxin is still sequestered. This suggests that proteolysis may function differently against plasmid-borne antitoxins like CcdA as compared to chromosomal antitoxins YefM and MqsA. If toxins are never freed or freed to a degree that does not produce a phenotype or confer an advantage in survival, perhaps those systems are activated much slower than previously thought, or by factors yet unknown.

As proteases are still responsible for degrading antitoxins in both models of toxin activation described above, it is imperative to design studies elucidating how antitoxins

can be selectively degraded (Chapter 4). Our studies importantly provide a framework for which antitoxin degradation can be studied by determining which residues and regions antitoxins utilize to sequester toxin. Then, this data can be compared with those from experiments determining which of those same regions are important for recognition by different proteases. Together, these data should provide insights on how antitoxins are recognized and degraded by proteases and will allow for further determination on how toxins are ultimately activated in bacteria.

5.6 Concluding Remarks

The last 25 years of toxin-antitoxin research has yielded an impressive number of confirmed and hypothesized roles for the two-component systems in bacteria. I hypothesize that with further exploration, the importance of toxin-antitoxin systems in bacterial physiology will grow as our understanding of them continues to evolve. Other classes of effector molecules like restriction enzymes and CRISPR-cas have proven to be significant in biology since their initial discovery. The function for which restriction enzymes were originally discovered was protection against phage DNA (55). Certain toxin-antitoxin systems have already been implicated in phage defense (56, 57) and there could be many more, given the ubiquity of these systems. Toxin-antitoxin systems have also recently been linked to the evolution of CRISPR-cas (58). In addition, toxin-antitoxin systems can safeguard CRISPR-cas loci from disruption by transposable elements, which is reminiscent of the role of toxin-antitoxins in plasmid maintenance (59). This is because the toxin-antitoxin systems are encoded within the CRISPR-cas loci and regulated by CRISPR RNA, which functions as the antitoxin. If the CRISPR-cas system becomes

damaged or is not inherited, the toxin gene is no longer repressed by the CRISPR RNA antitoxin and kills the cell. Thus, by encoding toxin-antitoxin pairs within a CRISPR-cas loci, the cells become addicted to that particular CRISPR-cas system, and it is maintained within the progeny. Given these examples, it's easy to imagine that toxin-antitoxin systems, with their various classes, components, and functions, represent another type of effector molecules in bacteria.

Considering recent studies (35, 44, 58-60), it will be important for the toxin-antitoxin field to acknowledge that these systems are more complex than was first realized. In response to this, the field should re-focus on the simplest questions, such as why there are so many toxin-antitoxin systems integrated into chromosomes, when and how they are activated, and what the consequences of their activation are.

5.7 Figures
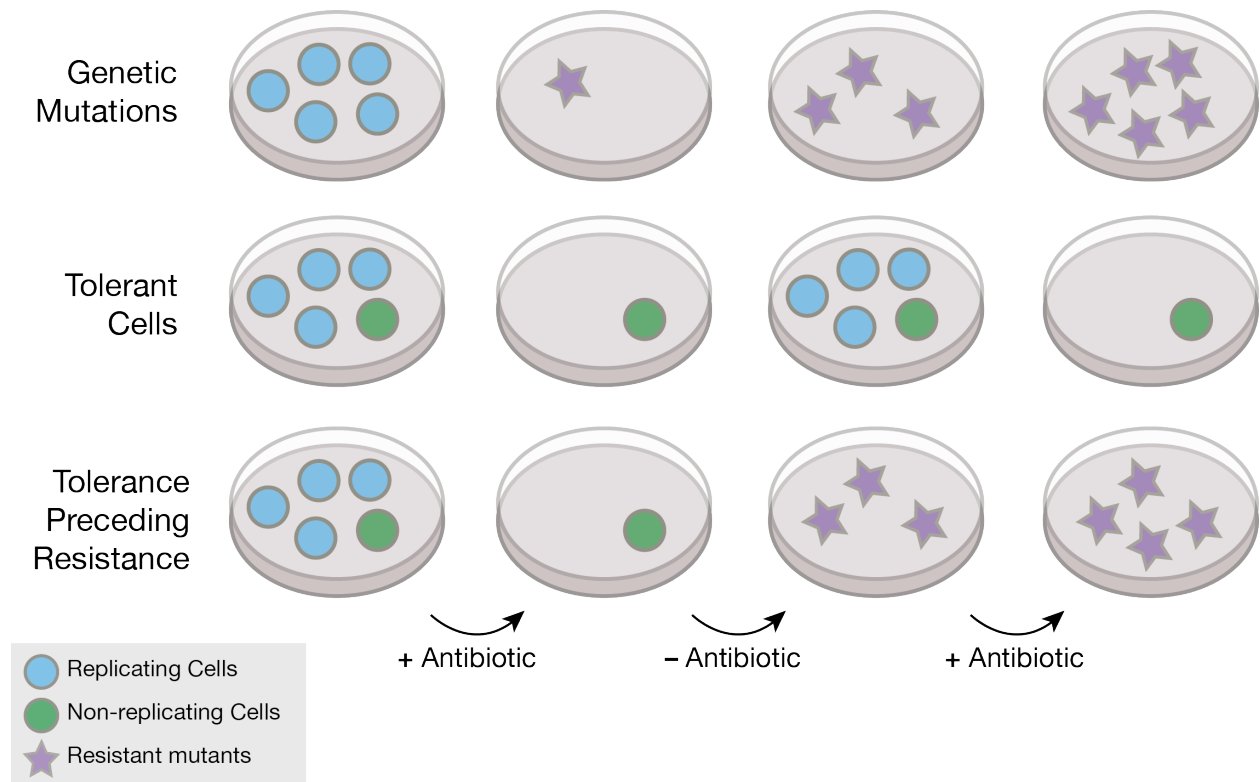
Figure 5.1 – Antibiotic tolerance versus resistance in bacteria.

Typically, upon antibiotic exposure, there would be some pressure of selection that gives rise to bacteria that are completely resistant by way of genetic mutations (top row). This contrasts with the formation of tolerant cells is a phenotypic change, where the cells are non-growing but can resume growth upon removal of the antibiotic stress (middle row). However, antibiotic tolerance may be a necessary pre-condition of antibiotic resistance (last row).
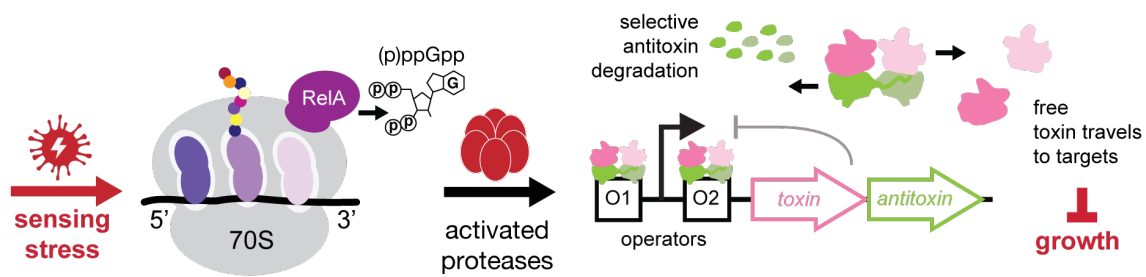
Figure 5.2 – The stringent response pathway regulated by (p)ppGpp was purported to function as a master regulator of toxin-antitoxin activity.

Through the RelA-dependent pathway, stress can be sensed by recognition of uncharged tRNAs on the ribosome that causes inactivation of protein synthesis by stalling. RelA produces the signaling second messenger guanosine (penta)tetraphosphate ((p)ppGpp) which activates numerous cellular responses to stress. This was thought to include global transcriptional activation of toxin-antitoxin genes through recruitment of proteases for the proteolysis of antitoxin proteins and freeing of toxin.
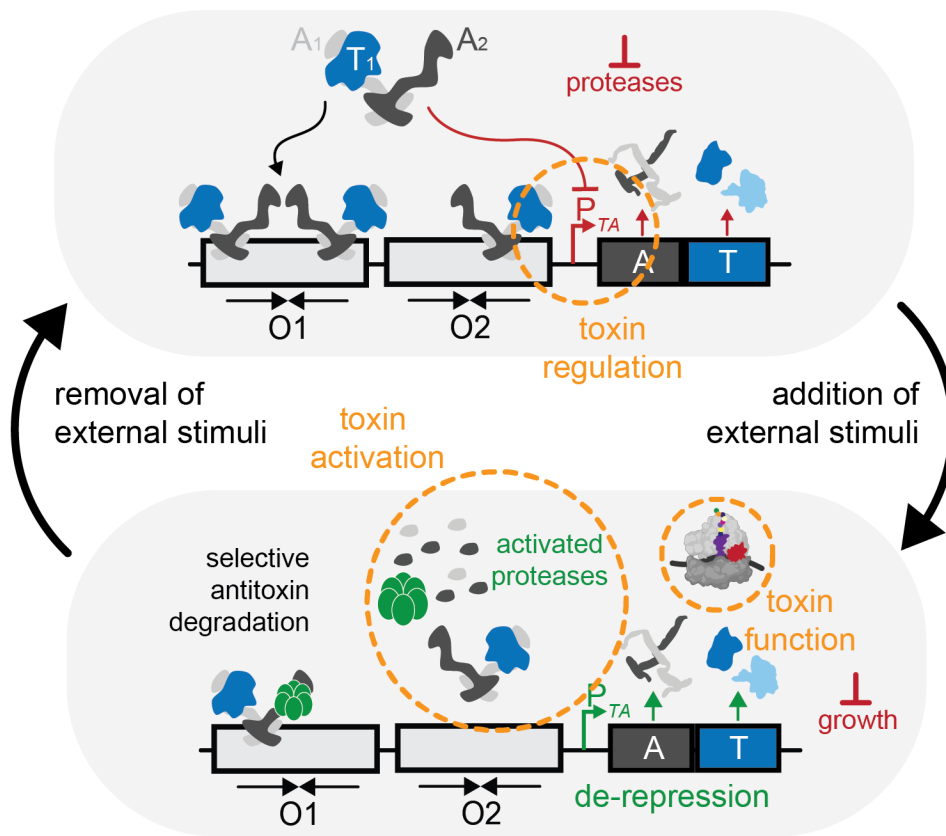
Figure 5.3 – The general toxin-antitoxin activation pathway.

Normally, expression of toxin (T) and antitoxin (A) result in the formation of a tight complex that binds upstream of the promoter (P_{TA}) at operator regions (O1, O2). Upon sensing external stimuli, proteases selectively degrade antitoxins, and the operon is de-repressed. The general focus of graduate work presented herein is indicated in dotted orange circles and by chapter.
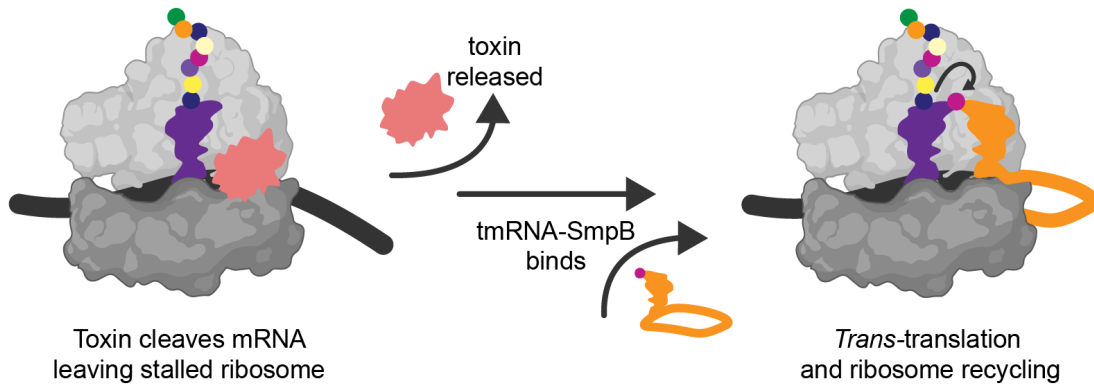
Figure 5.4 – Toxins in ribosome rescue.

A possible role for toxins in ribosomal rescue. Toxin cleavage in the A site (left) could allow ribosomal rescue agents like tmRNA-SmpB to bind (right) and alleviate stalled translation.
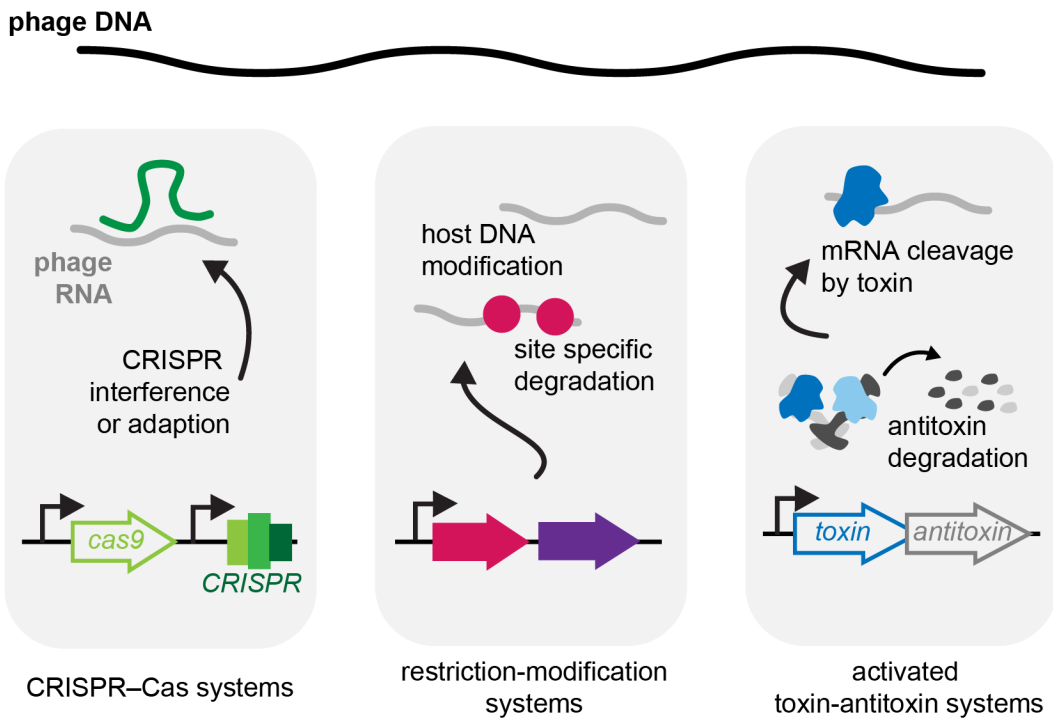
Figure 5.5 – Toxin-antitoxin systems compared with effector molecules.

Bacteria can utilize classes of effector molecules in response to environmental stimuli, such as phage infection. CRISPR-cas systems can interfere or aid in adaption to phage RNA. In a simpler scheme, restriction-modifications can modify host DNA or degrade phage DNA. Toxin-antitoxin systems function as another effector class, as they can cleave numerous mRNA and have been implicated in phage defense and CRISPR-cas.

5.8 References

1. Bigger JW. Treatment of staphylococcal infections with penicillin by intermittent sterilisation. The Lancet. 1944;244(6320):497-500. doi: https://doi.org/10.1016/S0140-6736(00)74210-3.

2. Lewis K. Persister cells, dormancy and infectious disease. Nat Rev Microbiol. 2007;5(1):48-56. Epub 2006/12/05. doi: 10.1038/nrmicro1557. PubMed PMID: 17143318.

3. Norton JP, Mulvey MA. Toxin-antitoxin systems are important for niche-specific colonization and stress resistance of uropathogenic *Escherichia coli*. PLoS Pathog. 2012;8(10):e1002954. Epub 2012/10/12. doi: 10.1371/journal.ppat.1002954. PubMed PMID: 23055930; PMCID: PMC3464220.

4. Kedzierska B, Hayes F. Emerging Roles of Toxin-Antitoxin Modules in Bacterial Pathogenesis. Molecules. 2016;21(6). Epub 2016/06/21. doi: 10.3390/molecules21060790. PubMed PMID: 27322231.

5. Levin-Reisman I, Ronin I, Gefen O, Braniss I, Shoresh N, Balaban NQ. Antibiotic tolerance facilitates the evolution of resistance. Science. 2017;355(6327):826-30. Epub 2017/02/12. doi: 10.1126/science.aaj2191. PubMed PMID: 28183996.

6. Moyed HS, Bertrand KP. *hipA*, a newly recognized gene of *Escherichia coli* K-12 that affects frequency of persistence after inhibition of murein synthesis. J Bacteriol. 1983;155(2):768-75. Epub 1983/08/01. PubMed PMID: 6348026; PMCID: PMC217749.

7. Schumacher MA, Piro KM, Xu W, Hansen S, Lewis K, Brennan RG. Molecular mechanisms of HipA-mediated multidrug tolerance and its neutralization by HipB. Science. 2009;323(5912):396-401. Epub 2009/01/20. doi: 10.1126/science.1163806. PubMed PMID: 19150849; PMCID: PMC2764309.

8. Germain E, Castro-Roa D, Zenkin N, Gerdes K. Molecular mechanism of bacterial persistence by HipA. Mol Cell. 2013;52(2):248-54. Epub 2013/10/08. doi: 10.1016/j.molcel.2013.08.045. PubMed PMID: 24095282.

9.   Kaspy I, Rotem E, Weiss N, Ronin I, Balaban NQ, Glaser G. HipA-mediated antibiotic persistence via phosphorylation of the glutamyl-tRNA-synthetase. Nat Commun. 2013;4:3001. Epub 2013/12/18. doi: 10.1038/ncomms4001. PubMed PMID: 24343429.

10.   Germain E, Roghanian M, Gerdes K, Maisonneuve E. Stochastic induction of persister cells by HipA through (p)ppGpp-mediated activation of mRNA endonucleases. Proceedings of the National Academy of Sciences of the United States of America. 2015;112(16):5171-6. doi: 10.1073/pnas.1423536112. PubMed PMID: 25848049; PMCID: PMC4413331.

11.   Schumacher MA, Balani P, Min J, Chinnam NB, Hansen S, Vulic M, Lewis K, Brennan RG. HipBA-promoter structures reveal the basis of heritable multidrug tolerance. Nature. 2015;524(7563):59-64. Epub 2015/07/30. doi: 10.1038/nature14662. PubMed PMID: 26222023.

12.   Maisonneuve E, Shakespeare LJ, Jorgensen MG, Gerdes K. Bacterial persistence by RNA endonucleases. Proc Natl Acad Sci U S A. 2011;108(32):13206-11. Epub 2011/07/27. doi: 10.1073/pnas.1100186108. PubMed PMID: 21788497; PMCID: PMC3156201.

13.   Maisonneuve E, Castro-Camargo M, Gerdes K. (p)ppGpp controls bacterial persistence by stochastic induction of toxin-antitoxin activity. Cell. 2013;154(5):1140-50. Epub 2013/09/03. doi: 10.1016/j.cell.2013.07.048. PubMed PMID: 23993101.

14.   Hauryliuk V, Atkinson GC, Murakami KS, Tenson T, Gerdes K. Recent functional insights into the role of (p)ppGpp in bacterial physiology. Nature reviews Microbiology. 2015;13(5):298-309. doi: 10.1038/nrmicro3448. PubMed PMID: 25853779; PMCID: PMC4659695.

15.   Kuroda A. A polyphosphate-lon protease complex in the adaptation of *Escherichia coli* to amino acid starvation. Biosci Biotechnol Biochem. 2006;70(2):325-31. Epub 2006/02/24. doi: 10.1271/bbb.70.325. PubMed PMID: 16495646.

16.   Goormaghtigh F, Fraikin N, Putrins M, Hallaert T, Hauryliuk V, Garcia-Pino A, Sjodin A, Kasvandik S, Udekwu K, Tenson T, Kaldalu N, Van Melderen L. Reassessing the Role of Type II Toxin-Antitoxin Systems in Formation of *Escherichia coli* Type II Persister Cells. Mbio. 2018;9(3). Epub 2018/06/14. doi: 10.1128/mBio.00640-18. PubMed PMID: 29895634.

17.   Harms A, Fino C, Sorensen MA, Semsey S, Gerdes K. Prophages and Growth Dynamics Confound Experimental Results with Antibiotic-Tolerant Persister Cells. Mbio. 2017;8(6). Epub 2017/12/14. doi: 10.1128/mBio.01964-17. PubMed PMID: 29233898; PMCID: PMC5727415.

18.   Maisonneuve E, Gerdes K. Molecular Mechanisms Underlying Bacterial Persisters. Cell. 2014;157(3):539-48. doi: 10.1016/j.cell.2014.02.050. PubMed PMID: 24766804.

19.   Helaine S, Cheverton AM, Watson KG, Faure LM, Matthews SA, Holden DW. Internalization of Salmonella by macrophages induces formation of nonreplicating persisters. Science. 2014;343(6167):204-8. Epub 2014/01/11. doi: 10.1126/science.1244705. PubMed PMID: 24408438.

20.   Dorr T, Vulic M, Lewis K. Ciprofloxacin causes persister formation by inducing the TisB toxin in *Escherichia coli*. PLoS Biol. 2010;8(2):e1000317. Epub 2010/02/27. doi: 10.1371/journal.pbio.1000317. PubMed PMID: 20186264; PMCID: PMC2826370.

21.   Tripathi A, Dewan PC, Siddique SA, Varadarajan R. MazF-induced Growth Inhibition and Persister Generation in *Escherichia coli*. The Journal of biological chemistry. 2014;289(7):4191-205. doi: 10.1074/jbc.M113.510511.

22.   De la Cruz MA, Zhao W, Farenc C, Gimenez G, Raoult D, Cambillau C, Gorvel JP, Meresse S. A toxin-antitoxin module of Salmonella promotes virulence in mice. PLoS Pathog. 2013;9(12):e1003827. Epub 2014/01/05. doi: 10.1371/journal.ppat.1003827. PubMed PMID: 24385907; PMCID: PMC3868539.

231

23.   Ross BN, Micheva-Viteva S, Hong-Geller E, Torres AG. Evaluating the role of *Burkholderia pseudomallei* K96243 toxins BPSS0390, BPSS0395, and BPSS1584 in persistent infection. Cell Microbiol. 2019;21(12):e13096. Epub 2019/08/11. doi: 10.1111/cmi.13096. PubMed PMID: 31400259.

24.   Kaper JB, Nataro JP, Mobley HL. Pathogenic *Escherichia coli*. Nat Rev Microbiol. 2004;2(2):123-40. Epub 2004/03/26. doi: 10.1038/nrmicro818. PubMed PMID: 15040260.

25.   Grady R, Hayes F. Axe-Txe, a broad-spectrum proteic toxin-antitoxin system specified by a multidrug-resistant, clinical isolate of *Enterococcus faecium*. Mol Microbiol. 2003;47(5):1419-32. Epub 2003/02/27. doi: 10.1046/j.1365-2958.2003.03387.x. PubMed PMID: 12603745.

26.   Janssen BD, Garza-Sanchez F, Hayes CS. YoeB toxin is activated during thermal stress. Microbiologyopen. 2015;4(4):682-97. Epub 2015/07/07. doi: 10.1002/mbo3.272. PubMed PMID: 26147890; PMCID: PMC4554461.

27.   Christensen SK, Mikkelsen M, Pedersen K, Gerdes K. RelE, a global inhibitor of translation, is activated during nutritional stress. Proceedings of the National Academy of Sciences of the United States of America. 2001;98(25):14328-33. doi: 10.1073/pnas.251327898. PubMed PMID: 11717402; PMCID: PMC64681.

28.   Christensen-Dalsgaard M, Jørgensen MG, Gerdes K. Three new RelE-homologous mRNA interferases of *Escherichia coli* differentially induced by environmental stresses. Molecular Microbiology. 2010;75(2):333-48. doi: 10.1111/j.1365-2958.2009.06969.x.

29.   Christensen SK, Pedersen K, Hansen FG, Gerdes K. Toxin-antitoxin loci as stress-response-elements: ChpAK/MazF and ChpBK cleave translated RNAs and are counteracted by tmRNA. J Mol Biol. 2003;332(4):809-19. Epub 2003/09/16. doi: 10.1016/s0022-2836(03)00922-7. PubMed PMID: 12972253.

30.   Christensen SK, Gerdes K. RelE toxins from bacteria and Archaea cleave mRNAs on translating ribosomes, which are rescued by tmRNA. Mol Microbiol. 2003;48(5):1389-400. Epub 2003/06/06. PubMed PMID: 12787364.

31.   Keiler KC, Feaga HA. Resolving nonstop translation complexes is a matter of life or death. J Bacteriol. 2014;196(12):2123-30. Epub 2014/04/08. doi: 10.1128/JB.01490-14. PubMed PMID: 24706739; PMCID: PMC4054194.

32.   Rae CD, Gordiyenko Y, Ramakrishnan V. How a circularized tmRNA moves through the ribosome. Science. 2019;363(6428):740-4. Epub 2019/02/16. doi: 10.1126/science.aav9370. PubMed PMID: 30765567; PMCID: PMC6440651.

33.   Prysak MH, Mozdzierz CJ, Cook AM, Zhu L, Zhang Y, Inouye M, Woychik NA. Bacterial toxin YafQ is an endoribonuclease that associates with the ribosome and blocks translation elongation through sequence-specific and frame-dependent mRNA cleavage. Molecular Microbiology. 2009;71(5):1071-87. doi: 10.1111/j.1365-2958.2008.06572.x. PubMed PMID: 19210620.

34.   Maehigashi T, Ruangprasert A, Miles SJ, Dunham CM. Molecular basis of ribosome recognition and mRNA hydrolysis by the *E. coli* YafQ toxin. Nucleic Acids Res. 2015;43(16):8002-12. Epub 2015/08/12. doi: 10.1093/nar/gkv791. PubMed PMID: 26261214; PMCID: PMC4652777.

35.   LeRoux M, Culviner PH, Liu YJ, Littlehale ML, Laub MT. Stress Can Induce Transcription of Toxin-Antitoxin Systems without Activating Toxin. Mol Cell. 2020;79(2):280-92 e8. Epub 2020/06/14. doi: 10.1016/j.molcel.2020.05.028. PubMed PMID: 32533919; PMCID: PMC7368831.

36.   Culviner PH, Nocedal I, Fortune SM, Laub MT. Global Analysis of the Specificities and Targets of Endoribonucleases from *Escherichia coli* Toxin-Antitoxin Systems. Mbio. 2021:e0201221. Epub 2021/09/22. doi: 10.1128/mBio.02012-21. PubMed PMID: 34544284.

37.   Ramisetty BCM, Ghosh D, Roy Chowdhury M, Santhosh RS. What Is the Link between Stringent Response, Endoribonuclease Encoding Type II Toxin–Antitoxin Systems and Persistence? Frontiers in Microbiology. 2016;7(R81):6059-15. doi: 10.3389/fmicb.2016.01882.

38.   Wang X, Wood TK. Toxin-antitoxin systems influence biofilm and persister cell formation and the general stress response. Appl Environ Microbiol. 2011;77(16):5577-83. Epub 2011/06/21. doi: 10.1128/AEM.05068-11. PubMed PMID: 21685157; PMCID: PMC3165247.

39.   Soo VW, Wood TK. Antitoxin MqsA represses curli formation through the master biofilm regulator CsgD. Sci Rep. 2013;3:3186. Epub 2013/11/12. doi: 10.1038/srep03186. PubMed PMID: 24212724; PMCID: PMC4894380.

40.   Fraikin N, Rousseau CJ, Goeders N, Van Melderen L. Reassessing the Role of the Type II MqsRA Toxin-Antitoxin System in Stress Response and Biofilm Formation: mqsA Is Transcriptionally Uncoupled from mqsR. Mbio. 2019;10(6). doi: ARTN e02678-19

10.1128/mBio.02678-19. PubMed PMID: WOS:000507988700022.

41.   Schureck MA, Meisner J, Hoffer ED, Wang D, Onuoha N, Ei Cho S, Lollar P, 3rd, Dunham CM. Structural basis of transcriptional regulation by the HigA antitoxin. Mol Microbiol. 2019. Epub 2019/02/23. doi: 10.1111/mmi.14229. PubMed PMID: 30793388.

42.   Talavera A, Tamman H, Ainelo A, Konijnenberg A, Hadzi S, Sobott F, Garcia-Pino A, Horak R, Loris R. A dual role in regulation and toxicity for the disordered N-terminus of the toxin GraT. Nat Commun. 2019;10(1):972. Epub 2019/03/01. doi: 10.1038/s41467-019-08865-z. PubMed PMID: 30814507; PMCID: PMC6393540.

43.   Brown BL, Lord DM, Grigoriu S, Peti W, Page R. The *Escherichia coli* toxin MqsR destabilizes the transcriptional repression complex formed between the antitoxin MqsA and the *mqsRA* operon promoter. J Biol Chem. 2013;288(2):1286-94. Epub 2012/11/23. doi: 10.1074/jbc.M112.421008. PubMed PMID: 23172222; PMCID: PMC3543012.

44.   Muthuramalingam M, White JC, Bourne CR. Toxin-Antitoxin Modules Are Pliable Switches Activated by Multiple Protease Pathways. Toxins. 2016;8(7):214. doi: 10.3390/toxins8070214. PubMed PMID: 27409636; PMCID: PMC4963847.

45.   Lehnherr H, Yarmolinsky MB. Addiction protein Phd of plasmid prophage P1 is a substrate of the ClpXP serine protease of *Escherichia coli*. Proc Natl Acad Sci U S A. 1995;92(8):3274-7. Epub 1995/04/11. doi: 10.1073/pnas.92.8.3274. PubMed PMID: 7724551; PMCID: PMC42148.

46.   Christensen SK, Gerdes K. Delayed-relaxed response explained by hyperactivation of RelE. Mol Microbiol. 2004;53(2):587-97. Epub 2004/07/02. doi: 10.1111/j.1365-2958.2004.04127.x. PubMed PMID: 15228536.

47.   Christensen SK, Maenhaut-Michel G, Mine N, Gottesman S, Gerdes K, Van Melderen L. Overproduction of the Lon protease triggers inhibition of translation in *Escherichia coli*: involvement of the *yefM-yoeB* toxin-antitoxin system. Molecular Microbiology. 2004;51(6):1705-17. doi: 10.1046/j.1365-2958.2003.03941.x. PubMed PMID: 10.1046/j.1365-2958.2003.03941.x.

48.   Overgaard M, Borch J, Gerdes K. RelB and RelE of *Escherichia coli* form a tight complex that represses transcription via the ribbon-helix-helix motif in RelB. Journal of molecular biology. 2009;394(2):183-96. doi: 10.1016/j.jmb.2009.09.006. PubMed PMID: 19747491; PMCID: PMC2812701.

49.   Winther KS, Gerdes K. Regulation of enteric *vapBC* transcription: induction by VapC toxin dimer-breaking. Nucleic Acids Res. 2012;40(10):4347-57. Epub 2012/01/31. doi: 10.1093/nar/gks029. PubMed PMID: 22287572; PMCID: PMC3378870.

50.   Diago-Navarro E, Hernandez-Arriaga AM, Kubik S, Konieczny I, Diaz-Orejas R. Cleavage of the antitoxin of the *parD* toxin-antitoxin system is determined by the ClpAP protease and is modulated by the relative ratio of the toxin and the antitoxin. Plasmid.

2013;70(1):78-85. Epub 2013/02/20. doi: 10.1016/j.plasmid.2013.01.010. PubMed PMID: 23419648.

51.   Hansen S, Vulić M, Min J, Yen T-J, Schumacher MA, Brennan RG, Lewis K. Regulation of the *Escherichia coli* HipBA Toxin-Antitoxin System by Proteolysis. PLoS ONE. 2012;7(6):e39185-10. doi: 10.1371/journal.pone.0039185; PMCID: 22720069.

52.   Van Melderen L, Bernard P, Couturier M. Lon-dependent proteolysis of CcdA is the key control for activation of CcdB in plasmid-free segregant bacteria. Molecular Microbiology. 1994;11(6):1151-7. PubMed PMID: 8022284.

53.   Wang X, Kim Y, Hong SH, Ma Q, Brown BL, Pu M, Tarone AM, Benedik MJ, Peti W, Page R, Wood TK. Antitoxin MqsA helps mediate the bacterial general stress response. Nat Chem Biol. 2011;7(6):359-66. Epub 2011/04/26. doi: 10.1038/nchembio.560. PubMed PMID: 21516113; PMCID: PMC3097263.

54.   Pedersen K, Christensen SK, Gerdes K. Rapid induction and reversal of a bacteriostatic condition by controlled expression of toxins and antitoxins. Mol Microbiol. 2002;45(2):501-10. Epub 2002/07/19. PubMed PMID: 12123459.

55.   Loenen WA, Dryden DT, Raleigh EA, Wilson GG, Murray NE. Highlights of the DNA cutters: a short history of the restriction enzymes. Nucleic Acids Res. 2014;42(1):3-19. Epub 2013/10/22. doi: 10.1093/nar/gkt990. PubMed PMID: 24141096; PMCID: PMC3874209.

56.   Fineran PC, Blower TR, Foulds IJ, Humphreys DP, Lilley KS, Salmond GP. The phage abortive infection system, ToxIN, functions as a protein-RNA toxin-antitoxin pair. Proc Natl Acad Sci U S A. 2009;106(3):894-9. Epub 2009/01/07. doi: 10.1073/pnas.0808832106. PubMed PMID: 19124776; PMCID: PMC2630095.

57.   Dy RL, Przybilski R, Semeijn K, Salmond GP, Fineran PC. A widespread bacteriophage abortive infection system functions through a Type IV toxin-antitoxin mechanism. Nucleic

Acids Res. 2014;42(7):4590-605. Epub 2014/01/28. doi: 10.1093/nar/gkt1419. PubMed PMID: 24465005; PMCID: PMC3985639.

58. Song S, Wood TK. A Primary Physiological Role of Toxin/Antitoxin Systems Is Phage Inhibition. Front Microbiol. 2020;11:1895. Epub 2020/09/10. doi: 10.3389/fmicb.2020.01895. PubMed PMID: 32903830; PMCID: PMC7438911.

59. Li M, Gong L, Cheng F, Yu H, Zhao D, Wang R, Wang T, Zhang S, Zhou J, Shmakov SA, Koonin EV, Xiang H. Toxin-antitoxin RNA pairs safeguard CRISPR-Cas systems. Science. 2021;372(6541). Epub 2021/05/01. doi: 10.1126/science.abe5601. PubMed PMID: 33926924.

60. Fraikin N, Goormaghtigh F, Van Melderen L. Type II Toxin-Antitoxin Systems: Evolution and Revolutions. J Bacteriol. 2020;202(7). Epub 2020/01/15. doi: 10.1128/JB.00763-19. PubMed PMID: 31932311; PMCID: PMC7167474.